THE UNIVERSITY
of EDINBURGH

Identifying the Disappeared: Testing a Novel Method for Sorting Commingled Human Remains

Mara A. Karell

Doctor of Philosophy

The University of Edinburgh

2019

Declaration

I declare that this thesis was composed solely by myself, that the words contained herein are my own except where explicitly stated otherwise in the text, and that this work has not been submitted for any other degree or professional qualification except as specified.

Parts of this work have been published in:

Karell MA, Lay M, Langstaff HK and Kranioti EF (2017) Pair-matching Temporals Using a Digital Mesh-to-mesh Value Comparison Method. *La Revue de Medicine Legale*. 8(4): 185

Karell MA, Langstaff H, Halazonetis DJ, Minghetti C, Frelat M, and Kranioti EF (2016) A Novel Method for Pair-matching Using Three-dimensional Digital Models of Bone: Mesh-to-mesh Value Comparison. *International Journal of Legal Medicine.* 130(5):1315-22

Mara A. Karell

30 April 2019

Abstract

Individualisation of commingled remains is the first step towards identification of skeletal remains, and thus to returning a loved one to their family or community after tragedy and to providing closure. Currently, there are limited methods of individualisation of commingled remains, which hinders the identification process. This dissertation explored the effectiveness of a novel individualisation technique, called mesh-to-mesh value comparison (MVC), on pair-matching four different sets of bones: humeri, clavicles, temporal bones and calcanei. This was done using two different MVC methods: one manual which uses the program Flexscan3D, and the other automatic which uses the program Viewbox. Both use three-dimensional models of bones to more accurately digitally match pairs using Iterative Closest Point algorithms. The resulting data from both programs were assessed using sensitivity, specificity, positive predictive value, and negative predictive values rates, calculated in two different manners: by Lowest Common Value selection and by Receiver Operating Characteristic (ROC) curves. Results varied by bone type and MVC type but generally both MVC methods were highly accurate at pair-matching, though the manual always outperformed the automatic. The single exception for both the manual and automatic MVC methods was the clavicle set, which produced significantly lower results.

Lay Summary

Forensic anthropology is the study of the human skeleton for identification purposes, to provide information for legal processes and closure for families and communities affected by tragedy. The main task of the forensic anthropologist is the creation of a biological profile, which estimates age, sex, stature, and often ancestry. However, in situations where multiple skeletons are commingled (mixed together), such as mass disasters, skeletal remains must be separated into individuals before a biological profile can be created. Currently there are limited methods for individualisation, which hinders the creation of a biological profile, and therefore identification of an individual.

This thesis tested a novel method for sorting commingled remains called mesh-to-mesh value comparison (MVC). This technique uses three-dimensional models of bones to test similarity in paired bones using Iterative Closest Point (ICP) algorithms, which expresses the overall similarity of three-dimensional objects. Four sets of bones, humeri (arm), clavicles (collarbones), temporals (skull) and calcanei (foot), were tested to explore the effects of three-dimensional geometry, asymmetry, and the algorithms on these paired elements. These sets of bones came from five different populations, covering different geographic locations and time periods. Two different versions of MVC were used, one manual which used the software Flexscan3D and the other automatic which used Viewbox 4.1. All of the resulting data were analysed using sensitivity, specificity, positive predictive value and negative predictive value rates. These rates more accurately describe the ability of a pair-matching method to distinguish between true pair-matches, true negatives (single bones), and other false matches.

Though the results varied across bone type and MVC type, generally MVC was a highly accurate method for pair-matching. The only exception was clavicles (collarbones), which were challenging to pair-match. MVC is therefore a valuable additional tool for sorting commingled human remains.

Dedication

For those who want to know, but do not.

Acknowledgements

To my friends and family for all of their support during this process.
I most definitely couldn't have done it without you.

My mom, my dad and Adam, for the endless encouragements and proof-reading. You are undoubtedly the reason I believed I could accomplish this, and I am forever grateful.

Elena Kranioti for being a wonderful, superhero supervisor.

The rotating IT staff over the years, including Karen Howie (the most amazing), Miles, Craig (1st), Craig (2nd), Josh, Amina, Malcolm, Kacper, Kevin, Michael and Ian. This project would have never been possible without you. Like physically, impossible. Thanks for moving and rebuilding all of the computers for me and putting up with the endless requests for more storage space!

Lynne Thompson, Siobhan McLaughlin and Ralph Bouhaidar for all of their help regarding CT scanning at Little France.

Laura Girdwood and Julieta Garcia-Donas for their Ballumbie and St. Andrews Collection work and expertise, especially sorting out the catalogue regarding age, sex and location!

The PhDs before and since – Laura, Julieta, Helen, Graeme, Anna… the list goes on and on. You made a PhD an actually enjoyable process.

The Marcella's folks for keeping me in food and good conversation.

Eric, for everything.

Table of Contents

List of Figures

Introduction

On the 14th of June 2017, Grenfell Tower went up in flames. By the 22nd of November 2017, the Westminster Coroner and the Metropolitan Police had released their final reports on the identification of the 71 individuals who died in the fire (Wilcox, 2019, Metropolitan Police, 2017b). From the point of view of the numerous agencies and personnel involved in the identification process of the disaster, the relative speed at which the processing of such a complex scene and the rigorous identification process took place was impressive (Jolly, 2017, Gregory, 2017, Press Association, 2018). The surviving victims of the fire, however, were distressed and angered about the slowness of the identification process only three weeks after the incident (Jolly, 2017).

A further six months after the disaster, the family of Mohamed Amied Neda were stunned and angered to learn that one of his bone fragments was found in a tumble dryer after his clothes were sent to be professionally cleaned in order to be returned (Press Association, 2018). As his wife described:

> "I'm angry with that. We are angry. Why didn't they check proper? Why did it take so long? Even the police aren't getting the answer for me…They tell the truth for us, I think it is respectful, but we are angry because why they didn't check first time and they didn't tell us? …This time is more difficult from the first time, it is more difficult, we did again. The ceremony ... reburied, everything." (Press Association, 2018)

During the approximately six month period of confirming the identification of those who died in the fire, those affected by the tragedy lived with not knowing if their family members and friends who were missing were alive or dead, in addition to other physical and emotional trauma from the event (Gregory, 2017).

This, unfortunately, is not a unique case. In the United Kingdom, numerous tragedies such as the sinking of the Marchioness, the Pan Am explosion over Lockerbie, the fire at King's Cross, and the Lakanal House fire have had similar impacts (Shepherd, 2019, Designing Buildings, 2018, Dangerfield, 2014). Judy Wellington, the mother of Marchioness victim Simon Senior, for example, described similar feelings of distress to the Grenfell victims: "All I kept thinking was my child is somewhere but I couldn't reach him. I couldn't eat or sleep and when I did sleep,

I'd wake up and that feeling of pain would come back inside of me. Then I started to realise he was not coming back" (Dangerfield, 2014).

The vast number of these testimonials do not mean that they have gone unheard. In fact, most of these testimonies have only served to strengthen the resolve of those practitioners involved in helping resolve these tragedies. Sergeant Alistair Hutchins, who led the Metropolitan Police's identification team for Grenfell, for example, expressed that his team understood the frustration of family and friends awaiting news of their loved ones (Gregory, 2017); he went on to explain that the team was "extremely passionate about what we do and that is fundamental…We believe in dignity in death, we believe in repatriating loved ones to their family members as fast as we can but also we believe in adhering to a safe system of identification" (Gregory, 2017).

The sheer number of personnel involved in helping the reconciliation process of disasters is generally astonishing. For example with Grenfell, there were approximately 670 firefighters, 340 police officers, and 340 ambulance staff involved in the rescue efforts, as reported by the Metropolitan Police (Metropolitan Police, 2017a). Another approximately 200 police officers were dedicated to the investigation after the incident, and there was a team of 42 individuals dedicated just to the identification process (Gregory, 2017, Metropolitan Police, 2017a). This does not count the numerous National Health Service staff members who have and continue to help survivors, including doctors, nurses and psychologists (Gregory, 2017, Metropolitan Police, 2017a).

Around the world, similar large-scale tragedies have occurred with similar impacts: the World Trade Centers' destruction in the United States; the 'disappeared' in Argentina; the genocide in Cambodia; the tsunamis in Indonesia. Smaller-scale tragedies and accidents happen around the world on a more frequent basis, without the global recognition but with the same impact on the friends, families and communities connected to these events.

Sometimes people prefer to move on directly from tragedies, not needing the particular type of closure that comes from seeing a set of remains or knowing without a doubt that their loved ones are dead. They already have what they need. But others do not.

With each of these types of situations, numerous forensic practitioners including police officers, firefighters, emergency workers, forensic scientists, forensic medicine practitioners, nurses, forensic pathologists and forensic anthropologists step forward to help. They step forward to provide aid, assistance, expertise, dignity, and hopefully justice.

This dissertation explores just one small aspect of that process, examining how forensic anthropologists and the creation of new individualisation techniques can potentially improve the identification process of commingled remains. In turn, these processes may help minimise the pain felt by friends, families and communities when human remains have lost their name, identity, and connections.

Aims and Objectives

The aims of this dissertation are to explore:

1) The potential of digital three-dimensional modelling for creating new methods for sorting commingled remains, specifically regarding pair-matching.
2) The potential of Iterative Closest Point (ICP) algorithms for creating new methods for sorting commingled remains, specifically regarding pair-matching.
3) The accuracy of these new potential methods as compared to current techniques.
4) The feasibility of these new potential methods as compared to current techniques.

In order to achieve these aims, the objectives of this dissertation are:

1) Compile a sample of four sets of different bone types (humeri, clavicles, temporals and clavicles) numbered at 100 bones per set, of known pair-matched bones.
2) Create digital three-dimensional models of all four sets of bones.
3) Test the four sets of known pair-matched bones with the two novel Mesh-to-mesh Value Comparison (MVC) methods, one manual and the other automatic, both of which use three-dimensional modelling and ICP algorithms for determining similarity and therefore pair-matching.
4) Report the accuracy of results of the MVC methods.
5) Interpret the results of the MVC methods, comparing their accuracy and feasibility to those of known individualisation techniques.

Literature Review

Forensic Anthropology

Purpose

Forensic anthropology is the study of the human skeleton for identification purposes. More specifically, the word forensic connotes the intersection of law and medicine. Thus, forensic anthropology focuses on situations which have legal importance, not just situations which may involve the human skeleton. In terms of identification, forensic anthropologists are generally tasked with the creation of a biological profile; in other words, the estimation of sex, age, stature, and ancestry. Forensic anthropologists can also assess the presence of certain types of pathology and trauma. The biological profile and any other resulting information regarding trauma or pathology are then used to help identify who that person was in life. The establishment of a positive identification, or matching a set of remains to a known individual, has rigorous standards that may vary slightly jurisdiction to jurisdiction, but are set at an intentionally high bar. They consist of three different types of identification: primary, secondary and accessory (College of Policing, 2018, Interpol, 2019). Primary identifiers include DNA, ridgeology (fingerprints, palm and footprints), and odontology (College of Policing, 2018, Interpol, 2019). Secondary identifiers include aspects like unique medical identifiers, scars, and tattoos (College of Policing, 2018, Interpol, 2019). Accessory, or assistance, identifiers consist of visual identification, jewellery, clothing and aspects such as location (College of Policing, 2018, Interpol, 2019). For positive identification, most jurisdictions require at least one primary identifier or at least two secondary identifiers (College of Policing, 2018, Interpol, 2019, Crown Office and Procurator Fiscal Service, 2019). Most forensic anthropological methods produce only secondary and accessory identifiers, though forensic anthropologists can aid in aspects like radiological comparison of dental records for odontological primary identifiers (Scientific Working Group for Forensic Anthropology, 2010, College of Policing, 2018, Interpol, 2019). Still, the main area of study of forensic anthropology continues to be connected directly to the identification of bone itself, which will be explored in more detail below.

Bone

Bone is a hard biological tissue made up of hydroxyapatite (an inorganic material) and collagen (an organic material) (White and Folkens, 2005). Cell-wise, the three main types of bone-related cells are osteoblasts, osteoclasts and osteocytes (White and Folkens, 2005, Manolagas, 2000). Osteoblasts are responsible for the creation of new bone tissue, while osteoclasts are responsible for the breakdown of bone tissue (White and Folkens, 2005, Manolagas, 2000). Thus, given they function normally, they maintain a balanced relationship where bone is a stabilised tissue (White and Folkens, 2005, Manolagas, 2000). However, this also means that activity has an impact on bone tissue growth (i.e. osteoblasts outperforming osteoclasts) and that imbalances between the two cell types have an impact on bone tissue growth (osteoclasts outperforming osteoblasts for example produces osteopenia/osteoporosis) (Manolagas, 2000, Haapasalo et al., 1998). Osteocytes are osteoblasts that have become trapped in the organic matrix of bone (otherwise known as the osteoid) (White and Folkens, 2005). In general terms, bone can be divided into two types, cancellous (trabecular/spongy) and cortical (compact) (White and Folkens, 2005). Cancellous bone is characterised by an open, less dense structure (White and Folkens, 2005). Cortical (compact) bone, on the other hand, is characterised by its compact, dense structure (White and Folkens, 2005). As these bone types serve different structural and biomechanical purposes, bones throughout the body are made up of different combinations of trabecular and compact bone (White and Folkens, 2005). For example, calcanei are mostly trabecular bone, with only a thin layer of compact bone. Femora, on the other hand, have a significant amount of compact bone, especially in the midshaft, and trabecular bone focused in the distal and proximal ends, plus the marrow cavity.

Commingled Remains

One of the main tasks of a forensic anthropologist is the creation of a biological profile, which is only possible when dealing with a single set of remains. However, forensic anthropologists often encounter situations where there are more than one set of remains mixed together, or commingled. In these situations, a forensic anthropologist must first separate or individualise the remains before a biological profile can be created. Despite early literature ignoring commingled

situations almost entirely, they occur relatively often (Ubelaker, 2008, Ubelaker, 2002). They can occur on as small a scale as a car crash, or as large a scale as mass disasters such as plane crashes, shipwrecks or wars. Due to the uniqueness of these types of situations, there is no 'cookbook approach' to commingled situations, only best practice (Ubelaker, 2008, Ubelaker, 2002). Best practice means selecting the best useable methods for the situation, with the highest accuracy possible. Additionally, it means preparing before an event takes place, to have good possible avenues from which to choose. This is important because there are also different goals for identification as well as different problems that will arise, depending on the situation.

For example, a main category of disaster victim identification situations is whether the situation is 'open' or 'closed' (College of Policing, 2019). An open situation is one where the remains could be anyone; there is no bounding list of possible people. This could include situations like a public transport disaster. While there are possible ways to narrow down who could be on a bus, for example, there is not an easily accessible and exhaustive list of people on that bus at the given time it crashed. Closed situations, on the other hand, are situations where there is a finite set of people who the remains could be. For example, with a plane crash there is a bounded list of possible people – the passenger manifest. There are not generally any other possible people on the plane besides the people listed on the passenger manifest. Thus, the identification becomes more of a matching process; one knows the people who are deceased, and only needs to match the sets of remains to the known individuals.

In terms of identification, there are also different goals for different situations. For example, in some commingled literature which deals mostly with animal remains or archaeological material, the main purpose of individualisation is the estimation of the minimum number of individuals (MNI) (Adams and Konigsberg, 2004). This process, which calculates the number of individuals recovered from an assemblage, can be calculated in three ways (Adams and Konigsberg, 2004). The first is to take the maximum number of left and right elements (Adams and Konigsberg, 2004). The second adds the left and right elements and divides the number by two, to account for pairs (Adams and

Konigsberg, 2004). The third method is similar to the second, in that it adds the number of the left and right elements, but instead subtracts the number of pairs (Adams and Konigsberg, 2004). In this way, the third method recognises that though the paired elements may be equal in number, they are not necessarily paired in the sense that they are from the same individual. The MNI is also different than the *most likely* number of individuals (MLNI), which is an estimate of the number of individuals from the *original* assemblage (Adams and Konigsberg, 2004). The MLNI is calculated using the same features, but in a different manner, where the equation is: $\left\lfloor \frac{(L+1)(R+1)}{P+1} - 1 \right\rfloor$ (Adams and Konigsberg, 2004). The type of brackets in this equation connote that the equation is rounded to the nearest integer, as it is not possible to have a partial pair (Adams and Konigsberg, 2004).

For most forensic commingled situations, the goal is not just MNI or MNLI estimation, though this calculation can be important as an initial estimate of individuals, and useful in situations such as cremated or burnt remains where other, more robust identification methods are not possible. Instead, the main goal of the forensic process is full identification of a set of remains, reuniting a person's name and identity with their physical remains. To start this process, two main questions must be asked regarding the potential human remains (Ubelaker, 2008):

1) Are the remains human or non-human?
2) Are the remains ancient or modern?

If the first question's answer is non-human, then the process does not continue as it likely has no forensic relevance (Ubelaker, 2008). If the first question's answer is human, then the second question must be answered. For the second question, if the answer is ancient then the process does not continue as there is no forensic relevance for ancient remains. However, ancient remains may produce useful information for other disciplines such as osteoarchaeology (Ubelaker, 2008). If the second question's answer is modern, then the anthropologist moves forward with the individualisation or sorting process, using a range of techniques explored below. The legal definition of modern varies in different jurisdictions but ranges from the past 50 to 100 years. The bulk of the methods (articulation, taphonomic comparison, visual pair-matching, osteometric sorting and the process of elimination) were originally described by Charles Snow after World War II, and have since been recently codified by Adams

and Byrd (Snow, 1948, Adams and Byrd, 2006). Other methods such as DNA, geometric morphometrics and some of the more esoteric methods like neutron activation come from more diverse sources and will also be examined in detail.

Current techniques

Articulation

Articulation uses the joint or juncture of bony elements to associate elements of an individual (Adams and Byrd, 2006). As the skeleton is made up of different types of articulation or bony junctures, there are therefore different reliabilities when it comes to articulating different skeletal elements (Adams and Byrd, 2006). Articulations where bone directly meets bone, for example the sacrum and innominates, have a high measure of reliability (Adams and Byrd, 2006). The humerus and the scapula, however, are not closely associated in terms of bony-joint connections and thus are not as reliable for articulation association (Adams and Byrd, 2006). Though Snow mentions articulation, Adams and Byrd formally codified the accuracy (confidence) rates of articulation into high, medium and low categories as seen in **Table 1** below (Adams and Byrd, 2006). They note that articulations which fall under the 'Low' category "cannot serve as evidence of a good match, but do have some potential for excluding very poor fits" (Adams and Byrd, 2006). In this manner, they also acknowledge that articulation is a qualitative and perhaps subjective method.

Table 1.

High	Moderate	Low
Cranium, mandible	Cranium, atlas	Ribs, thoracic vertebrae
Vertebrae	Tibia, fibula	Manubrium, clavicle
5th Lumbar vertebra, sacrum	Femur, tibia	Humerus, scapula
Humerus, ulna	Innominate, femur	
Innominate, sacrum	Patella, femur	
Tibia, talus	Scaphoid, radius	
Ulna, radius	Carpals[2]	
Metatarsals[1]	Carpals, metacarpals	
Metacarpals[1]		
Tarsals		
Tarsals, metatarsals		

After Adams and Byrd: [1]The 1st metacarpal and 1st metatarsal do not articulate closely with the others and are to be regarded as ''low'' confidence so far as their articulation with the others is concerned. [2]The articular surface of the pisiform is too small to articulate with confidence. (2006)

Taphonomic Comparison

Taphonomic comparison uses patterns of taphonomy to associate bony elements (Adams and Byrd, 2006). Taphonomy includes anything that can affect the appearance/condition of a bony surface, which usually results from differential types of preservation. This differential preservation can result in associations between bony surfaces through unique colour, textures and patterns. For instance, Adams and Byrd give the example of a rust stain on bony elements from a zipper, creating an association between otherwise non-associable elements (Adams and Byrd, 2006). They also give the example of associating elements taphonomically using trauma (Adams and Byrd, 2006); in that in a helicopter crash, they could associate a pattern of fractures in a humerus, ulna and radius, even though the elements were too fractured to articulate (Adams and Byrd, 2006). Though there have been various systems to codify the effects of taphonomy, it generally remains a qualitative and subjective method (Vietti, 2016, Moore and Norman, 2009, Blau, 2017).

Visual Pair-matching

Visual pair-matching is the association of paired, homologous skeletal elements using visual identification (Adams and Byrd, 2006, Adams and Konigsberg,

2004). Essentially, this is a qualitative method where the practitioner visually examines two bones (one left, one right) for similarity of features, looking at factors such as robusticity, overall shape, size, pathology, and non-metric traits (Adams and Byrd, 2006). This often also includes taphonomic comparison, but in a limited pair-matching context (Adams and Byrd, 2006). It is also important to note that while visual matching of other, un-paired elements has been tested, it is not recommended due to its unreliability with some exceptions (Adams and Byrd, 2006). One such possible exception would be in a small-scale situation, where there are only two individuals of markedly different sizes. Though this method is frequently suggested as a viable approach, there are only two studies to date on its use: one by Adams and Konigsberg, the other by Garrido-Varas (Adams and Konigsberg, 2004, Garrido-Varas et al., 2015). Adam and Konigsberg tested visual pair-matching for humeri, femora and tibia, while Garrido-Varas tested the method on pair-matching metacarpals (Adams and Konigsberg, 2004, Garrido-Varas et al., 2015).

Osteometric Sorting

Osteometric sorting is the association of bony elements, paired or not, using quantitative measurements and statistical tests (Byrd, 2008, Byrd and Adams, 2003, Adams and Byrd, 2006, Thomas et al., 2013, Lynch, 2018). This involves taking predetermined, repeatable measurements on bones, and then comparing them to the measurements from a known reference sample using statistical methods (Adams and Byrd, 2006). This reference sample should ideally cover a wide variety of biological variation, so as to accurately capture the full range of relational size and shape possibilities (Byrd and Adams, 2003). Though osteometric comparison can be used for pair-matching, it is generally used to associate non-paired elements, such as linking a humerus to a femur (Adams and Byrd, 2006). It is important to note that most osteometric comparison relies on the null hypothesis "that two bone specimens are of sizes consistent with having originated from the same individual" (Byrd and Adams, 2003). In this manner, most methods operate on the principle of exclusion. Two bones are expected to match, unless otherwise excluded. Adams and Byrd clearly visualise this principle in their graph from their paper 'Resolution of small-

scale commingled: A case report from the Vietnam War' as seen below in **Figure 1** (Adams and Byrd, 2006).

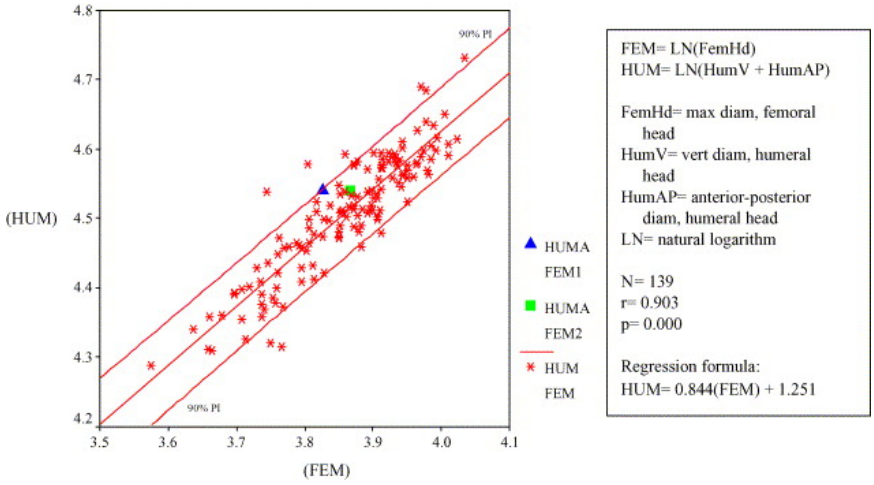

Figure 1 - From Adams and Byrd. Regression formula and table demonstrating the 90% confidence interval for determining whether two bones are excluded from coming from a single individual or not. More specifically, this graphic shows that the humerus tested is more closely associated with Individual 1 (FEM1) than Individual 2 (FEM2) (Adams and Byrd, 2006). The p-value (0.000) indicates that the regression is statistically significant.

There are different statistical methods for osteometric sorting of commingled remains, but generally it is a category of segregation involving quantitative measurements and associations (Byrd and Adams, 2003, Adams and Byrd, 2006, Thomas et al., 2013). The two main categories of statistical analysis include regression formulae, as also seen in **Figure 1**, and 'M' statistic tables, where 'M' is defined as $M = \frac{|L-R|}{\left(\frac{L+R}{2}\right)}$, with L and R representing the left and right paired elements (Byrd, 2008, Byrd and Adams, 2003, Adams and Byrd, 2006, Thomas et al., 2013). Regression formulae are more often used for the association of non-paired elements, and the 'M' statistic tables for paired elements (Byrd, 2008, Byrd and Adams, 2003, Adams and Byrd, 2006, Thomas et al., 2013).

Process of Elimination

The process of elimination, in terms of sorting commingled remains, is as simple as it sounds. It is a principle that relies on logical assumptions to exclude associations (Adams and Byrd, 2006). For example, if there are two crania, where one has an associated mandible and the other does not, it is most likely that a second

mandible found does not belong to the cranium with the associated mandible. Instead, it is most logical to associate the single mandible with the single cranium. Process of elimination is generally used in smaller scale commingled situations, as the deduction process is less reliable with a greater number of variables (Adams and Byrd, 2006).

DNA

There are many different types of DNA analyses in forensic science, but for forensic applications regarding commingled remains two main types are used: mitochondrial DNA analysis and nuclear genomic DNA analysis (Royal Society, 2017). Mitochondrial DNA analysis examines small, circular pieces of genomic material which are passed down via maternal inheritance (more specifically 16,569 base pairs in length) (Chial and Craig, 2008). Mitochondrial DNA tends to be used to show familial relationships and can be used for identification purposes in commingled situations, though more than one individual can have the same mitochondrial DNA (Garrido-Varas and Intriago Leiva, 2012, Chial and Craig, 2008).

For nuclear genomic DNA analysis, there are several options, especially given that the human genome is approximately 3.3 billion base pairs in length (Royal Society, 2017). The most common method uses patterns of Short Tandem Repeats (STRs) on non-coding regions of the genome to create unique DNA profiles for individuals. STRs are small, repeating portions of DNA that vary individual to individual, normally somewhere between one and six base pairs in length with an average of three to five (Royal Society, 2017). Thus, at certain genomic loci, one individual could have five copies of a STR (e.g. ATTATTATTATTATT) while another individual would only have one copy (ATT). Most STR methods use a minimum of 13 different loci, to create a unique DNA 'fingerprint,' though this varies jurisdiction to jurisdiction (Royal Society, 2017, Parliamentary Office of Science and Technology, 2006, Federal Bureau of Investigation, 2019). This is possible as the loci chosen for analysis are independently assorted, meaning one locus changing does not impact or co-vary with any other loci selected (Royal Society, 2017). In this manner, the minimum of 13 loci creates a high statistical

probability that a certain STR profile is unique to a single individual, usually at a magnitude of 1 in 10^9 (Royal Society, 2017).

Other possible genomic analyses include polymerase chain reactions (PCR) using Random Fragment Length Polymorphisms (RFLPs), and PCR using Single Nucleotide Polymorphism (SNPs). These methods take small amounts of DNA (measured in microliters, µl) and use polymerase enzymes to fragment and replicate specific portions of the nuclear genome. For example, RFLPs are different-sized portions of genomic DNA that when run using gel electrophoresis create unique bands at specific base pair sizes. This unique pattern of a collection of different sized fragments can be used for identification. In fact, it has been used as one of the gold standard methods of species identification (Lucchi et al., 2013). SNPs, on the other hand, are only mutations of a single nucleotide (U.S. National Library of Medicine, 2019). Thus, instead of different sized fragment lengths, SNPs examine different locations where a single base pair may have changed (U.S. National Library of Medicine, 2019); for example, one individual in a specific locus, base pair location, may have the base pair A, while another individual will have T.

Regardless of the nuclear genomic method used, it is worth noting that identical twins can potentially have identical genomic profiles, and thus other individualisation techniques would need to be used for positive identification (Bruder et al., 2008, Fraga et al., 2005). Crucially, DNA matching or individualisation relies on there being a sample for comparison; meaning, if a missing person does not have a DNA profile on file, there will need to be one collected. Occasionally this means using familial DNA as a reference, or collecting a sample from a person's home, such as hair from their hairbrush. It is critical, however, to ensure that samples are not cross-contaminated, else a proper comparison cannot be made.

The United Kingdom (UK) currently uses STR analysis and examines 17 different loci, 16 general loci plus one for sex (Royal Society, 2017, Home Office, 2019, Home Office, 2018). This maintains the statistical requirement of there being a one in 10^9 (one in one billion) chance that the same DNA profile is found in more than one individual (Home Office, 2018). Previously, the UK used a kit called SGM Plus®, which only utilised 10 loci plus an indicator for sex (Royal Society, 2017, Parliamentary Office of Science and Technology, 2006). Though Scotland and

Northern Ireland maintain their own DNA databases, the information is pooled in the UK's National DNA Database for reference.

Geometric Morphometrics

Geometric morphometrics is the analysis of shape data using the comparison (and transformation) of landmark data (measurement points). Though the technique is common when it comes to sex estimation studies and the analysis of ancestry, it has only rarely been used as a tool for sorting commingled remains (Garrido-Varas et al., 2015, Stull et al., 2014, Slice and Ross, 2009). The only study to date involves the pair-matching of metacarpals, though the method could theoretically be applied to other types of bone providing there were validation studies conducted (Garrido-Varas et al., 2015). As the method relies on the placing of landmarks on precise bony biological areas, it is key that the practitioner is familiar with the exact location of these areas, and reliably and consistently places the landmarks on the proper location.

Other techniques

Beyond the methods described by Snow and the newer methods of DNA and geometric morphometrics, there are several less frequently used techniques. These methods include neutron activation, comparison of bone densities, comparison of bone weights, serological testing (in a lot of ways, proto-DNA), ultraviolet fluorescence, and trace element analysis (Baker and Newman, 1957, Ubelaker, 2008, Eyman, 1965, McKern, 1958, Fulton et al., 1986, Gonzalez-Rodriguez and Fowler, 2013). These methods either have been shown to be ineffective (such as bone weight comparison) or have been replaced by newer methods (such as neutron activation) so will not be explored further.

Problems with current techniques

Commingled situations require planning combined with best practice (Ubelaker, 2008). Therefore to understand which methods are considered best practice and most applicable to a specific situation, the potential problems or downsides of a method must be examined. These problems or downsides can roughly

be grouped into four different categories: asymmetry, accuracy, UK admissibility/error rates, and cost. Each will be explored more fully below.

Asymmetry

For any method involving the examination or proportional measurement of paired elements, one of the main confounding factors is asymmetry. Humans are naturally asymmetrical, but the degree to which people are asymmetrical varies. The levels of asymmetry in the human body have been extensively studied, covering a wide range of bones (Tos and Stangerup, 1985, Steele and Mays, 1995, Ragab et al., 2003, Ćuk et al., 2001, Auerbach and Ruff, 2006, Abdel Fatah et al., 2012, Auerbach and Raxter, 2008). The majority of studies have focused on limbs, specifically looking at variation in humeri, femora and tibiae (Steele and Mays, 1995, Sládek et al., 2007, Ćuk et al., 2001, Auerbach and Ruff, 2006). This focus reflects the examination of bipedalism, and how it has evolved in modern humans (Sládek et al., 2007, Ćuk et al., 2001, Auerbach and Ruff, 2006). Other disciplines such as surgery have focused on asymmetry in terms of how to best repair pathological elements, using a homologous non-pathological element as the template (Ragab et al., 2003, Tomura et al., 1995, Loh et al., 2015, Hingsammer et al., 2015).

In terms of individualisation techniques, asymmetry is an issue for visual pair-matching, osteometric sorting, and geometric morphometric methods. For visual pair-matching, the process generally tries to circumvent problems of asymmetry qualitatively, by leaving the issue of how asymmetrical is asymmetrical up to the practitioner using the method (Adams and Byrd, 2006, Adams and Konigsberg, 2004). While this is sensible in some ways, as there is no absolute cut-off for what is asymmetrical or symmetrical and allows the practitioner to favour other aspects of bone similarity such as overall shape for pair-matching, it also means that this can vary practitioner to practitioner, an aspect which will be explored more later in the chapter.

Osteometric sorting, on the other hand, relies on a numeric value for asymmetry. This is true both in terms of regression formulae and 'M' statistic tables, though the calculation of that numeric value is slightly different for each. Still, what is 'asymmetrical' and what is 'symmetrical' for both are determined by what

reference population is used for either the calculation of regression formulae or 'M' statistic tables. This population asymmetry specificity has already been shown to be an issue, with other authors reporting that Byrd and Adam's osteometric sorting regression formulae allows too many false rejections (Vickers et al., 2015). In this sense, there are two different possibilities based on whether the rejections came from pair-matching elements or associating different elements. Either the population tested was less 'asymmetrical' than the original population used to calculate the regression formulae, or there are body proportional differences between the new population tested and the original population used to calculate the regression formulae. Byrd and Adams do highlight the necessity of a thorough reference sample in terms of population to counter this, but no sample can be fully exhaustive (Byrd, 2008, Byrd and Adams, 2003, Adams and Byrd, 2006).

Similarly for the one geometric morphometric method tested, there are the same population issues surrounding asymmetry. Though there has yet to be a validation study of the method using a different population for comparison, geometric morphometrics depends on unique shape differences between individuals, which may vary population to population.

Furthermore for both osteometric sorting and geometric morphometric methods, the measurements for (a)symmetry are only calculated in one or two dimensions, despite bones being three-dimensional objects. Byrd and Adams note this as an issue in a circular manner, in that for their method for osteometric sorting using regression formulae they do "not claim to sort individuals of the same size" (Byrd and Adams, 2003). Given the large portions of any population that are of similar sizes, this seems like a major oversight. Similarly, for geometric morphometrics, which prioritises shape over size, Byrd and Adams interestingly found that *size*, not shape, accounted for the majority of variation when assessed by Principal Component Analysis (Byrd and Adams, 2003). Thus, though geometric morphometrics attempts to account for (a)symmetry differences in shape alone, this may come with its own issues (Garrido-Varas et al., 2015).

Accuracy

With any individualisation method, accuracy is paramount. Without the assurance that remains have been individualised correctly, there is no way to accurately create a biological profile. Still, having any individualisation method, even if it is lower in accuracy, is essential if it is the only possible method. Thus, knowledge of any method's accuracy is essential. Of all the methods previously discussed, DNA is the most accurate, with the statistical probability of one in 10^9 generally backing the results. This statistical probability lessens when there are only partial DNA matches, due to either low recovery of DNA from a scene, or lack of a complete comparison sample. Again, however, DNA is only the most accurate method available provided there is a reference sample for comparison. With no comparative sample, it is not possible to make an identification.

Visual pair-matching and taphonomic comparison vary in accuracy fairly considerably, as both are heavily influenced by the practitioner. Though the study by Adams and Konigsberg showed high accuracy rates, correctly identifying the majority of bones regardless of type, both were highly experienced practitioners (Adams, for example, has worked at the Defense POW/MIA Accounting Agency specialising in sorting commingled remains, while Konigsberg is a longstanding Professor of human and faunal remains, used to dealing with large commingled situations of faunal remains) and this may not be indicative of general practitioners' accuracy rates. In the study by Garrido-Varas, for example, the accuracy of visual pair-matching was significantly reduced, with one practitioner identifying 82.9% of the pairs of metacarpals correctly and the other only 75.6% (Garrido-Varas et al., 2015). This was despite both practitioners being "trained physical anthropologists with broad experience in osteology" (Garrido-Varas et al., 2015). Thus, visual pair-matching may further vary beyond just the practitioner to the type of bone being matched.

For taphonomy, though some patterns of degradation are easily understood between practitioners, such as weathering patterns and faunal damage, other taphonomic changes can be harder to agree upon. Colour, for example, is notoriously difficult for multiple practitioners to agree upon (Pollock et al., 2018, Devlin et al., 2008). Where one person sees brown, another sees red. As long as the patterns of

associations remain the same, regardless of the colour named, this is generally fine. However, the complication comes when two practitioners disagree on patterns of association, based on that colour. Thus, this is one of the many ways taphonomic comparison's accuracy is highly variable. Byrd and Adams caution this in their article, though they still recommend the use of the method (Adams and Byrd, 2006).

For articulation, accuracy is only classed in terms of the general confidence categories of high, medium and low (Adams and Byrd, 2006). While this is understandable in a certain manner, as the existence of soft tissue provides a confounding factor for the accuracy of articulating two bones, this system is also rather vague. How high is high exactly? Are there different levels of 'high' accuracy within the category? Byrd and Adams even explain that the low confidence category does not indicate an actual connection between two bones, but rather should only be used for exclusionary purposes (Adams and Byrd, 2006).

Similarly, as the process of elimination is basically just deductive logic, there is no accuracy rate available.

The geometric morphometric method produces interesting accuracy issues. While it was highly accurate at matching metacarpals where their homologous pair was present, it has no way for indicating whether there is a single bone without a homologous match present (Garrido-Varas et al., 2015). In other words, as a method it is not capable of detecting negatives, or non-pair-matches. This is a significant issue, as in commingled situations there is often not perfect recovery of bony elements. Furthermore, as the method is based on the correct placements of landmarks on specific biological points, there is the possibility of introducing error by the practitioner when placing these points. If the points are not placed correctly, the shape comparison will not be conducted properly, producing skewed results.

UK Admissibility and Error Rates

While accuracy is inherently important for selecting the best individualisation technique, it is also essential to select methods which meet the specific jurisdiction's admissibility criteria. After all, if a method produces a high accuracy rate, but it is not admissible in a specific legal situation, it is still an ineffective method. In this

sense, knowing the criteria for admissibility of evidence is essential, and as it will be demonstrated, this often hinges on a method's accuracy and error rates.

In the context of the United Kingdom, the legal system is split between three different jurisdictions: England and Wales; Scotland; and Northern Ireland. While the extent of the differences between these three systems is beyond the scope of this project, it is important to keep this in mind when assessing the processes related to potential commingled situations in their respective jurisdictions. For example, England and Wales operate with a coroner-based system, while Scotland utilises a system with a procurator fiscal. Therefore, the person calling for an autopsy or assessment of skeletal remains may vary. Still, though there are different specific rules and regulations regarding admissibility of expert witness testimony and therefore evidence, for example the Criminal Practice Directions: Amendment 2 ([2014] EWCA Crim 1569) in England and Wales, and Dickson on Evidence, Third Edition, paragraph 398 in Scotland, they are both concerned with the reliability and accuracy of methods accepted in legal situations (Crown Office and Procurator Fiscal Service, n.d.). In Scotland, acceptable expert witness evidence "must be part of a recognised body of science or experience which is suitably acknowledged as being useful and reliable" (Crown Office and Procurator Fiscal Service, n.d.). For England and Wales, the court may take into account "if the expert's opinion relies on the results of the use of any method (for instance, a test, measurement or survey), whether the opinion takes proper account of matters, such as the degree of precision or margin of uncertainty, affecting the accuracy or reliability of those results" ([2014] EWCA Crim 1569, V Evidence 33A.5-6). Both systems acknowledge the relevance of peer-review in assessing these methods and levels of accuracy ([2014] EWCA Crim 1569, Crown Office and Procurator Fiscal Service, n.d.).

Therefore, reconsidering the accuracy rates of the current individualisation techniques with UK admissibility in mind, several conclusions can be made. Methods with known, acceptable error rates that are reliable in nature, such as DNA analysis, osteometric sorting, and geometric morphometric methods, would easily be acceptable. However, methods such as visual pair-matching, taphonomic comparison, and the process of elimination are likely to be excluded as they do not have acceptable, known error rates and are not necessarily easily reproducible.

Cost

In balancing the accuracy and admissibility of an individualisation technique, the third factor requiring consideration is cost. DNA, for example, while it is starting to decrease in cost, is still relatively expensive. This cost is quickly multiplied when considering both that samples are generally run in triplicate and that any fragmentation of bone must be tested separately. Though STR profiling of DNA has decreased in cost from approximately £100 per sample to only £15-17 per sample, with a triplicate cost of approximately £50, this adds up quickly when testing approximately 206 bones per person (ThermoFisher Scientific, 2019b, Promega, 2019a, ThermoFisher Scientific, 2019c, Qiagen, 2019, Home Office, 2019) [Calculations in **Appendix A**]. This easily adds up to £10,000 per person, possibly doubling or tripling that amount if there is fragmentation. Thus, a commingled situation's cost for DNA analysis can sky-rocket the more people who are involved in the situation. This of course assumes that DNA sampling is possible from a given bone sample with a 100% extraction success rate. Small bones or bone fragments may not be big enough to produce a usable amount of DNA, while DNA itself can be degraded or fully destroyed in bones that have been exposed to extreme conditions, such as being heavily burnt or left in water for long periods of time, or exposed to substances such as indigo dye (Butler, 2010). These costing estimates, furthermore, are based only on the cost of the reagents involved in DNA (specifically STR) analysis and does not take into account the cost of labour.

For articulation, visual pair-matching and taphonomic comparison, the cost of the methods is much lower, and only depends on the cost of the employment of the practitioner, as they do not require any specialised equipment or tools. For osteometric sorting there is a slight increase in cost, in that tools for accurate measurements and often statistical software packages are necessary to purchase, but again the cost is more or less restricted to the employment of the practitioner. Similarly for geometric morphometrics, there is a slight increase in cost for the specialised software and measurement tools required for the method, but generally it is fairly affordable.

New Technology and Digital Innovation

As these individualisation techniques have been developed, new hardware and software have been developed alongside them. There have, of course, been significant general technological changes, such as the fact that Charles Snow did not have the benefit of any type of computer or access to any automated statistical software. The changes which have the greatest potential to improve individualisation methods, however, are hardware and software changes related to imaging technology. The relevant hardware and software advances in imaging technology will be discussed below, examining the history of their creation and their potential relevance to the individualisation of commingled remains. The majority remain underutilised in the sorting of commingled remains, which this study aims selectively to address.

Hardware

This section will explore four different imaging technologies: x-rays, computed tomography scanners, three-dimensional structured/white light scanners, and laser scanners. Finally, it will also explore three-dimensional printing, though it is not strictly an imaging technique, and the relative cost of this hardware.

X-rays and Radiographs

The first relevant imaging technique hardware-wise is undoubtedly the x-ray, discovered in 1895 by Wilhelm Conrad Röntgen, which paved the way for future imaging techniques (Röntgen, 1896). The initial imaging technique from x-rays, the radiograph, was produced on glass plates. This changed in 1918 when George Eastman invented radiographic film (Thomas, n.d.-b). Diagnostic radiographs were first produced in the 1920's, and though the x-ray technology went through rigorous safety improvements from the 1920's onwards, the next major advance was the advent of the digital radiograph in the early 1980's (Thomas, n.d.-a).

It is apt that the first radiograph Röntgen produced was of his wife's hand, successfully imaging the living skeleton in situ for the first time (**Figure 2**). Radiographs have frequently been used in medical situations and by extension forensic anthropological applications since their invention. Sir Arthur Schuster in

1896, for example, identified a bullet in an individual's brain, less than a year after Röntgen first discovered x-rays (Wellcome Collection, 2019). Similarly, Brogden has reported that radiographs were used for a murder case conviction in Montreal in 1895 (Brogdon, 1998).

The use of radiographs to sort commingled remains has focused on areas of positive identification more than actual methods of individualisation. The majority of methods have been based on ante- and postmortem comparison of skeletal elements or features; this predominately includes dentition and sinuses, but also the skull generally, the chest, clavicles, the spine, the abdomen/pelvis, hands, lower limbs, the hyoid and trabecular bone patterns (Andersen and Wenzel, 1995, Rhine and Sperry, 1991, Sperry et al., 1992, Hogge et al., 1995, Kuehn et al., 2002, Adams and Maves, 2002, Valenzuela, 1997, Owsley and Mann, 1992, Koot et al., 2005, Owsley and Mann, 1989, Zviagin et al., 2005, Kahana and Hiss, 1994). Other studies have included identification of heavily decomposed, burned, and fragmented remains, identification from surgical implants and pathologies, and identification using facial superimposition (Sudimack et al., 2002, Owsley et al., 1993, Owsley, 1993, Kondo et al., 1995, Osipenkova and Mikhailova, 1996, Chai et al., 1989). However, methods specifically for individualisation have ranged from the use of radiographic atlases in the field for identification of juvenile remains, to positively identifying bone fragments and dentition (Warren et al., 2000, Kahana et al., 1997, Brkic et al., 2000).

It is worth noting that while the radiation dosage for radiographs is low, and if used on material post-mortem does not have a destructive impact, it must be used cautiously on living subjects (Friess, 2012, European Agency for Safety and Health at Work, 2019). The European Union, for example, has strict regulations regarding exposure to radiation unless strictly medically necessary (European Agency for Safety and Health at Work, 2019).

Figure 2. The bones of a hand with a ring on one finger, viewed through x-ray. Photoprint from radiograph by W.K. Röntgen, 1895. Credit: Wellcome Collection. CC-BY. (The first x-ray).

CT scanning

Computed tomography (CT) imaging, which took the x-ray based radiograph into three-dimensions, was developed by Godfrey Hounsfield in 1971 (Hounsfield, 1973). Though there has been variation over time in terms of how computed tomography scanners work, the essential principle is that radiation is used to detect

and represent different densities of materials, just like radiographs. The main difference between radiographs and CT scans, however, is that CT scans are essentially a collection of radiographs in sequence, taken at specific measurement intervals in order to achieve three-dimensional imaging (Hounsfield, 1973). In tribute to Hounsfield, the units used to measure radiodensity in computed tomography were named Hounsfield units, and serve as a unified measure across types of CT scanners (Zurl et al., 2014). These different density values or Hounsfield units are represented by grey-scale colour values ranging from true black (the least radiodense substance possible, usually air) to true white (the most radiodense substances, such as cortical bone), and will be explored further in the software section (Zurl et al., 2014).

The first generation scanner depended on an object being scanned in a container of water to both limit the dynamic range of the materials present to easily optimise the detectors and to correct for beam-hardening effects (Goldman, 2007). This was quickly followed by second-generation scanners in 1974, which allowed for waterless scanning and significantly sped up the scan time (Goldman, 2007). Third generation scanners appeared in late 1975, again marking a change in detector technology that drastically decreased scan time (Goldman, 2007). Fourth-generation scanners were introduced in 1976 and marked yet another reduction in scan time (Goldman, 2007). By this point, clinical use of computed tomography (CT) imaging was already taking place and CT research specifically relating to musculoskeletal elements on a relatively large scale started to be published (Wilson et al., 1978). CT technology remained relatively stable until 1987 with the advent of slip ring scanners, which attempted to eliminate interscan delays (Goldman, 2007). However, this technology was quickly surpassed by helical or spiral CT scanning methods in the early 1990's which have since remained the standard (Goldman, 2007).

In terms of the relevance to individualisation techniques, CT methods have included identifying and unifying skeletal elements from unidentifiable soft tissue body masses, positive identification via paranasal sinuses and surgical apparatuses, identification of personal effects, and biological profiling of skeletal elements in situ (O'Donnell et al., 2011, Blau et al., 2008, Ruder et al., 2012). As mentioned previously, the huge advantage of CT scans over radiographs is that the imaging technology allows for three-dimensional imaging and reconstruction of three-

dimensional bones, not just two-dimensional images. This also allows for the possibility of new measurements, such as in situ tissue thicknesses or cortical bone thicknesses, without sample destruction. Furthermore, for bone specifically, CT scans allow for measurements of different aspects of bones that may not be possible using traditional means (physical callipers) which will be explored more in the software section later in the chapter.

Finally, as mentioned previously with radiographs, CT scans do produce radiation and at a larger amount than a single radiograph (European Agency for Safety and Health at Work, 2019). Thus, while if used on material post-mortem it does not have a destructive impact, it must be used cautiously on living subjects.

3D Structured/White Light Scanning

While CT scanning evolved from radiographic techniques, three-dimensional scanning involving the use of structured/white light evolved from photography and the field of photogrammetry, or the stitching of photographic images into three-dimensional images. Though photography has been around since the early 1800's, photogrammetry only appeared in the 1950's (Friess, 2012). Three-dimensional structured/white light scanning emerged shortly after in the 1960's, though it was not until the common usage of computers that it started to become wider-spread, in part due to the computational nature of the process (Friess, 2012, Breuckmann, 2014). These three-dimensional structured/white light scanners initially were used in industrial applications for documenting wear of machining parts, but eventually spread to other disciplines and uses (Breuckmann, 2014, Friess, 2012). There are two main types of structured/white light scanners which will be explored below: *triangulation* based systems and *time-of-flight* based systems (Friess, 2012). Both types use a source of visible light (non-ionizing radiation) and some sort of detector to register the light once it has been reflected off the object being scanned, though they differ in how this process is conducted (Friess, 2012).

Triangulation systems use a source of visible light plus two or more cameras, in order to triangulate the object data, by recording the patterns of light projected on and then reflected from the object being scanned at two or more points (Friess, 2012). To create an accurate scan, the triangulation-based system must therefore be

calibrated to a known scale to which the recorded data can then be referenced. To capture data, the pattern of light shone at an object is a series of fixed-width beams (Friess, 2012); the deformation of these fixed-width patterns and therefore what light makes it back to the recording cameras is what creates the shape of the object (Friess, 2012). The data are initially recorded as point cloud data, then interpolated into point cloud meshes (Friess, 2012). These types of systems are often used to scan medium to small scale areas (Friess, 2012).

Time-of-flight systems also use a source of visible light but only require one detector instead of two or more, though multiple detectors can be used and the detector type does not have to be a camera (Friess, 2012). *Time-of-flight* systems only need one detector as they calculate the amount of time it takes for light to be reflected back from an object after leaving the light source in order to create the point cloud data, subsequent mesh and full model (Friess, 2012). These types of systems are also known as range finders and are more commonly used for scanning large areas (Friess, 2012).

For both types of systems, it is important to note that, unlike the ionizing radiation in CT scans and radiographs, normal white light cannot penetrate objects; thus, to create a complete three-dimensional object, these partial scans must be stitched together to create whole models (Friess, 2012). This aspect will be explored further later in the work, as it is a key aspect of the project, but it also why three-dimensional structured/white light scanners are also called surface scanners. They can only capture the surface data present, not the internal data (Friess, 2012). It is also worth noting that unlike radiographs and CT scanning, white (visible) light is non-ionizing and therefore can be used without restrictions for any subject type, living or deceased (Friess, 2012). Finally, unlike CT scans, three-dimensional structured/white light scanners can record and use texture/surface data (Friess, 2012, Breuckmann, 2014). This means that a model can be recreated three-dimensionally with the full-colour representation of how an object appears in life.

In terms of the relevance to sorting commingled remains, three-dimensional structure/white light scanners have been used in anthropology and archaeological contexts for scanning bone, but there have been no specific studies examining its use for individuation (Friess, 2012).

Laser Scanning

Laser scanning works on the same principle as three-dimensional structured/white light scanners, but uses a different type of light source (Friess, 2012). Laser, in fact, stands for **l**ight **a**mplification by **s**timulated **e**mission of **r**adiation (Hobarts, 2019). Lasers differ from visible light sources in that they have spatial coherence and sometimes temporal coherence, meaning that they can maintain a narrow beam width over large distances and that they can be focused on a narrow spectrum of light (Hobarts, 2019, Wikipedia, 2019). Though lasers vary in their visibility, most of the ones used for laser scanning fall within the visible spectrum (Hobarts, 2019). Again, laser scanners work in the same manner as structured/white light scanners, in that they can use *triangulation* or *time-of-flight* for model creation (Friess, 2012).

In terms of the relevance to sorting commingled remains, laser scanners also have been used in anthropology and archaeological contexts for scanning bone, but there have been no specific studies examining its use for individuation (Friess, 2012).

Three-dimensional printing

With the advent of three-dimensional scanning and imaging, new ways of using the resulting data started to emerge. One such new use was three-dimensional printing, which was originally invented in the early 1980's (Goldberg, 2018). Though generally an additive process, where material is added in very thin layers to create an object, currently there are different types of three-dimensional printing types which vary from using fused plastic materials to using a vat of liquid and resin curing (Goldberg, 2018). The important manner in which this process happens program-wise will be discussed more in the software section. Though there are numerous applications for three-dimensional printing related to anthropology, there has not yet been any specific research done on the possible applications regarding the sorting of commingled remains.

Cost

With each of these imaging methods, it is important to understand their costs, though prices are often hard to find as an individual consumer and vary country to

country. X-ray machines vary in cost between analogue and digital machines, as well as between stationary and portable versions. Generally, the digital and portable machines are more expensive. Estimated costs for a portable analogue machine range from approximately $40,000 to $80,000 USD (£30,600 to £62,100 GBP) with approximately $2,500 to $10,000 USD (£1,900 to £7,600 GBP) in upkeep costs, while a digital portable machine's cost range from $125,000 to $235,000 USD (£96,000 to £180,300 GBP) with approximately $11,000 to $29,000 USD (£8,500 to £23,300 GBP) in upkeep costs (Webb, 2019). Computed tomography scanners also vary considerably in cost, ranging from $55,000 to $350,00 USD (£42,000 to £268,000 GBP)(2019c). Three-dimensional structured/white light scanners range in cost from £160 to £50,000, while laser scanners range in cost from £20,000 to £100,000 (Lansard, 2019, 3D Natives, 2019). Three-dimensional printers also range in price considerably from £200 for home level models to £100,000 for industrial level models, not taking into account maintenance costs (3D Insider, 2018).

Software

Software solutions could have an equally large impact on new methods for sorting commingled remains. Three software program categories related to three-dimensional visualisation will be explored: three-dimensional imaging software for CT scans, three-dimensional imaging software for structured/white light scanning, and three-dimensional printing software. Finally, expanding beyond visualisation, the use of algorithms will be explored as well.

Computed Tomography Software

There are many programs that can visualise and manipulate CT scan data, including software packages built-in to the machines themselves and programs such as OsiriX, 3D Slicer, Mimics and AMIRA (2019f, 2019a, Materialise, 2019, ThermoFisher Scientific, 2019a). These programs are multifunctional and generally exceed working only with CT scan data, but this section will focus solely on CT scan data. Specifically, this section will explore two of the key features of all of these software programs which have potential use for individuation techniques: segmentation of CT scan data and three-dimensional measurements.

Segmentation background

Segmentation is the process of creating a three-dimensional mesh or model from CT scan data. In order to understand how the process works, especially as it could correspond to individualisation of bone, one has to return to examining the CT scan data itself.

Again, CT scan data is comprised of a range of grey values, measured in Hounsfield units, which in turn represent the different densities of the object(s) being scanned (Hounsfield, 1973). True black represents the least radiodense (or most radiolucent) substance present, usually air, and true white represents the most radiodense substance present, in this case generally bone, with intermediate other densities corresponding to the grey values in between (Hounsfield, 1973). In terms of Hounsfield units, these colour designations correspond to values generally ranging from -1000 (black/air) to +3000 (white/cortical bone). Taking into account the computed aspect of CT scan data, this density information and therefore grey value information is represented initially in pixels (Hounsfield, 1973). Pixels are two-dimensional square 'picture elements' which can be easily viewed in **Figure 3**. As they are squares, unsurprisingly this means that approximating a curved surface can be somewhat challenging. For an example of a curved surface represented by square pixels, also see **Figure 3**.

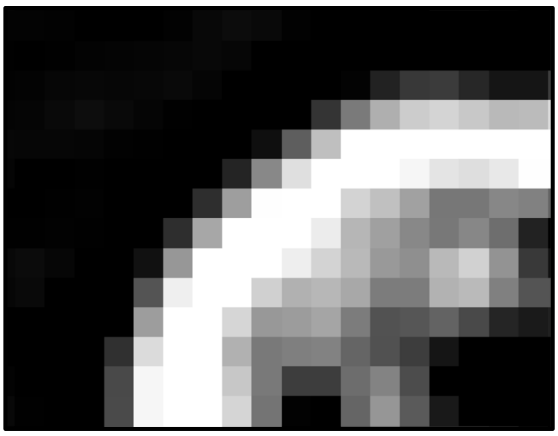

Figure 3. Example of pixels as found in CT scans taken from curved clavicle data

With the grey values of Hounsfield units of the data combined with the pixels of the computed aspect of the data, these two factors mean that to build a model of ('to segment') an object with curves, such as a bone, there needs to be a method of

accurately approximating the best grey value, or threshold value, which can determine the edge/colour boundary for that curve. For example, in **Figure 3**, there are three distinct bands of colour values that create the curved area: white, medium grey and a darker grey. Which is actually the edge of the bone? There are two possible answers for generating the key threshold value for segmentation. Spoor and colleagues' research answered this question with an example of averages – the Half Maximum Height Value – for thresholding (Spoor et al., 1993). The Half Maximum Height Value (HMHV) calculates the average maximum (most dense) grey value for an object, and then uses half that value for selection of the material to represent the true line of the object. The second answer is the alternative method for the edge selection of bone for segmentation called the histogram method, which examines the histogram or distribution data of the grey values to inform a visual threshold point (Frabris-Rotelli and Greeff, 2012, Karell et al., 2016).

Regardless of the thresholding method chosen, it is an essential step for segmentation and turning CT scan data into useable three-dimensional digital models, which have the possibility of being used for sorting commingled remains.

Three-dimensional measurements

Once a three-dimensional model is built via segmentation, one of the unique features of computed tomography software program is the ability to take measurements on these digital models that are either not possible or not advisable on real bone. Several examples include the ability to measure cortical bone thickness without any destruction of the bone, to easily measure angles on models directly, to easily measure features which are too small for callipers to reach, and to take volumetric measurements.

Three-dimensional Structured/White Light Scanning Software

Like CT scan software, there are many programs that can generate, visualise and manipulate point cloud and mesh/model data from three-dimensional structure/white light scanners, such as Cloud Compare, MeshLab, and Flexscan3D (2019b, 2019e, 2019d). Again, the normal visible light used by the scanners for detection of objects cannot penetrate the object, therefore requiring multiple scans of

a single object to be stitched together in order to create a full three-dimensional representation (Friess, 2012). While the software calculations involved with the creation of these partial scans is impressive, both for *triangulation* and *time-of-flight* systems, what is most impressive is the process by which this software aligns these partial scans. To accurately recreate an object from these partial scans requires exacting precision from the alignment process, else it is not a true, accurate representation of the object. The main innovation of these types of software is not just the generation, visualisation and manipulation of the point cloud and mesh data, but the algorithms written to perform this alignment process which will be explored further in the algorithm section, as they have potential uses for individualisation.

Three-dimensional Printing Software

Similarly to all the previously mentioned software types, there are a multitude of three-dimensional printing software including TinkerCad, Repetier, Netfabb (Autodesk, 2019b, Repetier, 2019, Autodesk, 2019a). Though three-dimensional printing software often covers similar aspects of mesh/model visualisation and manipulation as structured/white light scanner software, they were created for a different purpose and therefore have some tools other programs lack. Beyond the algorithmic slicing process of a model, which allows for a model to be properly three-dimensionally printed, they also have tools that easily hollow and repair models, making the models more useable for other applications. In this manner, they are another potential tool for individualisation techniques using newer technologies.

Algorithms

Within software programs, there are numerous processes coded into the program in order for it to perform various tasks. These processes generally follow mathematical and logical predefined sequences, which mutate or change as new information is input into the system. There are many types of these processes, but one of the most common is called algorithms: an idealized description of a process in the form of a set of instructions. Though there are numerous types of algorithms built into all the previously mentioned software, the category of algorithms that has the

most potential for sorting commingled remains are Iterative Closest Point (ICP) algorithms.

Iterative Closest Point Algorithms – Background

Iterative Closest Point algorithms were originally created as a method for helping solve a free-form surface matching problem in computer vision (Besl and McKay, 1992, Besl, 1988). Computer vision as a field of study is concerned with how computers 'see,' in or other words, how they process and interpret visual data (British Machine Vision Association and Society for Pattern Recognition, 2019). The initial problem of this free-form surface matching, as Besl and McKay define it is:

> "Given 3D data in a sensor coordinate system, which describes a data shape that may correspond to a model shape, and given a model shape in a model coordinate system in a different geometric shape representation, estimate the optimal rotation and translation that aligns, or registers, the model shape and the data shape minimizing the distance between the shapes and thereby allow determination of the equivalence of the shapes via mean-square distance metric" (1992, p. 239)

Though this appears complex, what this means is that they are looking for the best way to match two shapes in order to determine the similarity of the two shapes.

In reconsidering three-dimensional structured/white light scanning and how the software must merge partial scans in order to create a full, accurate three-dimensional model, the problem of how to best align and merge these partial scans has been solved by ICP algorithms. Though partial scan merging is not a computer vision problem, in that it does not directly help a computer 'see,' it fits the three-dimensional scanning issue perfectly. In fact, ICP algorithms have been used for a plethora of circumstances, including self-driving cars, inspection of wear of industrial parts, and facial recognition (Zhang, 1994, Boukebbab et al., 2007, Mohammadzade and Hatzinakos, 2013).

Though Besl and McKay created the first ICP algorithm, it is not the only such algorithm that has been created since; in fact, the variants of ICP are extensive (Mohammadzade and Hatzinakos, 2013, Du et al., 2010, Kaneko et al., 2003, Kapoutsis et al., 1999). Thus, a selection of different variations of ICP will be explored below. These variations differ in how they calculate distance between

models, what assumptions they use for the two models being compared, and how the algorithms process information. Four main variations will be explored in-depth in addition to the original ICP algorithm, followed by a summary of a number of other variations.

Types of Iterative Closest Point Algorithms

The Original Iterative Closest Point Algorithm

Though the mathematics behind the original ICP algorithm can seem daunting, it is easier to understand when viewed as an operational procedure. For the operational procedure, Peng and colleagues provide a concise definition, which is as follows (Besl and McKay, 1992, Peng et al., 2002):

> "Given point set *P* and surface *Q* where *P* is a subset of *Q:*
> 1) Nearest point search: For each point *p* in *P* find the closest point *q* on *Q*.
> 2) Compute registration: Evaluate the rigid transformation T that minimizes the sum of squared distances between pairs of closest points (*p*, *q*).
> 3) Transform: Apply the rigid transformation T to all points in set *P*.
> 4) Iterative: Repeat step 1 to 3 until convergence" (p. 449-450)

Key aspects of the original ICP algorithm, beyond the assumption that one model or point set must be the subset of the other, are that it is a quaternion-based algorithm, that it uses a least square registration for calculating minimum distances, and that it will converge to a local, not global, minimum (Besl and McKay, 1992). Quaternions are a specific type of number system, which allows for the extension of complex numbers. Converging to a local versus global minimum means that it is more important for points on a small (local) scale to match/align with the minimal amount of distance between points than it is for the whole (global) points sets to match/align overall (Besl and McKay, 1992, Du et al., 2010). Regarding the local minimum issue, Besl and McKay add that because of this aspect their ICP algorithm is not useful when models only barely overlap and include large amounts of other data that does not correspond (Besl and McKay, 1992). In other words, the original ICP does not handle outlying points well. This aspect is common to a majority of shape matching algorithms, which also converge to local minima (Besl and McKay, 1992,

Zhang, 1994). There is no way to communicate to the algorithm a preference for local *and* global alignment in these situations (Besl and McKay, 1992, Zhang, 1994). Finally, in terms of rigid transformations, more rotation states are preferred over more translational states (Besl and McKay, 1992).

The Range Image Registration Algorithm

In their article on object modelling, Chen and Medioni describe their Range Image Registration algorithm (Chen and Medioni, 1992). Geared towards early surface scanning, the algorithm differs from the original ICP in several key ways (Chen and Medioni, 1992). First, instead of aligning point-to-point for data sets and therefore requiring point-to-point correspondence, they use surface normals (rays tangent to the surface) to align data sets (Chen and Medioni, 1992) (**Figure 4**). The algorithm is still iterative and uses a least squares error measurement for alignment, but instead of point-to-point correspondence, it uses point-to-plane correspondence (Chen and Medioni, 1992). Second, the algorithm requires the placement of control points for the initial alignment process (Chen and Medioni, 1992). Third, the algorithm assumes that the two data sets/models are pre-aligned/pre-registered (Chen and Medioni, 1992). Finally, this method is not as susceptible to the issue of local minima as the original ICP algorithm (Lu et al., 2004).

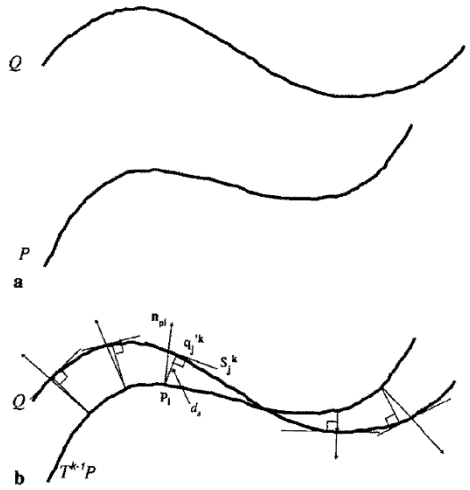

Figure 4. After Chen and Medioni. Example of matching to sets, *P* and *Q* using normals. (Chen and Medioni 1992).

The Iterative Pseudo Point Matching Algorithm

The Iterative Pseudo Point Matching algorithm as described by Zhang was developed to register (align) free-form curves and surfaces for autonomous cars (Zhang, 1994). Recognising that curve data is prone to noise (outliers), it essentially uses a mixture of the previous two methods. It uses surface normals for aiding in registration, but unlike the Range Image Registration algorithm, it limits their involvement to a specific degree range, thereby limiting the computational cost (Zhang, 1994). It still uses the point-to-point correspondence of the original ICP algorithm, but will the addition of partial normals, it become *pseudo* point matching (Zhang, 1994). Similarly to both previously mentioned algorithms, the algorithm converges to a local minimum and uses least-squares estimation (Zhang, 1994).

The Trimmed Iterative Closest Point Algorithm

The Trimmed Iterative Closest Point (TrICP) algorithm is an ICP variant that aims to increase the robusticity of the original algorithm (Chetverikov et al., 2005, Chetverikov et al., 2002). Instead of basing the distance measurement on least squares estimation, TrICP uses least trimmed squares (LTS) estimation (Chetverikov et al., 2005, Chetverikov et al., 2002). This effectively increases the algorithm's robusticity in handling outliers and means that it only needs a 50% overlap between the two data sets/models, unlike the original ICP's need for 100% overlap (Chetverikov et al., 2005, Chetverikov et al., 2002). Like the Iterative Pseudo Point Matching algorithm, TrICP requires pre-registration or alignment. TrICP differs as well in the descriptors of the type of outliers it can handle (Chetverikov et al., 2005). When describing the difference between least median of squares (LMedS) and LTS, Chetverikov and colleagues highlight that "The median is efficient in discarding strongly deviating outliers. However, the deterministic outliers are not necessarily strong outliers: the spectrum of residuals is often continuous" (Chetverikov et al., 2005). To expand upon this point, there are two different types of outliers, "1) the correctly measured points that have no pair in the other part and 2) the incorrectly measured points," and that there are different possibilities for handling these outlier types (Chetverikov et al., 2005).

Hybrid Iterative Closest Point Algorithm

For their paper on facial recognition, Lu and colleagues merged the algorithms of Besl and McKay and Chen and Medioni to create a 'hybrid' ICP (Lu et al., 2004). They first use the point-to-point feature of the original ICP for the initial distance calculation and then use the point-to-plane feature of the Range Image Registration algorithm to refine the alignment (Lu et al., 2004). They state that the use of both aspects produces a better alignment or registration result overall (Lu et al., 2004).

Other ICP variations

There are numerous other variations of ICP, all with slightly different goals. A major category in variants is the reduction of computational time it takes to run the algorithms and variations. The Morphological ICP algorithm uses Voronoi tessellation to serve as an alignment template in order to reduce computational time, while Kaneko and colleague integrate M-estimation into their variant of ICP to reduce computational time (Kapoutsis et al., 1999, Kaneko et al., 2003). Other variants seek to fix issues such as what happens when point correspondence and transformation are unknown, like the Affine ICP algorithm, or when there are objects that need to be matched even when they change shape (such as accounting for different facial expressions in facial recognition), like the Iterative Closest Normal Point algorithm (Du et al., 2010, Mohammadzade and Hatzinakos, 2013).

Other Distance-Based Algorithms

Finally, there are two other distance-based algorithms that are not ICP, but are important to mention in this context. The first is Active Contour Models, otherwise known as snakes, and their variant Active Shape Models (ASMs) (Cootes et al., 1995). What is interesting about these ASMs, is that they use training sets to shape the algorithms to be able to recognise the same object, but with a limited amount of variations (Cootes et al., 1995). One of the main examples the researchers give, for instance, is the automatic selection of heart valves. As living heart valves are constantly in motion, capturing images of them at different points in time create slightly different shapes for recognition (Cootes et al., 1995). By training a program

on a specific type of variation, the program is able to flexibly identify the correct variations present instead of any random outliers or other variations (Cootes et al., 1995). Also relevant are Hausdorff distances, which Zhao and colleagues describe as "a non-linear operator, which measures the mismatch of two sets," which "is not based on finding corresponding mode and image points" (Zhao et al., 2005). Hausdorff distance algorithms have similar issues to ICP algorithms in terms of dealing with outliers/noise, but there are numerous versions that have been applied to increase the algorithm's robusticity (Zhao et al., 2005, Vivek and Sudha, 2007, Huttenlocher et al., 1993).

Materials and Methods

Materials

Bone Types and Their Rationale

While not a universal classification system, anatomical complexity of bones in the skeleton can be loosely represented by five categories of bone (long, short, flat, irregular and sesamoid), which indicate features such as shape, function and the proportion of cortical bone versus trabecular bone (Wilson, 1840, Hamill, 2003).

For this study, four bones of varying anatomical complexity and bone category were chosen to test the mesh-to-mesh value comparison (MVC) method: humeri, clavicles, calcanei, and temporal bones.

Humeri are grouped in the long bone category, which describes bones that are longer than they are wide, have a dense cortical bone midshaft that often houses bone marrow production, have epiphyses with a high ratio of trabecular bone to cortical bone, and bear stress best along their long axis (Hamill, 2003). In addition to being used as a representative population for all other long bones, humeri were also chosen as they made up the original sample used for the pilot study, and therefore still required validation using a larger sample size (Karell et al., 2016). Furthermore, high levels of asymmetry have been previously documented in humeri (Auerbach and Ruff, 2006, Ćuk et al., 2001, Sládek et al., 2007, Steele and Mays, 1995).

Clavicles are also grouped in the long bone category though they lack a marrow cavity, unlike all other long bones (Hamill, 2003, Kulkarni, 2012). Clavicles were chosen not only for this distinctive anatomical difference in terms of structure and function, but also because of their unique bilateral asymmetry patterns which may impact pair-matching. Unlike other bones which tend to have asymmetry exclusively focused on one side, right clavicles tend to be more robust while left clavicles tend to be longer overall though the statistical significance varies (Abdel Fatah et al., 2012, Auerbach and Raxter, 2008, Bernat et al., 2014). The originating causes of this pattern are still being investigated, though it does appear to have some relationship to biomechanical movement, such as antagonistic muscle relationships and handedness (Loh et al., 2015, Abdel Fatah et al., 2012, Bernat et al., 2014). Though the overwhelming pattern of asymmetry has been documented as the right side being more robust and the left being longer, at least one set of researchers has

found the opposite pattern when looking exclusively at left-handed individuals though it was a very small sample size (Loh et al., 2015).

Calcanei are grouped in the short bone category, which describes bones that generally have a high ratio of trabecular bone to a layer of thin cortical bone and tend to play an important role in shock absorption (Hamill, 2003). Calcanei were chosen both for their different category type and to assess whether the shock absorption characteristics of a high ratio of trabecular bone to a thin layer of cortical bone would impact the pair-matching process. Furthermore, there is currently very little literature on the asymmetry patterns of calcanei though the articles span a significant time period. Of the few articles published, they tend to explore clinical aspects of the bone, and therefore have focused on features such as the presence of distinct or fused anterior and middle facets, and variation in locations of ligaments and tendons (Ragab et al., 2003, Laidlaw, 1905, Kumar et al., 1991, Linklater et al., 2009). Regardless, these articles still document a high amount of variation among calcanei, citing up to six different types and patterns of facets and fused facets, as well as approximately 10% asymmetry in these recorded features (Ragab et al., 2003). Given the variety and asymmetry of just the anterior and middle facets, it is likely other aspects of the bone are also variable and asymmetric to varying degrees.

Temporal bones are grouped in the irregular bone category, which tends to be a catch-all category describing bones that consist of a high ratio of trabecular bone to a thin layer of cortical bone but serve specialised functions (Hamill, 2003). In this case, the function of temporal bones includes housing the organ of Corti which controls balance and hearing, and protecting and supporting the brain. In terms of variation, temporal bones are surprisingly diverse. Most of the variation is accounted for in vascular anomalies but can also be seen in sutures and the other small canals present in the bone (Tomura et al., 1995, Koesling et al., 2005). In terms of asymmetry, the majority of these variations tend to be bilateral with the noted exception of the jugular foramen (Tomura et al., 1995, Koesling et al., 2005). In fact, Koesling and colleagues found jugular *symmetry* in only a quarter of their sample of 223 patients (446 temporal bones), with symmetry defined as jugular foramina that were within a left-right difference of 5 mm or less (Koesling et al., 2005). Tomura

and colleagues found similar results, with only 8% of their sample of 325 patients (650 temporal bones) (Tomura et al., 1995).

Sample Number

For each bone, the target sample size was 50 pairs (100 individual bones). This set the target total sample population at 200 pairs (400 individual bones).

Populations

All of the bones, regardless of type, were selected from five different populations across a relatively wide geographic and temporal span. Though the pilot study of the MVC method indicated that a wide geographic and temporal span of the samples should not affect the outcome of pair-matching each bone, geographic and temporal diversity were chosen in order to validate this finding (Karell et al., 2016). This diversity also allowed for a variety of other pilot testing conditions, including whether these aforementioned conditions would affect the pair-matching process in case the assertion in the pilot study proved untrue. The five populations are as follows:

Scottish, archaeological: The archaeological Scottish population consisted of bones from two different medieval sites: the Ballumbie Parish Church, located just outside of Dundee, and the Parish Church of the Holy Trinity, located in St. Andrews. The Ballumbie site was active in the late 15th century while the St. Andrews site, approximately 17 miles away, was active from the 15th to the early 17th century (Hall and Cachart, 2005, Rathmell Archaeology Ltd, 2003, Rees, 2003, Rees et al., 2008, Historic Environment Scotland, n.d.). For this study, the two sites are considered contemporaneous and geographically close enough to be grouped as one population. Though both sites were rescue excavations from the early 2000s, burials mostly consisted of single internments with articulated skeletons and therefore allowed for reliable known pairs to be chosen (Hall and Cachart, 2005, Rathmell Archaeology Ltd, 2003, Rees, 2003, Rees et al., 2008, Historic Environment Scotland, n.d.). However, there is only minimal information about the age-at-death and sex demographics (Girdwood and Karell, 2019, Garcia-Donas and Karell, 2019).

Both collections are housed at the University of Edinburgh. Bones sourced from this collection included humeri and calcanei.

Spanish, archaeological: The archaeological Spanish population consisted of bones from one site that was continuously active from the 13th to 18th century, the Ibizan Cathedral, in the Old Town of Ibiza (Guerra and Martín, 1999). Skeletal remains from this site were initially recovered in 1992, but were not analysed until 2013 due to the initial architectural focus of the excavation (Guerra and Martín, 1999). A combination of techniques including visual pair-matching, osteometric comparison, association by proximity, taphonomic analysis and the initial test of the MVC method insured that there were reliable known pairs. There is no known information on age-at-death and sex demographics of this collection, which is currently housed at the Archaeological Museum of Ibiza. The few bones sourced from this collection included humeri.

Italian, modern: The modern Italian population consisted of bones from the Frassetto Collection (Collezione Frassetto), which is comprised of 606 donated bodies that originate from Sassai (Sardinia) and whose deaths all date to the first decade of the 21st century (Karell et al., 2016, Facchini et al., 2006). As this collection is donated, known pairs are guaranteed, as they were documented upon donation (Karell et al., 2016, Facchini et al., 2006). Similarly, there is age-at-death and sex demographic information for the remains (Karell et al., 2016, Facchini et al., 2006). This collection is currently housed at the Anthropology Museum at the University of Bologna (Facchini et al., 2006). Bones sourced from this collection included humeri, all of which were male and adults.

Cypriot, modern: The modern Cypriot population consisted of bones from the Limassol Municipal ossuary, located inside the St. Nicholas cemetery in the city of Limassol, Cyprus (Kranioti et al., 2017). Death dates ranged from 1972 to 2003. As the ossuary contained individual skeletons in each box, the known pairs were guaranteed. In the same manner, there is age-at-death and sex demographic information for the remains. Ages-at-death ranged from six to 100, with this study only utilising adults with the age range of 20-100. Of the adults, the mean age of the population was 70 years old. Bones sourced from this collection included humeri and calcanei.

Greek, modern: The modern Greek population consisted of bones from the Cretan Collection, which is comprised of donated and reclaimed bodies. Death dates ranged from 1963 to 2004. The majority of the collection has age-at-death and sex demographics present, as well as medical records which note any injuries or illness. The population was mainly comprised of older individuals with a mean age-at-death of 70 years old, though the ages ranged from 19 to 101. The collection was balanced demographically in regard to sex, with almost equal males and females. As this is a donated collection, known pairs are guaranteed. This collection is housed at the Hellenic Republic Ministry of Justice and Human Rights, in Heraklion. Bones sourced from this collection included clavicles, calcanei and temporal bones.

For a breakdown of the number of bones used from each population, see **Table 2.**

For a breakdown of the number of bones separated by sex and population, see **Table 3.**

Ethics Approval

The use of all population data, whether in physical or digital form (i.e. scan data), was approved by the School of History, Classics and Archaeology at the University of Edinburgh in accordance with their guidelines regarding the ethical treatment of human remains. This included sourcing approval from all the relevant bodies connected to the remains, such as the Human Tissue Authority.

Table 2. Bones sourced from each population, separated by type.

Bone	**Scotland (Arch.)**	**Spain (Arch.)**	**Italy (Mod.)**	**Greece (Mod.)**	**Cyprus (Mod.)**	**Total* (891)**
Humeri	13 pairs (26 bones)	6 pairs + 3 singles (15 bones)	10 pairs (20 bones)		72 pairs (144 bones)	101 pairs + 3 singles (205 bones)
Clavicles				92 pairs + 5 singles (189 bones)		92 pairs + 5 singles (189 bones)
Calcanei	27 pairs + 8 singles (62 bones)			31 pairs + 26 singles (88 bones)	43 pairs + 1 single (87 bones)	101 pairs + 35 singles (237 bones)
Temporals				130 pairs (260 bones)		130 pairs (260 bones)

*Though an initially the target sample was 50 pairs (100 individual bones) per type, spread out across these five aforementioned populations, data collection resulted in almost double the number of bones expected, which will be explained further in the section.

Table 3. Bones sourced from each population, separated by type and sex*

Bone	Scotland (Arch.)	Spain (Arch.)	Italy (Mod.)	Greece (Mod.)	Cyprus (Mod.)	Total (891)
Humeri	M = 0 F = 4 U = 22	M = 0 F = 0 U = 15	M = 20 F = 0 U = 0		M = 66 F = 76 U = 2	M = 86 F = 80 U = 39
Clavicles				M = 107 F = 82 U = 0		M = 107 F = 82 U = 0
Calcanei	M = 13 F = 11 U = 28			M = 34 F = 44 U = 10	M = 35 F = 48 U = 4	M = 75 F = 99 U = 18
Temporals				M = 72 F = 56 U = 2		M = 72 F = 56 U = 2

* M = Male, F = Female, U = Unknown

Methods

Data Collection

Data collection consisted of seven distinct phases: three-dimensional scanning, model creation, hollowing, normals, mirror-imaging, decimation and pair-matching.

Three-dimensional Scanning, Types and Locations:

For the initial data acquisition, two different types of three-dimensional scanning were used: computed tomography (CT) scanning and three-dimensional (3D) structured light surface scanning. Though the target number of acquisition for number of bones was 400, data collection during the three-dimensional scanning phase produced scans for a total number of 891 bones, over double the target amount. The bulk of the sample, 552 bones, were CT scanned while roughly forty per cent of the sample, 339 bones, were 3D structured light surface scanned. The scanning method chosen for each population and bone type varied, and depended on a multitude of factors including availability of the collection, availability of scanning type, time, and potential for miniature pilot studies. For a breakdown of which bone types were CT and 3D surface scanned, see **Table 4.**

Table 4. Bones CT scanned versus 3D surface scanned by type

Bone	**CT Scanned**	**3D Surface Scanned**
Humeri	19 pairs + 3 singles (41 bones)	82 pairs (164 bones)
Clavicles	92 pairs + 5 singles (189 bones)	-
Calcanei	26 pairs + 8 singles (62 bones)	74 pairs + 27 singles (175 bones)
Temporals	130 pairs (260 bones)	-
Totals	552 bones	339 bones

For each population, the three-dimensional scan data were collected as follows:

Scottish, archaeological: All the bones from the Scottish archaeological population, including humeri and calcanei, were CT scanned in Edinburgh. The humeri were scanned at the Clinical Research Imaging Centre, the University of Edinburgh, with a Toshiba Aquilion ONE 320 Detector Row Computed Tomography multidetector scanner (Karell et al., 2016). The calcanei were scanned at the Royal Infirmary of Edinburgh with a Toshiba Aquilion 64 Computed Tomography multidetector scanner. Both data sets were collected using a slice thickness of 0.5 mm and a 512 x 512 matrix. Both CT scanners were properly calibrated, including x-ray tube calibration on start-up and weekly quality assurance phantom scanning to check noise, uniformity and Hounsfield units optimisation (Thomson and Karell, 2019). For a more detailed explanation of the calibration protocol, see **Appendix B**. All data were saved as Digital Imaging and Communications in Medicine (DICOM) files.

Spanish, archaeological: All the bones from the Spanish archaeological population were CT scanned at Can Misses Hospital, Ibiza (Eivissa). The humeri data were collected with a GE Medical System HiSpeed NX/I Computed Tomography multidetector scanner, using a slice thickness of 0.5 mm and a matrix of 512 x 512. This CT scanner was properly calibrated according to Can Misses Hospital protocols for quality assurance (Kranioti and Karell, 2019). Data were saved as Digital Imaging and Communications in Medicine (DICOM) files.

Italian, modern: All the bones from the modern Italian population were scanned using a 3D structured light surface scanner at the University of Bologna. The humeri data were collected using a ScanProbe Standard Structured Light Scanner, a two-camera system with 1.9 megapixels each. Data were saved as XOR (Geomagic) projects (Karell et al., 2016).

Cypriot, modern: All the bones from the modern Cypriot population were scanned using a 3D structured light surface scanner. Both the humeri and calcanei data were collected using a non-commercial two-camera surface scanner, which

utilised a Panasonic projector as the light source and two 1.3 megapixels uEye cameras (model number UI-154XLE). Data were saved as FlexScan3D projects.

Greek, modern: The modern Greek population is the only population which utilised both computed tomography and 3D surface scanning. The clavicles and temporals were scanned at the University Hospital of Iraklion (Heraklion), using a Siemens Sensation 16 Computed Tomography multidetector scanner. Both data sets were collected using a slice thickness of 0.75 mm and a 512 x 512 matrix. The CT scanner was properly calibrated according to the University Hospital of Iraklion (Heraklion)'s quality assurance protocol (Kranioti and Karell, 2019). Data were saved as Digital Imaging and Communications in Medicine (DICOM) files. The calcanei data were collected using the same non-commercial two-camera surface scanner, which utilised a Panasonic projector as the light source and two 1.3 megapixels uEye cameras (model number UI-154XLE), as the Cypriot population. Data were saved as FlexScan3D projects.

For a summary of bones CT scanned versus 3D surface scanned bones, by population, see **Table 5.**

Table 5. Bones CT scanned versus 3D surface scanned by population

Population	**CT Scanned**	**3D Surface Scanned**
Scotland (Arch.)	40 pairs + 8 singles (88 bones)	-
Spain (Arch.)	6 pairs + 3 singles (15 bones)	-
Italy (Mod.)	-	10 pairs (20 bones)
Greece (Mod.)	222 pairs + 5 singles (449 bones)	31 pairs + 26 singles (88 bones)
Cyprus (Mod.)	-	115 pairs + 1 single (231 bones)
Totals	552 bones	339 bones

Model Creation

Depending on the type of three-dimensional scanning, two different model creation protocols were followed. For CT scan data, a process called segmentation was used. For the 3D surface scanning, a process of merging multiple, incomplete meshes was used.

Segmentation (CT Scan Data)

For segmentation and model creation of CT scan data, the program AMIRA 5.3.3 was used. In AMIRA 5.3.3, segmentation is accomplished through the creation and application of a threshold value, which when applied to a scan selects the information needed from each individual slice of a scan so that it can be compiled into a single mesh, or model. Certain models were segmented initially for other projects, by other researchers. However, these models were all assessed and either corrected or excluded by the author where necessary due to model building errors or overall scan quality issues. Thus, the total initial number of segmented and built models is often slightly more than the final number for pair-matching analysis. Furthermore, it will be apparent that only a certain number of models were built from the large amount scanned due to time constraints. For the number of models built by segmentation by bone, plus notes on corrected, excluded and final number for analysis see **Table 6.**

Randomisation and Cropping

Before the threshold values were applied for the selection process in segmentation, all CT scan data were visualised using the *Isosurface* feature, cropped into individual bones when necessary using the *Bounding Box* feature, and renamed in order to randomise the sample when necessary.

Threshold Value Creation

Initially the program Image J was used to calculate the Half Maximum Height Value (HMHV), or threshold value, following Spoor et al. for all CT scan data (Spoor et al., 1993). In this program, the *Draw Line* tool was used to select the full range of grey values present and then the *Measure* feature was applied to record

the maximum and minimum values. This process was repeated every third slice throughout an entire scan. The resulting Excel spreadsheet of average maximum values was then summed and divided by two, in order to create the HMHV (Spoor et al., 1993). The HMHV was then entered as the lowest selection value in the *Display and Masking* window (**Figure 5**) in AMIRA 5.3.3 under the *Segmentation* tab which will be mentioned in greater detail further on.

As previously discussed, the HMHV does not always reflect the true line of bone due to factors such as the proportion of cortical to trabecular bone and the calibration of CT scanners' grey value ranges. Therefore, though the HMHV was calculated and applied where possible, it was not always applicable. In the situations where it was not appropriate, a histogram method for threshold value selection was used (Karell et al., 2016).

The histogram method for threshold value selection is an accurate and reproducible visual method for selecting half of the maximum grey value range present (Karell et al., 2016). It relies on two different grey value range windows AMIRA 5.3.3 displays: the *Zoom and Data* window and the previously mentioned *Display and Masking* window. In order to consistently view CT scan data in the same manner, regardless of scanner calibration, the sliding tool for viewing the CT scan information in the *Zoom and Data* window was always set in the same manner; the lowest (left-hand) slider was set to the lowest value of histogram data, while the highest (right-hand) slider was set to the highest value of the histogram data. This ensured that the lowest value present was now calibrated to true black (hypodense, the least radiodense), while the highest value was calibrated to true white (hyperdense, the most radiodense). For examples, see **Figures 5 & 6**. Additionally, this guaranteed that the next process of selection via a threshold value range, was done accurately and consistently. After the *Zoom and Data* window was calibrated, the *Display and Masking* window was then adjusted. To visually select the threshold value, the lowest (left-hand) slider was used to select the half-way point at which the histogram peak was the highest and the highest (right-hand) was set at the maximum value possible, i.e. as furthest to the right as possible.

For a breakdown of average threshold values created by the histogram method by bone, see **Table 7.**

Figure 5. *Display and Masking* Window, set for segmentation

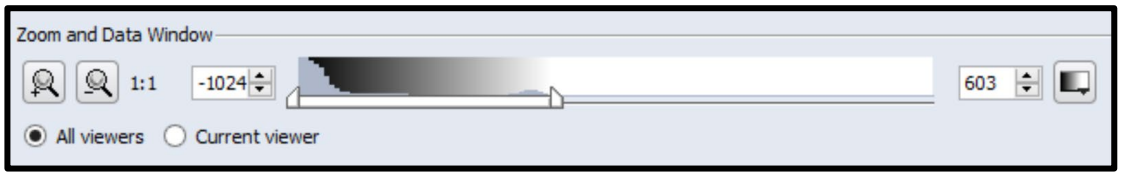

Figure 6. *Zoom and Data* Window, set for segmentation

Selection (Segmentation)

Once the threshold value had been calculated, either by the HMHV or histogram method, this value was applied to the selection process, which was completed using several different tools in AMIRA 5.3.3, and involved inspecting every slice of the now cropped and randomized CT scan (Spoor et al., 1993, Frabris-Rotelli and Greeff, 2012)

To start the process, a new set of *Labels* was created by selecting the *New* button next to the *Labels Data*. This creates an AMIRA specific file to which all the selection data will be saved, and then later used for model generations. These tools are explained further below.

The majority of the models were built using the *Magic Wand* selection tool. This tool selects contiguous pixels of the specified threshold value range, and allows for the precise selection of materials, while maximising the amount selected. It can be used in a slice by slice manner, where the user individually selects the portion of bone to add slice by slice, or the *All Slice* feature can be applied, which applies the threshold value range to the entire stack of images. The *Magic Wand* tool also has a *Draw Line Limit* feature, which allows the user to draw a line demarcating which areas not to select. This feature was especially useful when it came to cropping out the CT scanning bed, for example, which was observed to register a similar density to cortical bone. However, in the older versions of AMIRA, the *Draw Line Limit* tool could not be used with the *All Slices* setting, which meant that the majority of models were built in the slice by slice manner.

Occasionally the poorly named *Threshold* tool was used in addition to the *Magic Wand* tool. This tool, similar to the *Magic Wand*, selects all pixels which fall into the specified threshold value range. However, these pixels do not have to be contiguous. This means that it will select literally every pixel in the scan that falls within this range; for example, if there happens to be any other object present in the scan, such as a paper clip, this will be selected as well, even though it is obviously not connected to the bone. This feature was used sparingly, and generally only when the bone in question had large portions of thin, low-density trabecular bone. These portions of trabecular bone are often represented in CT scans as disconnected pixels slice by slice, and were therefore challenging to select with the *Magic Wand* tool.

Another sparingly used tool was the *Brush* tool. This tool will select any area, regardless of the threshold value range. Due to this, it was only used in the *Square* mode, at the smallest setting of one pixel, and only in instances where for some reason the *Magic Wand* tool had missed a very small area and created a false hole in the bone, such as incredibly thin parts of the squamosal area of the temporal bone. In this manner, only a couple of pixels were added at a time, and only to ensure the integrity of the model reflecting the true representation of the bone.

Finally, the *Lasso* tool was also sparingly used, and only to deselect areas. In a similar manner to the *Brush* tool, it will select any area, regardless of the threshold value range. While the *Brush* tool is a distinct size and shape, the *Lasso* tool is any size and shape as drawn freehand by the user, as long as the starting point and ending point connect. Due to this, as mentioned previously, it was only used to deselect areas, not select them, as selection it would create would be unreliable. It was useful, however, in situations such as the presence of another object such as a paper clip that could be easily deleted without affecting the selection of the bone.

After any selection was made using the aforementioned tools, the *Add Selected Voxels* button was pressed to ensure that the selection was added to the model. Once all the areas of bone were fully selected, the *Labels* information was then saved.

Table 7. Threshold values for segmentation by bone

Bone	Threshold Average	Threshold Range
Humeri	-689	-1050 to -490
Clavicles	-851	-902 to -743
Calcanei	-759	-1070 to -615
Temporals	-291	-696 to 0

Final Model Creation

After the bone selection data was saved as *Labels* data, the *Surface Gen* feature was applied to the *Labels* data in the *Object Pool* tab. The settings for the *Surface Gen* were always *Constrained Smoothing*. The model was then saved as a binary stereolithography (.stl) file with Little Endian formatting.

Table 6. Number of models built by Segmentation, by bone

Bone	Initial Number of Models Built	Number of Models Corrected	Number of Models Excluded	Final Number of Models Used
Humeri	61	0	16	45
Clavicles	203*	0	0	203*
Calcanei†	62	15	0	62
Temporals‡	130	39	6	124
Total	456	54	22	434

*As will be explained further in the chapter, certain bones were built multiple times to test intra-observer error for building by segmentation. Hence, the larger number of models built than bones scanned.
†Initially built by Kimberly Nash (Nash, 2015)
‡Initially built by Monika Lay (Lay, 2014)

Merging Meshes (3D Surface Scan Data)

For merging meshes, two different programs were used: Geomagic and FlexScan3D. Only the 20 Italian humeri were built in Geomagic, and this was done at the University of Bologna, independently of the current study by Caterina Minghetti (Karell et al., 2016). As this process was not undertaken for this dissertation, it will only be mentioned here briefly. In simplistic terms, data was acquired by the scanner in the form of point cloud information to create partial meshes, aligned appropriately, and then final meshes or models were generated from this information in Geomagic (Karell et al., 2016). For the remaining 319 surface scanned bones, the model creation was done in the program FlexScan3D and the process follows below. For the number of models built by merging by bone, plus notes on corrected, excluded and final number for analysis see **Table 8.** Similar to the segmentation process, only a certain number of models were built from the large amount scanned due to time constraints.

FlexScan3D Merging Protocol

Depending on the anatomical complexity and condition of the bone that was surface scanned, the number of the initial partial scans varied. Anywhere from 18 to upwards of 25 partial scans were manually moved and selected using the *CRTL, SHIFT* and *ALT* keys to align the partial scans for merging. For quality control, this process generally followed a consistent pattern, where one rotation around the bone was completed first, then added to using the second rotation around an object in a perpendicular reference to the first rotation to complete the object. To start the pattern, the first two partial scans were manually aligned as previously mentioned, then both selected using the *SHIFT* key and automatically aligned using the *Align* button on the setting '*Mesh Geometry*'. Once all of the partial scans had been added to create a cohesive object, all of the scans were selected and then automatically aligned for a second time using the *Align* button on the setting '*Fine Alignment*'. The *Fine Alignment* feature was set to 'Fast' for processing power and time purposes, meaning that it tested 300 iterations of alignments of the scans to accurately match partial scans. After *Fine Alignment*, the object was then checked to make sure that the computer had appropriately lined up all the partial scans. This was measured both

by a mesh-to-mesh value, a measurement in millimetres that indicates great similarity with a lower value, and visual inspection of the model. An overall *Fine Alignment* mesh-to-mesh value of under 0.05mm was considered a valid alignment. If all the partial scans lined up well, they were then all selected again using the *SHIFT* key and merged into a single object using the *Combine* button. The *Combine* button settings were generally set to just '*Apply Fine Alignment*'. After the combining process, the model was then completed by pressing the *Finalize* button, with the settings set to '*Precise Merge'*. This removed excess overlapping data where the partial scans were aligned (reducing file size) and preserved the original shape data. However, there was one set of scans where this '*Precise Merge'* was not possible. To minimise any differences in the quality between these scans, during the *Combine* process the '*Preserve Overlapping Data*' setting was used in addition to the '*Apply Fine Alignment*'. If the '*Preserve Overlapping Data*' feature was used, the *'Finalize'* settings were changed to '*Smoothed Merge'; 'Sample Density = High'; and 'Hole Filling = Low'.* Though this applies a slight smoothing to the model, the high sample density and low hole filling preserve the original shape data. The only difference in output between the two routes was the increased file size of the '*Preserve Overlapping Data*' models, as unsurprisingly, they retained the overlapping data of the partial scans; still, the overall shape for both settings was the same. Once a model was finalized, regardless of the *Combine* process, it was then exported and saved as a Wavefront (.obj) file.

Table 8. Number of models built by merging, by bone

Bone	Initial Number of Models Built	Number of Models Corrected	Number of Models Excluded	Final Number of Models Used
Humeri	7	0	7	0
Clavicles	0	0	0	0
Calcanei*	175	87†	0	175
Temporals	0	0	0	0
Total	456	54	22	434

* 87 models from Cyprus initially built by Kimberly Nash and Mary Gutekunst (Nash, 2015, Gutekunst, 2015), the other 88 were built by the author
† The only correction made to these models (from Cyprus) was to decimate them in size, as mentioned later in the chapter, due to the initial way they were built (*Preserving Overlapping Data*)

Hollowing

To test whether the best results for the MVC method were obtained from comparing all of the possible internal and external data at once or using only the external surfaces of bones, models were also hollowed. Therefore, all the models built via segmentation, i.e. those from CT scan data which still contained internal data, were hollowed using the program Viewbox 4 or Viewbox 4.1. To hollow the scans, the files were individually imported into Viewbox, then had their internal surfaces selected using the tool *Select Non-visible* or *Select by Visibility* depending on the respective version of the software. After the selection was made, it was then deleted using the feature *Delete Selection*. All the files were saved as Wavefront (.obj) files with the setting *'With Normals'*. For the average and range of hollowing percentages by bone, see **Table 9.**

Table 9. Hollowing percentages, by bone

Bone	Average	Average Left	Average Right	Range
Humeri	NP*	NP*	NP*	NP*
Clavicles	59.37%	59.19%	59.54%	13 - 73%
Calcanei	66.01%	66.09%	65.93%	44 - 77%
Temporals	33.83%	33.83%	33.83%	15 - 48%

*Originally hollowed by a collaborator, Dr. Demetrios J. Halazonetis, and thus values were not recorded (Karell et al., 2016). NP = Not Possible.

Normals

During the study, 'normals' – vectors perpendicular to three-dimensional surfaces of polygonal meshes – were discovered as a powerful option for better matching curved surfaces (see **Figure 7**). Thus, the default testing condition was models saved *'With Normals,'* though certain sets of bone also were tested without normals to investigate the full effects.

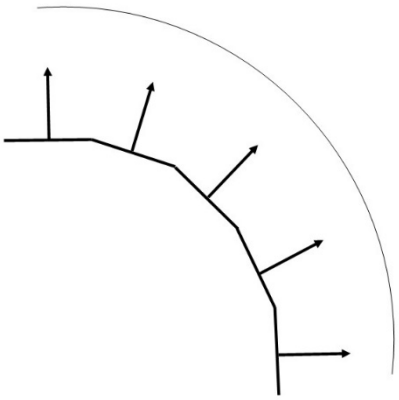

Figure 7. The squared lines represent the polygonal mesh, the arrowed rays are the normals, and the faint circular line represents the new more accurate curve produced by the normals.

Mirror Imaging

In order to pair-match two three-dimensional models of bones by placing one directly on top of the other, one of the bones must be appropriately mirror-imaged to fit properly. The right side was chosen to be mirror-imaged for all sets of bones for consistency, and this process was done using the free three-dimensional printer software program NetFabb basic (Karell et al., 2016). To mirror-image each model, it was individually loaded into the program and then the *Mirror Image* feature was applied. The files were saved as Wavefront (.obj) files.

Decimation

One set of 3D white light scans from Cyprus which were built using the '*Preserve Overlapping Data*' setting resulted in very large file sizes. All of these files were classed as 'Huge' by Windows – ranging in size from 28 to 144 MB, with 88% over 70 MB. These files were decimated by 25% using Flexscan3D and the '*Decimate*' feature. This reduced the number of triangles of the mesh, while preserving the level of detail, in order to reduce computational time.

The reduction amount (by 25%) was chosen after comparing a set of paired calcanei at 25% decimation intervals and assessing their mesh-to-mesh comparison values as compared to the undecimated versions in Flexscan3D, the same pair-matching process described below. As the reduced-by-25% versions differed from the original by only 0.002 mm, a value less than the model building error, they preserved the appropriate level of detail and were considered valid for further comparison. The other decimation amounts reduced the level of detail, differing by larger amounts, and therefore were not used.

Pair-matching – Mesh-to-Mesh Value Comparison

After all three-dimensional models were built, either through segmentation or merging, each group of the different types of bones was then compared and pair-matched using mesh-to-mesh value comparison (MVC). The MVC method compares the entire three-dimensional geometry of two models at once to indicate similarity in millimetres. Both manual and automatic versions of MVC were tested using the software programs FlexScan3D and Viewbox 4.1 respectively. Both programs

produce ‘mesh-to-mesh values’ in millimetres to indicate similarity of the two models, but differ slightly based on their algorithmic distance calculations. The details of the manual and automatic protocols and setting will be explored below.

FlexScan3D Protocol and Settings (Manual MVC)

To compare each group of bones in FlexScan3D, one left at a time was imported into the program and then subsequently manually compared to every mirror-imaged right. To compare the two bones, they were first manually aligned using the mouse and the *SHIFT* and *ALT* keys. After they were as manually aligned as possible, the two scans were selected using the *SHIFT* key and then algorithmically aligned using the *Align* button on the setting ‘*Fine Alignment*’. As mentioned previously, this *Fine Alignment* feature produced a mesh-to-mesh value which was then recorded in an Excel spreadsheet for further statistical analysis which will be explained later in this chapter. All lefts were subsequently compared to all mirror-imaged rights.

The comparison algorithms for Flexscan3D were based on trimmed iterative closest point algorithms, but generally unknown as they are proprietary (Chetverikov et al., 2002). It is known, however, that it does not use root-mean-squared for its distance calculations and that it has some prioritisation algorithms for preferentially matching flat surfaces (Langstaff and Karell, 2014).

Viewbox 4.1 Protocol and Settings (Automatic)

Unlike FlexScan3D, the comparison process in Viewbox 4.1 was automated in a feature called *Mesh Similarity*. This automated process has two main settings, both of which were used at various points. The first comparison option is *Compare reference mesh to all meshes in mesh folder,* which takes a single user-defined mesh (model) and compares it to a user-selected folder of meshes. The second comparison option is *Compare all meshes in mesh folder to each other,* which takes a user-defined folder and compares every mesh in that folder to each other. The dual use of these two options allowed for creative applications of data production versus time. Once the type of mesh analysis was selected, the other settings of the comparison were set. These included general options such as the *Estimated Overlap of Meshes*

and number of *Initial Positions for Rough Alignment*, and more specific options for rough and fine alignment such as *Nearest Neighbour Search*, *Point Sampling* percentage, *Matching Point-to-point* or *Point-to-plane*, and number of *Iterations*. For this study, two different sets of Viewbox 4.1 settings were used:

1. 'Exact Normal'

General

Estimated Overlap of Meshes: 100%

Initial Positions: 20

Options for Rough Alignment

Nearest Neighbour Search: Approximate (fast)

Point Sampling: 1%

Matching Point to: Point

Iterations: 100

Options for Fine Alignment

Nearest Neighbour Search: Exact (Normal Compatibility)

Point Sample: 100%

Matching Point to: Plane

Iterations: 100

2. 'Exact Slow'

General

Estimated Overlap of Meshes: 100%

Initial Positions: 20

Options for Rough Alignment

Nearest Neighbour Search: Approximate (fast)

Point Sampling: 1%

Matching Point to: Point

Iterations: 100

Options for Fine Alignment

Nearest Neighbour Search: Exact Slow

Point Sample: 100%

Matching Point to: Plane

Iterations: 100

All comparison data were sent to a new Excel spreadsheet, delimited by tab. This produced the same format of data as created by the manual method and allowed for the same type of statistical analysis. The primary settings used were 'Exact Normal' due to the presence of normals in most of the 3D models and were applied to all data regardless of bone type. The 'Exact Slow' settings were only used in an exploratory fashion to test the effects of normals on the matching process.

The comparison algorithm for Viewbox 4.1 was the trimmed iterative closest point algorithm, which uses the least trimmed squares approach to distance calculation (Chetverikov et al., 2002, dHal Software, Chetverikov et al., 2005). This algorithm, as described by Chetverikov et al, is summarised briefly below (2002, p. 546-547, 2005, p. 8):

1. For each point of P, find the closet point in M and compute the individual distances d_i^2 (Equation: $d_i(R,t) = \|M_{cl}(i,R,t) - p_i(R,t)\|$)
2. Sort d_i^2 in ascending order, select the N_{po} least values and calculate their sum S'_{LTS}.
3. If any of the stopping conditions is satisfied, exit; otherwise, $S_{LTS} = S'_{LTS}$ and continue.
4. Compute for the N_{po} selected pairs the optimal motion (R,t) that minimizes S'_{LTS}.
5. Transform P according to (R,t) (Equation = $p_i(R,t) = Rp_i + t,\ P(R,t) = \{p_i(R,t)\}_1^{N_p}$) and go to step 1.

P = Data set 1

M = Data set 2

N_{po} = Number of points (subset that is paired/aligned)

S_{LTS} = Sum of least trimmed squares

(R,t) = Rotation Matrix, Translation Vector

Pre-alignment / Pre-registration

As the comparison process in Viewbox 4.1 happens automatically by the computer randomly selecting the user-specified number of initial positions in space to test, there was the possibility that the original location/space data of the model could affect the outcome of the comparison process, both in terms of accuracy and time of the overall comparison. To test this possibility, some Viewbox 4.1 automatic comparisons were run twice. First without any orientation of the mesh data, and

second, with the mesh data roughly pre-aligned, or in other words pre-registered, to minimise the computing work and time required for comparison and to potentially increase the accuracy of the comparison.

To pre-align or pre-register the models for comparison in Viewbox 4.1, the models were manually aligned in FlexScan3D using the same features at the comparison process: aligning all the models using the mouse and the *SHIFT* / *ALT* keys, and pressing the *Align* button, on the setting *Fine Alignment*. After all the models were aligned in the same space/location, they were then exported using the *Export (Scan)* button. These exported models were then subsequently compared in Viewbox 4.1 using identical settings to the non-pre-aligned models. As the process for pre-alignment coincided directly with the manual comparison process in FlexScan3D, the first step of the manual comparison process was often the export of the aligned models for the aligned comparison in Viewbox 4.1.

Time

Where possible during the data collection process, the amount of time each step took was recorded to assess the overall feasibility of the entire process in terms of time. Accuracy ultimately is the most important feature of an individuation technique, but the time spent and general feasibility in the relevant applications are also essential considerations, especially for individuals awaiting information on their missing friends and relatives.

Hardware

Due to the intense computational nature of the comparison process, six different main computers were used. As hardware specifications can drastically affect aspects of the project such as calculation of processing time, the computers' specifications are listed below. These were all high-end, high-performance computers, with the exception of Luxor. The relative processing power/speed was also calculated to ensure a full understanding of the relative hardware specification across machines and how that might vary.

Rosetta

Manufacturer: Razer Inc.

Model: Blade (2014)

Processor: Intel® Core™ i7-4702HQ CPU @ 2.20GHz

Cores: 4

Logical Processors: 8

Installed memory (RAM): 8.00 GB

System type: 64-bit Operating system, x64-based processor

Graphics Card: GeForce GTX 870M

Driver Version: 391.01

Direct3D API Version: 12

Direct3D feature level: 11_0

CUDA Cores: 1344

Graphics clock: 941 MHz

Memory data rate: 5000 MHz

Memory interface: 192-bit

Memory bandwidth: 120.00 GB/s

Total available graphics memory: 7129 MB

Dedicated video memory: 3072 MB GDDR5

System video memory: 0 MB

Shared system memory: 4057 MB

Amarna

Manufacturer: IS Supported Desktop - HP

Model: Z240

Processor: Intel® Core™ i7-6700 CPU @ 3.40GHz

Cores: 4

Logical Processors: 8

Installed memory (RAM): 32.0 GB

System type: 64-bit Operating system, x64-based processor

Graphics Card: Quadro K1200

Driver Version: 347.88

Direct3D API Version: 11

Direct3D feature level: 11_0

CUDA Cores: 512

Graphics clock: 954 MHz

Memory data rate: 5010 MHz

Memory interface: 128-bit

Memory bandwidth: 80.00 GB/s

Total available graphics memory: 20184 MB

Dedicated video memory: 4096 MB GDDR5

System video memory: 0 MB

Shared system memory: 16088 MB

Elena

Manufacturer: ASUSTek COMPUTER INC.

Model: ASUS Desktop PC G30AB Series

Processor: Intel® Core™ i7-4770K CPU @ 3.50GHz 3.50GHz

Cores: 4

Logical Processors: 8

Installed memory (RAM): 24.0 GB

System type: 64-bit Operating system, x64-based processor

Graphics Card: GeForce GTX 760

Driver Version: 388.13

Direct3D API Version: 11.2

Direct3D feature level: 11_0

CUDA Cores: 1152

Graphics clock: 823 MHz

Memory data rate: 5600 MHz

Memory interface: 192-bit

Memory bandwidth: 134.00 GB/s

Total available graphics memory: 15329 MB

Dedicated video memory: 3072 MB GDDR5

System video memory: 0 MB

Shared system memory: 12257 MB

Romulus

Manufacturer: IS Supported Desktop - HP

Model: Elite Desk

Processor: Intel® Core™ i5-6500 CPU @ 3.20GHz

Cores: 4

Logical Processors: 4

Installed memory (RAM): 16.0 GB

System type: 64-bit Operating system, x64-based processor

Integrated Graphics: Intel® HD Graphics 530

Shader Version: 5.0

OpenGL Version: 4.4

OpenCL Version: 2.0

Remus

Manufacturer: IS Supported Desktop - HP

Model: Elite Desk

Processor: Intel® Core™ i5-6500 CPU @ 3.20GHz

Cores: 4

Logical Processors: 4

Installed memory (RAM): 16.0 GB

System type: 64-bit Operating system, x64-based processor

Integrated Graphics: Intel® HD Graphics 530

Shader Version: 5.0

OpenGL Version: 4.4

OpenCL Version: 2.0

Luxor

Manufacturer: Toshiba

Model: Satellite M645

Processor: Intel® Core™ i3 CPU @ 2.27GHz

Cores: 2

Logical Processors: 4
Installed memory (RAM): 4.0 GB
System type: 64-bit Operating system, x64-based processor
Integrated Graphics: Intel® HD Graphics

Statistical Analysis

Pair-matching Analysis– Sensitivity and Specificity

After the data collection was completed, statistical analysis on the resulting Excel sheets of mesh-to-mesh values was conducted using sensitivity and specificity as indicators of accuracy. Sensitivity is the ability of a test to correctly identify positive results, in this case true pair matches; Specificity is the ability of a test to correctly identify negative results, in this case non-pair matches or true negatives (single bones with no pair-match) (Loong, 2003, Metz, 1978). Though generally this type of analysis falls broadly under the heading of sensitivity and specificity, two different types of value selection for sensitivity and specificity were assessed: Lowest Common Value analysis and Receiver Operating Characteristic analysis. Generally, however, both processes use mesh-to-mesh values as a proxy for pair-matching; the lower the mesh-to-mesh value, the better the match. In general, however, the advantage of either method is that they both provide *rates* of pair-matching instead of just the simple number of cases (Metz, 1978).

Lowest Common Value - Single Pair Match Selection

For the Lowest Common Value analysis method, the three lowest mesh-to-mesh values for each individual bone were selected and assessed. This means that each left and each right had their three lowest values highlighted in the pivot table like format of the Excel spreadsheet. To be considered a pair-match, both sides had to agree that they were each other's shared lowest values. In other words, this was done to assure that bone A couldn't be matched with bone B, if bone B matched with bone C. In this manner, a bone could have only one possible pair-match, or none at all. This was initially done manually for the pilot study but was later automated by the author using an Excel macro [**Appendix C**]. After this selection process, the veracity of the pair chosen was assessed for each individual bone. If the proper pair-

match was indicated, it was recorded as a true positive. If a bone was paired, but with the wrong bone, it was recorded as a false positive. If the bone did not have a pair, and was indicated as such, it was recorded as a true negative. If the bone did have a pair, but was indicated not to, it was recorded as a false negative. When complete, all of the instances of true positives, true negatives, false positives and false negatives were summed for each respective category. These values were then entered into the formulae for sensitivity, specificity, positive predictive value and negative predictive value which follow below:

$$Sensitivity = \frac{number\ of\ true\ positives}{number\ of\ true\ positives + number\ of\ false\ negatives}$$

$$Specificity = \frac{number\ of\ true\ negatives}{number\ of\ true\ negatives + false\ positives}$$

$$Positive\ Predictive\ Value = \frac{number\ of\ true\ positives}{number\ of\ true\ positives + number\ of\ false\ positives}$$

$$Negative\ Predictive\ Value\ = \frac{number\ of\ true\ negatives}{number\ of\ true\ negatives + number\ of\ false\ negatives}$$

It must be noted that due to the selection process of the three lowest values for each bone, the order in which this process happens can affect the outcome of the results. Thus, the Excel spreadsheets were always formatted in the same manner with the right bones across the top and the left bones going down the side, and the selection of the lowest value for both sides was always conducted in the same manner, first across and then down the sheet.

Furthermore, this selection method also does not take into account the actual numeric mesh-to-mesh value, but instead relies on the relative relationship of all of the values to each other. In this manner, there is no significance attached to a mesh-to-mesh value of 1.5 mm for example, but instead to the condition that 1.5 mm is a low value as compared to all the other values present. This is important as due to the nature of three-dimensional models and the variation among different bone shapes

and sizes, mesh-to-mesh values fluctuate. For a full, detailed example of this method, see **Appendix C**.

The numeric mesh-to-mesh values were initially investigated for a possible threshold value using the standard deviation, but this selection process but did not work so were abandoned (Karell et al., 2016).

Receiver Operating Characteristic (ROC) Curve Analysis - Multi-Pair Match Selection

As there was the possibility of user selection affecting the outcome of the sensitivity and specificity results, a different selection process which eliminated this problem was also tested. This version of sensitivity and specificity is called a Receiver Operating Characteristic (ROC) curve and is a visual way of representing the dynamic relationship of sensitivity and specificity information (Metz, 1978, Fawcett, 2006, Hanley and McNeil, 1983). This method relies on the numeric values of mesh-to-mesh values themselves, creating a dynamic threshold range from the mesh-to-mesh values entered. In this manner, the first type of sensitivity and specificity described could be visualised as a single point, whereas a ROC curve is a step-function that gradually creates a curve by plotting the resulting data points of sensitivity and specificity calculated at different thresholds (Metz, 1978, Fawcett, 2006). A threshold cut-off value can then be adjusted along this curve, to maximise the desired result of the relationship between sensitivity and specificity.

To assess the resulting ROC curves for significance, the Area Under the Curve (AUC) was calculated for each ROC curve. Though there are slightly different ways to calculate the AUC based on different shape fitting, in general it is a mathematical calculation of the physical space that falls beneath the ROC curve (Fawcett, 2006, Obuchowski, 2003, Marzban, 2004, DeLong et al., 1988). As a ROC curve is always graphed on a 1 X 1 scale, the AUC is always between zero and one, with higher AUC values (i.e. closer to one) representing better models. This corresponds directly to the aspect of ROC curves that the closer the curve is to convex and reaching the top right corner of a graph, the better it should be, as it represents high sensitivity and high specificity. The AUC is also equivalent to Wilcoxon test of ranks, which means that it displays the probability of the test that it

'will rank a randomly chosen positive higher than a randomly chosen negative' (Fawcett, 2006).

Furthermore, ROC curves can be assessed by comparing them directly to each other using a non-parametric approach based on U-statistics (DeLong et al., 1988). In this manner, it is possible to calculate confidence regions for ROC curves, in addition to the possibility of partial AUCs for assessment of the validity of the methods tested (DeLong et al., 1988, Obuchowski, 2003).

Finally, it is important to note that as ROC curves create dynamic threshold values, theses threshold values created will change bone to bone, as it relies on the actual numeric aspect of mesh-to-mesh values. In this manner, it is essential that each bone is thoroughly tested with known samples and an accurate threshold value created. It is important to note that using a threshold value, albeit a dynamic one, does allow for a single bone to have multiple 'pair-matches'. While obviously impossible, this pair selection method allows the use of a null hypothesis that bones are assumed to be a match unless they fall above the threshold given which is a common current framework in pair-matching literature (Byrd, 2008, Lynch et al., 2018).

For all ROC analysis, the following settings were used:

Methodology: DeLong et al.
Binomial exact Confidence Interval for the AUC: ✓
Disease Prevalence (or pre-test probability of disease): Unknown

Options
List criterion values with test characteristics: ✓
Include all observed criterion values: Blank
95% Confidence Interval for:
    Sensitivity/Specificity: ✓
    Likelihood ratios: ✓
Advanced options:
    Estimation of sensitivity and specificity at fixed specificity and sensitivity: ✓
    Bootstrap Youden index and/or optimal criterion confidence interval
    Bootstrap replications: 1000
    Random-number seed: 978

Graphs
Display ROC curve window: ✓
Mark points corresponding to criterion values: Blank
Include 95% Confidence Bounds: ✓

Replicability

To confirm that the three-dimensional models and the subsequent mesh-to-mesh values were replicable, four miniature studies were conducted to test intra-observer error.

To test the intra-observer error of the model building process using segmentation, 11 random clavicles models were built a second time approximately a year later, and then three were rebuilt a third time approximately another six months later. All these clavicles were then compared to each other in the same manner as pair-matching in FlexScan3D to acquire mesh-to-mesh values and assess their similarity. These values were assessed individually and as an average model building error. Unfortunately, there was not time to test the inter-observer error of the model building process.

To test the intra-observer error for the merging process, the fine alignment values for 142 calcanei models were recorded and assessed to see if they fell below the accepted 0.05 mm. Though there was not a specific test of inter-observer error for the merging process, the criteria of the fine alignment values falling below the accepted 0.05 mm would be the same. Due to time, this was not tested.

To test the potential intra-observer error of producing mesh-to-mesh values in FlexScan3D, 69 left calcanei were compared to 69 right calcanei in triplicate (Nash, 2015). The mesh-to-mesh values were then compared for similarity using the relative technical error of measurement (TEM), as described by Perini et al (Perini et al., 2005). The inter-observer error was not tested, as the computer algorithm creating the mesh-to-mesh values remains the same, regardless of user input.

Though the comparison process in Viewbox 4.1 is automated and thus varies only based on the algorithm, not human input, it was still tested for intra-observer error. Two sets, one of clavicles and one of temporals, were run in triplicate and then analysed using the relative TEM (Perini et al., 2005). Each set consisted of one left compared to 10 rights. The inter-observer error was not tested specifically, as it would be identical to the intra-observer error given the comparison process' algorithmic nature.

Software

All statistical analysis was conducted in Excel and MedCalc.

Results

Time

Model Building

Models, regardless of scan type, took approximately 30 minutes to 2 hours to build, with an average time of approximately 1 hour. Thus, for the 413 models built or corrected by the author, model building took approximately 413 hours, or a straight 17 days and 5 hours.

Hardware Calibration

To give a rough calibration of all the different hardware sets used, the same two sets of test runs were conducted in Viewbox on every machine used. The first set was one left clavicle compared against ten right clavicles, while the second was one left temporal compared against ten right temporals. The time was compared for all runs, and then relative percentages were calculated. The relative percentages varied set to set, but generally showed the same pattern hardware-wise. Amarna was the fastest computer, while Luxor was the slowest. The slowest computer was 2.9 times slower than the fastest computer, though the second slowest was only 1.4 times slower. Furthermore, the slowest computer was only used for one comparison set, as will be explained later in the chapter. For the complete time calculations and relative percentages, see **Tables 10 & 11**.

Table 10.

Computer	Clavicles - Run Time	Time Per Run	Relative Percentage
Luxor	0:11:09	0:01:07	274.18%
Rosetta	0:05:53	0:00:35	144.67%
Amarna	0:04:04	0:00:24	100.00%
Elena	0:04:32	0:00:27	111.48%
Romulus	0:04:10	0:00:25	102.46%
Remus	0:04:25	0:00:26	108.61%

Table 11.

Computer	Temporals - Run Time	Time Per Run	Relative Percentage
Luxor	0:33:51	0:03:23	296.93%
Rosetta	0:16:14	0:01:37	142.40%
Amarna	0:11:24	0:01:08	100.00%
Elena	0:13:04	0:01:18	114.62%
Romulus	0:13:07	0:01:19	115.06%
Remus	0:16:04	0:01:36	140.94%

Error Calculation

Model Building Error

Segmentation (Computed Tomography Data)

To test the intra-observer segmentation error, eleven random clavicles were built a second time, one year after initially being built, and then compared to the original models using Flexscan3D. The lowest difference between two models was 0.007 mm, while the highest was 0.117 mm, though the majority were below 0.021 mm. The average difference was 0.03 mm including the two highest values (0.117 mm and 0.116 mm), and 0.01 mm excluding those two highest values. Three of these random clavicles were also built a third time six months later, and again compared using Flexscan3D. The difference between the first models and this set ranged from 0.02 mm to 0.025 mm. The average difference was 0.022 mm. The difference between the second models and this set averages at 0.007 mm. Due to the low intra-observer error across these built sets, the models built by segmentation were considered valid and usable for comparison.

Merging (3D Surface Scan Data)

To test the intra-observer error for the merging process, the fine alignment values for all of the calcanei models from Crete (88 models) were recorded and assessed to see if they fell below the accepted 0.05 mm. The values ranged from 0.027 mm to 0.039 mm, with an average of 0.031 mm. This is well below the 0.05 mm limit. The fine alignment values for 54 of the calcanei from Cyprus were also recorded by Kimberley Nash (Nash, 2015). The values ranged from 0.024 mm to 0.05 mm (Nash, 2015). The average value was 0.028 mm, and thus these models were also considered valid and usable for comparison.

Comparison Error

Flexscan3D

To test the intra-observer comparison error for Flexscan3D, the 69 left/right pairs of calcanei from Scotland and Cyprus were compared in Flexscan3D in triplicate by Kimberley Nash (Nash, 2015). These values were then assessed using the technical error of measurement (TEM), as described by Perini et al, by the author (Perini et al., 2005). A relative TEM under 5% was considered valid. As the 69 left/right pairs included pairs from both Scotland and Cyprus (26 and 43 respectively), this assured comparison was valid across model building type (Scotland – Segmentation, Cyprus – Merging). All three comparison values sets were compared using the TEM, resulting in three relative TEMs: 1.60% for the first and second alignment sets, 1.48% for the first and third alignment sets, and 1.68% for the first and third alignment sets. All relative TEMs were well under 5% and considered valid.

Though not a TEM calculation, it is also worth noting that Monika Lay also tested the alignment of a single pair of temporal bones 250 times (Lay, 2014). Lay found that these values had a standard deviation of 0.0187 mm, another acceptable margin of error calculation (Lay, 2014).

Viewbox

To test the intra-observer error for Viewbox, two different sets were analysed. The first set was one left clavicle compared against ten right clavicles, while the second was one left temporal compared against ten right temporals. Both sets were run three times, and analysed using the technical error of measurement (Perini et al., 2005). Again, a relative TEM under 5% was considered valid. The resulting three relative TEMs for the clavicle set were: 0.14% for the first and second alignment sets, 0.11% for the first and third alignment sets, and 0.20% for the first and third alignment sets. The resulting three relative TEMs for the temporal set was: 0.12% for the first and second alignment sets, 0.15% for the first and third alignment sets, and 0.26% for the first and third alignment sets. All relative TEMs for both sets were well under 5%, and thus considered valid.

Pair-matching Results

For each of the four sets of bones, results will be presented in a consistent format. Results are separated by bone, with Flexscan3D comparison results first, followed by the Viewbox comparison results. Each Flexscan3D/Viewbox section will start by explaining the sample size, time taken for comparison, and hardware used. For every testing condition, it will then present the Lowest Common Value (LCV) analysis results followed by the Receiver Operating Characteristic (ROC) Curve analysis results, including the optimal sensitivity and specificity, at a fixed 97.5% sensitivity, and at a fixed 97.5% specificity. The number of true positives, true negatives, false positives and false negatives will also be presented for each condition and analysis type. The results are also described in evaluative categories of ideal/perfect (100%), excellent (≥ 95%), good (≥ 85%), mediocre (84-40%), poor (39-20%), very poor (19-0%). Ideal/perfect results would indicate perfect usage, and therefore perfect pair-matching. Excellent indicates a method that performs higher than accepted techniques, such as osteometric sorting which use 90% as an acceptable error cut-off (Byrd and Adams, 2003). Good indicates a method which performs at or slight below current methods, such as osteometric sorting, and could be considered viable for use. Mediocre indicates results below current techniques, but may be better than nothing should no alternative method exist. Poor indicates results that are low enough that they would not be useable. Very poor indicates results that should not be used.

Humeri

Flexscan3D

Though 61 humeri were initially built and compared, due to the quality of the scanning and model creation, only 45 humeri were used for the final comparison (Karell et al., 2016). The comparison took place on Luxor and took approximately 45 hours (Karell et al., 2016). The analysis of the results took approximately 1 hour.

Lowest Common Value Results

The results for the LCV analysis were ideal, with perfect sensitivity, specificity, positive and negative predictive value rates (PPV, NPV) (**Tables 12 & 13**) (Karell et al., 2016):

Table 12.

Flexscan3D - Humeri - LCV Results	
Sensitivity	100%
Specificity	100%
Positive Predictive Value	100%
Negative Predictive Value	100%

Table 13.

Flexscan3D - Humeri - LCV Matches	
True positives	42
False negatives	0
False positives	0
True negatives	3

ROC Optimal

The optimal ROC results also include the respective threshold value, the Area Under the Curve (AUC), and the p-value for the AUC's validity, in addition to sensitivity, specificity, PPV and NPV. The threshold values and the AUC can be represented graphically as well as numerically. As with the LCV, the results for all rates were excellent, with the exception of the PPV which was mediocre (**Table 14 & 15**).

Table 14.

Flexscan3D – Humeri - ROC Optimal Results				
		Threshold Value	**AUC**	**p-value**
Sensitivity	95.24%	0.849	0.994	<0.0001
Specificity	99.18%			
Positive Predictive Value	83.41%			
Negative Predictive Value	99.79%			

Table 15.

Flexscan3D – Humeri - ROC Optimal Sample Size	
True Positives	21
True Negatives	485
Total Sample	506

The humeri ROC optimal results show an almost perfect AUC which is clearly visualised graphically in **Figure 8**:

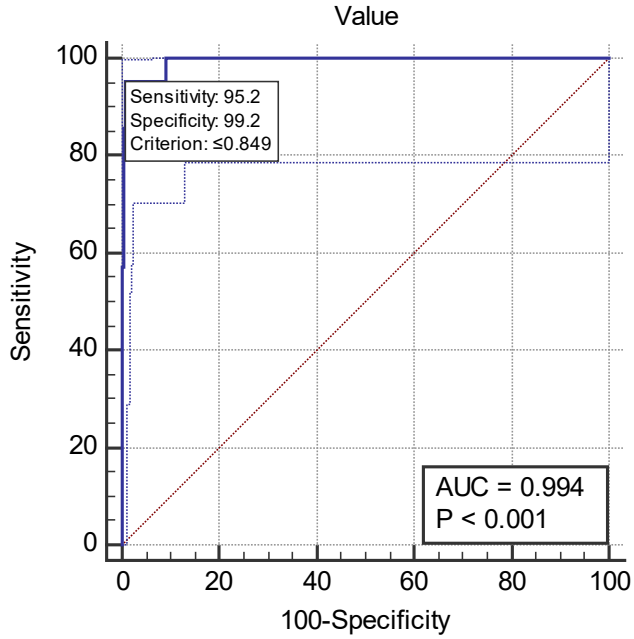

Figure 8. The AUC is calculated from the solid line, with the diagonal dashed line representing random allocation, and the two other dashed lines representing the 95% confidence intervals. The closer the solid line to the top left corner, the closer the AUC is to 1, and the better the AUC.

Though the sensitivity, specificity, PPV, NPV, and AUC are very high, these values can potentially be affected by sample size. This is easily assessed by a dot diagram, however **(Figure 9)**.

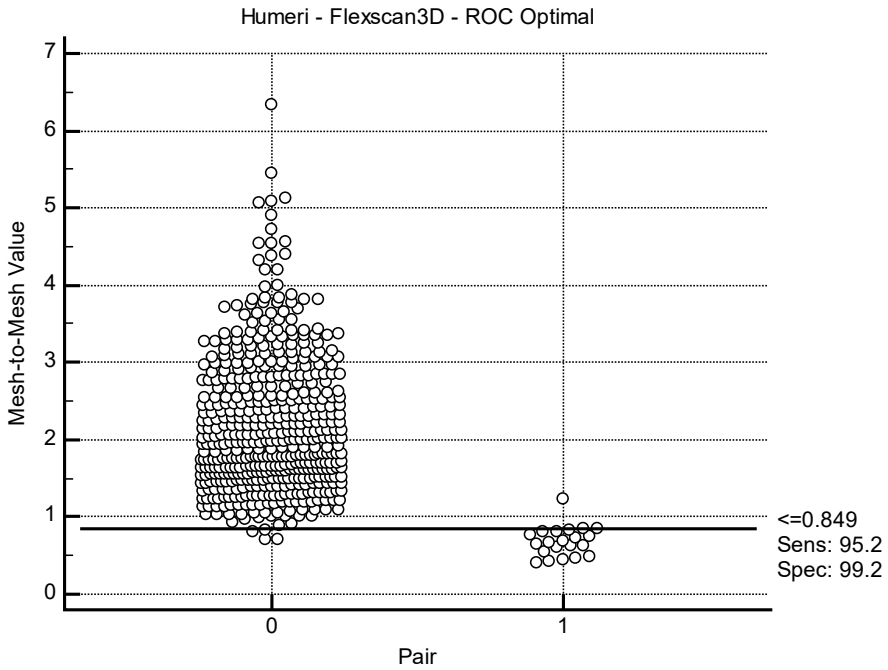

Figure 9. The threshold value is represented by the solid line, 0 represents the negative group, 1 represents the positive group, with each circle representing a mesh-to-mesh comparison value.

This dot diagram (**Figure 9.**) illustrates a good sample size and distribution, with the threshold value easily distinguishing between the positive group and the negative group. However, this will not be the case for all examples, hence the examination of both the 97.5% sensitivity and specificity thresholds.

ROC 97.5% Sensitivity

For the 97.5% fixed sensitivity ROC, the sample size, AUC and p-value remain stable, with only the threshold value and sensitivity/specificity rates changing. As the Flexscan3D humeri results were generally good at the optimal values, the 97.5% fixed sensitivity rates were unsurprisingly also good (**Table 16**).

Table 16.

Flexscan3D – Humeri – ROC 97.5% Sensitivity Results		
		Threshold Value
Sensitivity	97.5%	1.2213
Specificity	90.72%	

The dot diagram for the 97.5% fixed sensitivity clearly visualises the difference between the 97.5% sensitivity rates and the optimal results (**Figure 10.**).

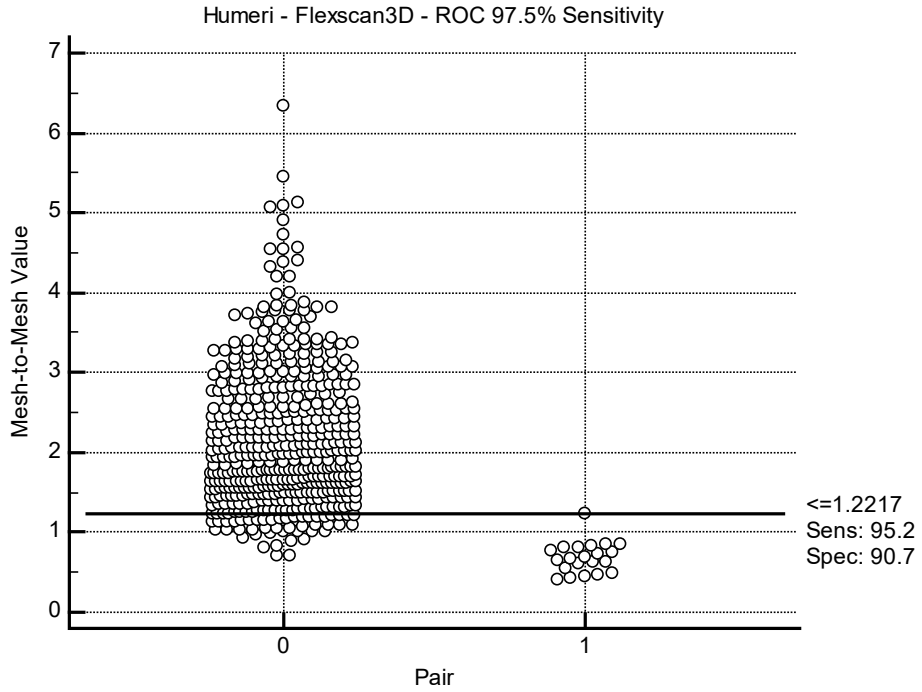

Figure 10. Dot diagram for ROC fixed 97.5% sensitivity, reflecting new threshold value and resulting sensitivity and specificity rates.

As the threshold changed to ensure that every true positive value was captured, it is easy to see that is has resulted in more true negatives being classed as false positives, as the number of circles in the 0 category has increased.

ROC 97.5% Specificity

In the same manner as the 97.5% fixed sensitivity, the 97.5% fixed specificity produced excellent results (**Table 17**).

Table 17.

Flexscan3D – Humeri – ROC 97.5% Specificity Results		
		Threshold Value
Sensitivity	95.24%	1.003
Specificity	97.5%	

Viewbox

For the Viewbox comparison, the same 45 humeri were used. As Viewbox cannot compare models with different types of internal data, these humeri were hollowed and saved with normals. These models were unaligned, or not pre-

registered. The comparison took place on Rosetta and took approximately five minutes of user set up and 45 hours of run time. The comparison was only done with the 'Exact Normal' settings. The analysis of the results took approximately 1 hour.

Lowest Common Value Results

The Viewbox LCV results were not as good as the Flexscan3D results, with a small drop in sensitivity and PPV and a significant drop in specificity and NPV (**Table 18 & 19**).

Table 18.

Viewbox - Humeri – U, H, N - LCV Results	
Sensitivity	95%
Specificity	60%
Positive Predictive Value	95%
Negative Predictive Value	60%

Table 19.

Viewbox - Humeri – U, H, N - LCV Matches	
True positives	38
False negatives	2
False positives	2
True negatives	3

ROC Optimal

The ROC optimal results were on par with the Flexscan3D results and showed only a slight drop in specificity. The PPV decreased significantly, while the NPV increased dramatically. The threshold value was also significantly different (**Table 20 & 21**).

Table 20.

Viewbox – Humeri – U, H, N - ROC Optimal Results				
		Threshold Value	**AUC**	**p-value**
Sensitivity	95.24%	1.498	0.985	<0.0001
Specificity	95.04%			
Positive Predictive Value	45.44%			
Negative Predictive Value	99.78%			

Table 21.

Viewbox – Humeri -1- ROC Optimal Sample Size	
True Positives	21
True Negatives	485
Total Sample	506

ROC 97.5% Sensitivity

The ROC fixed 97.5% sensitivity results reflected the optimal, with another slight drop in specificity and an increased threshold value (**Table 22**).

Table 22.

Viewbox – Humeri – U, H, N - ROC 97.5% Sensitivity Results		
		Threshold Value
Sensitivity	97.5%	1.844
Specificity	84.54%	

ROC 97.5% Specificity

The ROC fixed 97.5% specificity results were unsurprisingly worse than the others, with a significant decrease in sensitivity (**Table 23**).

Table 23.

Viewbox – Humeri – U, H, N - ROC 97.5% Specificity Results		
		Threshold Value
Sensitivity	76.19%	1.356
Specificity	97.5%	

Summary

Time

The combined Flexscan3D and Viewbox comparison took approximately 90 hours for a total of 1104 comparison values. This is an average iteration time of 4 minutes and 53 seconds, as calculated by Rosetta's specifications. The analysis of both comparison methods took approximately 2 hours.

Flexscan3D versus Viewbox Results

Overall, the sensitivity and specificity results for the Flexscan3D and Viewbox comparisons were both excellent/good and comparable, regardless of LCV or ROC optimal analysis. The one exception was the LCV specificity for Viewbox, which was significantly below the other specificity values. The PPV values for the LCV analysis for both the Flexscan3D and the Viewbox comparisons were identical to their sensitivity and specificity rates respectively. The PPV rates for the ROC optimal analysis, however, were both significantly worse, though mediocre in the case of the Flexscan3D comparison. The NPV rates were almost perfect. (**Tables 24, 25 & 26**)

All ROC Results

All the sensitivity and specificity results for the ROC analysis were high and comparable in accuracy, with two exceptions: the specificity for the 97.5% fixed sensitivity ROC for Viewbox, which was slightly lower than other values, and the sensitivity for the 97.5% fixed specificity, which was significantly below the other values. The results of the PPV and the NPV rates were summarised in the previous section. (**Table 26**)

Overall Optimal Method

Of the two comparison methods and two analysis methods, the best result for the humeri was the Flexscan3D comparison using LCV analysis.

Table 24.

Comparison	Batch	LCV Sensitivity	LCV Specificity	ROC (Optimal) Sensitivity	ROC (Optimal) Specificity
Flexscan3D	Mixed Hollowed	100%	100%	95.24%	99.18%
Viewbox	Unaligned - Hollowed - w/ Normals - Exact Normal	95%	60%	95.24%	95.05%

Table 25.

Comparison	Batch	LCV - PPV	LCV - NPV	ROC (Optimal) - PPV	ROC (Optimal) - NPV
Flexscan3D	Mixed Hollowed	100%	100%	83.41%	99.79%
Viewbox	Unaligned - Hollowed - w/ Normals - Exact Normal	95%	60%	45.44%	99.78%

Table 26.

Comparison	Batch	ROC (Optimal) Sensitivity	ROC (Optimal) Specificity	ROC (Fixed 97.5 Sens) Sensitivity	ROC (Fixed 97.5 Sens) Specificity	ROC (Fixed 97.5 Spec) Sensitivity	ROC (Fixed 97.5 Spec) Specificity
Flexscan3D	Mixed Hollowed	95.24%	99.18%	97.5%	90.72%	95.24%	97.5%
Viewbox	Unaligned - Hollowed - w/ Normals - Exact Normal	95.24%	95.05%	97.5%	84.54%	76.19%	97.5%

Clavicles

Flexscan3D

For the Flexscan3D comparison, 99 clavicles were used. All of the clavicles were unhollowed. The comparison took place on Rosetta and took approximately 43 hours to complete 2294 iterations. This averages to 1 minute and 7 seconds per iteration. The analysis of the data took approximately 2 hours.

Lowest Common Value Results

The LCV results for the Flexscan3D comparison of the clavicles were mediocre across the board, and far below the humeri (**Tables 27 & 28**).

Table 27.

Flexscan3D - Clavicles - LCV Results	
Sensitivity	81.79%
Specificity	57.89%
Positive Predictive Value	75.76%
Negative Predictive Value	66.67%

Table 28.

Flexscan3D – Clavicles - LCV Matches	
True positives	50
False negatives	11
False positives	16
True negatives	22

ROC Optimal

The ROC optimal results, however, were very good and on par with the humeri results in terms of sensitivity and specificity. The AUC was high and valid. The NPV was excellent, and almost perfect; the PPV, however, was very poor (**Tables 29 & 30**).

Table 29.

Flexscan3D – Clavicles - ROC Optimal Results				
		Threshold Value	**AUC**	**p-value**
Sensitivity	94.44%	0.9	0.978	<0.0001
Specificity	92.16%			
Positive Predictive Value	16.11%			
Negative Predictive Value	99.90%			

Table 30.

Flexscan3D – Clavicles - ROC Optimal Sample Size	
True Positives	36
True Negatives	2258
Total Sample	2294

The associated dot diagram **(Figure 11)** shows that there are a number of negatives below the threshold line, despite the high sensitivity, specificity, and AUC. This is an effect of the sample size, as mentioned previously, and makes the 97.5% fixed ROC more useful for interpretation.

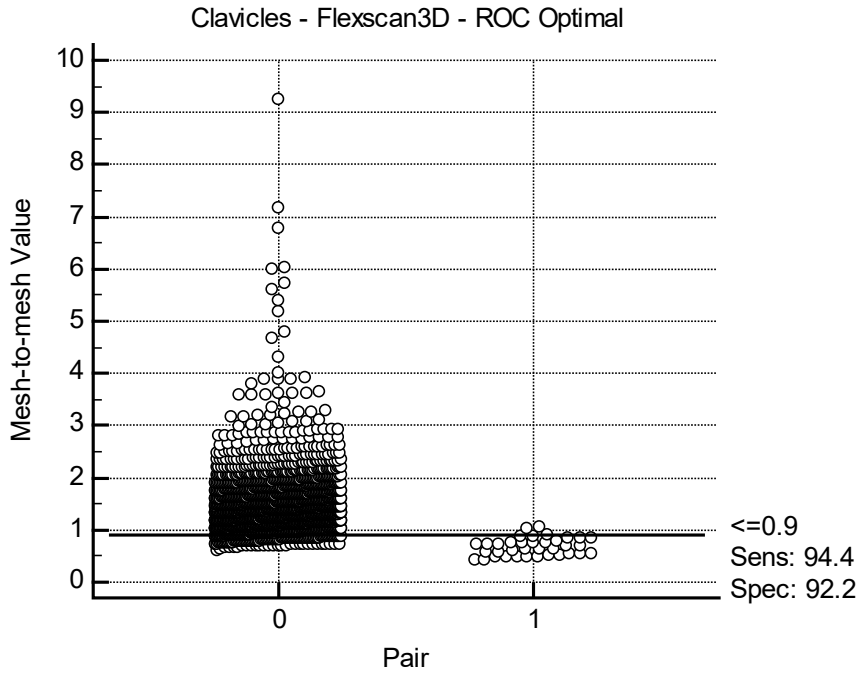

Figure 11. Dot diagram for Clavicles - Flexscan3D – ROC Optimal

ROC 97.5% Sensitivity

The fixed 97.5% sensitivity results had a lower, mediocre specificity than the optimal, as was expected based on the dot diagram for the optimal (**Table 31**).

Table 31.

Flexscan3D – Clavicles – ROC 97.5% Sensitivity Results		
		Threshold Value
Sensitivity	97.5%	1.0421
Specificity	80.73%	

ROC 97.5% Specificity

The fixed 97.5% specificity results had a mediocre sensitivity, as was expected based on the other ROC results (**Table 32**).

Table 32.

Flexscan3D – Clavicles – ROC 97.5% Specificity Results		
		Threshold Value
Sensitivity	75%	0.780
Specificity	97.5%	

Viewbox

For the Viewbox comparisons, eight different conditions of variable sample sizes were tested. Therefore, all the details regarding sample size, time, and parameters of the run will be listed individually along with the respective results.

1 - Aligned - Unhollowed - Exact Normal (Flexscan3D Comparable)

To directly compare with the Flexscan3D, the same number and type of clavicles, 99 aligned and unhollowed, were compared using the 'Exact Normal' setting. The analysis was conducted on Rosetta. Time-wise, this set of parameters was not run on its own, but as part of a larger sample. Therefore, the time calculation of the comparison is calculated in a different parameter set. The average time per iteration of this larger sample in the different parameter set, however, was 49 seconds. This means 99 clavicles would take approximately 5 days, 12 hours, 3 minutes and 18 seconds for the 9702 necessary iterations, assuming the 'All Against All' setting in Viewbox. The analysis took an additional 2 hours.

Lowest Common Value Results

The LCV results were overall mediocre or poor, with sensitivity, specificity, PPV and NPV under 45% (**Tables 33 & 34**).

Table 33.

Viewbox - Clavicles -1- LCV Results	
Sensitivity	37.74%
Specificity	43.48%
Positive Predictive Value	43.48%
Negative Predictive Value	37.74%

Table 34.

Viewbox – Clavicles -1- LCV Matches	
True positives	20
False negatives	33
False positives	26
True negatives	20

ROC Optimal

The optimal ROC results were considerably better than the LCV results, with a good sensitivity rate and a mediocre specificity. The PPV was very poor, while the NPV was excellent and almost perfect. The AUC was decently high and valid. (**Tables 35 & 36**)

Table 35.

Viewbox – Clavicles -1- ROC Optimal Results				
		Threshold Value	**AUC**	**p-value**
Sensitivity	88.89%	0.941	0.861	<0.0001
Specificity	70.46%			
Positive Predictive Value	4.57%			
Negative Predictive Value	99.79%			

Table 36.

Viewbox – Clavicles -1- ROC Optimal Sample Size	
True Positives	36
True Negatives	2258
Total Sample	2294

ROC 97.5% Sensitivity

The fixed 97.5% sensitivity results were poor, as seen in **Table 37.**

Table 37.

Viewbox– Clavicles -1- ROC 97.5% Sensitivity Results		
		Threshold Value
Sensitivity	97.5%	1.268
Specificity	37.11%	

ROC 97.5% Specificity

The fixed 97.5% specificity results were also poor, and slightly below the fixed 97.5% sensitivity (**Table 38**).

Table 38.

Viewbox– Clavicles -1- ROC 97.5% Specificity Results		
		Threshold Value
Sensitivity	30.56%	0.608
Specificity	97.5%	

2 - Aligned - Unhollowed - Exact Slow (Flexscan3D comparable)

The same, aligned, unhollowed, 99 clavicles were run using the 'Exact Slow' settings. The analysis was run on Amarna, and similarly to the first condition (aligned, unhollowed, run Exact Normal), was part of a larger sample. Therefore, the time calculation of the comparison is again calculated in a different parameter set. The average time per iteration of this larger sample in the different parameter set was 1 minute and 7 seconds. This means 99 clavicles would take approximately 7 days, 12 hours, 33 minutes and 54 seconds to complete the 9702 necessary iterations, assuming the 'All Against All' setting in Viewbox. The analysis took an additional 2 hours.

Lowest Common Value Results

The results for the LCV analysis were poor, with sensitivity, specificity, PPV and NPV all under 40% (**Tables 39 & 40**).

Table 39.

Viewbox - Clavicles -2- LCV Results	
Sensitivity	36.73%
Specificity	36%
Positive Predictive Value	36%
Negative Predictive Value	36.73%

Table 40.

Viewbox – Clavicles -2- LCV Matches	
True positives	18
False negatives	31
False positives	32
True negatives	18

ROC Optimal

The optimal ROC results were much better, with a good sensitivity, AUC and respective p-value. The specificity, however, was mediocre. The NPV was excellent; the PPV was very poor. (**Tables 41 & 42**)

Table 41.

Viewbox – Clavicles -2- ROC Optimal Results				
		Threshold Value	**AUC**	**p-value**
Sensitivity	88.89%	0.8564	0.844	<0.0001
Specificity	70.37%			
Positive Predictive Value	4.56%			
Negative Predictive Value	99.74%			

Table 42.

Viewbox – Clavicles -2- ROC Optimal Sample Size	
True Positives	36
True Negatives	2258
Total Sample	2294

ROC 97.5% Sensitivity

The 97.5% fixed sensitivity results were poor, as seen in **Table 43** and the respective dot diagram **(Figure 12**).

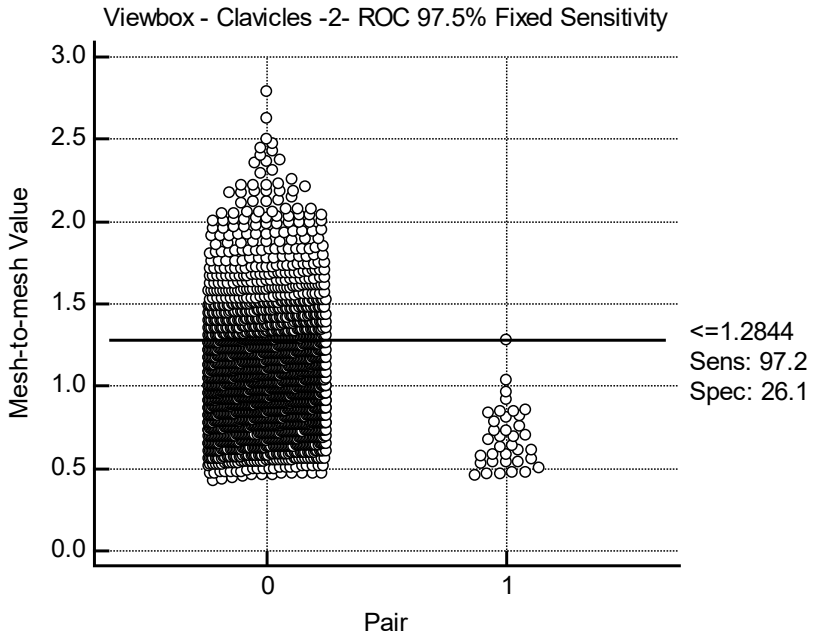

Figure 12. Dot diagram of Clavicle -2- ROC 97.5% Fixed Sensitivity with a poor result.

Table 43.

Viewbox– Clavicles -2- ROC 97.5% Sensitivity Results		
		Threshold Value
Sensitivity	97.5%	1.285
Specificity	25.95%	

ROC 97.5% Specificity

The 97.5% fixed specificity ROC results were similarly poor to the 97.5% fixed sensitivity, with the sensitivity and specificity rates reversed (**Table 44**).

Table 44.

Viewbox– Clavicles -2- ROC 97.5% Specificity Results		
		Threshold Value
Sensitivity	27.78%	0.547
Specificity	97.5%	

3 - Aligned - Unhollowed - Exact Normal (Larger Sample)

A total of 203 clavicles, unhollowed and aligned, were run on Amarna using the 'Exact Normal' settings. The run took 23 days, 1 hour and 1 minute for a total of 41006 iterations. This is an average time per iteration of 49 seconds. The analysis, of the 189 unique clavicles, took an additional 2 hours.

Lowest Common Value Results

The results for the LCV method were mostly poor and very poor, especially the specificity and NPV which fell below 5% **(Tables 45 & 46).**

Table 45.

Viewbox - Clavicles -3- LCV Results	
Sensitivity	30.53%
Specificity	3.45%
Positive Predictive Value	41.67%
Negative Predictive Value	2.15%

Table 46.

Viewbox – Clavicles -3- LCV Matches	
True positives	40
False negatives	91
False positives	56
True negatives	2

ROC Optimal

The optimal ROC results produced mediocre sensitivity and specificity rates, with a valid AUC. The PPV result was again very poor, while the NPV was excellent. The threshold value is close to the threshold value of Viewbox parameter set 1, as was expected due to the same test parameters with a larger sample size. **(Tables 47 & 48)**

Table 47.

Viewbox – Clavicles -3- ROC Optimal Results				
		Threshold Value	**AUC**	**p-value**
Sensitivity	82.61%	0.9077	0.849	<0.0001
Specificity	73.81%			
Positive Predictive Value	3.17%			
Negative Predictive Value	99.75%			

Table 48.

Viewbox – Clavicles -3- ROC Optimal Sample Size	
True Positives	92
True Negatives	8836
Total Sample	8928

ROC 97.5% Sensitivity

The fixed 97.5% sensitivity resulting specificity was poor (**Table 49**).

Table 49.

Viewbox– Clavicles -3- ROC 97.5% Sensitivity Results		
		Threshold Value
Sensitivity	97.5%	1.32
Specificity	33.11%	

ROC 97.5% Specificity

Similar to the fixed 97.5% sensitivity results, the fixed 97.5% specificity results were poor, as seen in **Table 50**.

Table 50.

Viewbox– Clavicles -3- ROC 97.5% Specificity Results		
		Threshold Value
Sensitivity	29.35%	0.612
Specificity	97.5%	

4 - Aligned - Unhollowed - Exact Slow (Larger Sample)

A total of 203 clavicles, unhollowed and aligned, were run on Amarna using the 'Exact Slow' settings. The run took 31 days, 21 hours and 42 minutes for a total of 41006 iterations. This is an average time per iteration of 1 minute and 7 seconds. The analysis, of the 189 unique clavicles, took an additional 2 hours.

Lowest Common Value Results

All of the LCV results were poor or very poor, with the specificity and NPV falling below 2%, as seen in **Tables 51 & 52**.

Table 51.

Viewbox - Clavicles -4- LCV Results	
Sensitivity	25.37%
Specificity	1.85%
Positive Predictive Value	39.08%
Negative Predictive Value	0.99%

Table 52.

Viewbox – Clavicles -4- LCV Matches	
True positives	34
False negatives	100
False positives	53
True negatives	1

ROC Optimal

The ROC optimal results were overall mediocre. The PPV was very poor, and the NPV was excellent. The AUC was decently high and valid. **(Tables 53 & 54).**

Table 53.

Viewbox – Clavicles -4- ROC Optimal Results				
		Threshold Value	**AUC**	**p-value**
Sensitivity	84.78%	0.8675	0.830	<0.0001
Specificity	69.31%			
Positive Predictive Value	2.79%			
Negative Predictive Value	99.77%			

Table 54.

Viewbox – Clavicles -4- ROC Optimal Sample Size	
True Positives	92
True Negatives	8836
Total Sample	8928

ROC 97.5% Sensitivity

The fixed 97.5% sensitivity ROC values were also poor, unsurprisingly given the optimal results were also poor (**Table 55**).

Table 55.

Viewbox– Clavicles -4- ROC 97.5% Sensitivity Results		
		Threshold Value
Sensitivity	97.5%	1.285
Specificity	26.55%	

ROC 97.5% Specificity

As expected, the fixed 97.5% specificity results were poor, as seen in **Table 56**.

Table 56.

Viewbox– Clavicles -4- ROC 97.5% Specificity Results		
		Threshold Value
Sensitivity	25%	0.556
Specificity	97.5%	

5 - Aligned – Hollowed – Without Normals - Exact Normal

A total of 200 clavicles were aligned, hollowed, and saved without Normals. They were run on Amarna using the 'Exact Normal' settings. The run took 6 days, 10 hours and 26 minutes for a total of 39800 iterations. This is an average time per iteration of 14 seconds. The analysis, of the 186 unique clavicles, took an additional 2 hours.

Lowest Common Value Results

The sensitivity and PPV rates were mediocre, while the specificity and NPV rates were very poor (**Tables 57 & 58**).

Table 57.

Viewbox - Clavicles -5- LCV Results	
Sensitivity	65.82%
Specificity	14.29%
Positive Predictive Value	81.25%
Negative Predictive Value	6.90%

Table 58.

Viewbox – Clavicles -5- LCV Matches	
True positives	104
False negatives	54
False positives	24
True negatives	4

ROC Optimal

The sensitivity and specificity were good, with a high and valid AUC. This is the best results of the clavicle sets thus far. While the PPV was still very poor, it was three times better than previous results, and the NPV remained excellent. (**Table 59 & 60**).

Table 59.

Viewbox – Clavicles -5- ROC Optimal Results				
		Threshold Value	**AUC**	**p-value**
Sensitivity	85.56%	1.429	0.947	<0.0001
Specificity	93.66%			
Positive Predictive Value	12.42%			
Negative Predictive Value	99.83%			

Table 60.

Viewbox – Clavicles -5- ROC Optimal Sample Size	
True Positives	90
True Negatives	8555
Total Sample	8645

ROC 97.5% Sensitivity

The results for the 97.5% fixed sensitivity were mediocre, but a marked improvement on the other parameter sets thus far (**Table 61**).

Table 61.

Viewbox– Clavicles -5- ROC 97.5% Sensitivity Results		
		Threshold Value
Sensitivity	97.5%	1.879
Specificity	63.68%	

ROC 97.5% Specificity

The fixed 97.5% specificity results were also mediocre, but again a marked improvement on the other parameter sets thus far (**Table 62**).

Table 62.

Viewbox– Clavicles -5- ROC 97.5% Specificity Results		
		Threshold Value
Sensitivity	67.78%	1.285
Specificity	97.5%	

6 - Aligned - Hollowed – Without Normals - Exact Slow

A total of 200 clavicles were aligned, hollowed, and saved without Normals. They were run on Remus using the 'Exact Slow' settings. The run took 6 days, 3 hours and 35 minutes for a total of 39800 iterations. This is an average time per iteration of 13 seconds. The analysis, of the 186 unique clavicles, took an additional 2 hours.

Lowest Common Value Results

The sensitivity and PPV for LCV were mediocre, with very poor specificity and NPV rates (**Tables 63 & 64**).

Table 63.

Viewbox - Clavicles -6- LCV Results	
Sensitivity	64.56%
Specificity	14.29%
Positive Predictive Value	80.95%
Negative Predictive Value	6.67%

Table 64.

Viewbox – Clavicles -6- LCV Matches	
True positives	102
False negatives	56
False positives	24
True negatives	4

ROC Optimal

The optimal ROC results were surprisingly good considering the other parameter sets, with good sensitivity and specificity rates. The PPV was still poor, while the NPV was still excellent. The AUC was high and valid. (**Tables 65 & 66**)

Table 65.

Viewbox – Clavicles -6- ROC Optimal Results				
		Threshold Value	**AUC**	**p-value**
Sensitivity	86.67%	1.357	0.942	<0.0001
Specificity	91.92%			
Positive Predictive Value	10.13%			
Negative Predictive Value	99.84%			

Table 66.

Viewbox – Clavicles -6- ROC Optimal Sample Size	
True Positives	90
True Negatives	8555
Total Sample	8645

ROC 97.5% Sensitivity

The fixed 97.5% sensitivity results were mediocre, as seen in **Table 67.**

Table 67.

Viewbox– Clavicles -6- ROC 97.5% Sensitivity Results		
		Threshold Value
Sensitivity	97.5%	1.793
Specificity	54.13%	

ROC 97.5% Specificity

The fixed 97.5% specificity results were mediocre (**Table 68)**.

Table 68.

Viewbox– Clavicles -6- ROC 97.5% Specificity Results		
		Threshold Value
Sensitivity	63.33%	1.187
Specificity	97.5%	

7 - Aligned - Hollowed – With Normals - Exact Normal

A total of 203 clavicles were aligned, hollowed and saved with normals. They were run on Remus using the 'Exact Normal' settings. The run took 7 days, 12 hours and 13 minutes for a total of 41006 iterations. This is an average time per iteration of 16 seconds. The analysis, of the 189 unique clavicles, took an additional 2 hours.

Lowest Common Value Results

The sensitivity rate and PPV were mediocre. However, both the specificity and the NPV were very poor, with values well under 5%. (**Tables 69 & 70**).

Table 69.

Viewbox - Clavicles -7- LCV Results	
Sensitivity	60.25%
Specificity	3.57%
Positive Predictive Value	78.23%
Negative Predictive Value	1.54%

Table 70.

Viewbox – Clavicles -7- LCV Matches	
True positives	97
False negatives	64
False positives	27
True negatives	1

ROC Optimal

The optimal ROC results were good for both the sensitivity and specificity rates, and among the best results for the clavicle set thus far. This includes the NPV, which was excellent. The PPV was still very poor, however. (**Tables 71 & 72**)

Table 71.

Viewbox – Clavicles -7- ROC Optimal Results				
		Threshold Value	**AUC**	**p-value**
Sensitivity	88.04%	1.368	0.942	<0.0001
Specificity	92.01%			
Positive Predictive Value	10.28%			
Negative Predictive Value	99.86%			

Table 72.

Viewbox – Clavicles -7- ROC Optimal Sample Size	
True Positives	92
True Negatives	8836
Total Sample	8928

ROC 97.5% Sensitivity

The fixed 97.5% sensitivity results were mediocre, as seen in **Table 73**.

Table 73.

Viewbox– Clavicles -7- ROC 97.5% Sensitivity Results		
		Threshold Value
Sensitivity	97.5%	1.879
Specificity	50.12%	

ROC 97.5% Specificity

The fixed 97.5% specificity results were mediocre (**Table 74)**.

Table 74.

Viewbox– Clavicles -7- ROC 97.5% Specificity Results		
		Threshold Value
Sensitivity	69.57%	1.205
Specificity	97.5%	

8 - Aligned – Hollowed – With Normals - Exact Slow

A total of 203 clavicles were aligned, hollowed and saved with normals. They were run on Remus using the 'Exact Slow' settings. The run took 6 days, 16 hours and 51 minutes for a total of 41006 iterations. This is an average time per iteration of 14 seconds. The analysis, of the 189 unique clavicles, took an additional 2 hours.

Lowest Common Value Results

For the LCV results, the sensitivity and PPV were mediocre. The specificity and NPV, however, were both very poor. (**Tables 75 & 76)**

Table 75.

Viewbox - Clavicles -8- LCV Results	
Sensitivity	59.21%
Specificity	8.11%
Positive Predictive Value	72.58%
Negative Predictive Value	4.62%

Table 76.

Viewbox – Clavicles -8- LCV Matches	
True positives	90
False negatives	62
False positives	34
True negatives	3

ROC Optimal

The optimal ROC results were good, with high sensitivity and specificity rates, as well as a high and valid AUC. The PPV was still very poor, while the NPV was excellent. (**Tables 77 & 78**)

Table 77.

Viewbox – Clavicles -8- ROC Optimal Results				
		Threshold Value	**AUC**	**p-value**
Sensitivity	88.04%	1.304	0.933	<0.0001
Specificity	89.84%			
Positive Predictive Value	8.27%			
Negative Predictive Value	99.86%			

Table 78.

Viewbox – Clavicles -8- ROC Optimal Sample Size	
True Positives	92
True Negatives	8836
Total Sample	8928

ROC 97.5% Sensitivity

The fixed 97.5% sensitivity results were mediocre, as seen in **Table 79**.

Table 79.

Viewbox– Clavicles -8- ROC 97.5% Sensitivity Results		
		Threshold Value
Sensitivity	97.5%	1.790
Specificity	45.07%	

ROC 97.5% Specificity

The fixed 97.5% specificity results were mediocre, as seen in **Table 80**.

Table 80.

Viewbox– Clavicles -7- ROC 97.5% Specificity Results		
		Threshold Value
Sensitivity	59.78%	1.107
Specificity	97.5%	

Summary

Time

The total time for the Flexscan3D comparison was approximately 45 hours for 2294 iterations. This is an average iteration time of 1 minute and 7 seconds. The total time for all of the Viewbox comparisons were 81 days, 17 hours and 48 minutes for 243,624 iterations. Average iteration times ranged from 1 minute and 7 seconds to as low as 13 seconds. The unhollowed models ran the slowest, with average iteration times of 1 minute and 7 seconds, and 49 seconds respective to the different parameters of 'Exact Slow' and 'Exact Normal'. The hollowed models ran considerably faster with an average iteration time of 14 seconds, regardless of parameter. The average analysis time of each test condition was approximately 2 hours, for a total of 20 hours for every condition.

Flexscan3D versus Viewbox Results

For the LCV method, the Flexscan3D results were considerably better than either of the Viewbox conditions tested, though the sensitivity was mediocre and the specificity middling. Similarly, the PPV and NPV for Flexscan3D were mediocre, but well above the poor Viewbox results. For the ROC optimal results, the sensitivities for all comparison types were similar and good, though the Flexscan3D results were still the best. For the specificities, however, the Flexscan3D results were significantly better with a good result while the Viewbox results were both mediocre. The PPV values for all the ROC optimal results were poor, though the Flexscan3D value was four times the Viewbox. The NPV values, however, were all excellent with the Flexscan3D result almost reaching 100%. (**Tables 81, 82 & 83**)

All LCV Results

As the Flexscan3D and Viewbox results have been compared in the section above, this section will focus only on the LCV results for the six remaining Viewbox parameter sets. Generally, the LCV results were all poor to abysmal with only two parameter sets rising to mediocre in terms of sensitivity and PPV: 5 (Aligned - Hollowed – Without Normals - Exact Normal) and 6 (Aligned - Hollowed - Without

Normals - Exact Slow). Both parameter sets, however, had poor specificity and NPV. (**Table 84**)

All ROC Results

As the Flexscan3D and Viewbox results have been compared in the section above, this section will focus only on the ROC results for the six remaining Viewbox parameter sets. The optimal ROC sensitivity and specificity rates were generally good with the exception of the unhollowed models run both 'Exact Normal' and 'Exact Slow,' which were mediocre. The PPV rates, however, were very poor across the board with the highest value of any parameter set being 12.42%. The NPV rates were exceptional with the lowest value of 99.75%. The best 97.5% fixed sensitivity rate was parameter set 5 (Aligned - Hollowed – Without Normals - Exact Normal) at 63.68%. The best 97.5% fixed specificity rate was parameter set 7 (Aligned - Hollowed - with Normals - Exact Normal) at 69.75%. (**Tables 85 & 86**)

Overall Optimal Method

Of the two comparison methods and two analysis methods, there is no clear stand out best result, demonstrating that clavicles are harder to pair-match. Of the LCV results, Viewbox parameter sets 5 (Aligned - Hollowed – Without Normals - Exact Normal) and 6 (Aligned - Hollowed - Without Normals -Exact Slow) produced the best results, comparable in all ways except for parameter set 6 achieving a slightly higher NPV. Of the ROC results, the majority of the hollowed results were similar and decent in terms of sensitivity and specificity. However, due to the incredibly poor PPV rates, as well as both the 97.5% fixed sensitivity and specificity ROC values, the best two were Viewbox parameter sets 5 (Aligned - Hollowed – Without Normals - Exact Normal) and 7 (Aligned - Hollowed – With Normals - Exact Normal). Thus, though neither method is great, the two optimal methods are LCV analysis with parameter set 6 (Aligned - Hollowed - Without Normals -Exact Slow) and ROC analysis with parameter set 5 (Aligned - Hollowed – Without Normals - Exact Normal).

Table 81.

Comparison	Batch	LCV Sensitivity	LCV Specificity	ROC (Optimal) Sensitivity	ROC (Optimal) Specificity
Flexscan3D (99)	Unhollowed	81.79%	57.89%	94.44%	92.16%
Viewbox (99)	Aligned - Unhollowed - Exact Normal	37.74%	43.48%	88.89%	70.46%
Viewbox (99)	Aligned - Unhollowed - Exact Slow	36.73%	36%	88.89%	70.37%

Table 82.

Comparison	Batch	LCV - PPV	LCV - NPV	ROC (Optimal) - PPV	ROC (Optimal) - NPV
Flexscan3D (99)	Unhollowed	75.76%	66.67%	16.11%	99.9%
Viewbox (99)	Aligned - Unhollowed - Exact Normal	43.48%	37.74%	4.57%	99.79%
Viewbox (99)	Aligned - Unhollowed - Exact Slow	36%	36.73%	4.57%	99.74%

Table 83.

Comparison	Batch	ROC (Optimal) Sensitivity	ROC (Optimal) Specificity	ROC (Fixed 97.5 Sens) Sensitivity	ROC (Fixed 97.5 Sens) Specificity	ROC (Fixed 97.5 Spec) Sensitivity	ROC (Fixed 97.5 Spec) Specificity
Flexscan3D (99)	Unhollowed	94.44%	92.16%	97.5%	80.73%	75%	97.5%
Viewbox	Aligned - Unhollowed - Exact Normal	4.57%	99.79%	97.5%	37.11%	30.56%	97.5%
Viewbox	Aligned - Unhollowed - Exact Slow	4.57%	99.74%	97.5%	25.95%	27.78%	97.5%

Table 84.

Comparison	Batch	LCV Sensitivity	LCV Specificity	LCV - PPV	LCV - NPV
Viewbox	Aligned - Unhollowed - Exact Normal	30.53%	3.45%	41.67%	2.15%
Viewbox	Aligned - Unhollowed - Exact Slow	25.37%	1.85%	39.08%	0.99%
Viewbox	Aligned - Hollowed - w/o Normals - Exact Normal	65.82%	14.29%	81.25%	6.9%
Viewbox	Aligned - Hollowed - w/o Normals - Exact Slow	64.56%	14.29%	80.95%	14.29%
Viewbox	Aligned - Hollowed - w/ Normals - Exact Normal	60.25%	3.57%	78.23%	1.54%
Viewbox	Aligned - Hollowed - w/ Normals - Exact Slow	59.21%	8.11%	72.58%	4.62%

Table 85.

Comparison	Batch	ROC (Optimal) Sensitivity	ROC (Optimal) Specificity	ROC (Fixed 97.5 Sens) Sensitivity	ROC (Fixed 97.5 Sens) Specificity	ROC (Fixed 97.5 Spec) Sensitivity	ROC (Fixed 97.5 Spec) Specificity
Viewbox	Aligned - Unhollowed - Exact Normal	82.61%	73.81	97.5%	33.1%	29.35%	97.5%
Viewbox	Aligned - Unhollowed - Exact Slow	84.78%	69.31%	97.5%	26.55%	25%	97.5%
Viewbox	Aligned - Hollowed - w/o Normals - Exact Normal	85.56%	93.66%	97.5%	63.68%	67.78%	97.5%
Viewbox	Aligned - Hollowed - w/o Normals - Exact Slow	86.67%	91.92%	97.5%	54.13%	63.33%	97.5%
Viewbox	Aligned - Hollowed - w/ Normals - Exact Normal	88.04%	92.01%	97.5%	50.12%	69.75%	97.5%
Viewbox	Aligned - Hollowed - w/ Normals - Exact Slow	88.04%	89.84%	97.5%	45.07%	59.78%	97.5%

Table 86.

Comparison	Batch	ROC (Optimal) Sensitivity	ROC (Optimal) Specificity	ROC (Optimal) PPV	ROC (Optimal) NPV
Viewbox	Aligned - Unhollowed - Exact Normal	82.61%	73.81	3.17%	99.75%
Viewbox	Aligned - Unhollowed - Exact Slow	84.78%	69.31%	2.79%	99.77%
Viewbox	Aligned - Hollowed - w/o Normals - Exact Normal	85.56%	93.66%	12.42%	99.83%
Viewbox	Aligned - Hollowed - w/o Normals - Exact Slow	86.67%	91.92%	10.13%	99.84%
Viewbox	Aligned - Hollowed - w/ Normals - Exact Normal	88.04%	92.01%	10.28%	99.86%
Viewbox	Aligned - Hollowed - w/ Normals - Exact Slow	88.04%	89.84%	8.27%	99.86%

Temporals

Flexscan3D

For the Flexscan3D comparison, two different parameters sets were explored which will be explained in each section. All models were unhollowed. The initial comparison was done by Monika Lay and thus no time per iteration data was recorded nor were her computer specifications (Lay, 2014). However, her estimated total time for the comparison was just under 12 full working days for 8385 iterations (Lay, 2014). This is approximately 46 seconds an iteration, assuming a nine-hour workday. As certain models were corrected or excluded by the author, only a certain portion of these iterations were used by the author.

1 - Unhollowed – All Models

A total of 124 unhollowed temporals were used for the first parameter set. Assuming the previous estimated iteration speed, this would have taken approximately 49 hours, 6 minutes and 18 seconds, or in other words, 2 continuous days, 1 hour, 6 minutes and 18 seconds for 3843 iterations. The analysis of the data was done by the author and took approximately 2 hours.

Lowest Common Value Results

All the LCV results were excellent or ideal, with the exception of the mediocre NPV (**Table 87 & 88**).

Table 87.

Flexscan3D - Temporals -1- LCV Results	
Sensitivity	98.36%
Specificity	100%
Positive Predictive Value	100%
Negative Predictive Value	50%

Table 88.

Flexscan3D – Temporals -1- LCV Matches	
True positives	120
False negatives	2
False positives	0
True negatives	2

ROC Optimal

The ROC optimal results were excellent, with a nearly perfect and valid AUC. The PPV was good, while the NPV was excellent. (**Tables 89 & 90**)

Table 89.

Flexscan3D – Temporals -1- ROC Optimal Results				
		Threshold Value	**AUC**	**p-value**
Sensitivity	98.36%	0.688	0.999	<0.0001
Specificity	99.74%			
Positive Predictive Value	85.93%			
Negative Predictive Value	99.97%			

Table 90.

Flexscan3D – Temporals -1- ROC Optimal Sample Size	
True Positives	61
True Negatives	3782
Total Sample	3843

ROC 97.5% Sensitivity

The fixed 97.5% sensitivity results were excellent (**Table 91**).

Table 91.

Flexscan3D – Temporals -1- ROC 97.5% Sensitivity Results		
		Threshold Value
Sensitivity	97.5%	0.686
Specificity	99.74%	

ROC 97.5% Specificity

The fixed 97.5% specificity results were also excellent (**Table 92**).

Table 92.

Flexscan3D – Temporals -1- ROC 97.5% Specificity Results		
		Threshold Value
Sensitivity	98.36%	0.751
Specificity	97.5%	

2 - Unhollowed – Increased Negatives

As there were only two true negatives in the original batch of temporals analysed, three temporals were removed from the sample to create more true negatives and a more accurate result for the LCV results. This meant a total of 121

temporals were used. As this was part of a larger parameter set and originally compared by Monika Lay, the time calculation could only be estimated (Lay, 2014). Assuming the same, previously mentioned iteration speed, this would have taken approximately 46 hours, 44 minutes and 28 seconds, or in other words, 1 continuous day, 22 hours, 44 minutes and 28 seconds for 3658 iterations. The analysis of the data was done by the author and took approximately 2 hours.

Lowest Common Value Results

The LCV results were excellent or ideal with the exception of the NPV which was mediocre. Still, the increased negatives significantly improved the NPV from the initial NPV. (**Tables 93 & 94**).

Table 93.

Flexscan3D - Temporals -2- LCV Results	
Sensitivity	98.28%
Specificity	100%
Positive Predictive Value	100%
Negative Predictive Value	71.43%

Table 94.

Flexscan3D – Temporals -2- LCV Matches	
True positives	114
False negatives	2
False positives	0
True negatives	5

ROC Optimal

The optimal ROC results were generally excellent with an almost perfect, valid AUC. The sensitivity and specificity rates were excellent, as was the NPV. The PPV was lower, but still good. (**Tables 95 & 96**)

Table 95.

Flexscan3D – Temporals -2- ROC Optimal Results				
		Threshold Value	**AUC**	**p-value**
Sensitivity	98.28%	0.685	0.999	<0.0001
Specificity	99.75%			
Positive Predictive Value	86.39%			
Negative Predictive Value	99.97%			

Table 96.

Flexscan3D – Temporals -2- ROC Optimal Sample Size	
True Positives	58
True Negatives	3600
Total Sample	3658

ROC 97.5% Sensitivity

The fixed 97.5% sensitivity results were excellent with a nearly perfect, excellent specificity (**Table 97**).

Table 97.

Flexscan3D – Temporals -2- ROC 97.5% Sensitivity Results		
		Threshold Value
Sensitivity	97.5%	0.684
Specificity	99.76%	

ROC 97.5% Specificity

The 97.5% specificity results were also excellent, with an incredibly high sensitivity (**Table 98**).

Table 98.

Flexscan3D – Temporals -2- ROC 97.5% Specificity Results		
		Threshold Value
Sensitivity	98.28%	0.751
Specificity	97.5%	

Viewbox

For the Viewbox comparisons, ten different conditions of variable sample sizes were tested. Therefore, all the details regarding sample size, time, and parameters of the run will be listed individually along with the respective results.

1 - Aligned - Unhollowed - Exact Normal – (Flexscan3D comparable)

A total of 124 temporals, aligned and unhollowed, were run 'Exact Normal' on Amarna. This took 9 days, 21 hours and 4 minutes for 15252 iterations. This is an average time per iteration of 59 seconds. The analysis took an additional 2 hours.

Lowest Common Value Results

The sensitivity and PPV rates were both excellent, though the specificity and NPV rates were mediocre and poor respectively (**Tables 99 & 100**).

Table 99.

Viewbox - Temporals -1- LCV Results	
Sensitivity	93.33%
Specificity	50%
Positive Predictive Value	98.25%
Negative Predictive Value	20%

Table 100.

Viewbox – Temporals -1- LCV Matches	
True positives	112
False negatives	8
False positives	2
True negatives	2

ROC Optimal

The sensitivity and specificity rates were excellent and good respectively, with a high and valid AUC. The NPV was almost perfect, while the PPV was poor. (**Tables 101 & 102**)

Table 101.

Viewbox – Temporals -1- ROC Optimal Results				
		Threshold Value	**AUC**	**p-value**
Sensitivity	95.08%	0.967	0.986	<0.0001
Specificity	94.02%			
Positive Predictive Value	20.43%			
Negative Predictive Value	99.91%			

Table 102.

Viewbox – Temporals -1- ROC Optimal Sample Size	
True Positives	61
True Negatives	3782
Total Sample	3843

ROC 97.5% Sensitivity

The fixed 97.5% sensitivity results were good overall (**Table 103**).

Table 103.

Viewbox – Temporals -1- ROC 97.5% Sensitivity Results		
		Threshold Value
Sensitivity	97.5%	1.006
Specificity	89.45%	

ROC 97.5% Specificity

The 97.5% fixed specificity results were good, though not quite as good as the 97.5% fixed sensitivity results (**Table 104**).

Table 104.

Viewbox – Temporals -1- ROC 97.5% Specificity Results		
		Threshold Value
Sensitivity	86.89%	0.917
Specificity	97.5%	

2 - Aligned - Unhollowed - Exact Normal – Increased Negatives (Flexscan3D Comparable)

To achieve more accurate LCV results, three temporals were removed from the sample to create more true negatives than the original two. This reduced the sample size to 121 aligned and unhollowed temporals. Time-wise, this set of parameters was not run on its own, but as part of a larger sample. Therefore, the comparison is calculated by the above parameter set. The average time per iteration remains 59 seconds. This means 121 temporals would take approximately 9 days, 21 hours and 58 minutes for the 14520 necessary iterations, assuming the 'All Against All' setting in Viewbox.

Lowest Common Value Results

The sensitivity and PPV results were good and excellent respectively, while the specificity was mediocre and the NPV poor (**Tables 105 & 106).**

Table 105.

Viewbox - Temporals -2- LCV Results	
Sensitivity	92.98%
Specificity	71.43%
Positive Predictive Value	98.15%
Negative Predictive Value	38.46%

Table 106.

Viewbox – Temporals -2- LCV Matches	
True positives	106
False negatives	8
False positives	2
True negatives	5

ROC Optimal

The optimal ROC results were good, with high sensitivity, specificity and almost perfect NPV. The PPV was poor, however. The AUC was high and valid. (**Tables 107 & 108)**

Table 107.

Viewbox – Temporals -2- ROC Optimal Results				
		Threshold Value	**AUC**	**p-value**
Sensitivity	94.83%	0.967	0.986	<0.0001
Specificity	93.86%			
Positive Predictive Value	19.97%			
Negative Predictive Value	99.91%			

Table 108.

Viewbox – Temporals -2- ROC Optimal Sample Size	
True Positives	58
True Negatives	3600
Total Sample	3658

ROC 97.5% Sensitivity

The fixed 97.5% sensitivity results were good with a high specificity (**Table 109**).

Table 109.

Viewbox – Temporals -1- ROC 97.5% Sensitivity Results		
		Threshold Value
Sensitivity	97.5%	1.006
Specificity	89.33%	

ROC 97.5% Specificity

The fixed 97.5% specificity results were also good (**Table 110)**.

Table 110.

Viewbox – Temporals -1- ROC 97.5% Specificity Results		
		Threshold Value
Sensitivity	87.83%	0.915
Specificity	97.5%	

3 - Aligned - Unhollowed - Exact Slow (Flexscan3D Comparable)

A total of 124 temporals, aligned and unhollowed, were run 'Exact Slow' on Amarna. This took 7 days and 55 minutes for a total of 15252 iterations. This is an average time per iteration of 40 seconds. The analysis took an additional 2 hours.

Lowest Common Value Results

The sensitivity and PPV rates were good and excellent respectively, while the specificity was mediocre and the NPV very poor (**Tables 111 & 112**).

Table 111.

Viewbox - Temporals -3- LCV Results	
Sensitivity	90%
Specificity	50%
Positive Predictive Value	98.18%
Negative Predictive Value	14.29 %

Table 112.

Viewbox – Temporals -3- LCV Matches	
True positives	108
False negatives	12
False positives	2
True negatives	2

ROC Optimal

The sensitivity and specificity results for the ROC optimal were excellent and good respectively with a high and valid AUC. The PPV was very poor, while the NPV was excellent. (**Tables 113 & 114)**.

Table 113.

Viewbox – Temporals -3- ROC Optimal Results				
		Threshold Value	**AUC**	**p-value**
Sensitivity	95.08%	0.8921	0.982	<0.0001
Specificity	91.25%			
Positive Predictive Value	14.93%			
Negative Predictive Value	99.91%			

Table 114.

Viewbox – Temporals -3- ROC Optimal Sample Size	
True Positives	61
True Negatives	3782
Total Sample	3843

ROC 97.5% Sensitivity

The fixed 97.5% sensitivity results were good (**Table 115**).

Table 115.

Viewbox – Temporals -3- ROC 97.5% Sensitivity Results		
		Threshold Value
Sensitivity	97.5%	0.917
Specificity	87.76%	

ROC 97.5% Specificity

The fixed 97.5% specificity results were mediocre (**Table 116**).

Table 116.

Viewbox – Temporals -3- ROC 97.5% Specificity Results		
		Threshold Value
Sensitivity	77.05%	0.814
Specificity	97.5%	

4 - Aligned - Unhollowed - Exact Slow – Increased Negatives (Flexscan3D Comparable)

To achieve more accurate LCV results, three temporals were removed from the sample to create more true negatives than the original two. This reduced the sample size to 121 aligned and unhollowed temporals. Time-wise, this set of parameters was not run on its own but as part of a larger sample. Therefore, the comparison is calculated by the previous parameter set. The average time per iteration remains 40 seconds. This means 121 temporals would take approximately 6 days, 17 hours and 20 minutes for the 14520 necessary iterations, assuming the 'All Against All' setting in Viewbox.

Lowest Common Value Results

The sensitivity and PPV LCV results were good and excellent respectively, though the specificity was mediocre and the NPV poor (**Table 117 & 118**).

Table 117.

Viewbox - Temporals -4- LCV Results	
Sensitivity	91.07%
Specificity	55.56%
Positive Predictive Value	96.23%
Negative Predictive Value	33.33 %

Table 118.

Viewbox – Temporals -4- LCV Matches	
True positives	102
False negatives	10
False positives	4
True negatives	5

ROC Optimal

The optimal ROC results were generally excellent, with the exception of the PPV which was very poor. The AUC was high and valid. (**Tables 119 & 120**).

Table 119.

Viewbox – Temporals -4- ROC Optimal Results				
		Threshold Value	**AUC**	**p-value**
Sensitivity	96.55%	0.8921	0.983	<0.0001
Specificity	91.14%			
Positive Predictive Value	14.97%			
Negative Predictive Value	99.93%			

Table 120.

Viewbox – Temporals -4- ROC Optimal Sample Size	
True Positives	58
True Negatives	3600
Total Sample	3658

ROC 97.5% Sensitivity

The fixed 97.5% sensitivity results were good (**Table 121**).

Table 121.

Viewbox – Temporals -4- ROC 97.5% Sensitivity Results		
		Threshold Value
Sensitivity	97.5%	0.917
Specificity	87.67%	

ROC 97.5% Specificity

The fixed 97.5% specificity results, however, were mediocre (**Table 122**).

Table 122.

Viewbox – Temporals -4- ROC 97.5% Specificity Results		
		Threshold Value
Sensitivity	79.31%	0.813
Specificity	97.5%	

5 - Aligned - Hollowed - Without Normals - Exact Normal

A total of 120 temporals were aligned, hollowed and saved without normals. They were then run 'Exact Normal' on Amarna. This took 13 days, 4 hours and 43 minutes for a total of 14280 iterations. This is an average time per iteration of 1 minute and 20 seconds. The analysis took an additional 2 hours.

Lowest Common Value Results

The sensitivity and NPV LCV results were poor or very poor, while the specificity and PPV were very poor (**Tables 123 & 124**).

Table 123.

Viewbox - Temporals -5- LCV Results	
Sensitivity	5.56%
Specificity	33.33%
Positive Predictive Value	42.86%
Negative Predictive Value	3.77%

Table 124.

Viewbox – Temporals -5- LCV Matches	
True positives	6
False negatives	102
False positives	8
True negatives	4

ROC Optimal

The ROC optimal results had a low AUC and high associated p-value which invalidate the following results (**Figure 13**). Expectedly, the sensitivity was poor, while unexpectedly the specificity was good. Also, unsurprisingly the PPV was very poor, while the NPV was excellent. (**Tables 125 & 126**).

Table 125.

Viewbox – Temporals -5- ROC Optimal Results				
		Threshold Value	**AUC**	**p-value**
Sensitivity	20.69%	2.187	0.533	0.4612
Specificity	91.66%			
Positive Predictive Value	3.90%			
Negative Predictive Value	98.6%			

Table 126.

Viewbox – Temporals -5- ROC Optimal Sample Size	
True Positives	58
True Negatives	3538
Total Sample	3596

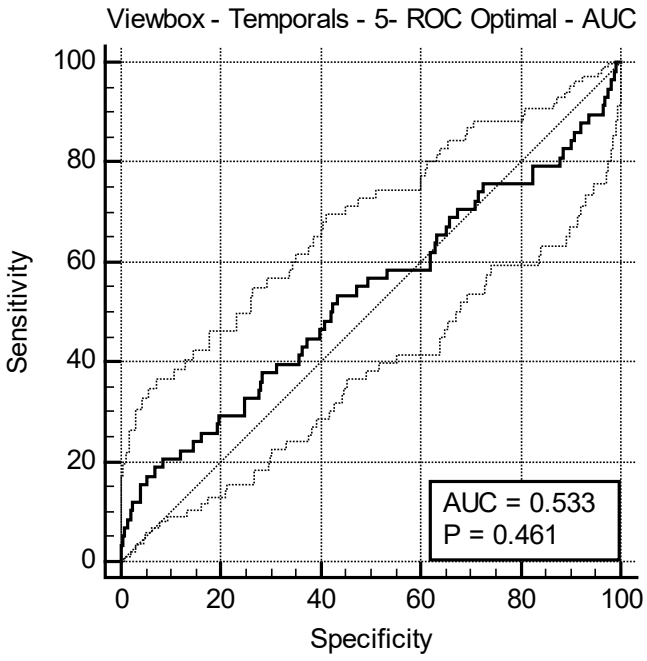

Figure 13. Invalid AUC and associated criterion for parameter set 5

ROC 97.5% Sensitivity

The fixed 97.5% sensitivity results, though invalid, were very poor (**Table 127**).

Table 127.

Viewbox – Temporals -5- ROC 97.5% Sensitivity Results		
		Threshold Value
Sensitivity	97.5%	3.328
Specificity	1.16%	

ROC 97.5% Specificity

The fixed 97.5% specificity results, also invalid, were very poor (**Table 128**).

Table 128.

Viewbox – Temporals -5- ROC 97.5% Specificity Results		
		Threshold Value
Sensitivity	12.07%	2.045
Specificity	97.5%	

6 - Aligned – Hollowed – Without Normals - Exact Slow

A total of 120 temporals were aligned, hollowed and saved without normals. They were then run 'Exact Slow' on Amarna. This took 3 days, 23 hours and 40 minutes for a total of 14280 iterations. This is an average time per iteration of 24 seconds. The analysis took an additional 2 hours.

Lowest Common Value Results

Amazingly, the specificity and PPV rates were perfect, with a high sensitivity. However, the NPV was mediocre. (**Tables 129 & 130**).

Table 129.

Viewbox - Temporals -6- LCV Results	
Sensitivity	96.55%
Specificity	100%
Positive Predictive Value	100%
Negative Predictive Value	50%

Table 130.

Viewbox – Temporals -6- LCV Matches	
True positives	112
False negatives	4
False positives	0
True negatives	4

ROC Optimal

The ROC optimal results were excellent or ideal with a high and valid AUC (**Figure 14**). The sensitivity was ideal and the specificity was excellent. The PPV was poor, while the NPV was perfect. (**Tables 131 & 132**).

Table 131.

Viewbox – Temporals -6- ROC Optimal Results				
		Threshold Value	**AUC**	**p-value**
Sensitivity	100%	1.1126	0.997	<0.0001
Specificity	96.24%			
Positive Predictive Value	30.32%			
Negative Predictive Value	100%			

Table 132.

Viewbox – Temporals -6- ROC Optimal Sample Size	
True Positives	58
True Negatives	3538
Total Sample	3596

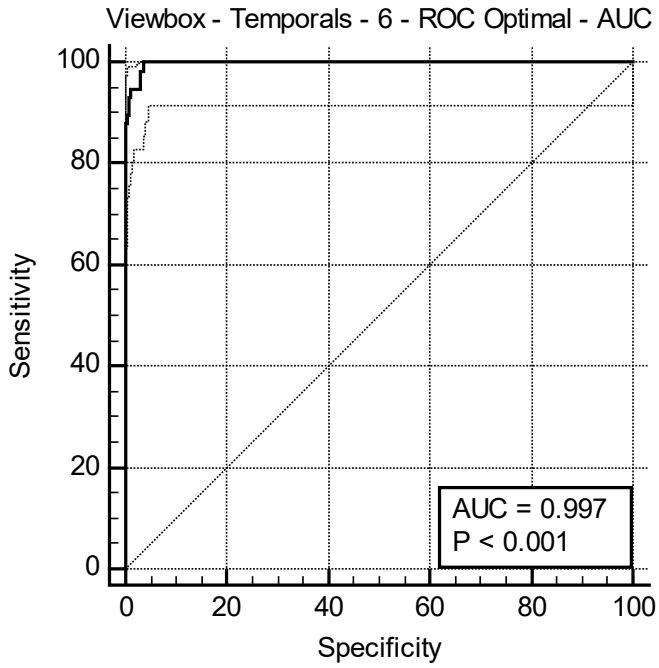

Figure 14. Almost perfect AUC, parameter set 6

ROC 97.5% Sensitivity

The fixed 97.5% sensitivity results were excellent, with the specificity over 95% (**Table 133**).

Table 133

Viewbox – Temporals -6- ROC 97.5% Sensitivity Results		
		Threshold Value
Sensitivity	97.5%	1.102
Specificity	96.86%	

ROC 97.5% Specificity

The fixed 97.5% specificity results were good, with the sensitivity just under 95% (**Table 134**).

Table 134.

Viewbox – Temporals -6- ROC 97.5% Specificity Results		
		Threshold Value
Sensitivity	94.83%	1.086
Specificity	97.5%	

7 - Aligned – Hollowed – With Normals - Exact Normal

A total of 123 temporals were aligned, hollowed and saved with normals. They were then run 'Exact Normal' on Remus. This took 6 days, 18 hours and 52 minutes for a total of 15006 iterations. This is an average time per iteration of 39 seconds. The analysis took an additional 2 hours.

Lowest Common Value Results

The LCV results were excellent with a high sensitivity, perfect specificity and perfect PPV. The NPV, however, was poor. (**Tables 135 & 136**).

Table 135.

Viewbox - Temporals -7- LCV Results	
Sensitivity	98.36%
Specificity	100%
Positive Predictive Value	100%
Negative Predictive Value	33.33%

Table 136.

Viewbox – Temporals -7- LCV Matches	
True positives	120
False negatives	2
False positives	0
True negatives	1

ROC Optimal

The optimal ROC results were excellent, with a very high and valid AUC. The PPV was mediocre, while the NPV was excellent. (**Tables 137 & 138**)

Table 137.

Viewbox – Temporals -7- ROC Optimal Results				
		Threshold Value	**AUC**	**p-value**
Sensitivity	96.72%	1.137	0.998	<0.0001
Specificity	98.82%			
Positive Predictive Value	57.28%			
Negative Predictive Value	99.94%			

Table 138.

Viewbox – Temporals -7- ROC Optimal Sample Size	
True Positives	61
True Negatives	3721
Total Sample	3782

ROC 97.5% Sensitivity

The fixed 97.5% sensitivity results were excellent (**Table 139**).

Table 139.

Viewbox – Temporals -7- ROC 97.5% Sensitivity Results		
		Threshold Value
Sensitivity	97.5%	1.201
Specificity	96.64%	

ROC 97.5% Specificity

The fixed 97.5% specificity results were also excellent (**Table 140**).

Table 140.

Viewbox – Temporals -7- ROC 97.5% Specificity Results		
		Threshold Value
Sensitivity	96.72%	1.182
Specificity	97.5%	

8 - Aligned – Hollowed – With Normals - Exact Normal – Increased Negatives

To achieve more accurate LCV results, three temporals were removed from the sample to create more true negatives than the original two. This reduced the sample size to 120 aligned, hollowed temporals which were saved with normals. Time-wise, this set of parameters was not run on its own but as part of a larger sample. Therefore, the comparison is calculated by the previous parameter set. The average time per iteration remains 39 seconds. This means 120 temporals would take approximately 6 days, 10 hours and 42 minutes for the 14280 necessary iterations, assuming the 'All Against All' setting in Viewbox.

Lowest Common Value Results

The LCV results were excellent or ideal, with the exception of the NPV which was mediocre. Still, it nearly doubled as compared to the previous parameter. (**Tables 141 & 142**)

Table 141.

Viewbox - Temporals -8- LCV Results	
Sensitivity	98.28%
Specificity	100%
Positive Predictive Value	100%
Negative Predictive Value	66.67%

Table 142.

Viewbox – Temporals -8- LCV Matches	
True positives	114
False negatives	2
False positives	0
True negatives	4

ROC Optimal

The optimal ROC results were excellent, with a high and valid AUC. The sensitivity, specificity and NPV were excellent. The PPV, however, was only mediocre. (**Tables 143 & 144**)

Table 143.

Viewbox – Temporals -8- ROC Optimal Results				
		Threshold Value	**AUC**	**p-value**
Sensitivity	96.55%	1.137	0.998	<0.0001
Specificity	98.76%			
Positive Predictive Value	56.02%			
Negative Predictive Value	99.94%			

Table 144.

Viewbox – Temporals -8- ROC Optimal Sample Size	
True Positives	58
True Negatives	3541
Total Sample	3599

ROC 97.5% Sensitivity

The fixed 97.5% sensitivity results were excellent (**Table 145**).

Table 145.

Viewbox – Temporals -8- ROC 97.5% Sensitivity Results		
		Threshold Value
Sensitivity	97.5%	1.201
Specificity	96.55%	

ROC 97.5% Specificity

The fixed 97.5% specificity results were also excellent (**Table 146**).

Table 146.

Viewbox – Temporals -8- ROC 97.5% Specificity Results		
		Threshold Value
Sensitivity	96.55%	1.178
Specificity	97.5%	

9 - Aligned - Hollowed – With Normals - Exact Slow

A total of 123 temporals were aligned, hollowed and saved with normals. They were then run 'Exact Slow' on Amarna. This took 3 days, 23 hours and 42 minutes for a total of 15006 iterations. This is an average time per iteration of 23 seconds. The analysis took an additional 2 hours.

Lowest Common Value Results

The LCV results were excellent, with a high sensitivity, perfect specificity and PPV. However, the NPV was poor. (**Tables 147 & 148**)

Table 147.

Viewbox - Temporals -9- LCV Results	
Sensitivity	96.72%
Specificity	100%
Positive Predictive Value	100%
Negative Predictive Value	20%

Table 148.

Viewbox – Temporals -9- LCV Matches	
True positives	118
False negatives	4
False positives	0
True negatives	1

ROC Optimal

The ROC optimal results were excellent, with a perfect sensitivity and high specificity. The AUC was high and valid. The PPV was poor, while the NPV was perfect. (**Tables 149 & 150**)

Table 149.

Viewbox – Temporals -9- ROC Optimal Results				
		Threshold Value	**AUC**	**p-value**
Sensitivity	100%	1.092	0.997	<0.0001
Specificity	95.06%			
Positive Predictive Value	24.88%			
Negative Predictive Value	100%			

Table 150.

Viewbox – Temporals -9- ROC Optimal Sample Size	
True Positives	61
True Negatives	3721
Total Sample	3782

ROC 97.5% Sensitivity

The fixed 97.5% sensitivity results were excellent (**Table 151**).

Table 151.

Viewbox – Temporals -9- ROC 97.5% Sensitivity Results		
		Threshold Value
Sensitivity	97.5%	1.078
Specificity	96.10%	

ROC 97.5% Specificity

The fixed 97.5% specificity results were excellent as well (**Table 152**).

Table 152.

Viewbox – Temporals -9- ROC 97.5% Specificity Results		
		Threshold Value
Sensitivity	95.08%	1.055
Specificity	97.5%	

10 - Aligned – Hollowed – With Normals - Exact Slow – Increased Negatives

To achieve more accurate LCV results, three temporals were removed from the sample to create more true negatives than the original two. This reduced the sample size to 120 aligned, hollowed temporals which were saved with normals.

Time-wise, this set of parameters was not run on its own but as part of a larger sample. Therefore, the comparison is calculated by the previous parameter set. The average time per iteration remains 23 seconds. This means 120 temporals would take approximately 3 days, 19 hours and 14 minutes for the 14280 necessary iterations, assuming the 'All Against All' setting in Viewbox.

Lowest Common Value Results

The LCV results were excellent with the exception of the mediocre NPV. The sensitivity was high and both the specificity and PPC were perfect. (**Tables 153 & 154**)

Table 153.

Viewbox - Temporals -10- LCV Results	
Sensitivity	96.55%
Specificity	100%
Positive Predictive Value	100%
Negative Predictive Value	50%

Table 154.

Viewbox – Temporals -10- LCV Matches	
True positives	112
False negatives	4
False positives	0
True negatives	4

ROC Optimal

The optimal ROC results were excellent or good. The sensitivity and NPV were perfect, while the specificity was good. The PPV, however, was poor. The AUC was high and valid. (**Tables 155 & 156**)

Table 155.

Viewbox – Temporals -10- ROC Optimal Results				
		Threshold Value	**AUC**	**p-value**
Sensitivity	100%	1.092	0.997	<0.0001
Specificity	94.92%			
Positive Predictive Value	24.36%			
Negative Predictive Value	100%			

Table 156.

Viewbox – Temporals -9- ROC Optimal Sample Size	
True Positives	58
True Negatives	3541
Total Sample	3599

ROC 97.5% Sensitivity

The fixed 97.5% sensitivity results were excellent (**Table 157**).

Table 157.

Viewbox – Temporals -9- ROC 97.5% Sensitivity Results		
		Threshold Value
Sensitivity	97.5%	1.078
Specificity	96.02%	

ROC 97.5% Specificity

The fixed 97.5% specificity results were good (**Table 158**).

Table 158.

Viewbox – Temporals -9- ROC 97.5% Specificity Results		
		Threshold Value
Sensitivity	94.83%	1.054
Specificity	97.5%	

Summary

Time

The total time for the Flexscan3D comparison was approximately 49 hours, 6 minutes and 18 seconds, or in other words, 2 continuous days, 1 hour, 6 minutes and 18 seconds for 3843 iterations. This is an average iteration time of 46 seconds, again assuming the calculation time information as described by Monika Lay (Lay, 2014). The total time for all of the Viewbox comparisons was 44 days, 20 hours and 56 minutes for 89,076 iterations. Average iteration times ranged from 1 minute and 20 seconds to as low as 23 seconds. The aligned, hollowed and saved without normals models run 'Exact Normal' ran the slowest with the average iteration time of 1 minute and 20 seconds. The unhollowed models followed with the second and third slowest iteration times, with average iteration times of 56 seconds and 40 seconds respective to the different parameters of 'Exact Normal' and 'Exact Slow'. The hollowed models generally ran considerably faster with an average iteration time of 28 seconds, with the noted exception of the aligned, hollowed and saved without normals models run 'Exact Normal'. The analysis time of each test condition averaged approximately 2 hours, for a total of 24 hours for every condition.

Flexscan3D verses Viewbox Results

For the LCV method, both Flexscan3D results were overall better than the four different Viewbox conditions tested, though all had good or excellent sensitivity and PPV rates. The Flexscan3D results were considerably better in terms of specificity (100% versus Viewbox's 50 - 71.42%). Both Flexscan3D and Viewbox had poor to mediocre NPV rates, though the Flexscan3D results were significantly better. For the ROC optimal results, the sensitivities and specificities for all comparison types were similar and good or excellent, though the Flexscan3D results were still the best. The Flexscan3D PPV and NPV rates were both good, with nearly perfect NPV and excellent PPV. All of the Viewbox parameter sets, however, had poor PPV rates (sub 21%), though they all had nearly perfect NPV rates. (**Tables 159, 160 & 161**)

All LCV Results

As the Flexscan3D and Viewbox results were compared in the section above, this section will focus only on the LCV results for the six remaining Viewbox parameter sets. Generally, the LCV results were all good or excellent, with high sensitivity and specificity rates. The glaring exception was parameter set 5 (Aligned - Hollowed - Without Normals - Exact Normal) which was poor or very poor: 5.56% sensitive and 33.3% specific. The LCV PPV rates were all good or excellent as well, again with the exception of parameter set 5 which was poor. The LCV NPV rates, however, were all mediocre or poor; the best NPV, parameter set 8 (Aligned – Hollowed – With Normals - Exact Normal – Increased Negatives) reached only 66.67%. **(Table 162)**

All ROC Results

As the Flexscan3D and Viewbox results were compared above, this section will focus only on the ROC results for the six remaining Viewbox parameter sets. The optimal ROC sensitivity and specificity rates were all good with the exception of parameter set 5 (Aligned - Hollowed - Without Normals - Exact Normal), which had a poor sensitivity but a good specificity. The PPV rates were mediocre to poor with parameter set 7 (Aligned – Hollowed – With Normals - Exact Normal) reaching the highest value at 57.28%, followed closely by parameter set 8 (Aligned – Hollowed – With Normals - Exact Normal – Increased Negatives) at 56.06%. Again, parameter set 5 was very poor, with a PPV of only 3.9%. All of the NPV rates were exceptional with the lowest value of 98.76% for parameter 5 (Aligned - Hollowed - Without Normals - Exact Normal). All of the 97.5% fixed sensitivity rates were excellent and above 96%, with the exception of parameter set 5 (Aligned - Hollowed - Without Normals - Exact Normal) at a very poor 1.16%. Similarly, all the 97.5% fixed specificity rates were good or excellent and above 94%, with the exception of parameter set 5 (Aligned - Hollowed - Without Normals - Exact Normal) at 12.07%. (**Tables 163 & 164)**

Overall Optimal Method

Of the two comparison methods and two analysis methods, generally all the results were quite good, indicating that temporal bones pair-match well. Of the LCV results, Flexscan3D parameter set 2 (Unhollowed – Increased Negatives) and Viewbox parameter set 8 (Aligned – Hollowed – With Normals - Exact Normal – Increased Negatives) produced the best results, identical except for Flexscan3D parameter set 2 achieving a slightly higher NPV. All of the sensitivity, specificity, and PPV rates were above 98%. Of the ROC results, both Flexscan3D sets and all the hollowed Viewbox parameter sets were similar and good in terms of sensitivity and specificity, with the noted exception of Viewbox parameter set 5 (Aligned - Hollowed - Without Normals - Exact Normal). Both Flexscan3D parameter sets had good PPV at above 85% while the closest Viewbox parameter set was 7 (Aligned – Hollowed – With Normals - Exact Normal) at 57.28%, followed closely by parameter set 8 (Aligned – Hollowed – With Normals - Exact Normal – Increased Negatives) at 56.06%. All of the NPV values, regardless of Flexscan3D or Viewbox, were excellent. Thus, though most of the methods produce good results, the two optimal methods are the Flexscan3D parameter set 2, regardless of LCV or ROC, and Viewbox parameter set 8 (Aligned – Hollowed – With Normals - Exact Normal – Increased Negatives) using LCV, though the ROC results are close.

Table 159.

Comparison	Batch	LCV Sensitivity	LCV Specificity	ROC (Optimal) Sensitivity	ROC (Optimal) Specificity
Flexscan3D (124)	Unhollowed	98.36%	100%	98.36%	99.74%
Flexscan3D (121 - Negs)	Unhollowed	98.28%	100%	98.28%	99.75%
Viewbox (124)	Aligned - Unhollowed - Exact Normal	93.33%	50%	95.08%	94.02%
Viewbox (121 - Negs)	Aligned - Unhollowed - Exact Normal	92.98%	71.43%	94.83%	93.86%
Viewbox (124)	Aligned - Unhollowed - Exact Slow	90%	50%	95.08%	91.25%
Viewbox (121 - Negs)	Aligned - Unhollowed - Exact Slow	91.07%	55.56%	96.55%	91.14%

Table 160.

Comparison	Batch	LCV - PPV	LCV - NPV	ROC (Optimal) - PPV	ROC (Optimal) - NPV
Flexscan3D (124)	Unhollowed	100%	50%	85.93%	99.97%
Flexscan3D (121 - Negs)	Unhollowed	100%	71.43%	86.39%	99.97%
Viewbox (124)	Aligned - Unhollowed - Exact Normal	98.25%	20%	20.43%	99.91%
Viewbox (121 - Negs)	Aligned - Unhollowed - Exact Normal	98.15%	38.46%	19.97%	99.91%
Viewbox (124)	Aligned - Unhollowed - Exact Slow	98.18%	14.29 %	14.93%	99.91%
Viewbox (121 - Negs)	Aligned - Unhollowed - Exact Slow	96.23%	33.33 %	14.97%	99.93%

Table 161.

Comparison	Batch	ROC (Optimal) Sensitivity	ROC (Optimal) Specificity	ROC (Fixed 97.5 Sens) Sensitivity	ROC (Fixed 97.5 Sens) Specificity	ROC (Fixed 97.5 Spec) Sensitivity	ROC (Fixed 97.5 Spec) Specificity
Flexscan3D (124)	Unhollowed	98.36%	99.74%	97.5%	99.74%	98.36%	97.5%
Flexscan3D (121 - Negs)	Unhollowed	98.28%	99.75%	97.5%	99.76%	98.28%	97.5%
Viewbox (124)	Aligned - Unhollowed - Exact Normal	95.08%	94.02%	97.5%	89.45%	86.89%	97.5%
Viewbox (121 - Negs)	Aligned - Unhollowed - Exact Normal	94.83%	93.86%	97.5%	89.33%	87.83%	97.5%
Viewbox (124)	Aligned - Unhollowed - Exact Slow	95.08%	91.25%	97.5%	87.76%	77.05%	97.5%
Viewbox (121 - Negs)	Aligned - Unhollowed - Exact Slow	96.55%	91.14%	97.5%	87.67%	79.31%	97.5%

Table 162.

Comparison	Batch	LCV Sensitivity	LCV Specificity	LCV - PPV	LCV - NPV
Viewbox (120)	Aligned - Hollowed - w/o Normals - Exact Normal	5.56%	33.3%	42.86%	3.77%
Viewbox (120)	Aligned - Hollowed - w/o Normals - Exact Slow	96.55%	100%	100%	50%
Viewbox (123)	Aligned - Hollowed - w/ Normals - Exact Normal	98.36%	100%	100%	33.33%
Viewbox (120 - Negs)	Aligned - Hollowed - w/ Normals - Exact Normal	98.28%	100%	100%	66.67%
Viewbox (123)	Aligned - Hollowed - w/ Normals - Exact Slow	96.72%	100%	100%	20%
Viewbox (120 - Negs)	Aligned - Hollowed - w/ Normals - Exact Slow	96.55%	100%	100%	50%

Table 163.

Comparison	Batch	ROC (Optimal) Sensitivity	ROC (Optimal) Specificity	ROC (Fixed 97.5 Sens) Sensitivity	ROC (Fixed 97.5 Sens) Specificity	ROC (Fixed 97.5 Spec) Sensitivity	ROC (Fixed 97.5 Spec) Specificity
Viewbox (120)	Aligned - Hollowed - w/o Normals - Exact Normal	20.69%	91.66%	97.5%	1.16%	12.04%	97.5%
Viewbox (120)	Aligned - Hollowed - w/o Normals - Exact Slow	100%	96.24%	97.5%	96.86%	94.83%	97.5%
Viewbox (123)	Aligned - Hollowed - w/ Normals - Exact Normal	96.72%	98.82%	97.5%	96.64%	96.72%	97.5%
Viewbox (120 - Negs)	Aligned - Hollowed - w/ Normals - Exact Normal	96.55%	98.76%	97.5%	96.55%	96.55%	97.5%
Viewbox (123)	Aligned - Hollowed - w/ Normals - Exact Slow	100%	95.06%	97.5%	96.1%	95.08%	97.5%
Viewbox (120 - Negs)	Aligned - Hollowed - w/ Normals - Exact Slow	100%	94.92%	97.5%	96.02%	94.08	97.5%

Table 164.

Comparison	Batch	ROC (Optimal) Sensitivity	ROC (Optimal) Specificity	ROC (Optimal) PPV	ROC (Optimal) NPV
Viewbox (120)	Aligned - Hollowed - w/o Normals - Exact Normal	20.69%	91.66%	3.9%	98.6%
Viewbox (120)	Aligned - Hollowed - w/o Normals - Exact Slow	100%	96.24%	30.32%	100%
Viewbox (123)	Aligned - Hollowed - w/ Normals - Exact Normal	96.72%	98.82%	57.28%	99.94%
Viewbox (120 - Negs)	Aligned - Hollowed - w/ Normals - Exact Normal	96.55%	98.76%	56.02%	99.94%
Viewbox (123)	Aligned - Hollowed - w/ Normals - Exact Slow	100%	95.06%	24.88%	100%
Viewbox (120 - Negs)	Aligned - Hollowed - w/ Normals - Exact Slow	100%	94.92%	24.36%	100%

Calcanei

Flexscan3D

For the Flexscan3D comparison, three different parameters sets were explored. These parameter sets are unique as they include both whole, entire surface bone models and models where the surface scanning created essentially fragmented surface models. These are separated out in the different parameter sets, as will be explained in a similar vein to hollowing. The initial comparisons were done by Mary Gutekunst and thus no time data were recorded nor were her computer specifications (Gutekunst, 2015).

1 - Mixed Hollowed – All Models (Mixed Fragmented)

A total of 149 calcanei were used for the first parameter set. Sixty-two were unhollowed and 87 were hollowed due to the respective initial scan type (CT scanning versus surface scanning). Of the 149, 68 were considered whole, entire surface models. The rest were partial, or fragmented surface scans. There was no time or hardware information recorded, as previously mentioned (Gutekunst, 2015). The analysis of the data was done by the author and took approximately 2 hours.

Lowest Common Value Results

The LCV results were ideal with 100% sensitivity, specificity, PPV and NPV rates (**Tables 165 & 166**).

Table 165.

Flexscan3D - Calcanei -1- LCV Results	
Sensitivity	100%
Specificity	100%
Positive Predictive Value	100%
Negative Predictive Value	100%

Table 166.

Flexscan3D – Calcanei -1- LCV Matches	
True positives	142
False negatives	0
False positives	0
True negatives	7

ROC Optimal

The optimal ROC results were generally excellent. The sensitivity and specificity were both excellent, with a high and valid AUC. The NPV was almost perfect, while the PPV was poor. (**Tables 167 & 168**)

Table 167.

Flexscan3D – Calcanei -1- ROC Optimal Results				
		Threshold Value	**AUC**	**p-value**
Sensitivity	98.59%	0.791	0.998	<0.0001
Specificity	96.88%			
Positive Predictive Value	29.06%			
Negative Predictive Value	99.98%			

Table 168.

Flexscan3D – Calcanei -1- ROC Optimal Sample Size	
True Positives	71
True Negatives	5479
Total Sample	5550

ROC 97.5% Sensitivity

The fixed 97.5% sensitivity results were excellent (**Table 169**).

Table 169.

Flexscan3D – Calcanei-1- ROC 97.5% Sensitivity Results		
		Threshold Value
Sensitivity	97.5%	0.79
Specificity	96.94%	

ROC 97.5% Specificity

The fixed specificity results were also excellent (**Table 170**).

Table 170.

Flexscan3D – Calcanei -1- ROC 97.5% Specificity Results		
		Threshold Value
Sensitivity	97.18%	0.765
Specificity	97.5%	

2 - Mixed Hollowed – Whole Surface Models

A total of 68 calcanei were used for this parameter set. Sixty-two were unhollowed and six were hollowed due to the respective initial scan type (CT scanning versus surface scanning). All models had their entire surface intact. There

was no time information recorded, as previously mentioned (Gutekunst, 2015). The analysis of the data was done by the author and took approximately 1 hour.

Lowest Common Value Results

The sensitivity, PPV and NPV were all excellent, while the specificity was mediocre (**Tables 171 & 172**).

Table 171.

Flexscan3D - Calcanei -2- LCV Results	
Sensitivity	100%
Specificity	80%
Positive Predictive Value	96.67%
Negative Predictive Value	100%

Table 172.

Flexscan3D – Calcanei -2- LCV Matches	
True positives	58
False negatives	0
False positives	2
True negatives	8

ROC Optimal

The optimal ROC results were good to ideal, with a perfect sensitivity and a good specificity. The NPV was perfect. The PPV, however, was poor. The AUC was high and valid. (**Tables 173 & 174**)

Table 173.

Flexscan3D – Calcanei -2- ROC Optimal Results				
		Threshold Value	**AUC**	**p-value**
Sensitivity	100%	0.746	0.994	<0.0001
Specificity	91.81%			
Positive Predictive Value	23.99%			
Negative Predictive Value	100%			

Table 174.

Flexscan3D – Calcanei -2- ROC Optimal Sample Size	
True Positives	29
True Negatives	1123
Total Sample	1152

ROC 97.5% Sensitivity

The fixed 97.5% sensitivity results were good (**Table 175**).

Table 175.

Flexscan3D – Calcanei-2- ROC 97.5% Sensitivity Results		
		Threshold Value
Sensitivity	97.5%	0.744
Specificity	91.81%	

ROC 97.5% Specificity

The fixed 97.5% specificity results were also good, though not as good as the fixed 97.5% sensitivity results (**Table 176**).

Table 176.

Flexscan3D – Calcanei -2- ROC 97.5% Specificity Results		
		Threshold Value
Sensitivity	89.66%	0.677
Specificity	97.5%	

3 - Unhollowed

A total of 62 calcanei were used for this parameter set. All were unhollowed. All models also had their entire surface intact. There was no time information recorded, as previously mentioned (Gutekunst, 2015). The analysis of the data was done by the author and took approximately 1 hour.

Lowest Common Value Results

The LCV results were ideal, with perfect sensitivity, specificity, PPV and NPV rates (**Tables 177 & 178**).

Table 177.

Flexscan3D - Calcanei -3- LCV Results	
Sensitivity	100%
Specificity	100%
Positive Predictive Value	100%
Negative Predictive Value	100%

Table 178.

Flexscan3D – Calcanei -3- LCV Matches	
True positives	56
False negatives	0
False positives	2
True negatives	6

ROC Optimal

The optimal ROC results were good, with perfect sensitivity and a high specificity. The NPV was perfect; the PPV was poor. The AUC was high and valid. (**Tables 179 & 180**)

Table 179.

Flexscan3D – Calcanei -3- ROC Optimal Results				
		Threshold Value	**AUC**	**p-value**
Sensitivity	100%	0.746	0.992	<0.0001
Specificity	90.13%			
Positive Predictive Value	23.35%			
Negative Predictive Value	100%			

Table 180.

Flexscan3D – Calcanei -3- ROC Optimal Sample Size	
True Positives	28
True Negatives	932
Total Sample	960

ROC 97.5% Sensitivity

The fixed 97.5% sensitivity results were good (**Table 181**).

Table 181.

Flexscan3D – Calcanei-3- ROC 97.5% Sensitivity Results		
		Threshold Value
Sensitivity	97.5%	0.744
Specificity	90.13%	

ROC 97.5% Specificity

The fixed 97.5% specificity results were also good (**Table 182**).

Table 182.

Flexscan3D – Calcanei -3- ROC 97.5% Specificity Results		
		Threshold Value
Sensitivity	89.29%	0.667
Specificity	97.5%	

Viewbox

For the Viewbox comparisons, seven different conditions of variable sample sizes were tested. Therefore, all the details regarding sample size, time, and parameters of the run will be listed individually along with the respective results.

1 - Aligned - Hollowed – With Normals - Exact Normal (Flexscan3D Comparable)

A total of 62 calcanei aligned, hollowed, and saved with normals were run 'Exact Normal' on Amarna. This took 1 day, 12 hours, 46 minutes and 10 seconds for 3782 iterations. This is an average iteration time of 35 seconds. All models were whole, entire surfaces. The analysis took an additional 1 hour.

Lowest Common Value Results

The specificity and PPV were perfect, while the sensitivity was good. The NPV, however, was mediocre. (**Tables 183 & 184**)

Table 183.

Viewbox - Calcanei-1- LCV Results	
Sensitivity	92.86%
Specificity	100%
Positive Predictive Value	100%
Negative Predictive Value	60%

Table 184.

Viewbox – Calcanei -1- LCV Matches	
True positives	52
False negatives	4
False positives	0
True negatives	6

ROC Optimal

The optimal ROC results were good, with high sensitivity and specificity rates. The NPV was almost perfect, while the PPV was poor. The AUC was high and valid. (**Tables 185 & 186**)

Table 185.

Viewbox – Calcanei -1- ROC Optimal Results				
		Threshold Value	**AUC**	**p-value**
Sensitivity	92.86%	1.1571	0.975	<0.0001
Specificity	93.03%			
Positive Predictive Value	28.60%			
Negative Predictive Value	99.76%			

Table 186.

Viewbox – Calcanei -1- ROC Optimal Sample Size	
True Positives	28
True Negatives	932
Total Sample	960

ROC 97.5% Sensitivity

The fixed 97.5% sensitivity results were mediocre (**Table 187**).

Table 187.

Viewbox – Calcanei -1- ROC 97.5% Sensitivity Results		
		Threshold Value
Sensitivity	97.5%	1.506
Specificity	58.69%	

ROC 97.5% Specificity

The 97.5% fixed specificity results were good (**Table 188**).

Table 188.

Viewbox – Calcanei -1- ROC 97.5% Specificity Results		
		Threshold Value
Sensitivity	85.71%	1.049
Specificity	97.5%	

2 - Aligned - Unhollowed - Exact Normal (Flexscan3D Comparable)

A total of 62 calcanei, aligned and unhollowed, were run 'Exact Normal' on Elena. This took 1 day, 15 hours and 16 minutes for 3906 iterations. This is an average time per iteration of 36 seconds. All models were whole, entire surfaces. The analysis took approximately 1 hour.

Lowest Common Value Results

The specificity and PPV were perfect, while the sensitivity was good. The NPV, however, was only mediocre. (**Tables 189 & 190**)

Table 189.

Viewbox - Calcanei-2- LCV Results	
Sensitivity	92.86%
Specificity	100%
Positive Predictive Value	100%
Negative Predictive Value	60%

Table 190.

Viewbox – Calcanei -2- LCV Matches	
True positives	52
False negatives	4
False positives	0
True negatives	6

ROC Optimal

The sensitivity was mediocre, while the specificity was good. The NPV was almost perfect, while the PPV was poor. The AUC was high and valid. (**Tables 191 & 192**)

Table 191.

Viewbox – Calcanei -2- ROC Optimal Results				
		Threshold Value	**AUC**	**p-value**
Sensitivity	78.57%	0.630	0.932	<0.0001
Specificity	94.85%			
Positive Predictive Value	31.45%			
Negative Predictive Value	99.32%			

Table 192.

Viewbox – Calcanei -2- ROC Optimal Sample Size	
True Positives	28
True Negatives	932
Total Sample	960

ROC 97.5% Sensitivity

The fixed 97.5% sensitivity results were poor (**Table 193**).

Table 193.

Viewbox – Calcanei -2- ROC 97.5% Sensitivity Results		
		Threshold Value
Sensitivity	97.5%	0.841
Specificity	34.76%	

ROC 97.5% Specificity

The 97.5% fixed specificity results were mediocre, but far better than the 97.5% fixed sensitivity results (**Table 194**).

Table 194.

Viewbox – Calcanei -2- ROC 97.5% Specificity Results		
		Threshold Value
Sensitivity	64.29%	0.613
Specificity	97.5%	

3 - Aligned - Unhollowed - Exact Slow (Flexscan3D Comparable)

A total of 62 calcanei, aligned and unhollowed, were run 'Exact Slow' on Elena. This took 1 day, 11 hours and 56 minutes for 3906 iterations. This is an average time per iteration of 33 seconds. All models were whole, entire surfaces. The analysis took approximately 1 hour.

Lowest Common Value Results

The specificity and PPV were perfect. The sensitivity was good, while the NPV was only mediocre. (**Table 195 & 196**)

Table 195.

Viewbox - Calcanei-3- LCV Results	
Sensitivity	89.29%
Specificity	100%
Positive Predictive Value	100%
Negative Predictive Value	50%

Table 96.

Viewbox – Calcanei -3- LCV Matches	
True positives	50
False negatives	6
False positives	0
True negatives	6

ROC Optimal

The specificity was good, while the sensitivity was only mediocre. The PPV was poor, while the NPV was almost perfect. The AUC was high and valid. (**Tables 197 & 198**)

Table 197.

Viewbox – Calcanei -3- ROC Optimal Results				
		Threshold Value	**AUC**	**p-value**
Sensitivity	78.57%	0.641	0.913	<0.0001
Specificity	92.60%			
Positive Predictive Value	24.20%			
Negative Predictive Value	99.30%			

Table 198.

Viewbox – Calcanei -3- ROC Optimal Sample Size	
True Positives	28
True Negatives	932
Total Sample	960

ROC 97.5% Sensitivity

The fixed 97.5% sensitivity results were poor (**Table 199**).

Table 199.

Viewbox – Calcanei -3- ROC 97.5% Sensitivity Results		
		Threshold Value
Sensitivity	97.5%	0.844
Specificity	38.73%	

ROC 97.5% Specificity

The 97.5% fixed specificity results were mediocre, though considerably better than the 97.5% fixed sensitivity results (**Table 200**).

Table 200.

Viewbox – Calcanei -3- ROC 97.5% Specificity Results		
		Threshold Value
Sensitivity	64.29%	0.605
Specificity	97.5%	

4 - Unaligned - Unhollowed - Exact Normal (Flexscan3D Comparable)

A total of 62 calcanei, unaligned and unhollowed, were run 'Exact Normal' on Elena. This was to test the effects of alignment, or pre-registration. It took 2 days, 4 hours and 31 minutes for 3906 iterations. This is an average time per iteration of 48 seconds. All models were whole, entire surfaces. The analysis took approximately 1 hour.

Lowest Common Value Result

The sensitivity was good, while the specificity and PPV were both perfect. The NPV, however, was only mediocre. (**Tables 201 & 202**)

Table 201.

Viewbox – Calcanei -4- LCV Results	
Sensitivity	89.29%
Specificity	100%
Positive Predictive Value	100%
Negative Predictive Value	50%

Table 202.

Viewbox – Calcanei -4- LCV Matches	
True positives	50
False negatives	6
False positives	0
True negatives	6

ROC Optimal

The sensitivity was mediocre, but the specificity was excellent. The PPV was mediocre, while the NPV was almost perfect. The AUC was high and valid. (**Tables 203 & 204**)

Table 203.

Viewbox – Calcanei -4- ROC Optimal Results				
		Threshold Value	**AUC**	**p-value**
Sensitivity	82.14%	0.693	0.950	<0.0001
Specificity	97.21%			
Positive Predictive Value	46.96%			
Negative Predictive Value	99.45%			

Table 204.

Viewbox – Calcanei -4- ROC Optimal Sample Size	
True Positives	28
True Negatives	932
Total Sample	960

ROC 97.5% Sensitivity

The fixed 97.5% sensitivity results were mediocre (**Table 205**).

Table 205.

Viewbox – Calcanei -4- ROC 97.5% Sensitivity Results		
		Threshold Value
Sensitivity	97.5%	0.854
Specificity	54.4%	

ROC 97.5% Specificity

The 97.5% fixed specificity results were mediocre (**Table 206**).

Table 206.

Viewbox – Calcanei -4- ROC 97.5% Specificity Results		
		Threshold Value
Sensitivity	78.57%	0.686
Specificity	97.5%	

5 - Unaligned - Unhollowed - Exact Slow (Flexscan3D Comparable)

A total of 62 calcanei, unaligned and unhollowed, were run 'Exact Slow' on Elena. This was to test the effects of alignment, or pre-registration. It took 2 days, 4 hours and 31 minutes for 3906 iterations. This is an average time per iteration of 24 seconds. All models were whole, entire surfaces. The analysis took approximately 1 hour.

Lowest Common Value Result

The sensitivity and specificity were mediocre. The PPV was good, while the NPV was poor. (**Tables 207 & 208**)

Table 207.

Viewbox – Calcanei -5- LCV Results	
Sensitivity	80.77%
Specificity	60%
Positive Predictive Value	91.3%
Negative Predictive Value	37.5%

Table 208.

Viewbox – Calcanei -5- LCV Matches	
True positives	42
False negatives	10
False positives	4
True negatives	6

ROC Optimal

The sensitivity was good, while the specificity was only mediocre. The PPV was poor, while the NPV was almost perfect. The AUC was high and valid. (**Tables 209 & 210**)

Table 209

Viewbox – Calcanei -5- ROC Optimal Results				
		Threshold Value	**AUC**	**p-value**
Sensitivity	92.86%	0.594	0.917	<0.0001
Specificity	77.90%			
Positive Predictive Value	11.23%			
Negative Predictive Value	99.72%			

Table 210.

Viewbox – Calcanei -5- ROC Optimal Sample Size	
True Positives	28
True Negatives	932
Total Sample	960

ROC 97.5% Sensitivity

The fixed 97.5% sensitivity results were poor (**Table 211**).

Table 211.

Viewbox – Calcanei -5- ROC 97.5% Sensitivity Results		
		Threshold Value
Sensitivity	97.5%	0.744
Specificity	33.91%	

ROC 97.5% Specificity

The 97.5% fixed specificity results were mediocre (**Table 212**).

Table 212.

Viewbox – Calcanei -5- ROC 97.5% Specificity Results		
		Threshold Value
Sensitivity	50%	0.505
Specificity	97.5%	

6 - Aligned – Hollowed – With Normals - Exact Normal - Whole Surface Models

A total of 91 calcanei, aligned, hollowed, and saved with normals were used. They were run 'Exact Normal' on Amarna. This took 7 days, 22 hours and 18 minutes for 8208 iterations. This is an average time per iteration of 1 minute and 23 seconds. All models were whole, entire surfaces. The analysis took approximately 2 hours.

Lowest Common Value Result

The LCV results were generally good. The specificity and PPV were perfect, while the sensitivity was good. The NPV, however, was only mediocre. (**Tables 213 & 214**)

Table 213.

Viewbox – Calcanei -6- LCV Results	
Sensitivity	94.74%
Specificity	100%
Positive Predictive Value	100%
Negative Predictive Value	78.95%

Table 214.

Viewbox – Calcanei -6- LCV Matches	
True positives	72
False negatives	4
False positives	0
True negatives	15

ROC Optimal

The optimal ROC results were good or excellent, with high sensitivity and specificity rates. The NPV was almost perfect, however, the PPV was poor. The AUC was high and valid. (**Tables 215 & 216**)

Table 215.

Viewbox – Calcanei -6- ROC Optimal Results				
		Threshold Value	**AUC**	**p-value**
Sensitivity	94.74%	1.157	0.985	<0.0001
Specificity	95.12%			
Positive Predictive Value	26.68%			
Negative Predictive Value	99.89%			

Table 216.

Viewbox – Calcanei -6- ROC Optimal Sample Size	
True Positives	38
True Negatives	2030
Total Sample	2068

ROC 97.5% Sensitivity

The fixed 97.5% sensitivity results were mediocre (**Table 217**).

Table 217.

Viewbox – Calcanei -6- ROC 97.5% Sensitivity Results		
		Threshold Value
Sensitivity	97.5%	1.506
Specificity	65.81%	

ROC 97.5% Specificity

The 97.5% fixed specificity results were good (**Table 218**).

Table 218.

Viewbox – Calcanei -6- ROC 97.5% Specificity Results		
		Threshold Value
Sensitivity	89.47%	1.089
Specificity	97.5%	

7 - Aligned – Hollowed – With Normals - Exact Normal - Mixed Fragmented, Random Selection

A total of 144 calcanei, aligned, hollowed, and saved with normals were used. They were run in 'Exact Normal' in 33 batches, spread across Amarna, Elena, Romulus and Remus. For a full breakdown of each run, see **Appendix D**. In total, all the runs took 36 days, 21 hours and 51 minutes for 5200 iterations. Though average iteration times ranged from 1 minute and 26 seconds to 1 hour, 28 minutes and 4 seconds, the overall average iteration time was 10 minutes and 13 seconds. Models were randomized and a mixture between whole, entire surfaces and incomplete or fragmented surfaces. The analysis took approximately 3 hours.

Lowest Common Value Result

The LCV results overall were good to excellent. The sensitivity, specificity and NPV were high. The PPV, however, was only mediocre. (**Tables 219 & 220**)

Table 219.

Viewbox – Calcanei -7- LCV Results	
Sensitivity	97.30%
Specificity	92.52%
Positive Predictive Value	81.82%
Negative Predictive Value	99%

Table 220.

Viewbox – Calcanei -7- LCV Matches	
True positives	36
False negatives	1
False positives	8
True negatives	99

ROC Optimal

The ROC optimal results were good, with a high and valid AUC. The sensitivity was high, and the specificity was almost perfect. The PPV was mediocre, and the NPV was almost perfect. (**Tables 221 & 222**)

Table 221.

Viewbox – Calcanei -7- ROC Optimal Results				
		Threshold Value	**AUC**	**p-value**
Sensitivity	94.74%	0.859	0.997	<0.0001
Specificity	99.86%			
Positive Predictive Value	81.80%			
Negative Predictive Value	99.96%			

Table 222.

Viewbox – Calcanei -7- ROC Optimal Sample Size	
True Positives	19
True Negatives	2861
Total Sample	2880

ROC 97.5% Sensitivity

The fixed 97.5% sensitivity results were good (**Table 223**).

Table 223.

Viewbox – Calcanei -7- ROC 97.5% Sensitivity Results		
		Threshold Value
Sensitivity	97.5%	1.120
Specificity	94.55%	

ROC 97.5% Specificity

The 97.5% fixed specificity results were also good (**Table 224**).

Table 224.

Viewbox – Calcanei -7- ROC 97.5% Specificity Results		
		Threshold Value
Sensitivity	94.74%	1.043
Specificity	97.5%	

Summary

Time

It was not possible to calculate the total time for the Flexscan3D comparisons, due to the lack of information recorded (Gutekunst, 2015). The total time for all Viewbox comparisons was 52 days, 19 hours, 3 minutes and 10 seconds for 32,814 iterations. Average iteration times ranged from 1 hour, 28 minutes and 4 seconds to as low as 24 seconds. The aligned, hollowed, saved with normals, mixed fragmentation/random selection models run 'Exact Normal' ran the slowest with the average iteration time of 10 minutes and 13 seconds (Viewbox parameter set 7). The unhollowed models ran the fastest, with average iteration times between 24 and 48 seconds. The aligned, hollowed, saved with normals models that were Flexscan3D comparable (Viewbox parameter set 1) were also fast, with an average iteration time of 35 seconds. The main difference between that average iteration time and the larger sample size of whole calcanei (Viewbox parameter 6) was the inclusion of a few calcanei models from Cyprus. While these models were accurate, they were considerably larger in size than other models and increased iteration time to 1 minute and 23 seconds. This is almost three times as long. The analysis time of each test condition ranged from 1 to 3 hours, for a total of 14 hours for every condition.

Flexscan3D versus Viewbox Results

For the LCV method, all of the Flexscan3D results were overall better than the five different Viewbox conditions tested, though all had good sensitivity, specificity and PPV rates. The two exceptions were Viewbox parameter set 5 (Unaligned - Unhollowed - Exact Slow) which mediocre sensitivity and specificity, and Flexscan3D parameter set 2 (Mixed Hollowed – Whole Surface Models) which had a mediocre specificity. All Flexscan3D parameter sets had perfect NPV, while the Viewbox parameter set's NPV rates were mediocre to poor. For the ROC optimal results, the Flexscan3D parameters all produced the best results in terms of sensitivity and specificity, regardless of parameter type. All of the Viewbox parameter sets produced good to excellent specificity rates with the exception of Viewbox parameter set 5 (Unaligned - Unhollowed - Exact Slow) which produced mediocre results. The only two good or excellent sensitivity rates Viewbox produced,

however, were parameter sets 1 (Aligned - Hollowed – With Normals - Exact Normal) and 5 (Unaligned - Unhollowed - Exact Slow). All of the PPV rates for the ROC optimal results, regardless of Flexscan3D or Viewbox comparison, were poor. All of the NPV rates, however, were nearly perfect regardless of Flexscan3D or Viewbox comparison type. (**Tables 225, 226, 227**)

All LCV Results

As the Flexscan3D and Viewbox results were compared in the section above, this section will focus only on the LCV results for the two remaining Viewbox parameter sets. Generally, the LCV results were all good or excellent, with high sensitivity and specificity rates. The two parameter sets had flipped PPV and NPV rates, with Viewbox parameter set 6 (Aligned – Hollowed – With Normals - Exact Normal - Whole Surface Models) having a perfect PPV and mediocre NPV, while Viewbox parameter set 7 (Aligned – Hollowed – With Normals - Exact Normal - Mixed Fragmented, Random Selection) had an almost perfect NPV and a mediocre PPV. (**Table 228**)

All ROC Results

As the Flexscan3D and Viewbox results were compared above, this section will focus only on the ROC results for the two remaining Viewbox parameter sets. The optimal ROC sensitivity and specificity rates for both were good or excellent and high. The main difference between the two parameter sets, however, was the PPV. The PPV rates for Viewbox parameter set 7 (Aligned – Hollowed – With Normals - Exact Normal - Mixed Fragmented, Random Selection) was mediocre (81.90%), while the PPV rate for Viewbox parameter set 6 (Aligned – Hollowed – With Normals - Exact Normal - Whole Surface Models) was poor (only 26.68%). Both NPV rates were exceptional and above 99%. For the 97.5% fixed sensitivity rates, Viewbox parameter set 7 (Aligned – Hollowed – With Normals - Exact Normal - Mixed Fragmented, Random Selection) was considerably better than Viewbox parameter set 6 (Aligned – Hollowed – With Normals - Exact Normal - Whole Surface Models), with a good specificity rate as opposed to parameter set 6's

mediocre results. Both 97.5% fixed specificity rates, however, were good or excellent. (**Tables 229 & 230**)

Overall Optimal Method

Of the two comparison methods and two analysis methods, generally all the results were good, indicating that calcanei pair-match well. Of the LCV results, Flexscan3D parameter sets 1 (Mixed Hollowed - All Models - Mixed Fragmented) and 3 (Unhollowed) produced the best results with perfect sensitivity, specificity, PPV and NPV rates. The closest Viewbox results were parameter sets 6 (Aligned – Hollowed – With Normals - Exact Normal – Whole Surface Models) and 7 (Aligned – Hollowed – With Normals - Exact Normal – Mixed Fragmented, Random Selection), though parameter set 6 had a much lower NPV and parameter set 7 had a much lower PPV. Of the ROC results, Viewbox parameter set 7 (Aligned – Hollowed – With Normals - Exact Normal – Mixed Fragmented, Random Selection) produced the best results, with high sensitivity, specificity and NPV rates, as well as a mediocre PPV rate. All of the Flexscan3D parameter sets produce high sensitivity, specificity and NPV rates, but their PPV rates were poor. Thus, the optimal methods are the Flexscan3D parameter sets 1(Mixed Hollowed - All Models - Mixed Fragmented) or 3 (Unhollowed) using LCV, and Viewbox parameter set 7 (Aligned – Hollowed – With Normals - Exact Normal – Mixed Fragmented, Random Selection) using ROC.

Table 225.

Comparison	Batch	LCV Sensitivity	LCV Specificity	ROC (Optimal) Sensitivity	ROC (Optimal) Specificity
Flexscan3D (149)	Mixed Hollowed (Mixed Frag)	100%	100%	98.59%	96.88%
Flexscan3D (68)	Mixed Hollowed (Whole)	100%	80%	100%	91.81%
Flexscan3D (62)	Unhollowed	100%	100%	100%	90.13%
Viewbox (62)	Aligned - Hollowed - With Normals - Exact Normal	92.86%	100%	92.86%	93.03%
Viewbox (62)	Aligned - Unhollowed - Exact Normal	92.86%	100%	78.57%	94.85%
Viewbox (62)	Aligned - Unhollowed - Exact Slow	89.29%	100%	78.57%	92.6%
Viewbox (62)	Unaligned - Unhollowed - Exact Normal	89.29%	100%	82.14%	97.21%
Viewbox (62)	Unaligned - Unhollowed - Exact Slow	80.77%	60%	92.86%	77.9%

Table 226.

Comparison	Batch	LCV - PPV	LCV - NPV	ROC (Optimal) - PPV	ROC (Optimal) – NPV
Flexscan3D (149)	Mixed Hollowed (Mixed Frag)	100%	100%	29.06%	99.98%
Flexscan3D (68)	Mixed Hollowed (Whole)	96.67%	100%	23.99%	100%
Flexscan3D (62)	Unhollowed	100%	100%	23.35%	100%
Viewbox (62)	Aligned - Hollowed - With Normals -Exact Normal	100%	60%	28.60%	99.76%
Viewbox (62)	Aligned - Unhollowed - Exact Normal	100%	60%	31.45%	99.32%
Viewbox (62)	Aligned - Unhollowed - Exact Slow	100%	50%	24.20%	99.30%
Viewbox (62)	Unaligned - Unhollowed - Exact Normal	100%	50%	46.96%	99.45%
Viewbox (62)	Unaligned - Unhollowed - Exact Slow	91.3%	37.5%	11.23%	99.72%

Table 227.

Comparison	Batch	ROC (Optimal) Sensitivity	ROC (Optimal) Specificity	ROC (Fixed 97.5 Sens) Sensitivity	ROC (Fixed 97.5 Sens) Specificity	ROC (Fixed 97.5 Spec) Sensitivity	ROC (Fixed 97.5 Spec) Specificity
Flexscan3D (149)	Mixed Hollowed (Mixed Frag)	98.59%	96.88%	97.5%	96.94%	97.18%	97.5%
Flexscan3D (68)	Mixed Hollowed (Whole)	100%	91.81%	97.5%	91.81%	89.66%	97.5%
Flexscan3D (62)	Unhollowed	100%	90.13%	97.5%	90.13%	89.29%	97.5%
Viewbox (62)	Aligned - Hollowed - With Normals - Exact Normal	92.86%	93.03%	97.5%	58.69	85.71%	97.5%
Viewbox (62)	Aligned - Unhollowed - Exact Normal	78.57%	94.85%	97.5%	34.76	64.29%	97.5%
Viewbox (62)	Aligned - Unhollowed - Exact Slow	78.57%	92.6%	97.5%	38.73	64.29%	97.5%
Viewbox (62)	Unaligned - Unhollowed - Exact Normal	82.14%	97.21%	97.5%	54.4	78.57%	97.5%
Viewbox (62)	Unaligned - Unhollowed - Exact Slow	92.86%	77.9%	97.5%	33.91	50%	97.5%

Table 228.

Comparison	Batch	LCV Sensitivity	LCV Specificity	LCV - PPV	LCV - NPV
Viewbox (91)	Aligned - Hollowed - w/ Normals - Exact Normal (Whole)	94.74%	100%	100%	78.95%
Viewbox (144)	Aligned - Hollowed - w/ Normals - Exact Normal (Mixed Frag)	97.3%	92.52%	81.82%	99%

Table 229.

Comparison	Batch	ROC (Optimal) Sensitivity	ROC (Optimal) Specificity	ROC (Fixed 97.5 Sens) Sensitivity	ROC (Fixed 97.5 Sens) Specificity	ROC (Fixed 97.5 Spec) Sensitivity	ROC (Fixed 97.5 Spec) Specificity
Viewbox (91)	Aligned - Hollowed - w/ Normals - Exact Normal (Whole)	94.74%	95.12%	97.5%	65.81%	89.74%	97.5%
Viewbox (144)	Aligned - Hollowed - w/ Normals - Exact Normal (Mixed Frag)	94.74%	99.86%	97.5%	94.55%	94.74%	97.5%

Table 230.

Comparison	Batch	ROC (Optimal) Sensitivity	ROC (Optimal) Specificity	ROC (Optimal) PPV	ROC (Optimal) NPV
Viewbox (91)	Aligned - Hollowed - w/ Normals - Exact Normal (Whole)	94.74%	95.12%	26.68%	99.89%
Viewbox (144)	Aligned - Hollowed - w/ Normals - Exact Normal (Mixed Frag)	94.74%	99.86%	81.90%	99.96%

Summary of All Results

Amongst the four different sets of bones compared for pair-matching, a total of 18,009 mesh-to-mesh values were analysed from Flexscan3D while a total of 366,066 values were analysed from Viewbox 4.1. This equals 384,075 values between the two programs. The Flexscan3D pair-matching process for three sets of bones (humeri, clavicles and temporals) took approximately a continuous 5 days, 19 hours, 6 minutes and 18 seconds. The final fourth set (calcanei) did not have time recorded (Gutekunst, 2015). The total time for all four sets of bones compared in Viewbox 4.1 was a continuous 181 days, 6 hours, 47 minutes and 10 seconds. The total time for analysis for all 384,075 values from all four sets was 60 hours. With the addition of the time it took to build the models, 17 days and 5 hours, this means that the entire process took approximately a continuous 206 days, 18 hours, 53 minutes and 28 seconds, excluding the scanning processes. Assuming a workday of 8 hours, this means that the process, again excluding scanning, took 620 workdays, 2 hours, 53 minutes and 28 seconds. This does not count runs that were interrupted or analyses that had to be redone, which will be discussed later.

Discussion

This dissertation explored the potential of digital three-dimensional modelling of bones and Iterative Closest Point (ICP) algorithms for creating new methods of pair-matching, an individualisation technique. It found that both digital three-dimensional modelling of bones and ICP algorithms are useful for the creation of new pair-matching techniques, as demonstrated by the project's creation and use of the mesh-to-mesh value comparison (MVC) method. Though the two different types of MVC, manual and automatic, vary in accuracy of results among bone types, both provide useful, additional tools to the sorting commingled remains arsenal. The MVC method is easy to use, highly accurate, not reliant on user expertise, cost-effective, and meets the criteria for evidence admissibility in most courts.

To contextualise the data generated by this study, the results of each bone set will be summarised, assessed in terms of how the (a)symmetry of the bone would affect the MVC process, assessed for any particular interactions with the comparison algorithms used, and then assessed as compared to other current methods of pair-matching.

Humeri

A total of 45 humeri from three populations (modern Italian, archaeological Spain and archaeological Scotland) were compared using Flexscan3D and Viewbox 4.1. Only one condition was tested using Viewbox 4.1: models that were unaligned, hollowed and saved with normals. Overall the best humeri results were the Flexscan3D results, which had 100% sensitivity, specificity, positive predictive value (PPV) and negative predictive value (NPV) rates. The Viewbox results were not as good and showed problems with specificity using the LCV technique, or PPV and sensitivity issues using ROC analysis. To explore why this was the case, several factors are examined below.

Asymmetry effects

Humeri have a unique pattern of asymmetry, often related to differential hand usage and the respective muscles involved (Auerbach and Raxter, 2008, Auerbach and Ruff, 2006, Steele and Mays, 1995, Ćuk et al., 2001, Sládek et al., 2007). While this can impact other individuation techniques, how does it specifically affect the mesh-to-mesh value comparison (MVC) methods, either automatic or manual? Based on the Flexscan3D results for the manual MVC, the asymmetry of humeri has no detrimental effect; it appears, in fact, that is has a positive effect on the matching process. Overall, most humeri seem to vary along their major muscle attachments, but this variation appears to preserve the overall shape of the bone. Muscles on the left and right sides may be worked slightly more due to handedness, but barring extreme differences in usage, the muscles are still being used in the *same way*. This means that the enlargement or reduction of the bone happens in the same manner, side to side, based on shape. This can be easily visualised using the deviation analysis feature in Flexscan3D, or the distance map feature in Viewbox 4.1, both of which show the areas of difference between two models by colour-coordinating the model surface appearance based on the amount of difference present. For example, blue would indicate where one model is smaller than the other, while red would indicate where it is bigger. Below are pictures of both a true pair-match (**Figure 15**) and a non-pair-match (**Figure 16**).

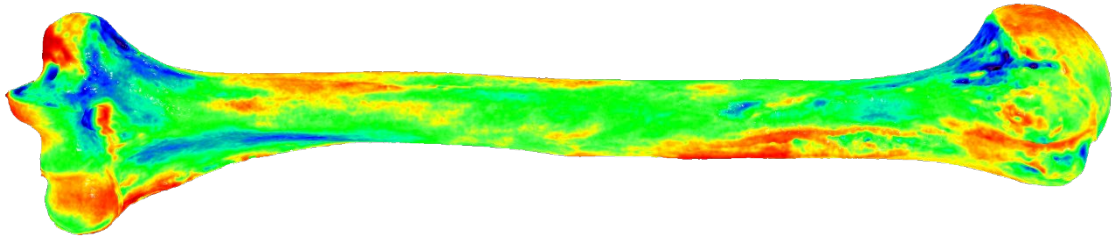

Figure 15. True pair-match, colours scaled -2 mm (blue) to 2 mm (red) – Humeri 13 and 18 (Italy). Humeri 13 as reference mesh.

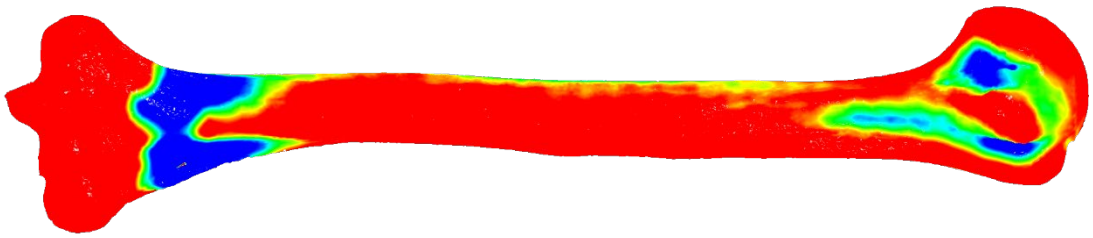

Figure 16. Non-pair-match (negative), colours scaled -2 mm (blue) to 2 mm (red) – Humeri 13 and 24 (Italy and Spain respectively)

Algorithm Interactions

Algorithmically, Flexscan3D worked quite well and appeared to have no specific issues. Viewbox 4.1, however, seemed to have some issues which produced less accurate results. While Viewbox's poorer results may be due to the slightly different algorithms that Flexscan3D uses, these could also be due to the complications of the bone type in combination with Viewbox's Trimmed Iterative Closest Point (TrICP) algorithm specifically, or due to the Viewbox settings for TrICP. In this case, only unaligned humeri models were run, but TrICP, like most ICP algorithms, assumes that the models being compared have been roughly pre-aligned, or pre-registered (Chetverikov et al., 2005, Chetverikov et al., 2002). As the initial conditions for the TrICP algorithm were not met, this could be one potential cause of the poorer results. This lack of initial pre-alignment or pre-registration could also cause another type of error resulting in poorer results, as without an initial pre-alignment or registration certain parts of models will be prioritised for matching, often incorrectly. In the case of humeri, for example, midshafts are often prioritised for alignment (as they exhibit many similar linear points), but this could result in the distal and proximal ends being flipped/mismatched. (**Figure 17**). Humeri, however, were the first bone set tested and thus this pre-alignment/pre-registration issue was corrected for the subsequent sets.

Figure 17. Mismatched humeri midshafts – Humeri 13 and 18 (Italy)

Overall Pros and Cons (As compared to other known methods on this bone)

When considering a method's usability and desirability overall, it must be compared to existing techniques whenever possible to assess both the results and feasibility in context. In terms of visual pair-matching, there is only one known study on humeri: Adams and Konigsberg (Adams and Konigsberg, 2004). Though there are plenty of articles that mention visual pair-matching as a viable technique, Adams and Konigsberg appear to have the only actual validation study (Adams and Byrd, 2006, Adams and Byrd, 2008, Snow, 1948, Adams and Konigsberg, 2004). Though Adams and Konigsberg do not express their findings in terms of sensitivity, specificity, PPV and NPV rates, the values are simple to calculate from their findings (Karell et al., 2016). For visual pair-matching, the sensitivity was 93%, the specificity was 95%, the NPV was 83% and the PPV was 99% (Karell et al., 2016). This, of course, is a qualitative method that is dependent upon the expertise of the practitioner and it must be considered that both Adams and Konigsberg are experienced practitioners; other, less experienced practitioners may not fare as well, and a study has yet to be published addressing this aspect. An additional confounding consideration for visual pair-matching is population variation. Traits like extremity of sexual dimorphism vary between populations, and thus aspects of pair-matching such as extremity of robustness (more variation of which often aids pair-matching) can also have a significant impact on the process (Byrd, 2008). Population variation is not limited to sexual dimorphism and even cultural practices of activity could have an effect on the pair-matching process (Ubelaker and Grant, 1989).

Humeri are also mentioned in osteometric sorting method articles, but generally in the manner of associating them to other, non-paired elements, such as a humerus to a

femur (Byrd and Adams, 2003, Byrd, 2008). The main exception to this is an article by Thomas et al. which uses the statistic 'M' (defined as $M = \frac{|L-R|}{\left(\frac{L+R}{2}\right)}$) to create tables of metric values which reflect maximum parameters of homologs (correct pair-matches) to use for osteometric pair-matching (Thomas et al., 2013). It is important to note, however, that they operate on the null hypothesis that two bones are assumed to match and therefore operate on the principle of exclusion (Thomas et al., 2013). It is also worth noting that the studies which include other element associations as well as osteometric pair-matching have received criticism for poor performance and allowing too many false rejections (Vickers et al., 2015). To this claim, the authors of the original publication have offered a more sophisticated statistical rebuttal and improved upon the method (Lynch et al., 2018). Interestingly, there are numerous humeral asymmetry studies, but no other publications specifically on pair-matching humeri (Steele and Mays, 1995, Sládek et al., 2007, Ćuk et al., 2001, Auerbach and Ruff, 2006).

Clavicles

A total of 203 modern clavicles from Crete (Greece) were compared using Flexscan3D and Viewbox 4.1. For Flexscan3D, 99 clavicles were tested. For Viewbox 4.1, eight different parameter sets were tested, including two of 99 clavicles and the rest of 203 clavicles. Flexscan3D produced the best results, regardless of LCV or ROC analysis; however, all the results regardless of Flexscan3D/Viewbox were generally mediocre. In fact, clavicles were the worst performing set of bones tested. In assessing both the asymmetry of the bone itself and the way ICP/TrICP algorithms function, this is unsurprising, as will be discussed below.

Asymmetry effects

Clavicles' bilateral asymmetry patterns are unusual, even amongst normal skeletal symmetrical variation. Though they are classed as long bones, the lack of a marrow cavity and the specific type of muscular biomechanical antagonism create both their unique shape and type of asymmetry (Loh et al., 2015, Abdel Fatah et al., 2012,

Bernat et al., 2014, Hamill, 2003). While other bones tend to have asymmetry focused on a single side, left and right clavicles present different patterns of asymmetry (Abdel Fatah et al., 2012, Auerbach and Raxter, 2008, Bernat et al., 2014). Left clavicles tend to be longer while right clavicles tend to be more robust, though this is possibly linked to handedness (Abdel Fatah et al., 2012, Auerbach and Raxter, 2008, Bernat et al., 2014, Loh et al., 2015). This pattern seems to flip sides for left-handed individuals (Loh et al., 2015). The fact that the majority of individuals are right-handed may account for the majority of studies finding the first asymmetry trend. Regardless of the direction of this pattern, it still poses a problem for any pair-matching technique, as the overall three-dimensional shape between the two sides is different. Again, this particular pattern can be visualised using the deviation analysis feature. For example, here are pictures of both a true pair-match (**Figure 18)**, the length difference visible between a true pair-match (**Figure 19**), and a non-pair-match (**Figure 20**).

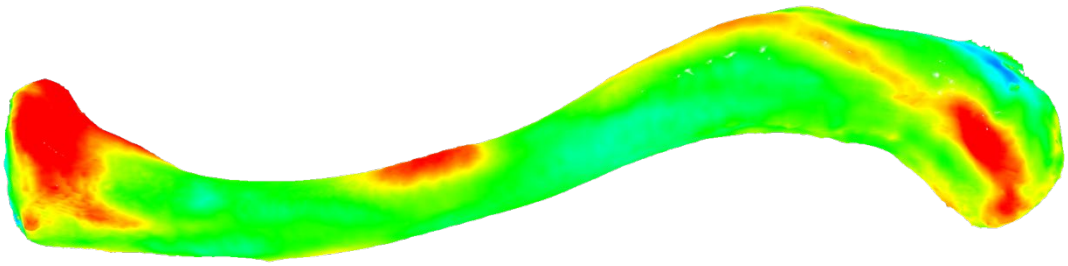

Figure 18. True pair-match, colours scaled -2 mm (blue) to 2 mm (red) – Clavicle Left 3 and Right 3 (Crete)

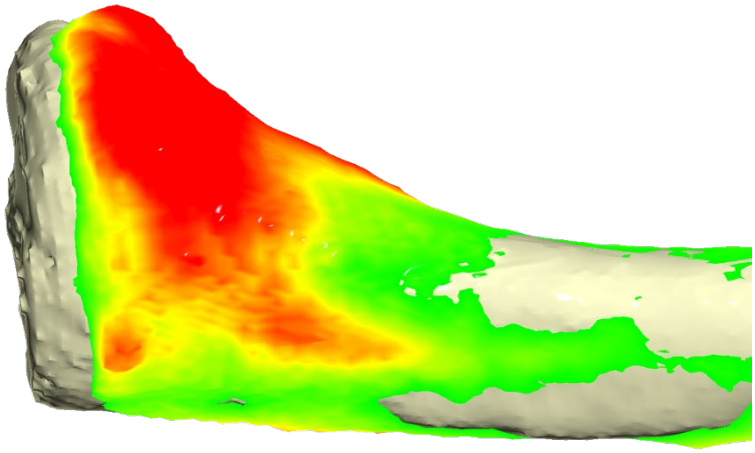

Figure 19. True pair-match, colours scaled -2 mm (blue) to 2 mm (red) – Clavicle Left 3 (coloured) and Right 3 (white) [Both Crete] – Close up on medial end, showing the difference in length between the two sides

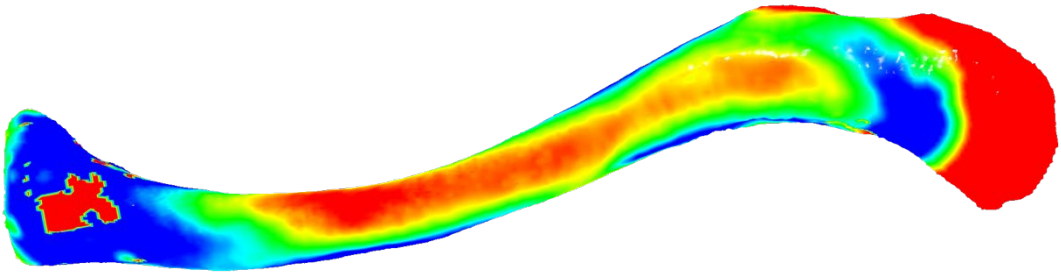

Figure 20. Non-pair-match (negative), colours scaled -2 mm (blue) to 2 mm (red) – Clavicle Left 3 and Right 55 (Crete)

The poor effects of this particular type of asymmetry can also clearly be seen in the mediocre algorithm matching results, and also as a problem for osteometric pair-matching as well, which will be explored further below. Finally, as the medial aspect of the clavicle is generally the last bone in the body to fuse and because of its connection with the manubrium, there is a good amount of variation in the medial end shape of clavicles side to side; though all the clavicles in this study were adults, and thus fusion itself was not a factor, the side to side variation could have an effect (Ekizoglu et al., 2015a, Ekizoglu et al., 2015b, Schulz et al., 2005). See **Figure 19** for a visual

representation of the length variation on the medial end, as well as **Figure 21** below for a close up of the variation on the medial end itself.

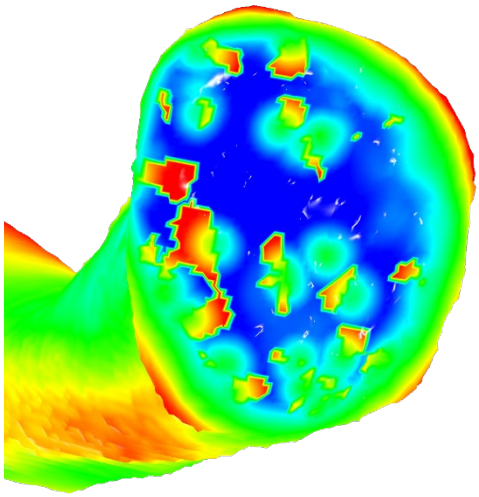

Figure 21. True pair-match, colours scaled -2 mm (blue) to 2 mm (red) – Clavicle Left 3 and Right 3 (Crete) – Close up on medial end, showing the difference in shape between the two sides

Algorithm Interactions

Beyond the effects of asymmetry, ICP and TrICP algorithms also have particular aspects which make pair-matching clavicles algorithmically challenging. While all ICP algorithms, regardless of variant, occasionally incorrectly register/align models, there are specifics for both Flexscan3D and Viewbox 4.1's variation that hinders accurately pair-matching clavicles.

For Flexscan3D, though the specific algorithms are unknown, during the comparison process it was noted that the midshafts of clavicles preferentially aligned over other aspects of the bone. This was unsurprising for two reasons. First, as the models used for comparison were unhollowed, the density of the cortical bone at the midshaft creates a bulk of data points in that area. This greater density means that there are more points to match, as compared to other areas of the bone and that the algorithm will preferentially match that bulk of points. Second, with the confounding factor of the two patterns for clavicular asymmetry, it means that shape-wise, the midshaft is actually the area of greatest similarity. The overall robusticity of each bone varies, but shape-wise it is at its most similar. Furthermore, due to the length differences between the two

sides, it is harder for the algorithms to match either the distal or proximal ends over the shape similarity and density of points at the midshaft.

For Viewbox 4.1, these general shape/asymmetry issues remain the same, but there are several key differences. First, as models were also run hollowed, this negated the bulk-of-points-matching issues found in Flexscan3D. Though the Viewbox 4.1 results were overall mediocre to poor, hollowing did have a significant impact on improving the matching process, almost doubling the LCV results and slightly improving the ROC results. This suggests that the bulk–of–points issue is significant and that hollowed models could improve the Flexscan3D results in the future.

Beyond the effects of hollowing, the TrICP algorithm itself also can produce particular misregistrations based on its underlying assumptions. The most significant aspect is that TrICP converges to a local minimum; this means that where there are multiple aspects of similarity between two models, there is no way to automatically force the algorithm to select the optimal result using other smaller bits of information in the model (Chetverikov et al., 2005, Zhang, 1994). Though this may seem complex, it is straightforward to visualise, as shown in **Figure 22**.

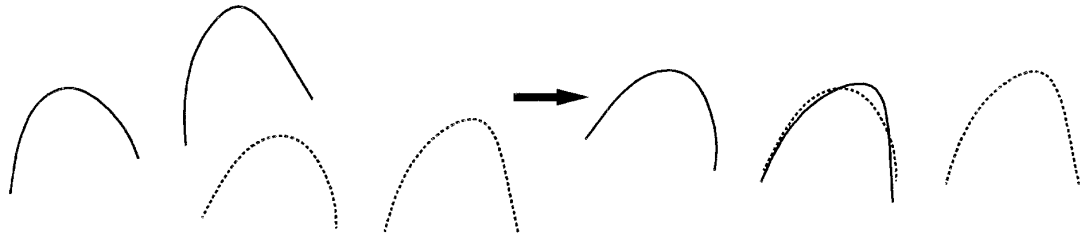

Figure 22. From Zhang – demonstrating how local matching techniques which converge to the closest local minimum do not necessarily produce the optimal result (Zhang, 1994). The two models are identical, one shown with the solid line and the other with the dotted line. Still, using a local matching technique which converges to the closest local minimum does not produce the expected, or optimal, result due to the multiple aspects of similarity (in this case, curves).

While the TrICP is not the only ICP variant with this issue, it is a significant one, especially in regard to overlapping aspects of models which are highly symmetrical. Though it seems counterintuitive after the discussion of shape differences and asymmetry in the clavicle, the *overall* shape of the clavicle is actually highly

symmetrical in its *S*-shape form. For the same reason forensic anthropology students find determining the side of a clavicle challenging (*Is it a left? Is it a right? It looks correct either way),* the algorithm can have a hard time aligning clavicles. As the initial conditions of the algorithm in Viewbox 4.1 use 20 different rotation positions to find the best fit between the two models, this can create a misalignment, matching the proximal end of one clavicle to the distal end of another. Though not demonstrated identically by Chetverikov et al, **Figure 23** is a good example of how an *S*-shaped form can produce misalignments using TrICP, providing an analogue to two clavicles (2005).

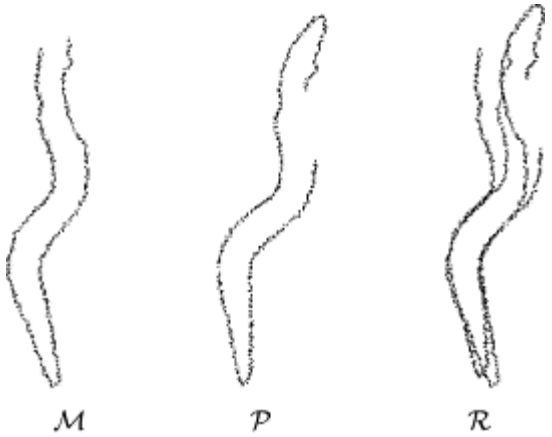

Figure 23. From Chetverikov et al – Example of TrICP misalignment from an *S*-shape form (2005). M is the first set of points, or model; P is the second set of points, or model. R is the aligned/registered version of M and P.

The last confounding factor for both these challenging aspects of similarity and *S*-shaped forms in general are normals. While they can provide smoother curve information in most models, this can exacerbate both the similarity of curves (especially in *S*-shaped forms, depending on the initial positioning effects) and the local minima issue. This is why clavicles are the only set of bones tested where the comparison process performs slightly better using models without normals. For a visualisation of how normals can create similarity problems, see **Figures 24-26** for a basic visualisation, a visualisation of a clavicle with the normals displayed, and a close-up of the normals visualisation along the midshaft.

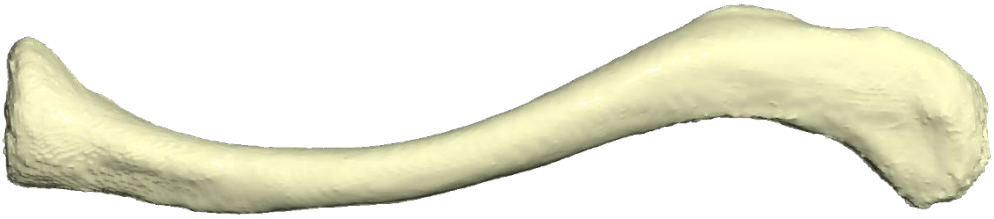

Figure 24. Basic visualisation of a clavicle (Left 3 – Crete)

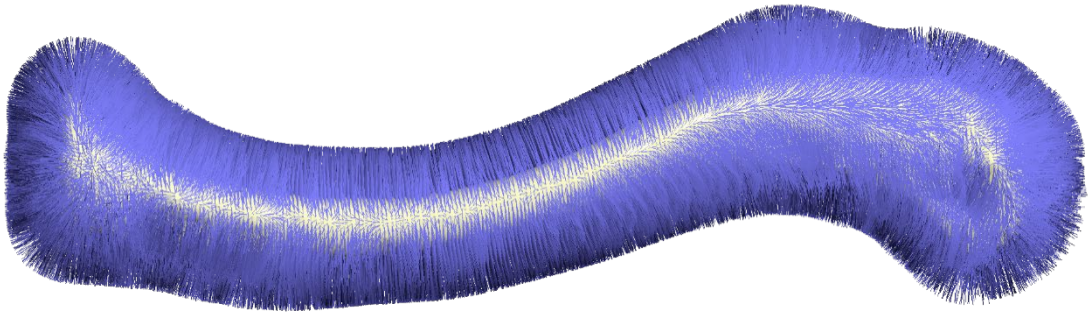

Figure 25. Visualisation of a clavicle with normals displayed (Left 3 – Crete)

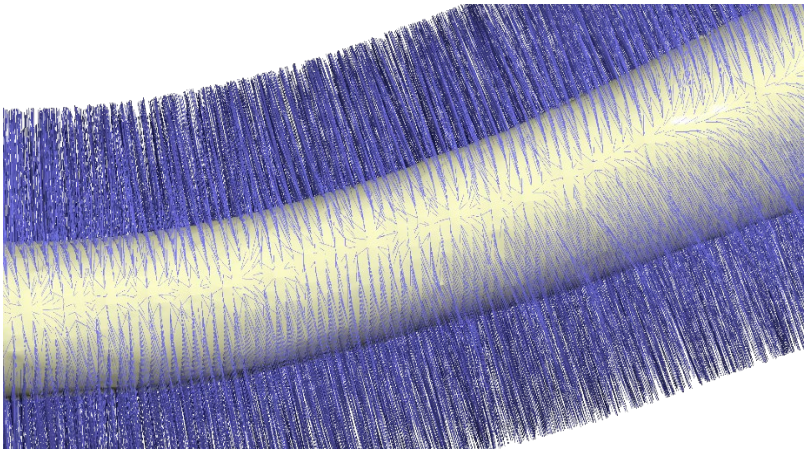

Figure 26. Visualisation of a clavicle with normals displayed (Left 3 –Crete), close-up.

Overall Pros and Cons (As compared to other known methods on this bone)

Given the clavicle is only of limited biological profiling use – occasionally being used to determine age – it is unsurprising that there are very few studies on pair-matching clavicles, or even individualisation of clavicles. There are no studies specifically on visual pair-matching of clavicles, and only one on osteometric sorting (Thomas et al., 2013). Even the one osteometric study, again on the 'M' statistic (defined as $M = \frac{|L-R|}{\left(\frac{L+R}{2}\right)}$) tables, had significant issues with clavicles (Thomas et al., 2013); of the three measurements assessed on the clavicle (Maximum length, Midshaft diameter – Anterior/Posterior, Midshaft diameter – Medial/Lateral), only two were not significantly different between the sexes in terms of bilaterality and thus considered valid (Thomas et al., 2013). The midshaft diameter (Anterior/Posterior) had significant differences between sexes (Thomas et al., 2013); an interesting feature also considering the issues with the midshaft previously mentioned. The only other specific mention of clavicles individuation-wise was in reference to articulation with the manubrium (Adams and Byrd, 2006). The reliability of this articulation is considered low, though it has the potential of being used in an exclusionary manner (Adams and Byrd, 2006). In terms of other studies, the only other relevant articles were ones which used 3D modelling for other applications, such as how to select the best surgical approach for correcting malunited clavicles or investigated different anatomical variations (Hingsammer et al., 2015, Bernat et al., 2014). For the study on mal-united clavicles by Hingsammer et al, ICP algorithms were used to model the symmetry differences between the pathological clavicle split into two pieces and the contralateral side that was complete (Zhang and Chen, 2001, Hingsammer et al., 2015). While this study overall had a different goal and used fragmented clavicles, it had similar issues with alignment, in which eight of the subjects, out of a total of 102, failed completely (Hingsammer et al., 2015). This can be seen below in **Figure 27.**

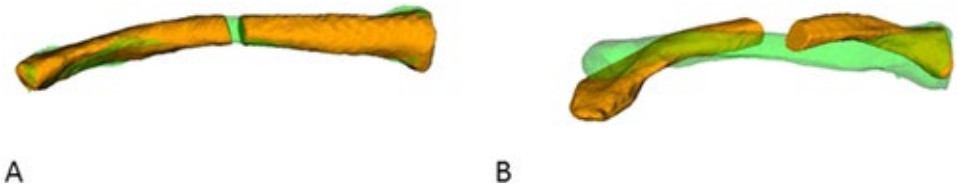

Figure 27. After Hingsammer et al – (A) is an example of a well-aligned clavicle, (B) is an example of misalignment (Hingsammer et al., 2015).

Temporals

A total of 124 modern temporals from Crete (Greece) were compared using Flexscan3D and Viewbox 4.1. For Flexscan3D, two different conditions were tested, one with 124 unhollowed temporals and one with only 121 unhollowed temporals so as to increase the non-pair-matches (negatives) in the sample. For Viewbox 4.1, ten different conditions were tested, with sample sizes ranging from 120 to 124 temporals. Flexscan3D produced the best results overall, though the Viewbox results for one test condition — increased negatives, hollowed models saved with normals, run 'Exact Normal'— produced almost identical results, both in terms of LCV and ROC analysis. In fact, the majority of the results were good regardless of Flexscan3D/Viewbox 4.1 and LCV/ROC results. The one glaring exception was the Viewbox test condition 5 (aligned, hollowed without normals, run Exact Normal), whose ROC results were not statistically significant and whose LCV results were also poor. This has interesting implications for the use and comparison of normals in three-dimensional modelling, as will be discussed below.

Asymmetry effects

Temporals' asymmetry pattern is intriguing, in that certain aspects of the bone are highly asymmetrical while others are highly symmetrical. For instance, while the squama is generally highly symmetrical (a factor that makes sense given the overall structure of the skull), certain aspects like the jugular foramen are notoriously asymmetrical (Koesling et al., 2005, Tomura et al., 1995). In various studies, the jugular foramen is notable in that it is only *symmetrical* in approximately 20% of the population (Tomura et al., 1995, Koesling et al., 2005). This variation is also extreme, in that one side can be five millimetres across, while the opposite side can be up to 20mm across.

The temporal bone only accounts for part of the structure of the jugular foramen, however, with the adjoining occipital making up the other portion. Thus, though size differences of the jugular foramen can be extreme, it may not have a significant effect on pair-matching. Other aspects which can vary in terms of symmetry are the size and shape of the mastoid process, the presence of accessory ossicles (such as an epiteric bone, a parietal notch bone, an asterionic bone, and ossicles in the occipito-mastoid suture), the number of mastoid emissary foramina and the persistence of the petromastoid suture (sometimes known as a divided mastoid) (Paiva and Segre, 2003, Tos and Stangerup, 1985, Watson-Williams, 1937, Mann et al., 2016, Buikstra and Ubelaker, 1994, Murlimanju et al., 2014).

Algorithm Interactions

In general, temporal bones worked well with both versions of the ICP algorithms, regardless of Flexscan3D or Viewbox, though normals were essential. In part, both ICP algorithms worked well due to the overall shape of the temporal. While the squamosal portion of temporals can be very similar bone to bone and could provide confusion algorithmically, the petrous portion along with the mastoid process provide characteristic features which help the two models align properly. Though it is possible for the squamosal portions to misalign, a large bulk of data in terms of points/vertices are present in the petrous portion, which effectively weights alignment to the correct orientation.

The nature of the temporal shape, slightly point-heavy medially and inferiorly, is what makes it a good bone to match algorithmically, unlike clavicles for example. In other words, temporals are shaped in a manner which takes advantage of local minima matching. A caveat to this, however, is that the bone must be matched using normals. This is because normals create a greater diversity of shape changes and therefore distinctive shape patterns on a temporal bone than just the bone model alone. This fact is clear when visualised. For example, **Figure 28** is a picture of a normal temporal bone, visualised in a standard fashion to mimic the look of bone. **Figure 29** of the same bone, however, visualises the normals of that model. In both **Figure 29** and **Figure 30** (a

close-up of this visualisation), it is clear that the normals information provided greater nuance and diversity in terms of shape than just the model itself, especially as the 'Exact Normal' setting is also taking into account the normals best matching each other, not just the overall points of the model.

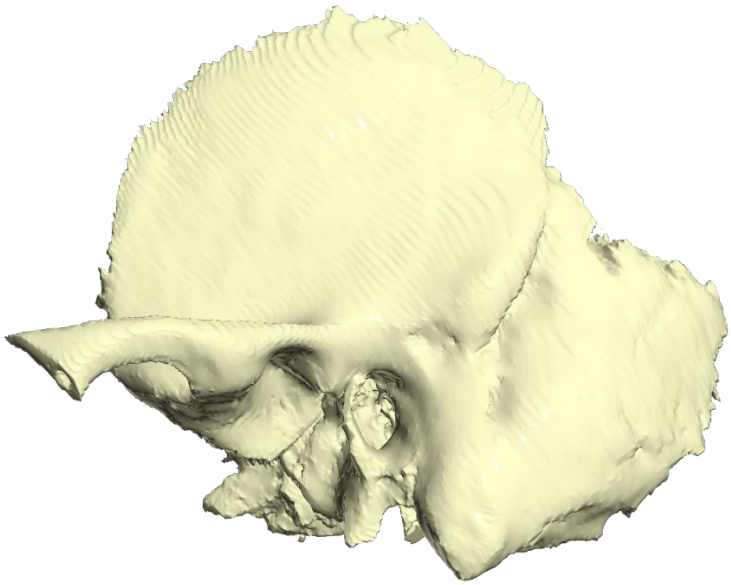

Figure 28. Basic visualisation of Temporal Left N1 (Crete)

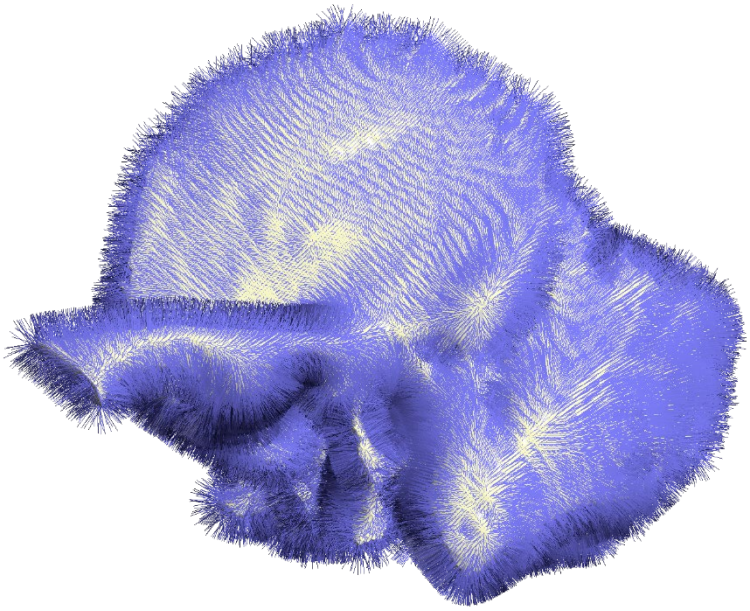

Figure 29. Temporal Left N1 (Crete) visualised with normals shown in purple (i.e. the small purple lines)

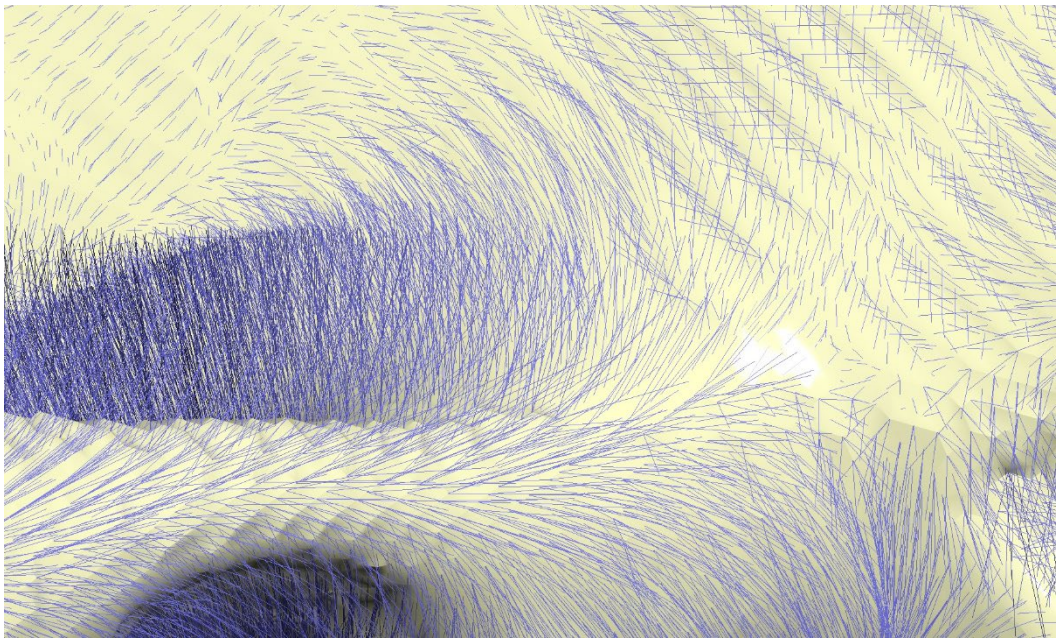

Figure 30. Temporal Left N1 (Crete) visualised with normals shown in purple (i.e. the small purple lines), close up

Overall Pros and Cons (As compared to other known methods on this bone)

While the petrous portion of the temporal is routinely used for estimating minimum number of individuals (MNI), the inner ear can be used to estimate sex even in infants, and there are a wealth of studies on craniometrics in general, there are no studies regarding temporals and pair-matching, or any other individualisation technique (Fairgrieve, 2009, Osipov et al., 2013, Ross et al., 2002, Kranioti et al., 2008, Stull et al., 2014, Tise et al., 2014, Mahakkanukrauh et al., 2015). Thus, there is no direct method for comparison of the two MVC methods. However, this means that should a situation arise which needs to pair-match temporals, and does not solely rely on DNA, both MVC methods are good options with highly accurate results, provided the models are built and saved with normals.

<u>Calcanei</u>

A total of 201 calcanei from Crete (Greece, modern), Cyprus (modern), and Scotland (archaeological) were compared using Flexscan3D and Viewbox 4.1. Three

different conditions were tested for Flexscan3D: 149 mixed hollowed, mixed fragmented models; 68 mixed hollowed, whole surface models, and 62 unhollowed models. Seven different conditions were tested in Viewbox 4.1, with sample sizes ranging from 62 to 144. Though Flexscan3D generally outperformed Viewbox, the majority of both sets of results were very good regardless of LCV selection or ROC analysis, with high to perfect sensitivity and specificity rates. Negative and positive predictive value rates alternated between high and low, with LCV producing high PPV rates and middling NPV rates, while ROC analysis produced high NPV rates and low PPV rates. There were two main exceptions; Viewbox parameter 5 (unaligned, unhollowed, run Exact Slow) produced a low sensitivity rate using LCV and Viewbox parameter 7 (aligned, hollowed with normals, run Exact Normal, mixed fragmented and random selection) which produced both an almost perfect LCV NPV rate and a good ROC PPV rate. The different calcanei test parameters for both Flexscan3D and Viewbox 4.1 were unique as compared to the other bone sets, as they allowed for both a direct comparison of hollowed/unhollowed parameters, aligned/unaligned parameters, and run Exact Normal/Exact Slow. Furthermore, they were the only set that explored the possible effects of fragmentation or partial models on the pair-matching process. As with temporals, normals improved the matching process, as did pre-alignment/pre-registration and hollowing. Excitingly, fragmentation seemed to have a minimal effect on the pair-matching process, which still performed quite well.

Asymmetry effects

Calcanei asymmetry studies have mostly focused on the patterns of the anterior and middle articular facets, in pursuit of surgical solutions for aspects such as flat-footed-ness (Ragab et al., 2003, Finnegan, 1978). A study by Ragab et al. demonstrated a rate of 10% asymmetry in side to side variation of anterior and middle articular facets, which is significant as regards to the overall three-dimensional geometry of a pair of calcanei (Ragab et al., 2003). An additional asymmetrical aspect of calcanei shape due to normal variation is that of osteophyte formation on the posterior aspect of the calcanei (the calcaneal tuberosity), otherwise known as calcaneal spurs (Alatassi et al., 2018).

This is thought to increase due to age and genetic factors, and is generally bilateral, but can be asymmetrical in formation (Alatassi et al., 2018, Beytemür and Öncü, 2018). Furthermore, there are numerous normal variations in the shape of the calcanei, such as Sever's disease, pseudofractures and variation in nutrient foramen locations, as seen in Kumar et al, but there is very little documented evidence of (a)symmetry of these features or of how they affect the three-dimensional geometry of the bone (Kumar et al., 1991). Similarly, there several documented non-metric traits on the calcaneus, including the accessory bones of calcaneus secundarius and os subcalsis, plus features such as the difference size and types of the peroneal tubercle (Krapf et al., 2015, Milliken, 1937, Shibata et al., 2014, Bulut et al., 2014, Keles-Celik et al., 2017, Ceroni et al., 2006, Finnegan, 1978). Again, there is almost no information documenting the asymmetry rates of these features, though there is some information regarding the effects on the calcaneus' three-dimensional shape (Shibata et al., 2014).

Algorithm Interactions

Algorithmically, the calcanei generally match well regardless of ICP variant in Flexscan3D and Viewbox. This is due in part to the sheer variation of calcanei shapes including size and arrangement of articular facets, but also due to the algorithms' preference for 'characteristic features' (Chetverikov et al., 2005). Like the temporals, calcanei have a unique orientation of planes and features that orient the models to match correctly more consistently. Even when models were 'fragmented,' meaning the bone itself did not scan well and created only a partial surface model, these models matched well due, again, to their characteristic shape. For example, there is no shape similarity between the anterior multi-faceted aspect of the calcanei and the posterior, single curved aspect of the calcanei (see **Figure 31**).

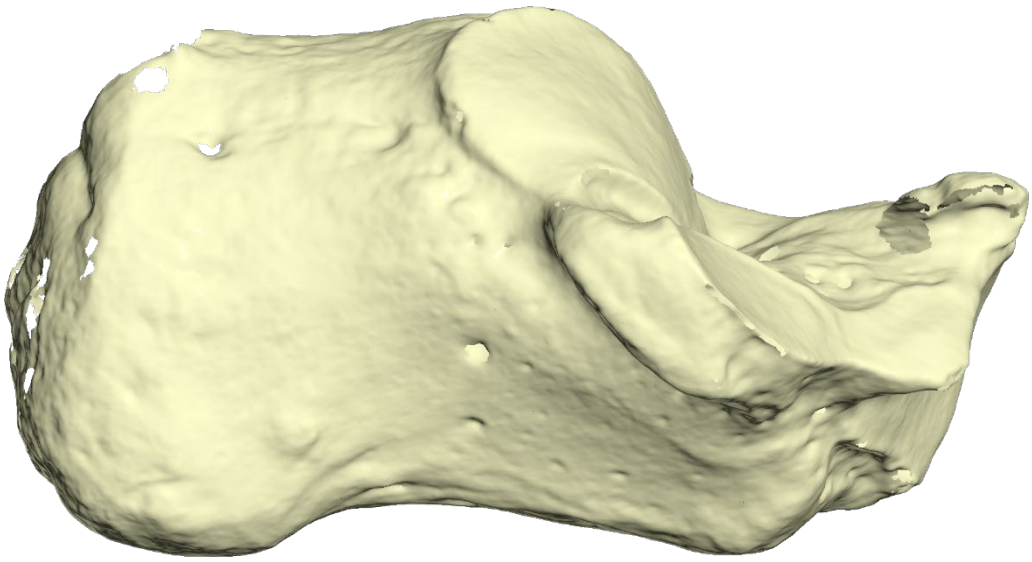

Figure 31. Basic visualisation of calcanei (Cyprus, Left, 1). Notice the distinctive and characteristic differences between the left (posterior) and right (anterior) sides.

Though the articular facets could be similar shape-wise, the orientation of all of the articular facets in connection does not rotate well to fit in any other configuration than the correct one. This is also aided by the fact that the ICP algorithms in this case only match the aspects of the model that are present. Thus, if a fragmented portion of a bone model is matched to a whole model, it will only calculate the similarity on the fragmented portion, not the entire whole model. This is, in fact, a central tenant of most ICP algorithms, that one of the sets being matched is assumed to be a subset of the other (Chetverikov et al., 2005, Chetverikov et al., 2002, Besl and McKay, 1992). While hollowing the models also improved the matching process, like temporals, the presence of normals was a more significant matching factor. This is because normals further highlight the differences between the characteristic aspects of the calcanei, as can be seen in **Figures 32, 33, and 34.**

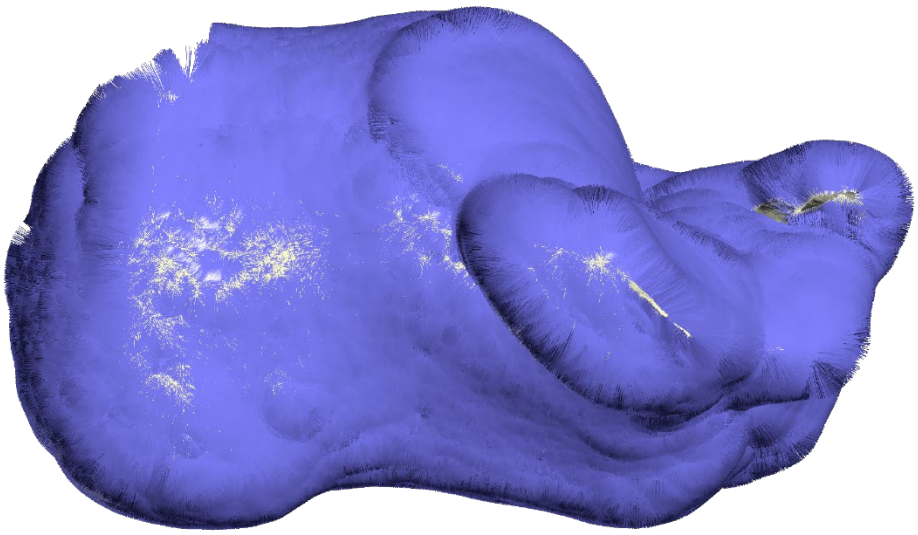

Figure 32. Left Cyprus 1 visualised with normals shown in purple (i.e. the small purple lines). Notice the distinctive shapes between the anterior and posterior sides are emphasized even more than in the basic visualisation.

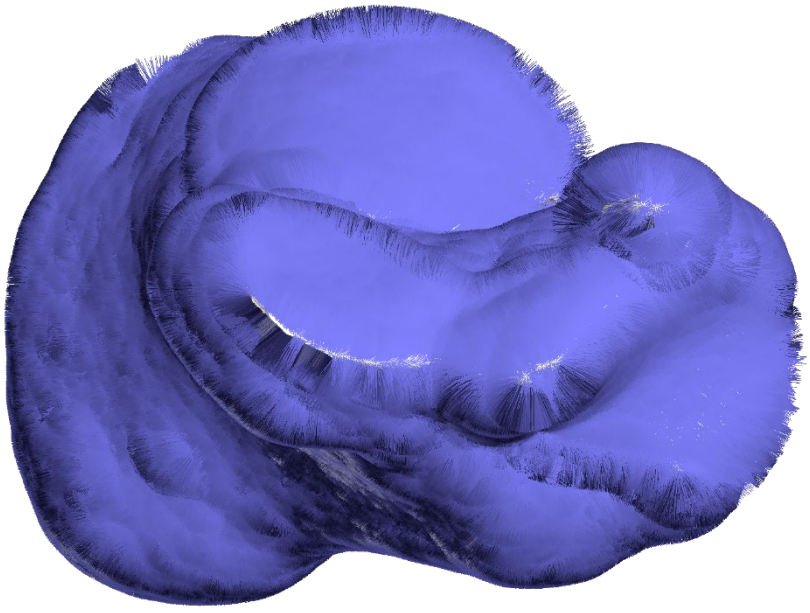

Figure 33. Anterior portion of Left Cyprus 1 visualised with normals shown in purple (i.e. the small purple lines). Notice the emphasis on the articular surfaces.

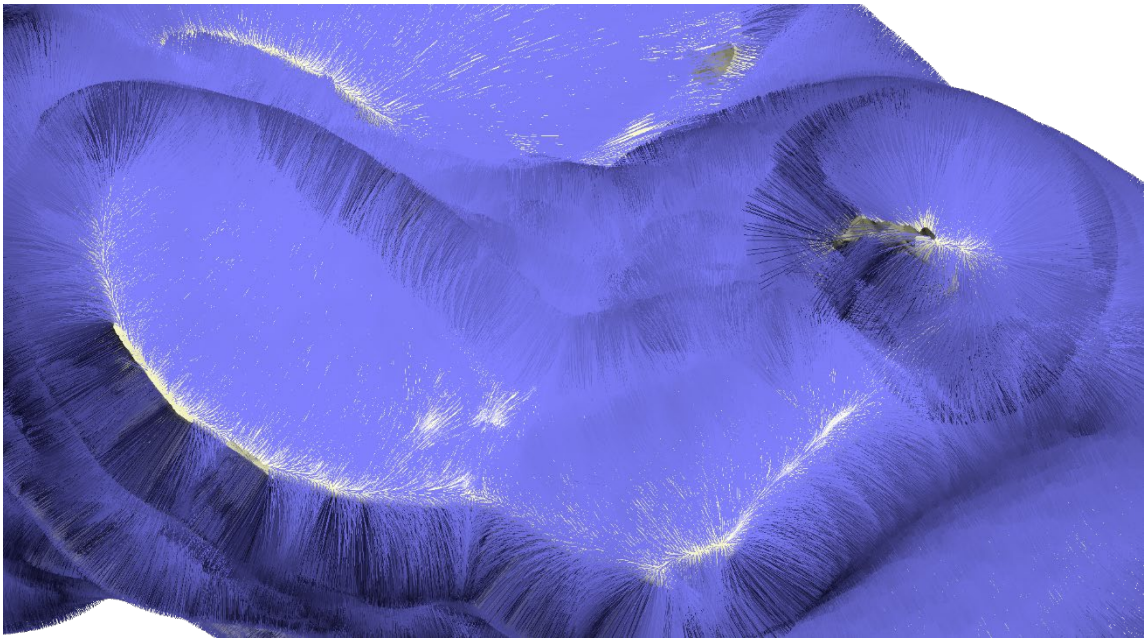

Figure 34. Close up of anterior portion and articular surfaces of Left Cyprus 1 visualised with normals shown in purple (i.e. the small purple lines).

Overall Pros and Cons (As compared to other known methods on this bone)

As calcanei provide limited information for the creation of a biological profile – usually limited to general ageing (adult/juvenile) and stature (though not a preferred method of choice) – there are only a limited number of methods for pair-matching. Unsurprisingly the only other pair-matching method for calcanei is the osteometric sorting technique which uses 'M-statistic' tables (again, defined as $= \frac{|L-R|}{\left(\frac{L+R}{2}\right)}$) (Thomas et al., 2013). Only two measurements were assessed for the calcaneus, that of the length and middle breadth (Thomas et al., 2013). There have been no previous studies done on visual pair-matching of the calcanei. The only other study related specifically to sorting commingled calcanei is by Anastopoulou et al, using osteometric measurements to associate calcanei and tali (Anastopoulou et al., 2018). Intriguingly, they did not have any issues with bilateral asymmetry, which is surprising given the 10% rate of articular facet variation reported by Ragab et al (Ragab et al., 2003). Still, this has interesting implications for pair-matching tali in the future, as well as potentially using algorithmic methods for articulation of the tali and calcanei. The studies by Anastopoulou et al and

Byrd and Adams regarding the high reliability of articulation of the tarsals, give further support to this possibility. Similarly, the tibia has a high reliability of association by articulation with the talus, suggesting that the entire ankle joint may be a good candidate for articulation using algorithmic methods (Adams and Byrd, 2006). Returning to calcanei specifically, both ICP variations in Flexscan3D and Viewbox 4.1 are highly accurate and reliable at associating calcanei and are therefore good options for pair-matching.

Real-World Example

Given the large variation amongst the four sets of bones, two comparison programs and two analysis methods, some mock test cases of real-world scenarios will be explored. As Ubelaker explained, there is no 'cookbook' approach to sorting commingled remains, only good preparation and best practice (Ubelaker, 2008). Thus, these will serve as a suggested guide on how to incorporate MVC methods as best practice in different types of commingled situations. Note that these examples will not distinguish between 'open' and 'closed' situations, as it is assumed that this will affect the final ante- and postmortem positive identification process (i.e. reconciling Disaster Victim Identification forms), but not necessarily the pair-matching process. Similarly, it will focus specifically on pair-matching elements, not the full association of all skeletal elements, though this is, of course, the ultimate goal. It will also not discuss what the scanning options are, or could be, in different situations, as this will be discussed later in the chapter.

<u>Mock Test Case 1 – Small scale, bone type has been tested previously</u>

For a small-scale commingling situation of 15 individuals, which happened to only include humeri, clavicles, temporals and calcanei, and assuming reasonable access to some, but not complete, DNA analysis, the individualisation process might look like this:

Say there are 27 humeri, 25 clavicles, 27 temporals and 23 calcanei recovered from the scene. Given the small number of individuals and only reasonable access to

DNA, the prime comparison program would be Flexscan3D, across the board. For the 27 humeri, this would mean that all the possible pairs and single bones would be identified correctly using the LCV analysis method, with a 100% confidence for both the positive identification and negative identification. DNA would then be used to test only a single side of each pair, or each negative, to link the bones to an individual. For all 25 clavicles, given the low results using the LCV analysis method, it would be ideal if they could be identified solely using DNA. If this was not possible budget-wise, the second-best option would be ROC analysis after Flexscan3D comparison. Though ROC analysis results can be prioritised and changed based on the requirements of the situation, such as using an exclusionary method as opposed to an inclusionary method, only one method will be explored here. For example, this would specifically mean that for clavicles and ROC analysis, an exclusionary approach could be taken using the fixed 97.5% sensitivity rate. For comparison values over the threshold of 1.04, they would be considered negatives, or non-matches. For values that fell below the threshold of 1.04, they would be tested using DNA to confirm the matches. The resulting successful positive and negative matches would therefore directly be linked to the mesh-to-mesh values of the models tested. For the 27 temporals, the best option would be ROC analysis, specifically using the ROC optimal results with a threshold value of 0.688. This would mean that at this threshold value 98.36% of all the positives would be correctly identified and 99.74% of the negatives would be correctly identified, with only 85.93% confidence in those positive matches being correctly identified but 99.97% confidence in the negatives being correctly identified. Thus, the DNA testing would be focused just on the positive matches, and not confirming the negatives. For the 23 calcanei, all the possible pairs and single bones could be correctly identified using the LCV analysis method, with a 100% confidence for both the positive identification and negative identification. All of these assessments, of course, could be improved using excavation/recovery information. For example, if there are different strata present, there is no need to attempt pair-matching for bones that could not be physically (strata) associated. If there was a disturbance of these strata, this could exclude this information.

Mock Test Case 2 – Large scale, known bone type

For a large-scale commingling situation of 100 individuals, which happened to only include humeri, clavicles, temporals and calcanei, and assuming reasonable access to some, but not complete, DNA analysis, the individualisation process might look like this:

For all cases, though Flexscan3D produces more accurate results, the manual MVC method would not be feasible. Thus, Viewbox could be used for all comparisons. In certain cases, for example temporals, LCV analysis would produce better results. Because LCV is not as feasible time-wise as ROC analysis is at that scale, all bones would use ROC analysis. For humeri, temporals and calcanei, this would mean using aligned and hollowed with normals models. For clavicles, this would mean using aligned and hollowed without normals models. Again, in the same manner as the small-scale scenario, there are different possibilities for how to interpret or use the ROC analysis results, which could be adjusted to the necessary requirements. Additional information that would be helpful for interpreting ROC results, though there was not time in this study to explore it fully, would be likelihood ratios. Likelihood ratios can be either positive or negative, and are defined as $\frac{Sensitivity}{1-Specificity}$ and $\frac{1-Specificity}{Sensitivity}$ respectively (Brown and Reeves, 2003, McGee, 2002, MedCalc, 2019a); they can be utilised in a similar fashion to Bayes' Theorem to interval specific post-test odds ratios, where the post-test odds are equal to the pre-test odds multiplied by the likelihood ratio ($posttest\ odds = pretest\ odds \times likelihood\ ratio$) (MedCalc, 2019b, Sonis, 1999, McGee, 2002). In practice, this means that the specific mesh-to-mesh value intervals can be used to further distinguish true pair-matches and negative pair-matches. For an example, see the likelihood ratio chart generated from the Flexscan3D-compared unhollowed temporals (Flexscan3D parameter set 1), shown in **Table 231**. From the interval of mesh-to-mesh values 0.4-0.6, the positive likelihood ratio is ∞, which means that a mesh-to-mesh value that falls below 0.6 is infinitely more times likely to be a positive pair-match than a negative. This can be easily seen in that there were no negative pair-match values which fell within that interval. When the interval rises from

0.6 to 0.8, however, the likelihood ratio is only 3.46. So while it is still more likely that a mesh-to-mesh value between the interval of 0.6 and 0.8 is a positive, it does not have the same assurance. The intervals in **Table 231** are set at 0.2 increments but can be adjusted as desired and set to the two fixed 97.5% sensitivity and specificity rates as well as the optimal, in order to gain a better decision-making tool for commingled situations.

Table 231.

Interval	Positive	Negative	Likelihood ratio	95% CI
0.4 - 0.6	42	0	∞	324.683 to ∞
0.6 - 0.8	16	287	3.460	2.248 to 5.327
0.8 - 1.0	0	1960	0.000	0.000 to 0.250
1.0 - 1.2	0	1150	0.000	0.000 to 0.427
1.2 - 1.4	0	178	0.000	0.000 to 2.765
1.4 - 1.6	0	25	0.000	0.000 to 20.158
Total	58	3600		

Mock Test Case 3 – Unknown bone type

The cases explored so far have only included bones which have already been tested using both MVC methods and analysis methods. Obviously, this does not come close to cataloguing all paired bones in the human body. What happens when there is an untested bone present? Can either of the MVC methods be effectively and reliably used?

This depends on several factors. First, in a forensic context, it is not possible to solely use an untested method for positive identification, due to evidentiary standards in most jurisdictions (2014, Christensen and Crowder, 2009). Thus, it is unlikely that using MVC method on untested bones would be admissible. In an archaeological context, this would be more flexible. Aside from the context for the commingled situation, the bone itself would be the largest consideration, mostly in terms of three-dimensional shape. For example, it is likely that tali will match well, as they tightly articulate with the calcanei, which also match well. This similarly shaped surface (though the inverse), combined with the orienting aspect of the lateral process, make it a good candidate for successful algorithmic matching. Other bones may be harder or less likely. For example, while femurs are very distinctive proximally and distally, they might have similar problems to the humeri using Viewbox's TrICP, in that the midshafts may preferentially

align over the correct ends. Still, the use of MVC without a known, tested sample has unknown sensitivity, specificity, PPV and NPV rates, making any comparison more or less conjecture. Beyond bone shape, another factor to consider is ROC analysis itself. Without a known sample, a threshold value for matching cannot be used. Threshold values change based on the overall size of the elements tested; for example, a positive match threshold for phalanges will be about 0.3, while a positive match threshold for humeri is around 0.8. In theory, bones can be excluded from matching using relative values (i.e. all the bones compared create a range of values from 0.5 to 3, with only a few values at 3, then the values around 3 are not likely to be matches). The LCV method could still be used, as it is only dependent on the relative relationships, not the actual numeric mesh-to-mesh values.

Key Points to Consider

After exploring some mock test cases, a few key points become clear. First, the scale of the commingled situation is the largest factor for determining the utility and type of MVC and analysis method used. Small-scale situations favour Flexscan3D as the comparison method of choice, and it is more feasible to use LCV analysis in addition to ROC analysis. For large-scale situations, it is unfeasible to use Flexscan3D as it is a manual comparison method. Thus, Viewbox is the program of choice. The large scale of the situation also makes LCV analysis more challenging. The optimal method, therefore, is ROC analysis, though it may be a slight trade-off in terms of accuracy. Still, the use of likelihood ratios could improve these results. Furthermore, it is essential to use MVC in consideration with all other information possible from the situation, such as excavation/recovery data and a thorough analysis of resources available (i.e. money for DNA).

Limitations

This study tested pair-matching four sets of different types of bones using both the manual and automatic Mesh-to-mesh Value Comparison methods, and as such was limited in its scope. Of all the potential paired skeletal elements, only four types were

tested; though the four sets were chosen to cover a wide range of shape and structural complexity, this cannot account for all potential variation in paired skeletal elements. The four sets of bones also varied in sample size, and some were stronger sets than others. For example, the humeri set fell below the 100-bone sample size target at only 61 bones. The other sets, though they exceeded the initial target sample size easily (e.g. 203 clavicle models), were not exhaustive in terms of sample size either; this factor was increased by the limitation of time as regards to the pair-matching process. There were only five different populations used, which also cannot count for all potential global and temporal variation. Additionally, all bones used were complete and in good taphonomic condition. The effects of fragmentation and taphonomic differences were thus not fully explored. Preliminary research suggests that fragmented remains can be pair-matched using MVC, and that taphonomy can affect the MVC method (McWhirter, 2018). The effects of taphonomy are generally seen in the scanning process, in that certain bones do not scan well which leads to poor or incomplete models. Modern bones, for instance, often still have fatty residue and are therefore shiny, and 3D structured/white light scanners cannot easily scan shiny surfaces without modification. As the 'fragmented' calcanei results show, however, this does not seem to have a deleterious effect on the pair-matching process, assuming a certain amount of shape complexity. Other taphonomic factors such as fire, however, could warp the shape of bone and cause problems for the MVC process. Beyond the effects of fragmentation and taphonomy, this study also did not examine the potential effects of pathology generally, nor was it able to account for unknown, underlying, potential pathology in the specimens used.

Beyond the sample itself, there were also limitations in terms of the software and algorithms used. As mentioned previously, the matching algorithm for Flexscan3D is known only generally, and not specifically in terms of precise calculations (Langstaff and Karell, 2014). This would likely exclude it for use in court situations, as there is generally a need for methods introduced as part of evidence to be easily reproducible and have calculable, known error rates, and the algorithm itself may not meet the necessary requirements (2014, Christensen and Crowder, 2009, Crown Office and Procurator Fiscal Service, n.d.). For Viewbox 4.1, the algorithms are known but are

limited and slightly different than the Flexscan3D algorithms in both function and accuracy. Furthermore, the full parameters of Viewbox 4.1 were not explored due to time. For example, the program has different settings for the estimation of overlap of the two models, as well as settings that allow for the user to define which parts of models get preferentially matched, both of which have the possibility of drastically improving results. Similarly, not all conditions of the different types of models (aligned, unaligned, hollowed with normals, hollowed without normals, and unhollowed) were able to be tested for every set of bone type, again due to time and computing power limitations.

Iterative closest point (ICP) algorithms in general also have computational limits and rely on certain parameters being met regardless of the models being compared. As an example, the TrICP algorithm assumes 'that the overlapping part of the two sets [models] is characteristic enough to allow for unambiguous matching' (Chetverikov et al., 2002) and requires a 50% overlap between the two models (Chetverikov et al., 2005, Chetverikov et al., 2002). While this works well for whole models (and therefore whole bones), it could be a possible issue for fragmentation pair-matching or for bone shapes that are not characteristic enough. Additionally, there are numerous other ICP variations which could be tested but were not due to the limited scope of this study and the lack of necessary programming resources (Mohammadzade and Hatzinakos, 2013, Du et al., 2010, Kapoutsis et al., 1999). For example, the Iterative Pseudo Point Matching algorithm does not rely on one set of points being a subset of another, so may be a better alternative for fragmented models (Zhang, 1994). Similarly, the Iterative Closest-Normal Point algorithm has a method for three-dimensional face identification using machine learning, regardless of expression, using a variation on normals (Mohammadzade and Hatzinakos, 2013). This process could be modified for bones to take into account variation due to age for example, excluding random asymmetrical osteophyte formation. Additionally, other ICP variants use different methods for calculating the distance between points, with some utilising Root Mean Squared (RMS) values, some Least Squares (LS), some Least Median Squares (LMS) and some Least Trimmed Squares (LTS) (Chetverikov et al., 2005, Chetverikov et al., 2002, Zhang, 1994). Though Trimmed ICP (and thus Viewbox) uses LTS, potentially other options

are equally or more valid (Chetverikov et al., 2005, Chetverikov et al., 2002). Likewise, there are different ways for different ICP variants to handle coordinate systems: some use quaternions, some Voronoi tessellation, and some other distance-based algorithms use Hausdorff distances (Besl and McKay, 1992, Kapoutsis et al., 1999, Zhao et al., 2005). Though the current TrICP and main ICP use quaternions, the other options could potentially improve the pair-matching process (Besl and McKay, 1992, Chetverikov et al., 2005, Chetverikov et al., 2002).

Statistically speaking, there were also limitations with the two types of sensitivity and specificity analyses. The Lowest Common Value (LCV) method is dependent on the initial formatting of the values and has a greater possibility of being influenced by user error. ROC curve analysis, on the other hand, is less prone to user error, but is also insensitive to class distribution, which means that multiple sample populations, skewed or not, can produce similar ROC curves (Marzban, 2004). This means that ROC curves are very successful in distinguishing between good and bad models, but not necessarily good and better models (Marzban, 2004). Similarly, as the Area Under the Curve (AUC), the main way of assessing ROC curves, is calculated from the ROC curve directly, it also does not depend on the prevalence rate of a sample and while it is good at determining good/bad models, it is also not necessarily good at distinguishing between good/better models (Obuchowski, 2003, Marzban, 2004).

Time and processing power were the most significant limitations. Every stage of the MVC process takes time, and often a significant amount. This was compounded by the effect of computational power (or lack thereof), as well as some software bugs. As the MVC component in Viewbox was kindly programmed by a colleague who is an expert dentist and researcher but not free to program full-time, there were several small bugs in the software that caused significant time issues. For example, Viewbox can only be paused mid-comparison at certain points. If it is interrupted at any other point, all data from that run is lost. This was a significant problem when comparison runs would take weeks or even months, as interruptions due to shared working spaces or power cuts were surprisingly frequent. For this study, multiple runs lasting 3 weeks to over 5 weeks were lost, totalling several months of work at minimum. Moreover, the lack of an ability to

compare only left bones against only right bones added significant time as well. For example, if 50 lefts could be compared to only 50 rights, that would only be 2,500 comparisons; with the current settings, this could only be achieved by individually running each of the 50 lefts against the 50 rights (2,500 comparisons but with extra set up time) or by running all 100 lefts and rights against each other for 9,990 comparisons.

Finally, the last limitation is related to data storage. Three-dimensional modelling often produces a huge amount of data. For example, one day of scanning Cretan calcanei created about 30 gigabytes of data for approximately 12 calcanei. In testing hundreds of bones, this adds up incredibly quickly, especially with different model conditions being created from the initial data.

Advantages

Three Dimensional Digital Models

Methods for sorting commingled remains that use three-dimensional, digital models of bones as opposed to just dry bone have several advantages. First, there is a permanent record of the bone. Dry bone naturally degrades over time, especially with excessive handling. Using three-dimensional models instead not only helps prevent this degradation, but also provides a way to work with bone in its original condition, without compromising its integrity. Furthermore, should something happen to the real bone, either accidentally or with malicious intent (as in wilful destruction of evidence from mass graves, for example), three-dimensional models provide an accurate and usable record. Instead of disappearing completely, a three-dimensional model can be 3D printed as many times as necessary. Additionally, while photographs and other measurement methods are still important, especially in forensic contexts, three-dimensional scanning methods can often incorporate both accurate visualisation and dimensions. This means that, unlike photographs and other measurements, models are both more accurate and more complete representations of real bone dimensionally-speaking, and can be thus treated as effectively the same. Digital models also allow for measurements that are either not possible or not feasible in real bone, such as volumetric measurements and measurements of internal structure. Measurements produced digitally are furthermore

saveable and easily shown to other researchers for confirmation or correction. These saveable processes, including the model itself, are also helpful in that they are easy to transfer and store around the world. Specimens need not be analysed solely in the location they were found but can be easily transported for analysis around the world without the same need for biological permitting as real bone. Furthermore, specimens can be easily analysed in situ. Bone, for example, can be easily identified and subsequently analysed (together or individually) in heavily decomposed remains via CT without the need to alter the remains in any way.

Mesh-to-mesh Value Comparison as a Method

In addition to the advantages of using three-dimensional digital models, the mesh-to-mesh value comparison (MVC) method also has several advantages of its own. MVC is a method that can be easily and accurately reproduced, both in terms of model building and comparison for pair-matching. It does not rely on user expertise for accuracy or reliability, unlike visual pair-matching (Adams and Byrd, 2006, Adams and Konigsberg, 2004); this includes both model building accuracy and method of algorithmic model comparison. Both the model building process and algorithmic comparison process have known error rates and would meet the criteria for admissibility in court. Beyond admissibility, these known algorithms also allow other researchers to contribute to testing the comparison method, even if they don't have access to either of the manual or automatic software. The known algorithms for comparison also eliminate issues connected to a user's expertise, or lack thereof.

Though it cannot yet match un-paired skeletal elements, the MVC method also has two distinct advantages over traditional osteometric comparison: the measurement of three-dimensional geometry and the ability to easily visualise variation. In its simplest form, the MVC method shows rough visual similarity by the superimposition of the left and right sides. As mentioned previously, in both Flexscan3D and Viewbox 4.0/4.1 there is also a feature called 'deviation analysis,' which will colour code every aspect of difference between the two models, on a sliding scale. This visualisation tool makes it

easy to see areas of bony difference due to differential muscle use, as well as any other potential anomalies, as seen in previous Figures.

As compared to DNA, though MVC can be expensive, it can also be cost-effective. With DNA, regents need to be purchased for every new sample, and generally tests are run in triplicate. At a price of £15-17 per sample, the initial cost is high, and more so when run in triplicate (Qiagen, 2019, ThermoFisher Scientific, 2019b, ThermoFisher Scientific, 2019c, Promega, 2019a, Promega, 2019b). With MVC, though the equipment and software can be expensive, the price is a one-off purchase and does not need to be repeated. Scanners for example range in price, and as long as the accuracy is good, the cheapest models can still be effective. Additionally, the cheapest models, 3D structured/white light scanners, require almost no maintenance; at most you are generally paying for a replacement bulb for the project part of the scanner. As the author has also personally travelled across various countries for this project carrying a portable 3D structured/white light scanner, she can also vouch for its feasibility in both transportation and set up. It is also worth noting that the MVC process is non-destructive, unlike DNA, which often requires the destruction of large portions of bone in order to secure enough genetic material. This destruction can limit or entirely erase other opportunities for analysis, a significant problem should the DNA extraction and analysis fail. Finally, MVC can also (and should, ideally) be used concurrently with other methods. While a handful of DNA samples are being run, or antemortem data is being collected, the MVC process can simultaneously be taking place, adding and confirming more information to the identification process. Similarly, if remains are partially articulated due to soft tissue, this factor can be taken into account for both the DNA and MVC analysis processes.

Further Research, Improvements, and Other Considerations

In any research, there always remains more to be tested. The mesh-to-mesh value comparison (MVC) method was no exception; in fact, the project produced more avenues of research with every new condition tested. To confirm the findings of the project and increase MVC's flexibility for a greater range of commingled situations,

more paired skeletal elements must be tested. Though the method works well across several populations, more populations will also need to be tested. The effects of pathology need to be explored, in addition to the effects of taphonomy and fragmentation. All three have the possibility of drastically changing and improving the method. Another avenue of exploration should be a method of using MVC and iterative closest point algorithms for articulation, adding a hopefully reliable osteometric method for that technique to the currently used, only qualitative method (Adams and Byrd, 2006).

Algorithmically there are also numerous variations of ICP that could be tested, and which might improve the method overall (Mohammadzade and Hatzinakos, 2013, Du et al., 2010, Kapoutsis et al., 1999). Additionally, trialling different prioritisation algorithms in addition to the TrICP algorithm in Viewbox would be the best way to improve the automated MVC method, hopefully re-creating the accuracy of Flexscan3D, but with known factors that would be admissible in court settings.

The pair-matching programs could be improved, addressing the software bugs and matching issues, hopefully making it free or low-cost in the process. Instead of having to build models by hand, hollow and align by hand, compare the results by hand, statistically analyse in a different program, and every step in between, the improved and specialised program could do it all automatically. It could run different algorithms for different bones, should it be found that other algorithms work better for clavicles for example, and could even produce the requisite error rates and confidence intervals. One possible avenue to accomplish this automation could be the introduction of machine learning to the process, or some other form of artificial intelligence.

Technology is constantly improving, both hardware and software-wise. When the models for this study were being 3D white/structured light scanned, for example, the models had to be built by hand with the user aligning and stitching the partial models that the software program would then confirm. With more recent scanners, however, the partial scans are automatically stitched during the scanning process, so that the user has a complete and usable model as soon as the object is scanned. This would save a significant amount of time, whether models were built for MVC or other applications,

possibly cutting scanning/building time in half or even more. Additionally, with the advent of supercomputing, computing clusters, and virtual machines, the processing of comparison runs could be significantly sped up, and interruptions due to power cuts and shared working spaces could be minimised or prevented entirely. A virtual machine ensures that there is not a single machine (computer) that will be accidentally logged on to or turned off by another user, and the processing power of that virtual machine, or cluster, will be at least equal to, and generally greater than, a single user desktop situation. As a concrete example, though the University of Edinburgh's virtual machine cluster, Eleanor, did not exist until the end of this project, its hardware calibration as compared to the other machines used for this study is only 19 seconds per iteration, based on the clavicle data set, which is a 25% reduction in computational time. However, Eleanor is still significantly less powerful as a virtual machine system than Eddie, the University of Edinburgh's supercomputing cluster (Information Services, 2018b, Information Services, 2018a). Currently, most supercomputing clusters only run Linux based operating systems, which would require a new software design for either the manual or automatic MVC methods. If applied to the automatic version with the other software and hardware tweaks mentioned previously, however, MVC could be drastically sped up.

As a final note on technological considerations, there is also the issue of data storage. As mentioned previously, digital model data can be huge and requires proper storage space. With the improvement and cost reduction of storage, these issues will hopefully become minimal. Beyond hardware issues, however, remain the ethical considerations surrounding the storage of information regarding human remains or patient data. Patient data protection in the United Kingdom, and most other countries, is subject to rigorous standards and rightly so (National Health Services, 2019, Health and Human Services, 2009). Physical human remains, skeletal or otherwise, are also subject to strict regulation and protection under the Human Tissue Act 2004 (c. 30)and the Human Tissue (Scotland) Act 2006 (asp 4). However, three-dimensional, digital models of bone can end up somewhere in a grey area. Should there be specific patient information connected to the model, such as a name, this would undoubtedly fall under

normal patient confidentiality schemes (National Health Services, 2019). Once anonymized, this could also fall under normal pseudo-anonymization protection measures (National Health Services, 2019). What is more challenging is when a researcher has both sets of information available. The National Health Services, for example, have very strict regulations about how their un-anonymized data can be stored and used (Academic and Clinical Central Office for Research and Development, n.d.). Similarly, normal forensic anthropological research goes through institutional review boards for ethical considerations and has similar policies (School of History Classics and Archaeology, 2017). To the author's knowledge, however, there is no specific institutional or legal considerations for storing 3D medical modelling data for research purposes beyond general suggestions (National Health Services, 2019, Academic and Clinical Central Office for Research and Development, n.d.). While that may be generally enough of a policy, it seems prudent to establish a specific policy on 3D modelling data, both forensically and archaeologically speaking, before it becomes an issue. This is especially important as many researchers are unfamiliar with certain aspects of digital data, such as metadata.

Beyond technological hardware/software improvements, a real-world test case for the MVC method would be an ideal next step. Two cases that are immediately possible would be Malaysian Airlines Flight 17 which was shot down over the Ukraine, and any of the recent Italian ship disasters (Langstaff and Karell, 2015, Piscitelli et al., 2016). Both situations made use of on-the-scene or post-scene CT scanning, meaning the digital data already exists for testing (Langstaff and Karell, 2015, Olivieri et al., 2017). Furthermore, the Ukrainian situation would be ideal as it is a closed situation, meaning the passengers on board are part of a finite and known list, and that there have already been traditional methods of individualisation applied for comparison (Langstaff and Karell, 2015, College of Policing, 2018). The Italian ship disasters would be an interesting test case as well, even though it is an open situation (the people on the boat could be from anywhere), because although they have been DNA testing remains, the waterlogged conditions of the boat have significantly hampered the results (Olivieri et al., 2017, Bertoglio et al., 2017). The waterlogging has been producing results with only

a 1 in 10^6 probabilistic chance of a match, whereas in most forensic contexts one would need a 1 in 10^9 probabilistic chance of a match to be considered valid (Bertoglio et al., 2017, Olivieri et al., 2017, Crown Prosecution Service, 2014).

Final considerations about the MVC method and using ICP algorithms include that pair-matching is not the only possible use for ICP algorithms and, beyond the previous suggestion, it can be used to compare or match any two or more digital objects (think weapon and wound comparison, or surgically speaking for prothesis building). Additionally, MVC is by no means designed to be used as the *only* individualisation technique for a commingled situation. Ideally in commingled situations one uses as many reliable methods as is possible in combination to obtain the best, most accurate result, and return as many people as possible to their loved ones and communities. This includes utilising information such as stratigraphic information and orientation or remains, clothing/personal effects, taphonomy, articulation, osteometric data, DNA where feasible and possible, and new techniques such as MVC.

Conclusion

Situations involving commingled human remains are generally marked by tragedy. In order to give a name to an individual and return their remains to their loved ones and community, commingled remains must first be sorted, or individualised. There are only limited methods, however, to aid in this individualisation process. This dissertation tested a new method for individualisation called mesh-to-mesh value comparison (MVC). MVC is a method for pair-matching, or associating homologous bony elements, which uses three-dimensional models of bones and compares their three-dimensional shape digitally to assess similarity. This similarly was measured in millimetres.

Two different version of the MVC method, one manual and the other automatic, were tested. The manual method used the program Flexscan3D, while the automatic method used the program Viewbox 4.1. Both methods use Iterative Closest Point algorithms for their comparison process, though the specific details of the algorithms were slightly different program to program. Four different sets of bones were tested using both MVC methods: humeri, clavicles, temporals and calcanei. This resulted in 384,075 unique comparison values. All of the comparison data were analysed using sensitivity, specificity, positive predictive value and negative predictive value rates. These rates were calculated using two different methods: Lowest Common Value (LCV) analysis and Receiver Operating Characteristic (ROC) curve analysis.

Results varied between the different bone types and analysis methods but overall were high in terms of accuracy. The most accurate bone for pair-matching using the MVC method, regardless of the manual or automatic method, was temporals. The lowest-performing bone set for both the automatic and manual MVC methods were the clavicles, which were the single exception to the high performance of the method overall. When comparing the MVC method to currently available individualisation techniques, the accuracy of the MVC method is generally higher and is advantageous in that it has known error rates.

There are still many avenues of MVC methods to explore. The method needs to be tested on different bone sets and could be used for comparing fragmented remains or assessing individualisation through articulation. Furthermore, there are numerous variants of the ICP algorithms that could improve aspects of the MVC method, such as time taken or the accuracy of matching clavicles.

Citations

2004. Human Tissue Act. *c. 30.* United Kingdom: The Stationary Office Limited.

2006. Human Tissue (Scotland) Act. *asp 4.* United Kingdom: The Stationary Office Limited.

2014. Criminal Practice Directions: Amendment No. 2. United Kingdom: England and Wales Court of Appeal (Criminal Division).

2019a. *3D Slicer* [Online]. Available: https://www.slicer.org/ [Accessed 22 April 2019].

2019b. *CloudCompare* [Online]. Available: https://www.cloudcompare.org/main.html [Accessed 22 April 2019].

2019c. *CT Scanner Buyers Guide* [Online]. Available: https://info.blockimaging.com/hs-fs/hub/21795/file-29903060-pdf/Non-searchables/ct-scanner-buyers-guide.pdf [Accessed 22 April 2019].

2019d. *FlexScan3D* [Online]. Available: https://www.polyga.com/hdi-3d-scanner/flexscan3d/ [Accessed 22 April 2019].

2019e. *MeshLab* [Online]. [Accessed 22 April 2019].

2019f. *OsiriX DICOM Viewer | The world famous medical imaging viewer* [Online]. Available: https://www.osirix-viewer.com/ [Accessed 22 April 2019].

3D INSIDER. 2018. *3D Printer Price: How Much Does a 3D Printer Cost?* [Online]. Available: https://3dinsider.com/cost-of-3d-printer/ [Accessed 22 April 2019].

3D NATIVES. 2019. *TOP 13 Best Low Cost 3D Scanners (2019 Update)* [Online]. Available: https://www.3dnatives.com/en/top-10-low-cost-3d-scanners280320174/ [Accessed 22 April 2019].

ABDEL FATAH, E. E., SHIRLEY, N. R., MAHFOUZ, M. R. & AUERBACH, B. M. 2012. A three-dimensional analysis of bilateral directional asymmetry in the human clavicle. *American Journal of Physical Anthropolology,* 149**,** 547-59.

ACADEMIC AND CLINICAL CENTRAL OFFICE FOR RESEARCH AND DEVELOPMENT. n.d. *Lothian Researcher Safe Haven* [Online]. Available: http://www.accord.ed.ac.uk/researcher-access-research-data/lothian-researcher-safe-haven [Accessed 27 March 2019].

ADAMS, B. J. & BYRD, J. E. 2006. Resolution of small-scale commingling: a case report from the Vietnam War. *Forensic Sci Int,* 156**,** 63-69.

ADAMS, B. J. & BYRD, J. E. 2008. Recovery, analysis, and identification of commingled human remains. Totowa, N.J.: Humana Press,.

ADAMS, B. J. & KONIGSBERG, L. W. 2004. Estimation of the most likely number of individuals from commingled human skeletal remains. *Am J Phys Anthropol,* 125**,** 138-151.

ADAMS, B. J. & MAVES, R. C. 2002. Radiographic identification using the clavicle of an individual missing from the Vietnam conflict. *Journal of Forensic Sciences,* 47**,** 369-73.

ALATASSI, R., ALAJLAN, A. & ALMALKI, T. 2018. Bizarre calcaneal spur: A case report. *International Journal of Surgery Case Reports,* 49**,** 37-39.

ANASTOPOULOU, I., KARAKOSTIS, F. A., BORRINI, M. & MORAITIS, K. 2018. A Statistical Method for Reassociating Human Tali and Calcanei from a Commingled Context. *Journal of Forensic Sciences,* 63**,** 381-385.
ANDERSEN, L. & WENZEL, A. 1995. Individual identification by means of conventional bitewing film and subtraction radiography. *Forensic Sci Int,* 72**,** 55-64.
AUERBACH, B. M. & RAXTER, M. H. 2008. Patterns of clavicular bilateral asymmetry in relation to the humerus: variation among humans. *J Hum Evol,* 54**,** 663-674.
AUERBACH, B. M. & RUFF, C. B. 2006. Limb bone bilateral asymmetry: variability and commonality among modern humans. *J Hum Evol,* 50**,** 203-218.
AUTODESK. 2019a. *Netfabb* [Online]. Available: https://www.autodesk.com/education/free-software/netfabb-premium [Accessed 22 April 2019].
AUTODESK. 2019b. *Tinkercad | Create 3D digital designs with online CAD* [Online]. Available: https://www.tinkercad.com/ [Accessed 22 April 2019].
BAKER, P. T. & NEWMAN, R. W. 1957. The use of bone weight for human identification. *Am J Phys Anthropol,* 15**,** 601-618.
BERNAT, A., HUYSMANS, T., VAN GLABBEEK, F., SIJBERS, J., GIELEN, J. & VAN TONGEL, A. 2014. The anatomy of the clavicle: a three-dimensional cadaveric study. *Clin Anat,* 27**,** 712-23.
BERTOGLIO, B., GRIGNANI, P., DI SIMONE, P., POLIZZI, N., BERTUGLIA, C., CATTANEO, C., PRESCIUTTINI, S. & PREVIDERÈ, C. 2017. Preliminary results of the genetic identifications of the Lampedusa 2013 shipwreck victims. *La Revue de Médecine Légale,* 8**,** 184.
BESL, P. J. 1988. Geometric modeling and computer vision. *Proceedings of the IEEE,* 76**,** 936-958.
BESL, P. J. & MCKAY, N. D. 1992. A method for registration of 3-D shapes. *IEEE Transactions on Pattern Analysis and Machine Intelligence,* 14**,** 239-256.
BEYTEMÜR, O. & ÖNCÜ, M. 2018. The age dependent change in the incidence of calcaneal spur. *Acta Orthopaedica et Traumatologica Turcica,* 52**,** 367-371.
BLAU, S. 2017. The Effects of Weathering on Bone Preservation. *In:* SCHOTSMANS, E. M. J., MARQUEZ-GRANT, N. & FORBES, S. L. (eds.) *Taphonomy of Human Remains: Forensic Analysis of the Dead and the Depositional Environment.*
BLAU, S., ROBERTSON, S. & JOHNSTONE, M. 2008. Disaster victim identification: new applications for postmortem computed tomography. *J Forensic Sci,* 53**,** 956-61.
BOUKEBBAB, S., BOUCHENITFA, H., BOUGHOUAS, H. & LINARES, J. M. 2007. Applied iterative closest point algorithm to automated inspection of gear box tooth. *Computers & Industrial Engineering,* 52**,** 162-173.
BREUCKMANN, B. 2014. 25 Years of High Definition 3D Scanning: History, State of the Art, Outlook. *Proceedings of the EVA London 2014 on Electronic Visualisation and the Arts.* London, UK: BCS.

BRITISH MACHINE VISION ASSOCIATION AND SOCIETY FOR PATTERN RECOGNITION. 2019. *What is computer vision?* [Online]. Available: http://www.bmva.org/visionoverview [Accessed 22 April 2019].

BRKIC, H., STRINOVIC, D., KUBAT, M. & PETROVECKI, V. 2000. Odontological identification of human remains from mass graves in Croatia. *International Journal of Legal Medicine,* 114**,** 19-22.

BROGDON, B. G. 1998. *Forensic Radiology*, CRC-Press.

BROWN, M. D. & REEVES, M. J. 2003. Interval likelihood ratios: Another advantage for the evidence-based diagnostician. *Annals of Emergency Medicine,* 42**,** 292-297.

BRUDER, C. E., PIOTROWSKI, A., GIJSBERS, A. A., ANDERSSON, R., ERICKSON, S., DIAZ DE STAHL, T., MENZEL, U., SANDGREN, J., VON TELL, D., POPLAWSKI, A., CROWLEY, M., CRASTO, C., PARTRIDGE, E. C., TIWARI, H., ALLISON, D. B., KOMOROWSKI, J., VAN OMMEN, G. J., BOOMSMA, D. I., PEDERSEN, N. L., DEN DUNNEN, J. T., WIRDEFELDT, K. & DUMANSKI, J. P. 2008. Phenotypically concordant and discordant monozygotic twins display different DNA copy-number-variation profiles. *American Journal of Human Genetics,* 82**,** 763-71.

BUIKSTRA, J. E. & UBELAKER, D. H. 1994. Standards for data collection from human skeletal remains. *Arkansas Archeological Survey Research Series.* Fayetteville, Arkansas: Arkansas Archeological Survey.

BULUT, M. D., YAVUZ, A., BORA, A., GOKALP, M. A., OZKACMAZ, S. & BATUR, A. 2014. Three-Dimensional CT Findings of Os Calcaneus Secundarius Mimicking a Fracture. *Case Rep Radiol,* 2014**,** 537062.

BUTLER, J. M. 2010. Chapter 5 - DNA Extraction. *In:* BUTLER, J. M. (ed.) *Fundamentals of Forensic DNA Typing.* San Diego: Academic Press.

BYRD, J. E. 2008. Models and Methods for Osteometric Sorting. *In:* ADAMS, B. J. & BYRD, J. E. (eds.) *Recovery, Analysis, and Identification of Commingled Human Remains.* Humana Press.

BYRD, J. E. & ADAMS, B. J. 2003. Osteometric sorting of commingled human remains. *J Forensic Sci,* 48**,** 717-24.

CERONI, D., DE COULON, G., SPADOLA, L., DE ROSA, V. & KAELIN, A. 2006. Calcaneus Secundarius Presenting as Calcaneonavicular Coalition: A Case Report. *The Journal of Foot and Ankle Surgery,* 45**,** 25-27.

CHAI, D. S., LAN, Y. W., TAO, C., GUI, R. J., MU, Y. C., FENG, J. H., WANG, W. D. & ZHU, J. A. 1989. A study on the standard for forensic anthropologic identification of skull-image superimposition. *J Forensic Sci,* 34**,** 1343-56.

CHEN, Y. & MEDIONI, G. 1992. Object modelling by registration of multiple range images. *Image and Vision Computing,* 10**,** 145-155.

CHETVERIKOV, D., STEPANOV, D. & KRSEK, P. 2005. Robust Euclidean alignment of 3D point sets: the trimmed iterative closest point algorithm. *Image and Vision Computing,* 23**,** 299-309.

CHETVERIKOV, D., SVIRKO, D., STEPANOV, D. & KRSEK, P. The Trimmed Iterative Closest Point Algorithm. Proceedings of 16th International Conference on Pattern Recognition, 2002. 545-548.

CHIAL, H. & CRAIG, J. 2008. mtDNA and Mitochondrial Diseases. *Nature Education,* 1**,** 217.
CHRISTENSEN, A. M. & CROWDER, C. M. 2009. Evidentiary standards for forensic anthropology. *J Forensic Sci,* 54**,** 1211-6.
COLLEGE OF POLICING. 2018. *Recovering and identifying the deceased and human remains* [Online]. Available: https://www.app.college.police.uk/app-content/civil-emergencies/disaster-victim-identification/recovering-and-identifying-the-deceased-and-human-remains/#identification-criteria [Accessed 22 April 2019].
COLLEGE OF POLICING. 2019. *Disaster Victim Identification: Definitions* [Online]. Available: https://www.app.college.police.uk/app-content/civil-emergencies/disaster-victim-identification/definitions/ [Accessed 22 April 2019].
COOTES, T. F., TAYLOR, C. J., COOPER, D. H. & GRAHAM, J. 1995. Active Shape Models-Their Training and Application. *Computer Vision and Image Understanding,* 61**,** 38-59.
CROWN OFFICE AND PROCURATOR FISCAL SERVICE. 2019. *Our role in investigating deaths (Diaster Victim Identification)* [Online]. Available: http://www.copfs.gov.uk/investigating-deaths/our-role-in-investigating-deaths [Accessed 22 April 2019].
CROWN OFFICE AND PROCURATOR FISCAL SERVICE. n.d. *Guidance booklet for expert witnesses: The role of the expert witness and disclosure* [Online]. Available: http://www.copfs.gov.uk/images/Documents/Prosecution_Policy_Guidance/Guidelines_and_Policy/Guidance%20booklet%20for%20expert%20witnesses.PDF [Accessed 22 April 2019].
CROWN PROSECUTION SERVICE. 2014. *Crown Prosecution Service: Guidance on Expert Evidence* [Online]. Judiciary UK. Available: http://ukafn.org/wp-content/uploads/2015/07/Expert-Evidence-First-edition-2014.pdf [Accessed 22 April 2019].
DANGERFIELD, A. 2014. *Remembering the Marchioness disaster* [Online]. BBC News. Available: https://www.bbc.com/news/uk-england-london-28839099 [Accessed 22 April 2019].
DELONG, E. R., DELONG, D. M. & CLARKE-PEARSON, D. L. 1988. Comparing the areas under two or more correlated receiver operating characteristic curves: a nonparametric approach. *Biometrics,* 44**,** 837-45.
DESIGNING BUILDINGS. 2018. *Lakanal House fire - Designing Buildings Wiki* [Online]. Available: https://www.designingbuildings.co.uk/wiki/Lakanal_House_fire [Accessed 22 April 2019].
DEVLIN, J. B., HERRMANN, N. P., SCHMIDT, C. W. & SYMES, S. A. 2008. Bone color as an interpretive tool of the depositional history of archaeological cremains. *The Analysis of Burned Human Remains.* San Diego: Academic Press.
DHAL SOFTWARE. Kifissa, Greece.
DU, S., ZHENG, N., YING, S. & LIU, J. 2010. Affine iterative closest point algorithm for point set registration. *Pattern Recognition Letters,* 31**,** 791-799.

EKIZOGLU, O., HOCAOGLU, E., INCI, E., CAN, I. O., AKSOY, S. & SAYIN, I. 2015a. Estimation of forensic age using substages of ossification of the medial clavicle in living individuals. *International Journal of Legal Medicine,* 129**,** 1259-1264.

EKIZOGLU, O., HOCAOGLU, E., INCI, E., SAYIN, I., SOLMAZ, D., BILGILI, M. G. & CAN, I. O. 2015b. Forensic age estimation by the Schmeling method: computed tomography analysis of the medial clavicular epiphysis. *Int J Legal Med,* 129**,** 203-10.

EUROPEAN AGENCY FOR SAFETY AND HEALTH AT WORK. 2019. *Directive 2013/59/Euratom - protection against ionising radiation - Safety and health at work - EU-OSHA* [Online]. Available: https://osha.europa.eu/en/legislation/directives/directive-2013-59-euratom-protection-against-ionising-radiation [Accessed 22 April 2019].

EYMAN, C. E. 1965. Ultraviolet fluorescence as a means of skeletal identification. *American Antiquity,* 31**,** 109-112.

FACCHINI, F., MARIOTTI, V., BONFIGLIOLI, B. & BELCASTRO, M. 2006. *Les collections ostéologiques et ostéoarchéologiques du musée d'Anthropologie de l'université de Bologne (Italie)*.

FAIRGRIEVE, S. I. 2009. *Forensic Cremation: Recovery and Analysis,* Boca Raton, CRC Press.

FAWCETT, T. 2006. An introduction to ROC analysis. *Pattern Recognition Letters,* 27**,** 861-874.

FEDERAL BUREAU OF INVESTIGATION. 2019. *Combined DNA Index System (CODIS) — FBI* [Online]. FBI. Available: https://www.fbi.gov/services/laboratory/biometric-analysis/codis [Accessed 22 April 2019].

FINNEGAN, M. 1978. Non-metric variation of the infracranial skeleton. *Journal of anatomy,* 125**,** 23-37.

FRABRIS-ROTELLI, I. N. & GREEFF, J.-F. 2012. *An overview of image segmentation techniques* [Online]. Available: https://repository.up.ac.za/bitstream/handle/2263/21974/FabrisRotelli_Overview(2012).pdf [Accessed 22 April 2019].

FRAGA, M. F., BALLESTAR, E., PAZ, M. F., ROPERO, S., SETIEN, F., BALLESTAR, M. L., HEINE-SUNER, D., CIGUDOSA, J. C., URIOSTE, M., BENITEZ, J., BOIX-CHORNET, M., SANCHEZ-AGUILERA, A., LING, C., CARLSSON, E., POULSEN, P., VAAG, A., STEPHAN, Z., SPECTOR, T. D., WU, Y. Z., PLASS, C. & ESTELLER, M. 2005. Epigenetic differences arise during the lifetime of monozygotic twins. *Proceedings of the National Academy of Sciences (U.S.A.),* 102**,** 10604-9.

FRIESS, M. 2012. Scratching the Surface? The use of surface scanning in physical and paleoanthropology. *J Anthropol Sci,* 90**,** 7-31.

FULTON, B. A., MELOAN, C. E. & FINNEGAN, M. 1986. Reassembling scattered and mixed human remains by trace element ratios. *Journal of Forensic Science,* 31**,** 1455-1462.

GARCIA-DONAS, J. G. & KARELL, M. A. 2019. *RE: St. Andrews Database.*

GARRIDO-VARAS, C. & INTRIAGO LEIVA, M. 2012. Managing commingled remains from mass graves: considerations, implications and recommendations from a human rights case in Chile. *Forensic Science International,* 219**,** e19-24.
GARRIDO-VARAS, C., RATHNASINGHE, R., THOMPSON, T. & SAVRIAMA, Y. 2015. A New Method to Pair-match Metacarpals Using Bilateral Asymmetry and Shape Analysis. *Journal of Forensic Sciences,* 60**,** 118-123.
GIRDWOOD, L. K. & KARELL, M. A. 2019. *RE: Ballumbie Database.*
GOLDBERG, D. 2018. *History of 3D Printing: It's Older Than You Think [Updated]* [Online]. Available: https://www.autodesk.com/redshift/history-of-3d-printing/ [Accessed 22 April 2019].
GOLDMAN, L. W. 2007. Principles of CT and CT technology. *J Nucl Med Technol,* 35**,** 115-28; quiz 129-30.
GONZALEZ-RODRIGUEZ, J. & FOWLER, G. 2013. A study on the discrimination of human skeletons using X-ray fluorescence and chemometric tools in chemical anthropology. *Forensic Sci Int,* 231**,** 407.e1-6.
GREGORY, J. 2017. *Grenfell Tower investigator tells of painstaking process of recovering remains* [Online]. The Guardian. Available: http://www.theguardian.com/uk-news/2017/jul/12/grenfell-tower-investigator-vows-to-provide-answers-for-victims-families [Accessed 22 April 2019].
GUERRA, R. & MARTÍN, Á. 1999. Excavaciones arqueológicas en la Catedral de Eivissa. Eivissa (Ibiza).
GUTEKUNST, M. 2015. *Commingled Human Remains: Testing the Mesh-to-Mesh Method on the Calcanei.* MSc, University of Edinburgh.
HAAPASALO, H., KANNUS, P., SIEVANEN, H., PASANEN, M., UUSI-RASI, K., HEINONEN, A., OJA, P. & VUORI, I. 1998. Effect of long-term unilateral activity on bone mineral density of female junior tennis players. *J Bone Miner Res,* 13**,** 310-9.
HALL, D. & CACHART, R. 2005. Ballumbie Church (Murroes parish), long cist cemetery; medieval church and graveyard. *Discovery Excavation Scotland,* 6**,** 21.
HAMILL, J. 2003. *Biomechanical basis of human movement,* Philadelphia ; London, Philadelphia ; London : Lippincott Williams & Wilkins.
HANLEY, J. A. & MCNEIL, B. J. 1983. A method of comparing the areas under receiver operating characteristic curves derived from the same cases. *Radiology,* 148**,** 839-43.
HEALTH AND HUMAN SERVICES. 2009. *Summary of the HIPAA Security Rule | HHS.gov* [Online]. United States Government. Available: https://www.hhs.gov/hipaa/for-professionals/security/laws-regulations/index.html [Accessed 22 April 2019].
HINGSAMMER, A. M., LAZAROS, V., DOMINIK, M. C. & FURNSTAHL, P. 2015. Three-dimensional corrective osteotomies of mal-united clavicles--is the contralateral anatomy a reliable template for reconstruction? *Clin Anat,* 28**,** 865-71.
HISTORIC ENVIRONMENT SCOTLAND. n.d. *St. Andrews, South Street, The Parish Church of the Holy Trinity* [Online]. Available: http://www.scotlandsplaces.gov.uk/record/rcahms/34347/st-andrews-south-

street-parish-church-holy-trinity/rcahms?item=1258667#carousel [Accessed 1 August 2016].
HOBARTS. 2019. *The ultimate guide to lasers* [Online]. Available: https://hobarts.com/guide-to-lasers [Accessed 22 April 2019].
HOGGE, J. P., MESSMER, J. M. & FIERRO, M. F. 1995. Positive identification by post-surgical defects from unilateral lambdoid synostectomy: a case report. *J Forensic Sci,* 40**,** 688-91.
HOME OFFICE. 2018. *National DNA Database annual report 2017-18* [Online]. Available: https://assets.publishing.service.gov.uk/government/uploads/system/uploads/attachment_data/file/778065/National_DNA_Database_anuual_report_2017-18_print.pdf [Accessed 22 April 2019].
HOME OFFICE. 2019. *Information fact sheet for the introduction of new DNA-17 profiling chemistries for the National DNA Database (NDNAD)* [Online]. Available: https://www.keyforensic.co.uk/docs/dna17-factsheet1.pdf [Accessed 22 April 2019].
HOUNSFIELD, G. N. 1973. Computerized transverse axial scanning (tomography). 1. Description of system. *Br J Radiol,* 46**,** 1016-1022.
HUTTENLOCHER, D. P., KLANDERMAN, G. A. & RUCKLIDGE, W. J. 1993. Comparing images using the Hausdorff distance. *IEEE Transactions on Pattern Analysis and Machine Intelligence,* 15**,** 850-863.
INFORMATION SERVICES. 2018a. *High-performance computing* [Online]. Available: https://www.ed.ac.uk/information-services/research-support/research-computing/ecdf/high-performance-computing [Accessed 22 April 2019].
INFORMATION SERVICES. 2018b. *Services* [Online]. University of Edinburgh. Available: https://www.ed.ac.uk/information-services/about/organisation/iti/division-iti-who/division-iti-units/research/services [Accessed 22 April 2019].
INTERPOL. 2019. *Disaster Victim Identification (DVI)* [Online]. Available: https://www.interpol.int/en/How-we-work/Forensics/Disaster-Victim-Identification-DVI [Accessed 22 April 2019].
JOLLY, J. 2017. *The painstaking task of naming Grenfell's victims* [Online]. BBC News. Available: https://www.bbc.com/news/magazine-40517658 [Accessed 22 April 2019].
KAHANA, T. & HISS, J. 1994. Positive identification by means of trabecular bone pattern comparison. *J Forensic Sci,* 39**,** 1325-30.
KAHANA, T., RAVIOLI, J. A., L URROZ, C. & HISS, J. 1997. *Radiographic Identification of Fragmentary Human Remains from a Mass Disaster*.
KANEKO, S. I., KONDO, T. & MIYAMOTO, A. 2003. Robust matching of 3D contours using iterative closest point algorithm improved by M-estimation. *Pattern Recognition,* 36**,** 2041-2047.
KAPOUTSIS, C. A., VAVOULIDIS, C. P. & PITAS, I. 1999. Morphological iterative closest point algorithm. *IEEE Transactions on Image Processing,* 8**,** 1644-1646.
KARELL, M. A., LANGSTAFF, H. K., HALAZONETIS, D. J., MINGHETTI, C., FRELAT, M. & KRANIOTI, E. F. 2016. A novel method for pair-matching

using three-dimensional digital models of bone: mesh-to-mesh value comparison. *Int J Legal Med*.
KELES-CELIK, N., KOSE, O., SEKERCI, R., AYTAC, G., TURAN, A. & GÜLER, F. 2017. Accessory Ossicles of the Foot and Ankle: Disorders and a Review of the Literature. *Cureus,* 9**,** e1881.
KOESLING, S., KUNKEL, P. & SCHUL, T. 2005. Vascular anomalies, sutures and small canals of the temporal bone on axial CT. *European Journal of Radiology,* 54**,** 335-343.
KONDO, T., OHTSUJI, M. & OHSHIMA, T. 1995. A new surgical method from the viewpoint of personal identification: a case of identification based on the presence of a metallic Z-stent. *Forensic Sci Int,* 73**,** 101-7.
KOOT, M. G., SAUER, N. J. & FENTON, T. W. 2005. Radiographic human identification using bones of the hand: a validation study. *J Forensic Sci,* 50**,** 263-8.
KRANIOTI, E. F., ISCAN, M. Y. & MICHALODIMITRAKIS, M. 2008. Craniometric analysis of the modern Cretan population. *Forensic Sci Int,* 180**,** 110.e1-5.
KRANIOTI, E. F. & KARELL, M. A. 2019. *RE: CT Scan Calibration Protocol.*
KRANIOTI, E. K., GARCIA-DONAS, J. G., ALMEIDA PRADO, P. S., KYRIAKOU, X. P. & LANGSTAFF, H. C. 2017. Sexual dimorphism of the tibia in contemporary Greek-Cypriots and Cretans: Forensic applications. *Forensic Sci Int,* 271**,** 129.e1-129.e7.
KRAPF, D., KRAPF, S. & WYSS, C. 2015. Calcaneus secundarius--a relevant differential diagnosis in ankle pain: a case report and review of the literature. *J Med Case Rep,* 9**,** 127.
KUEHN, C. M., TAYLOR, K. M., MANN, F. A., WILSON, A. J. & HARRUFF, R. C. 2002. Validation of chest X-ray comparisons for unknown decedent identification. *J Forensic Sci,* 47**,** 725-9.
KULKARNI, N. V. 2012. *Clinical anatomy : (a problem solving approach),* New Delhi, Jaypee Brothers Medical Pub.
KUMAR, R., MATASAR, K., STANSBERRY, S., SHIRKHODA, A., DAVID, R., MADEWELL, J. E. & SWISCHUCK, L. E. 1991. The calcaneus: normal and abnormal. *Radiographics,* 11**,** 415-40.
LAIDLAW, P. P. 1905. The Os Calcis: Part II. *Journal of anatomy and physiology,* 39**,** 161-177.
LANGSTAFF, H. & KARELL, M. A. 2014. *RE: Flexscan3D Algorithms.*
LANGSTAFF, H. & KARELL, M. A. 2015. *RE: Conference Details Regarding Malaysian Airlines Flight 17.*
LANSARD, M. 2019. *The best portable and handheld 3D scanners in 2019 - Reviews and guide* [Online]. Available: https://www.aniwaa.com/best-handheld-and-portable-3d-scanner/ [Accessed 22 April 2019].
LAY, M. 2014. *The Use of Three Dimensional Modelling of the Temporal Bones in the Sorting of Commingled Human Skeletal Remains.* MSc, University of Edinburgh.
LINKLATER, J., HAYTER, C. L., VU, D. & TSE, K. 2009. Anatomy of the subtalar joint and imaging of talo-calcaneal coalition. *Skeletal Radiol,* 38**,** 437-49.

LOH, J. L., WONG, K. L., HWANG, S., SHEN, L., MURPHY, D. P. & DARUWALLA, Z. J. 2015. Orthopedic asymmetry and clavicle length. *Clinical Anatomy,* 28**,** 964-964.

LOONG, T.-W. 2003. Understanding sensitivity and specificity with the right side of the brain. 327**,** 716.

LU, X., COLBRY, D. & JAIN, A. K. Three-dimensional model based face recognition. Proceedings of the 17th International Conference on Pattern Recognition, 2004. ICPR 2004., 26-26 Aug. 2004 2004. 362-366 Vol.1.

LUCCHI, N. W., NARAYANAN, J., KARELL, M. A., XAYAVONG, M., KARIUKI, S., DASILVA, A. J., HILL, V. & UDHAYAKUMAR, V. 2013. Molecular Diagnosis of Malaria by Photo-Induced Electron Transfer Fluorogenic Primers: PET-PCR. *PLoS ONE,* 8**,** e56677.

LYNCH, J. J. 2018. The Automation of Regression Modeling in Osteometric Sorting: An Ordination Approach. *Journal of Forensic Sciences,* 63**,** 798-804.

LYNCH, J. J., BYRD, J. & LEGARDE, C. B. 2018. The Power of Exclusion using Automated Osteometric Sorting: Pair-Matching. *Journal of Forensic Sciences,* 63**,** 371-380.

MAHAKKANUKRAUH, P., SINTHUBUA, A., PRASITWATTANASEREE, S., RUENGDIT, S., SINGSUWAN, P., PRANEATPOLGRANG, S. & DUANGTO, P. 2015. Craniometric study for sex determination in a Thai population. *Anatomy & cell biology,* 48**,** 275-283.

MANN, R. W., HUNT, D. R. & LOZANOFF, S. 2016. *Photographic Regional Atlas of Non-metric Traits and Anatomical Variants in the Human Skeleton*, Charles C. Thomas, Publisher, Limited.

MANOLAGAS, S. C. 2000. Birth and Death of Bone Cells: Basic Regulatory Mechanisms and Implications for the Pathogenesis and Treatment of Osteoporosis*. *Endocrine Reviews,* 21**,** 115-137.

MARZBAN, C. 2004. The ROC Curve and the Area under It as Performance Measures. *Weather and Forecasting,* 19**,** 1106-1114.

MATERIALISE. 2019. *Mimics* [Online]. Available: https://www.materialise.com/en/medical/software/mimics [Accessed 22 April 2019].

MCGEE, S. 2002. Simplifying Likelihood Ratios. *Journal of General Internal Medicine,* 17**,** 647-650.

MCKERN, T. W. 1958. The Use of Shortwave Ultraviolet Rays for the Segregation of Commingled Skeletal Remains. Natick, MA, U.S.A.

MCWHIRTER, Z. 2018. *Exploring the Functionality of Mesh-to-Mesh Value Comparison, an Innovative Three-Dimensional Pair-Matching Method, and the Implications for Re-Associating Commingled and Disarticulated Remains.* MSc, University of Edinburgh.

MEDCALC. 2019a. *Free statistical calculators* [Online]. Available: http://www.medcalc.org/calc/diagnostic_test.php [Accessed 22 April 2019].

MEDCALC. 2019b. *Interval-specific likelihood ratios* [Online]. [Accessed 22 April 2019].

METROPOLITAN POLICE. 2017a. *Grenfell Tower investigation update* [Online]. Available: https://web.archive.org/web/20180614015058/http://news.met.police.uk/news/grenfell-tower-investigation-update-260888 [Accessed 22 April 2019].
METROPOLITAN POLICE. 2017b. *Number of victims of the Grenfell Tower fire formally identified is 70* [Online]. Available: https://web.archive.org/web/20180616144730/http://news.met.police.uk/news/family-tributes-to-victims-of-grenfell-tower-fire-247006 [Accessed 22 April 2019].
METZ, C. E. 1978. Basic principles of ROC analysis. *Semin Nucl Med,* 8**,** 283-98.
MILLIKEN, R. A. 1937. Os subcalcis. *The American Journal of Surgery,* 37**,** 116-117.
MOHAMMADZADE, H. & HATZINAKOS, D. 2013. Iterative Closest Normal Point for 3D Face Recognition. *IEEE Transactions on Pattern Analysis and Machine Intelligence,* 35**,** 381-397.
MOORE, J. R. & NORMAN, D. B. 2009. Quantitatively evaluating the sources of taphonomic biasing of skeletal element abundances in fossil assemblages. 24**,** 591-602.
MURLIMANJU, B. V., CHETTIAR, G. K., PRAMEELA, M. D., TONSE, M., KUMAR, N., SARALAYA, V. V. & PRABHU, L. V. 2014. Mastoid emissary foramina: an anatomical morphological study with discussion on their evolutionary and clinical implications. *Anatatomy & Cell Biology,* 47**,** 202-6.
NASH, K. 2015. MSc, University of Edinburgh.
NATIONAL HEALTH SERVICES. 2019. *Caldicott Priniciples* [Online]. Available: https://www.igt.hscic.gov.uk/Caldicott2Principles.aspx [Accessed 22 April 2019].
OBUCHOWSKI, N. A. 2003. Receiver operating characteristic curves and their use in radiology. *Radiology,* 229**,** 3-8.
OLIVIERI, L., MAZZARELLI, D., CAPPELLA, A., DE ANGELIS, D., PISCITELLI, V. & CATTANEO, C. 2017. The importance of "secondary methods" in the identification of the victims of the 3rd of October 2013 shipwreck. *La Revue de Médecine Légale,* 8**,** 190-191.
OSIPENKOVA, T. K. & MIKHAILOVA, L. N. 1996. [The establishment of osteogenesis imperfecta for personal identification]. *Sud Med Ekspert,* 39**,** 21-6.
OSIPOV, B., HARVATI, K., NATHENA, D., SPANAKIS, K., KARANTANAS, A. & KRANIOTI, E. F. 2013. Sexual dimorphism of the bony labyrinth: a new age-independent method. *Am J Phys Anthropol,* 151**,** 290-301.
OWSLEY, D. W. 1993. Identification of the fragmentary, burned remains of two U.S. journalists seven years after their disappearance in Guatemala. *J Forensic Sci,* 38**,** 1372-82.
OWSLEY, D. W. & MANN, R. W. 1989. Positive identification based on radiographic examination of the leg and foot. A case report. *J Am Podiatr Med Assoc,* 79**,** 511-3.
OWSLEY, D. W. & MANN, R. W. 1992. Positive personal identity of skeletonized remains using abdominal and pelvic radiographs. *J Forensic Sci,* 37**,** 332-6.

OWSLEY, D. W., MANN, R. W., CHAPMAN, R. E., MOORE, E. & COX, W. A. 1993. Positive identification in a case of intentional extreme fragmentation. *J Forensic Sci,* 38**,** 985-96.
O'DONNELL, C., IINO, M., MANSHARAN, K., LEDITSCKE, J. & WOODFORD, N. 2011. Contribution of postmortem multidetector CT scanning to identification of the deceased in a mass disaster: Experience gained from the 2009 Victorian bushfires. *Forensic Science International,* 205**,** 15-28.
PAIVA, L. A. S. D. & SEGRE, M. 2003. Sexing the human skull through the mastoid process. *Revista do Hospital das Clínicas,* 58**,** 15-20.
PARLIAMENTARY OFFICE OF SCIENCE AND TECHNOLOGY 2006. Postnote: The National DNA Database.
PENG, X., ZHANG, Z. & TIZIANI, H. J. 2002. 3-D imaging and modeling – Part I: acquisition and registration. *Optik,* 113**,** 448-452.
PERINI, T. A., OLIVEIRA, G. L. D., ORNELLAS, J. D. S. & OLIVEIRA, F. P. D. 2005. Technical error measurement in anthropometry/Cálculo do erro técnico de medição em antropometria. *Revista Brasileira de Medicina do Esporte,* 11**,** 81-85.
PISCITELLI, V., IADICICCO, A., DE ANGELIS, D., PORTA, D. & CATTANEO, C. 2016. Italy's battle to identify dead migrants. *The Lancet Global Health,* 4**,** e512-e513.
POLLOCK, C. R., POKINES, J. T. & BETHARD, J. D. 2018. Organic staining on bone from exposure to wood and other plant materials. *Forensic Sci Int,* 283**,** 200-210.
PRESS ASSOCIATION. 2018. *Grenfell fire: police apologise after victim's bone fragment found* [Online]. The Guardian. Available: http://www.theguardian.com/uk-news/2018/feb/01/grenfell-fire-police-apologise-after-victims-bone-fragment-found-tumble-dryer [Accessed 22 April 2019].
PROMEGA. 2019a. *PowerPlex® ESX 17 and ESI 17 Pro Systems* [Online]. Available: https://www.promega.co.uk/products/genetic-identity/genetic-identity-workflow/str-amplification/powerplex-esx-17-and-esi-17-pro-systems/?catNum=DC7780 [Accessed].
PROMEGA. 2019b. *PowerPlex® ESX and ESI 17 Fast Systems* [Online]. Available: https://www.promega.co.uk/products/genetic-identity/genetic-identity-workflow/str-amplification/powerplex-esx-17-and-esi-17-fast-systems/?catNum=DC1721 [Accessed 22 April 2019].
QIAGEN. 2019. *Investigator ESSplex SE Plus Kit - QIAGEN Online Shop* [Online]. Available: https://www.qiagen.com/gb/shop/detection-solutions/investigator-essplex-se-plus-kit/#orderinginformation [Accessed 22 April 2019].
RAGAB, A. A., STEWART, S. L. & COOPERMAN, D. R. 2003. Implications of subtalar joint anatomic variation in calcaneal lengthening osteotomy. *J Pediatr Orthop,* 23**,** 79-83.
RATHMELL ARCHAEOLOGY LTD 2003. St Andrews Library: Archaeological Excavation - Data Structure Report. Dundee, Scotland: Rathmell Archaeology Ltd.

REES, T. 2003. St. Andrews Public Library. *Discovery and Excavation in Scotland,* 4**,** 78.
REES, T., GORDON, D. & MATTHEWS, A. 2008. Excavations within the graveyard of the Holy Trinity, St Andrews, Fife. *Tayside and Fife Archaeological Journal,* 14**,** 56-68.
REPETIER. 2019. *Repetier Software* [Online]. Available: https://www.repetier.com/ [Accessed 22 April 2019].
RHINE, S. & SPERRY, K. 1991. Radiographic identification by mastoid sinus and arterial pattern. *J Forensic Sci,* 36**,** 272-9.
ROSS, A. H., UBELAKER, D. H. & FALSETTI, A. B. 2002. Craniometric Variation in the Americas. *Human Biology,* 74**,** 807-818.
ROYAL SOCIETY. 2017. *Forensic DNA analysis: a primer for courts* [Online]. Available: https://royalsociety.org/-/media/about-us/programmes/science-and-law/royal-society-forensic-dna-analysis-primer-for-courts.pdf [Accessed 22 April 2019].
RUDER, T. D., KRAEHENBUEHL, M., GOTSMY, W. F., MATHIER, S., EBERT, L. C., THALI, M. J. & HATCH, G. M. 2012. Radiologic identification of disaster victims: a simple and reliable method using CT of the paranasal sinuses. *Eur J Radiol,* 81**,** e132-8.
RÖNTGEN, W. C. 1896. On a New Kind of Rays. *Nature,* 53**,** 274-276.
SCHOOL OF HISTORY CLASSICS AND ARCHAEOLOGY. 2017. *Ethics Procedures* [Online]. University of Edinburgh. Available: https://www.ed.ac.uk/history-classics-archaeology/research/ethics-procedures/procedures [Accessed 22 April 2019].
SCHULZ, R., MUHLER, M., MUTZE, S., SCHMIDT, S., REISINGER, W. & SCHMELING, A. 2005. Studies on the time frame for ossification of the medial epiphysis of the clavicle as revealed by CT scans. *Int J Legal Med,* 119**,** 142-5.
SCIENTIFIC WORKING GROUP FOR FORENSIC ANTHROPOLOGY 2010. Personal Identification. National Institute of Standards and Technology.
SHEPHERD, R. 2019. *How to identify a body: the Marchioness disaster and my life in forensic pathology* [Online]. The Guardian. Available: http://www.theguardian.com/science/2019/apr/18/how-to-identify-a-body-the-marchioness-disaster-and-my-life-in-forensic-pathology [Accessed 22 April 2019].
SHIBATA, Y., SAKUMA, E., YOSHIDA, Y., WAKABAYASHI, K., IGUCHI, H., SEKIYA, I., OTSUKA, T. & WADA, I. 2014. Morphometric analysis of the peroneal tubercle using a three-dimensional computed tomography model. *The Foot,* 24**,** 200-202.
SLICE, D. E. & ROSS, A. 2009. *3D-ID: Geometric Morphometric Classification of Crania for Forensic Scientists,* United States.
SLÁDEK, V., BERNER, M., SOSNA, D. & SAILER, R. 2007. Human manipulative behavior in the Central European Late Eneolithic and Early Bronze Age: Humeral bilateral asymmetry. *American Journal of Physical Anthropology,* 133**,** 669-681.

SNOW, C. E. 1948. The identification of the unknown war dead. *Am J Phys Anthropol,* 6**,** 323-328.
SONIS, J. 1999. How to use and interpret interval likelihood ratios. *Fam Med,* 31**,** 432-7.
SPERRY, K., MARLIN, D. C., BONNELL, H. J. & HAGLUND, W. D. 1992. Remains identification by frontal sinus radiographs [2]. *Journal of Forensic Sciences,* 37**,** 1205-1207.
SPOOR, C. F., ZONNEVELD, F. W. & MACHO, G. A. 1993. Linear measurements of cortical bone and dental enamel by computed tomography: applications and problems. *Am J Phys Anthropol,* 91**,** 469-484.
STEELE, J. & MAYS, S. 1995. Handedness and directional asymmetry in the long bones of the human upper limb. *International Journal of Osteoarchaeology,* 5**,** 39-49.
STULL, K. E., KENYHERCZ, M. W. & L'ABBE, E. N. 2014. Ancestry estimation in South Africa using craniometrics and geometric morphometrics. *Forensic Sci Int,* 245**,** 206.e1-7.
SUDIMACK, J. R., LEWIS, B. J., RICH, J., DEAN, D. E. & FARDAL, P. M. 2002. Identification of decomposed human remains from radiographic comparisons of an unusual foot deformity. *J Forensic Sci,* 47**,** 218-20.
THERMOFISHER SCIENTIFIC. 2019a. *Amira for Life & Biomedical Sciences - UK* [Online]. Available: https://www.thermofisher.com/uk/en/home/industrial/electron-microscopy/electron-microscopy-instruments-workflow-solutions/3d-visualization-analysis-software/amira-life-sciences-biomedical.html [Accessed 22 April 2019].
THERMOFISHER SCIENTIFIC. 2019b. *AmpFLSTR NGM PCR Amplification Kit - Thermo Fisher Scientific* [Online]. Available: https://www.thermofisher.com/order/catalog/product/4415020?SID=srch-srp-4415020 [Accessed 22 April 2019].
THERMOFISHER SCIENTIFIC. 2019c. *AmpFLSTR NGM SElect PCR Amplification Kit - Thermo Fisher Scientific* [Online]. Available: https://www.thermofisher.com/order/catalog/product/4457890?SID=srch-srp-4457890 [Accessed 22 April 2019].
THOMAS, A. n.d.-a. *History of Radiology* [Online]. The British Institute of Radiology. Available: https://www.bir.org.uk/patients-public/history-of-radiology/ [Accessed 2017].
THOMAS, A. n.d.-b. *Origins of Radiology* [Online]. The British Institute of Radiology. Available: https://www.bir.org.uk/patients-public/history-of-radiology/origins-of-radiology/ [Accessed 2017].
THOMAS, R. M., UBELAKER, D. H. & BYRD, J. E. 2013. Tables for the metric evaluation of pair-matching of human skeletal elements. *J Forensic Sci,* 58**,** 952-6.
THOMSON, L. & KARELL, M. A. 2019. *RE: CT Scan Calibration Protocol.*
TISE, M. L., KIMMERLE, E. H. & SPRADLEY, M. K. 2014. CRANIOMETRIC VARIATION OF DIVERSE POPULATIONS IN FLORIDA:

IDENTIFICATION CHALLENGES WITHIN A BORDER STATE. *Annals of Anthropological Practice,* 38**,** 111-123.
TOMURA, N., SASHI, R., KOBAYASHI, M., HIRANO, H., HASHIMOTO, M. & WATARAI, J. 1995. Normal variations of the temporal bone on high-resolution CT: their incidence and clinical significance. *Clin Radiol,* 50**,** 144-8.
TOS, M. & STANGERUP, S. E. 1985. The causes of asymmetry of the mastoid air cell system. *Acta Otolaryngol,* 99**,** 564-70.
U.S. NATIONAL LIBRARY OF MEDICINE. 2019. *What are single nucleotide polymorphisms (SNPs)?* [Online]. Available: https://ghr.nlm.nih.gov/primer/genomicresearch/snp [Accessed].
UBELAKER, D. H. 2002. Approaches to the study of commingling in human skeletal biology. *In:* HAGLUND, W. D. & SORG, M. H. (eds.) *Advances in Forensic Taphonomy: Method, Theory and Archaeological Perspectives.* Boca Raton, FL: CRC Press.
UBELAKER, D. H. 2008. Methodology in Commingling Analysis: An Historical Overview. *In:* ADAMS, B. J. & BYRD, J. E. (eds.) *Recovery, Analysis, and Identification of Commingled Human Remains.* Humana Press.
UBELAKER, D. H. & GRANT, L. G. 1989. Human skeletal remains: Preservation or reburial? *American Journal of Physical Anthropology,* 32**,** 249-287.
VALENZUELA, A. 1997. Radiographic comparison of the lumbar spine for positive identification of human remains. A case report. *Am J Forensic Med Pathol,* 18**,** 215-7.
VICKERS, S., LUBINSKI, P. M., HENEBRY DELEON, L. & BOWEN, J. T., JR. 2015. Proposed method for predicting pair matching of skeletal elements allows too many false rejections. *J Forensic Sci,* 60**,** 102-6.
VIETTI, L. A. 2016. Quantifying bone weathering stages using the average roughness parameter Ra measured from 3D data. *Surface Topography: Metrology and Properties,* 4**,** 034006.
VIVEK, E. P. & SUDHA, N. 2007. Robust Hausdorff distance measure for face recognition. *Pattern Recognition,* 40**,** 431-442.
WARREN, M., SMITH, K., STUBBLEFIELD, P., MARTIN, S. & WALSH-HANEY, H. 2000. Use of Radiographic Atlases in a Mass Fatality.
WATSON-WILLIAMS, E. 1937. Three Cases of Mastoid Asymmetry. *Proc R Soc Med,* 30**,** 423-4.
WEBB, L. 2019. *Purchasing Insight: Portable X-ray* [Online]. Healthcare Finance. Available: https://www.healthcarefinancenews.com/blog/purchasing-insight-portable-x-ray [Accessed 22 April 2019].
WELLCOME COLLECTION. 2019. *A bullet in the base of a brain, viewed through x-ray. Photoprint from radiograph after Sir Arthur Schuster, 1896.* [Online]. Wellcome Collection. Available: https://wellcomecollection.org/works/padbg8jw [Accessed 22 April 2019].
WHITE, T. D. & FOLKENS, P. A. 2005. *The Human Bone Manual*, Elsevier Science.
WIKIPEDIA. 2019. *Laser* [Online]. Available: https://en.wikipedia.org/wiki/Laser [Accessed 22 April 2019].

WILCOX, F. J. 2019. *Regulation 28: Report to prevent future deaths* [Online]. Judiciary (UK). Available: https://www.judiciary.uk/wp-content/uploads/2018/09/Grenfell-Tower-2018-0262.pdf [Accessed 22 April 2019].

WILSON, E. 1840. *The anatomist's vade mecum : a system of human anatomy,* London, John Churchill.

WILSON, J. S., KOROBKIN, M., GENANT, H. K. & BOVILL, E. G. 1978. Computed tomography of musculoskeletal disorders. *American Journal of Roentgenology,* 131**,** 55-61.

ZHANG, C. & CHEN, T. Efficient feature extraction for 2D/3D objects in mesh representation. Proceedings 2001 International Conference on Image Processing (Cat. No.01CH37205), 7-10 Oct. 2001 2001. 935-938 vol.3.

ZHANG, Z. 1994. Iterative point matching for registration of free-form curves and surfaces. *International Journal of Computer Vision,* 13**,** 119-152.

ZHAO, C., SHI, W. & DENG, Y. 2005. A new Hausdorff distance for image matching. *Pattern Recognition Letters,* 26**,** 581-586.

ZURL, B., TIEFLING, R., WINKLER, P., KINDL, P. & KAPP, K. S. 2014. Hounsfield units variations: impact on CT-density based conversion tables and their effects on dose distribution. *Strahlenther Onkol,* 190**,** 88-93.

ZVIAGIN, V. N., MAL'TSEVA, N. L., ALEKSINA, L. A. & GALITSKAIA, O. I. 2005. [Criteria of personal identification by the hyoid bone]. *Sud Med Ekspert,* 48**,** 27-34.

ĆUK, T., LEBEN-SELJAK, P. & ŠTEFANČIČ, M. 2001. Lateral asymmetry of human long bones. *Variability and Evolution,* 9**,** 19-32.

Appendix A

Company	Kit Type	Cost (£)	# Reactions	Cost per single reaction	Cost per sample in triplicate
Promega	PowerPlex® ESI 17 Pro	6255	400	15.6375	46.9125
	PowerPlex® ESX 17 and ESI 17 Fast Systems	6879	400	17.1975	51.5925
		2127	100	21.27	63.81
Applied Biosystems (ThermoFisher)	AmpFLSTR™ NGM™ PCR Amplification Kit	17810	1000	17.81	53.43
		3395	200	16.975	50.925
	AmpFLSTR™ NGM SElect™ PCR Amplification Kit	3050	200	15.25	45.75
Qiagen	Investigator ESSplex SE Plus Kit (400)	6475	400	16.1875	48.5625
		1754	100	17.54	52.62

Appendix B

Daily Tube Calibration

The calibration of the tube is designed to protect the life of the tube. It runs up the tube from cold, with small exposures, building up to larger patient type exposures. This prevents the tube from overloading with a large exposure from cold.

At the end of the morning calibration, the scanner runs air calibrations on the most frequently used collimations and kV's. These are set by the applications team when the system is initially built, and would vary depending on the sites workload and protocols. At the RIE yours will be 32x1mm, 64x0.5mm, 4x0.5mm collimations, and 120kV. These daily calibrations are designed to keep these commonly used settings within specification allowing for environmental fluctuations in terms of room temperature and humidity.

Full Air Calibrations

Full air calibrations are run, to calibrate all collimations and all kV's to the environmental conditions.

Multi pin Phantom (TOS Phantom)

The multi pin phantom is performed to allow for checking of Hounsfield Units drift.

The pins in the phantom are made from the following materials and under specific scan conditions should display a HU within the tolerances described

- Air (-1015 to -975HU)
- Delrin (330 to 350 HU)
- Acrylic (115 to 135 HU)
- Nylon (90 to 110 HU)
- Polypropylene (-115 to -95 HU)
- Water (-5 to 5 HU)

Any drift in HU could be as a result of a kV or reconstruction issue.

Water Phantoms

The water Phantoms are sized to match the Scan Fields of View, these are scanned to allow for visual checking of ring artefact.

In addition they are used to check for noise and uniformity of the x-ray beam. The noise levels recorded in multiple regions of interest will highlight any issues with uniformity of the x-ray beam.

Written by: Lynne Thomson (Thomson and Karell, 2019)

Appendix C

Instructions for Lowest Common Value Match Selection

1) Excel sheet must be formatted with the Lefts listed along the left-hand side (rows) and the Rights listed across the top (columns).

If the Excel sheet has been generated by Viewbox, it will start like this:

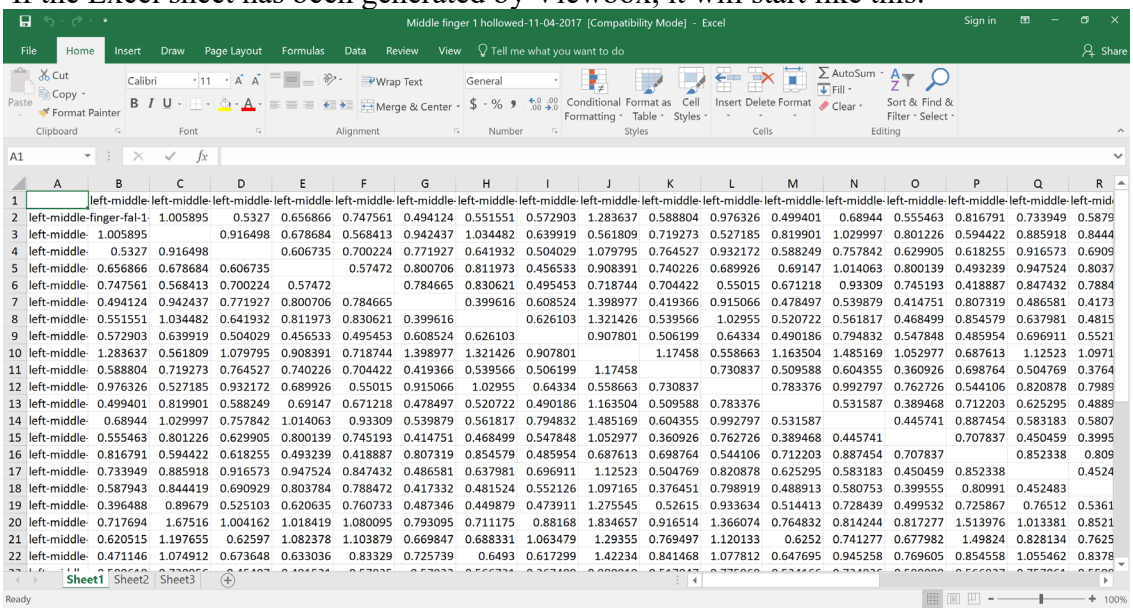

To format it in the way described, delete the Rights from the left-hand side (rows):

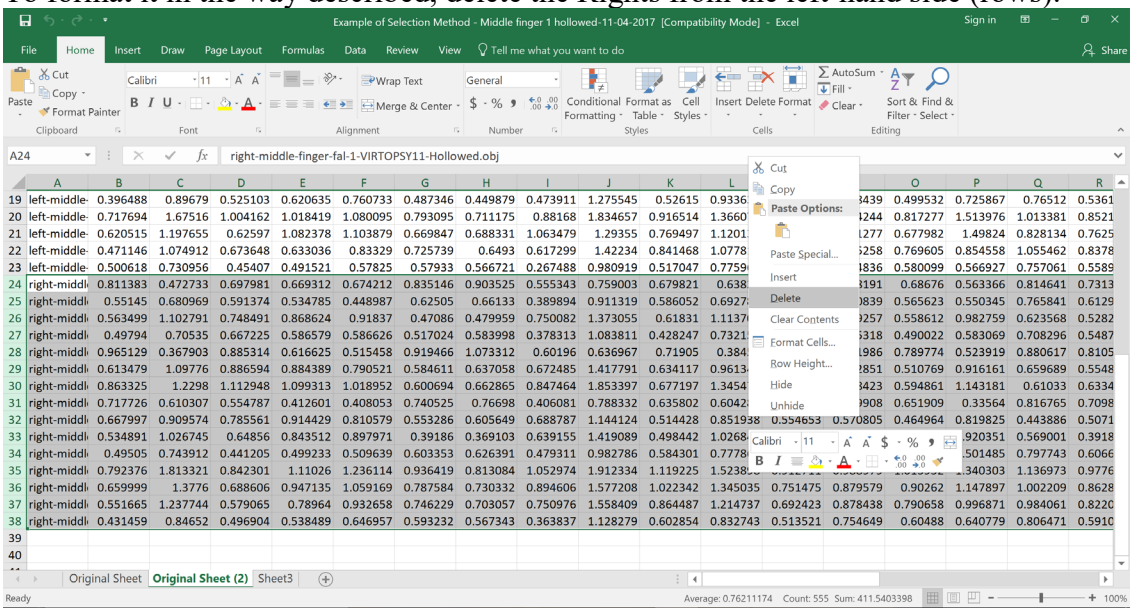

And delete the Lefts from the top (columns):

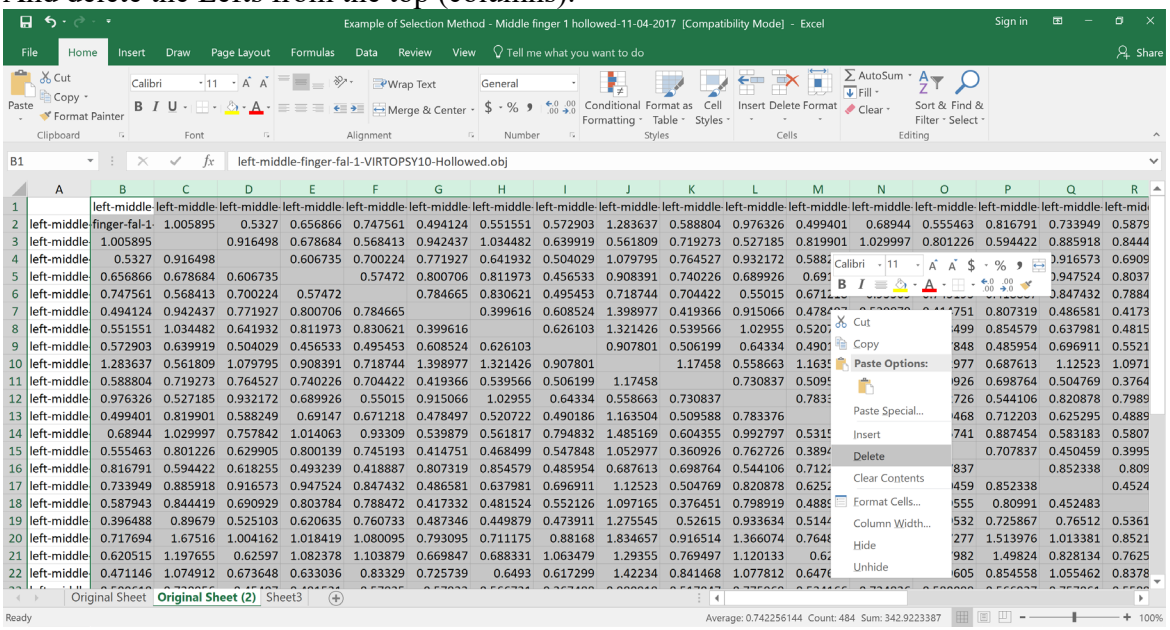

To end up with the final result of:

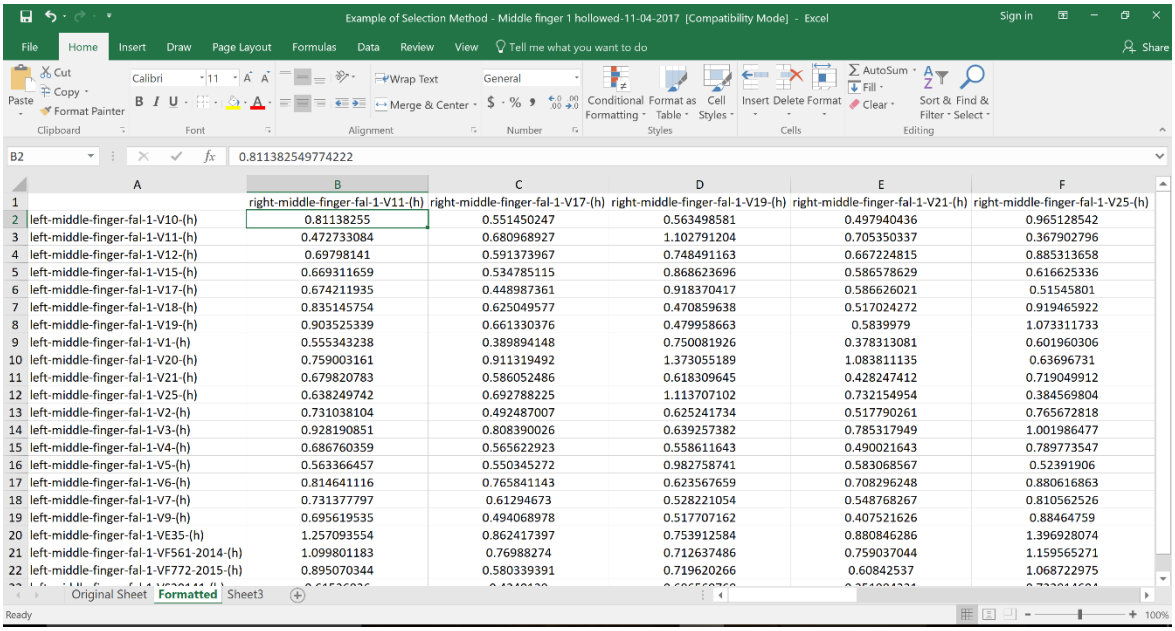

	A	B	C	D	E	F
1		right-middle-finger-fal-1-V11-(h)	right-middle-finger-fal-1-V17-(h)	right-middle-finger-fal-1-V19-(h)	right-middle-finger-fal-1-V21-(h)	right-middle-finger-fal-1-V25-(h)
2	left-middle-finger-fal-1-V10-(h)	0.81138255	0.551450247	0.563498581	0.497940436	0.965128542
3	left-middle-finger-fal-1-V11-(h)	0.472733084	0.680968927	1.102791204	0.705350337	0.367902796
4	left-middle-finger-fal-1-V12-(h)	0.69798141	0.591373967	0.748491163	0.667224815	0.885313658
5	left-middle-finger-fal-1-V15-(h)	0.669311659	0.534785115	0.868623696	0.586578629	0.616625336
6	left-middle-finger-fal-1-V17-(h)	0.674211935	0.448987361	0.918370417	0.586626021	0.51545801
7	left-middle-finger-fal-1-V18-(h)	0.835145754	0.625049577	0.470859638	0.517024272	0.919465922
8	left-middle-finger-fal-1-V19-(h)	0.903525339	0.661330376	0.479958663	0.5839979	1.073311733
9	left-middle-finger-fal-1-V1-(h)	0.555343238	0.389894148	0.750081926	0.378313081	0.601960306
10	left-middle-finger-fal-1-V20-(h)	0.759003161	0.911319492	1.373055189	1.083811135	0.63696731
11	left-middle-finger-fal-1-V21-(h)	0.679820783	0.586052486	0.618309645	0.428247412	0.719049912
12	left-middle-finger-fal-1-V25-(h)	0.638249742	0.692788225	1.113707102	0.732154954	0.384569804
13	left-middle-finger-fal-1-V2-(h)	0.731038104	0.492487007	0.625241734	0.517790261	0.765672818
14	left-middle-finger-fal-1-V3-(h)	0.928190851	0.808390026	0.639257382	0.785317949	1.001986477
15	left-middle-finger-fal-1-V4-(h)	0.686760359	0.565622923	0.558611643	0.490021643	0.789773547
16	left-middle-finger-fal-1-V5-(h)	0.563366457	0.550345272	0.982758741	0.583068567	0.52391906
17	left-middle-finger-fal-1-V6-(h)	0.814641116	0.765841143	0.623567659	0.708296248	0.880616863
18	left-middle-finger-fal-1-V7-(h)	0.731377797	0.61294673	0.528221054	0.548768267	0.810562526
19	left-middle-finger-fal-1-V9-(h)	0.695619535	0.494068978	0.517707162	0.407521626	0.88464759
20	left-middle-finger-fal-1-VE35-(h)	1.257093554	0.862417397	0.753912584	0.880846286	1.396928074
21	left-middle-finger-fal-1-VF561-2014-(h)	1.099801183	0.76988274	0.712637486	0.759037044	1.159565271
22	left-middle-finger-fal-1-VF772-2015-(h)	0.895070344	0.580339391	0.719620266	0.60842537	1.068722975

*Note – I also shortened the names of the files to make it easier to read by using the 'Find and Replace' tool:

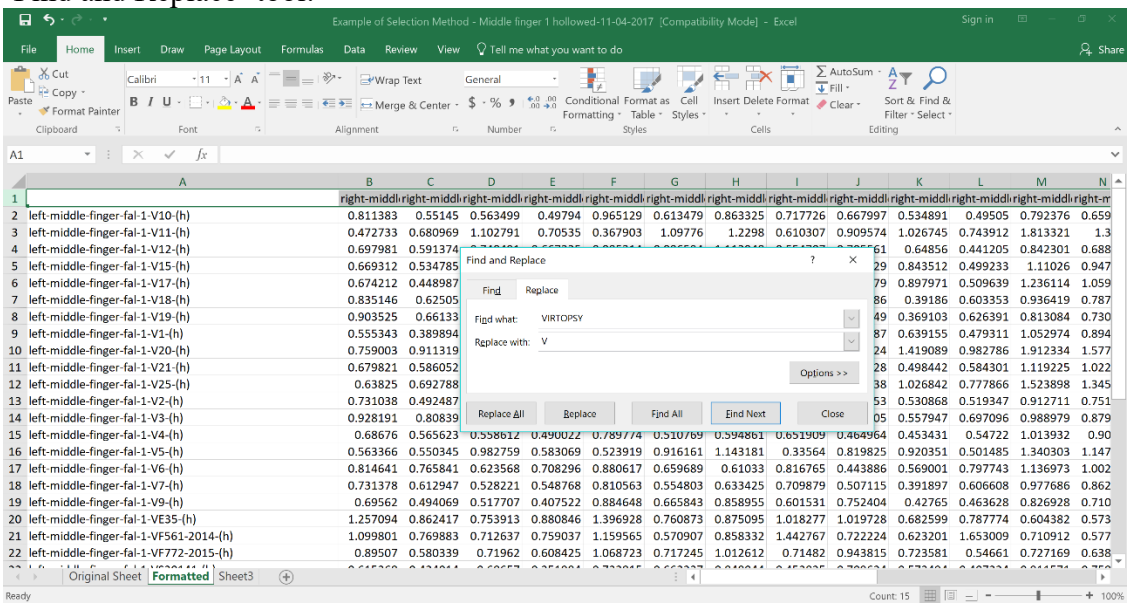

And 'Autofit' the columns (1st step), including centring the text afterwards (2nd step):

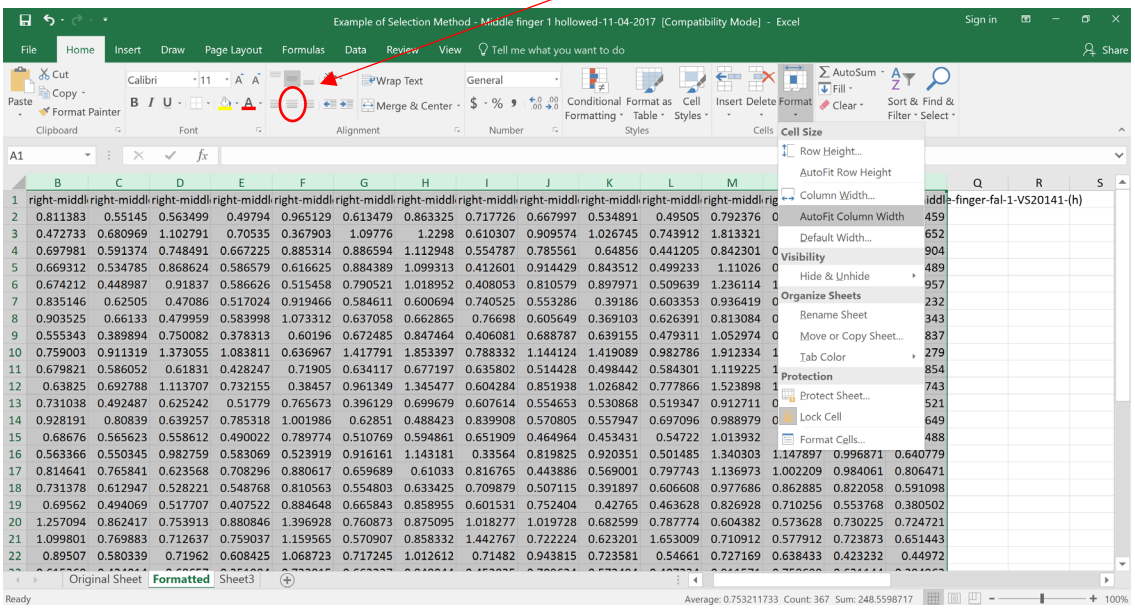

2) 'Freeze the Panes' of the top row and column in order to be able to read everything easily in future steps:

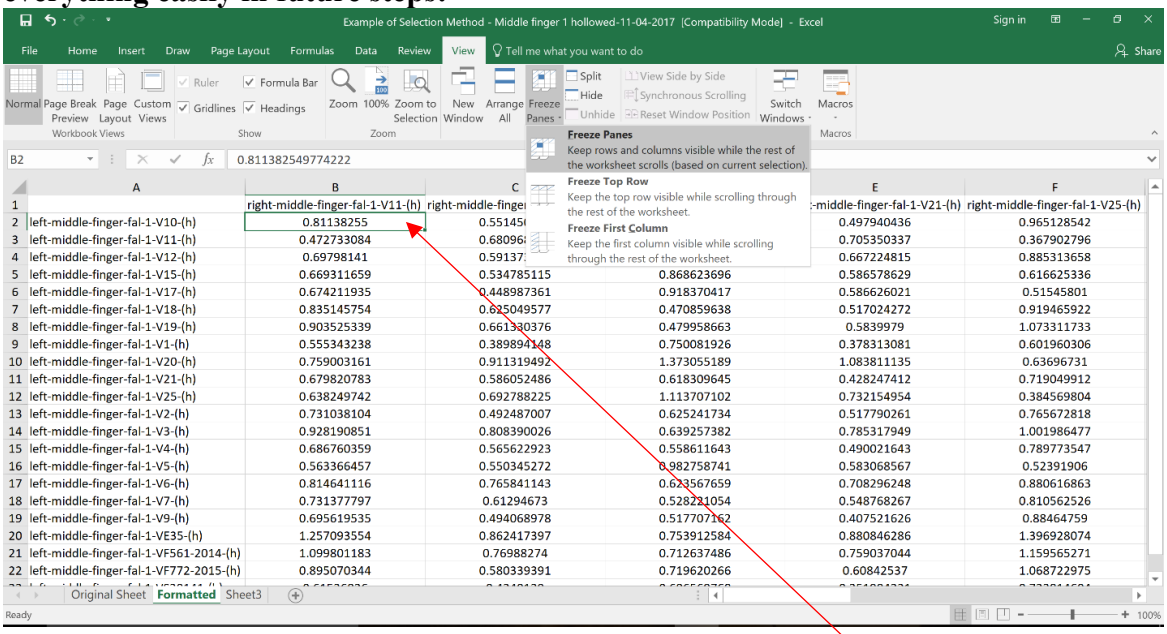

*Note – for this selection to work you need to have 'selected' the first cell of data (i.e. not the names of the bones)

3) Change the font colour of the true pair match values to RED in order to see them better

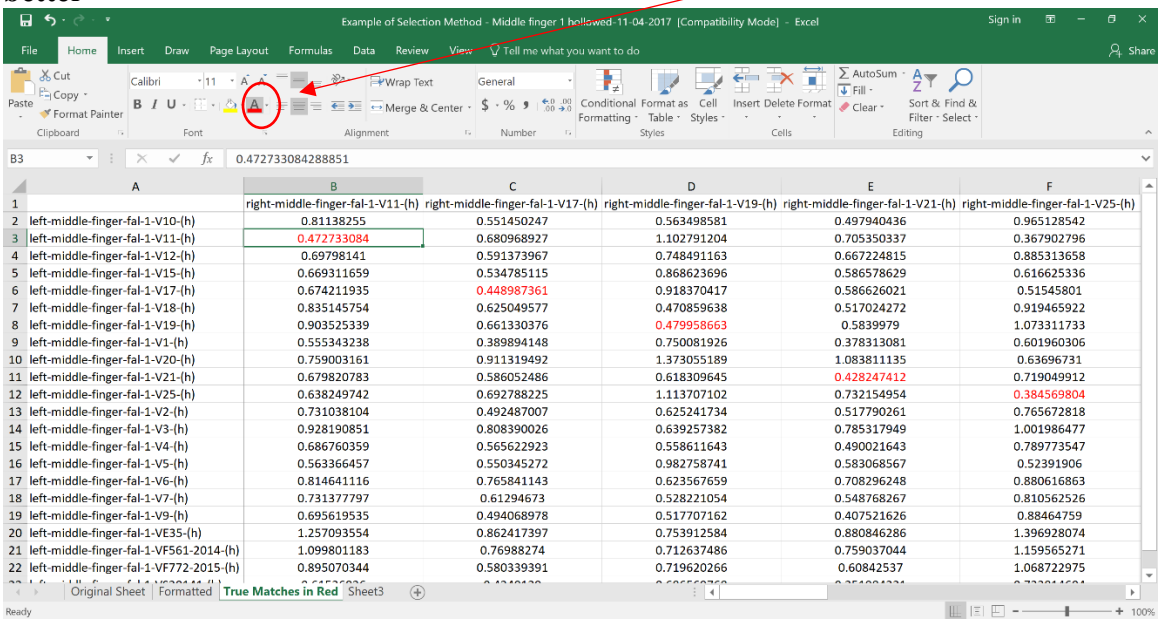

	A	B	C	D	E	F
1		right-middle-finger-fal-1-V11-(h)	right-middle-finger-fal-1-V17-(h)	right-middle-finger-fal-1-V19-(h)	right-middle-finger-fal-1-V21-(h)	right-middle-finger-fal-1-V25-(h)
2	left-middle-finger-fal-1-V10-(h)	0.81138255	0.551450247	0.563498581	0.497940436	0.965128542
3	left-middle-finger-fal-1-V11-(h)	0.472733084	0.680968927	1.102791204	0.705350337	0.367902796
4	left-middle-finger-fal-1-V12-(h)	0.69798141	0.591373967	0.748491163	0.667224815	0.885313658
5	left-middle-finger-fal-1-V15-(h)	0.669311659	0.534785115	0.868623696	0.586578629	0.616625336
6	left-middle-finger-fal-1-V17-(h)	0.674211935	0.448987361	0.918370417	0.586626021	0.51545801
7	left-middle-finger-fal-1-V18-(h)	0.835145754	0.625049577	0.470859638	0.517024272	0.919465922
8	left-middle-finger-fal-1-V19-(h)	0.903525339	0.661330376	0.479958663	0.5839979	1.073311733
9	left-middle-finger-fal-1-V1-(h)	0.555343238	0.389894148	0.750081926	0.378313081	0.601960306
10	left-middle-finger-fal-1-V20-(h)	0.759003161	0.911319492	1.373055189	1.083811135	0.63696731
11	left-middle-finger-fal-1-V21-(h)	0.679820783	0.586052486	0.618309645	0.428247412	0.719049912
12	left-middle-finger-fal-1-V25-(h)	0.638249742	0.692788225	1.113707102	0.732154954	0.384569804
13	left-middle-finger-fal-1-V2-(h)	0.731038104	0.492487007	0.625241734	0.517790261	0.765672818
14	left-middle-finger-fal-1-V3-(h)	0.928190851	0.808390026	0.639257382	0.785317949	1.001986477
15	left-middle-finger-fal-1-V4-(h)	0.686760359	0.565622923	0.558611643	0.490021643	0.789773547
16	left-middle-finger-fal-1-V5-(h)	0.563366457	0.550345272	0.982758741	0.583068567	0.52391906
17	left-middle-finger-fal-1-V6-(h)	0.814641116	0.765841143	0.623567659	0.708296248	0.880616863
18	left-middle-finger-fal-1-V7-(h)	0.731377797	0.61294673	0.528221054	0.548768267	0.810562526
19	left-middle-finger-fal-1-V9-(h)	0.695619535	0.494068978	0.517707162	0.407521626	0.88464759
20	left-middle-finger-fal-1-VE35-(h)	1.257093554	0.862417397	0.753912584	0.880846286	1.396928074
21	left-middle-finger-fal-1-VF561-2014-(h)	1.099801183	0.76988274	0.712637486	0.759037044	1.159565271
22	left-middle-finger-fal-1-VF772-2015-(h)	0.895070344	0.580339391	0.719620266	0.60842537	1.068722975

4) Duplicate this final sheet to work on (so in case something goes wrong, you have a backup)

To do this, 'Right Click' on the tab to duplicate and select the 'Move or Copy' option:

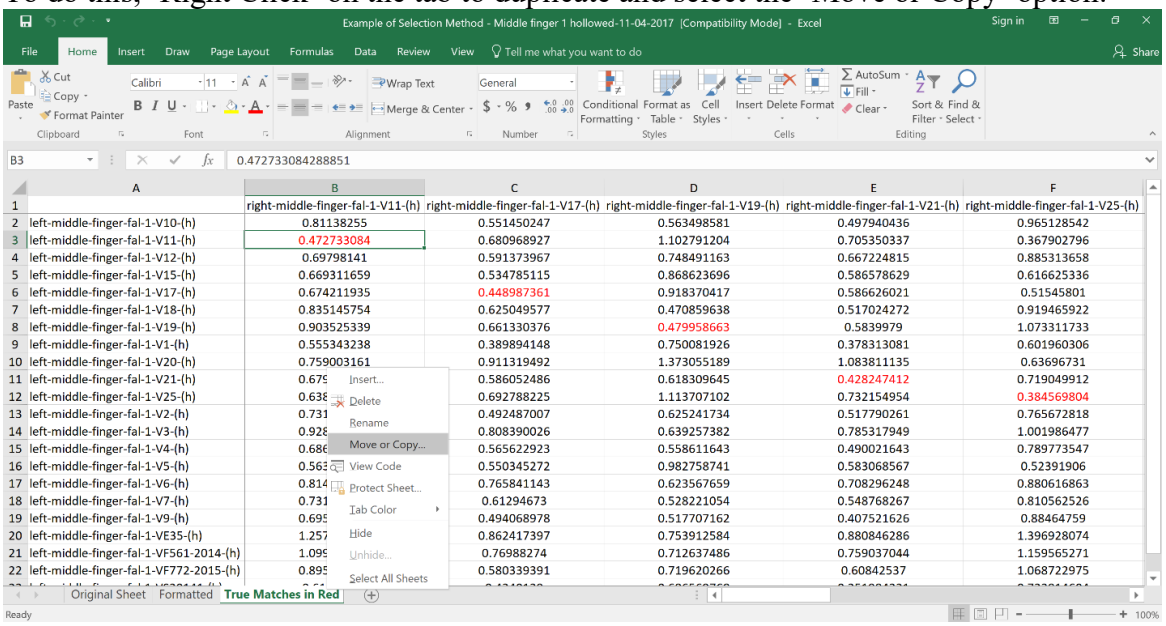

In the Move or Copy box, tick the 'Create a copy' box and highlight the '(move to end)' and then click 'Okay'

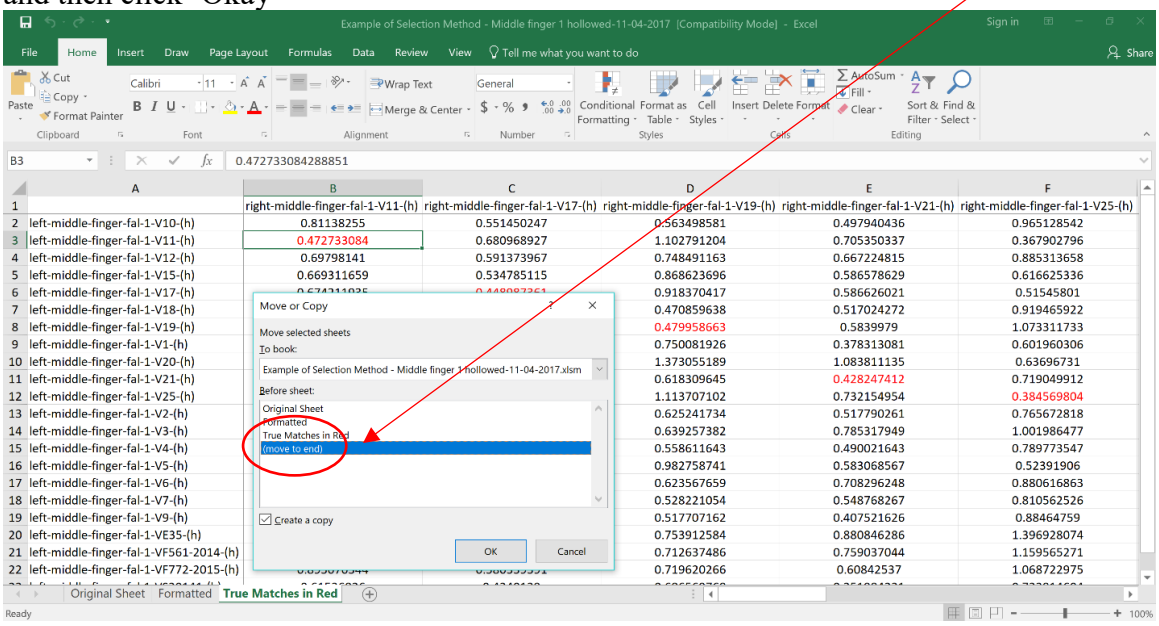

This will result in a duplicated sheet with the same name:

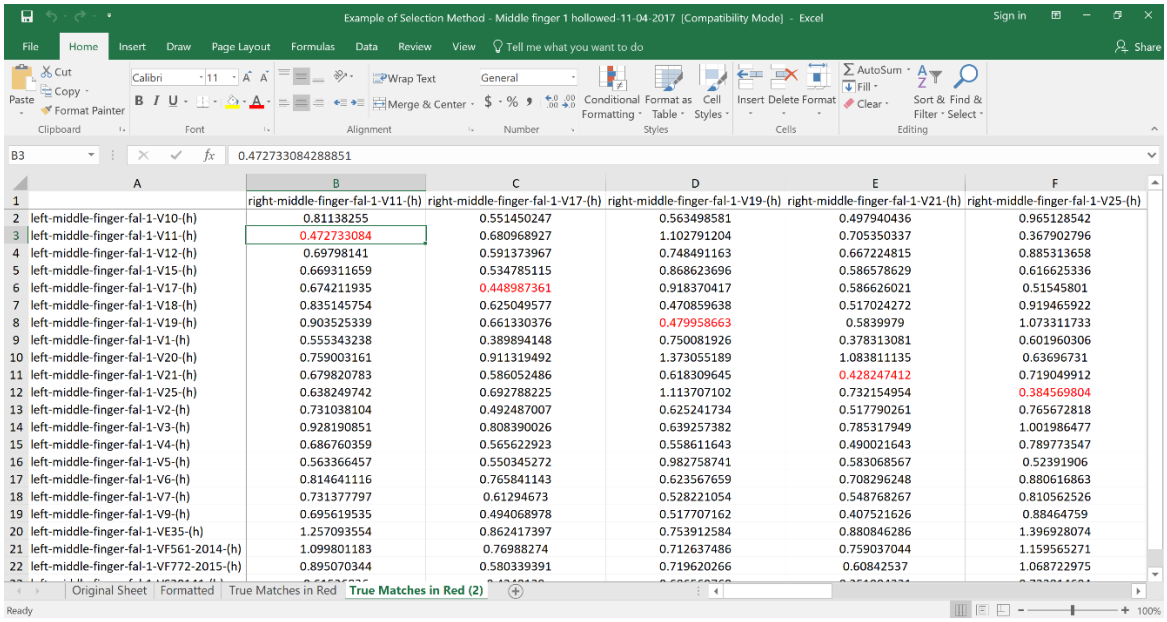

To re-name the sheet, 'Double Click' on the name and type in the new name:

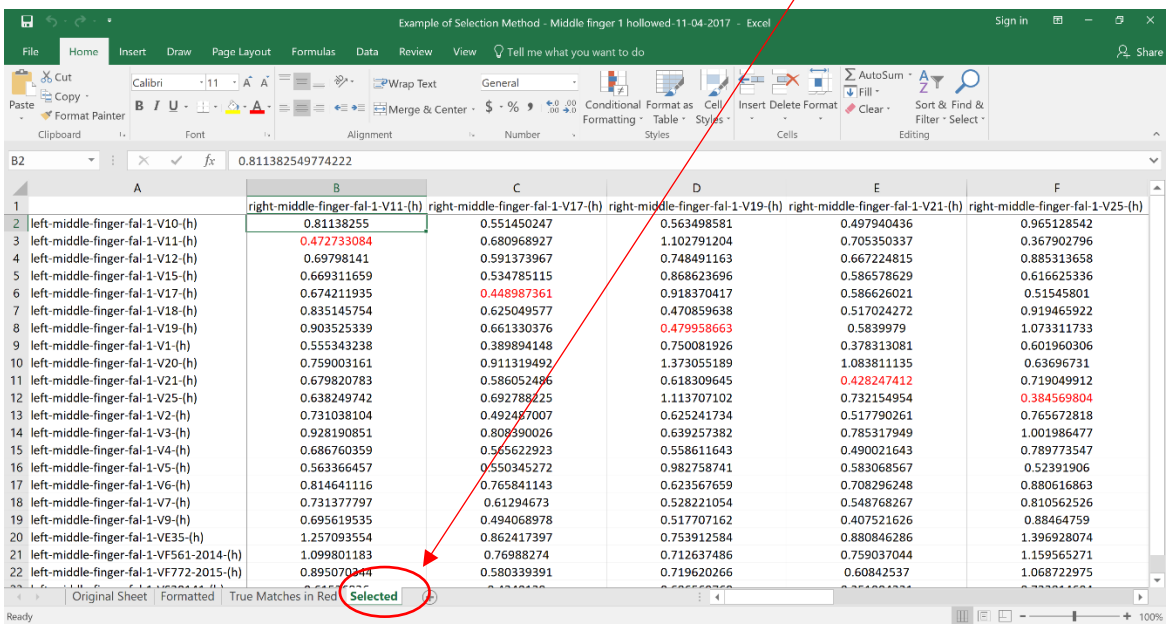

5) Selection of lowest values – First, the three lowest values of the lefts are selected (across, rows) are selected, followed by all the lowest values for the rights (down, columns)

To do this quickly, Excel Macros are needed. Macros allow you to use key combinations [as an example - CRTL + ALT + DLT] to instantly complete a process of multiple steps at once. So, the first step is to ‘Record’ a macro for the selection of the three lowest values for the lefts (across, rows).

This is done in the ‘View’ tab:

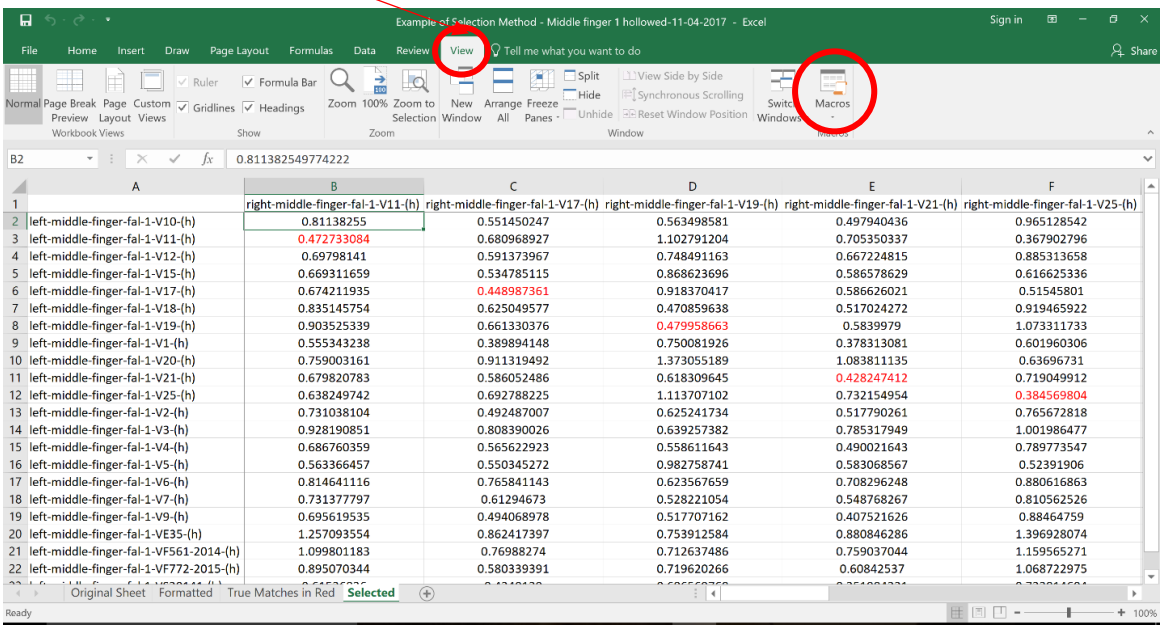

	A	B	C	D	E	F
1		right-middle-finger-fal-1-V11-(h)	right-middle-finger-fal-1-V17-(h)	right-middle-finger-fal-1-V19-(h)	right-middle-finger-fal-1-V21-(h)	right-middle-finger-fal-1-V25-(h)
2	left-middle-finger-fal-1-V10-(h)	0.81138255	0.551450247	0.563498581	0.497940436	0.965128542
3	left-middle-finger-fal-1-V11-(h)	0.472733084	0.680968927	1.102791204	0.705350337	0.367902796
4	left-middle-finger-fal-1-V12-(h)	0.69798141	0.591373967	0.748491163	0.667224815	0.885313658
5	left-middle-finger-fal-1-V15-(h)	0.669311659	0.534785115	0.868623696	0.586578629	0.616625336
6	left-middle-finger-fal-1-V17-(h)	0.674211935	0.448987361	0.918370417	0.586626021	0.51545801
7	left-middle-finger-fal-1-V18-(h)	0.835145754	0.625049577	0.470859638	0.517024272	0.919465922
8	left-middle-finger-fal-1-V19-(h)	0.903525339	0.661330376	0.479958663	0.5839979	1.073311733
9	left-middle-finger-fal-1-V1-(h)	0.555343238	0.389894148	0.750081926	0.378313081	0.601960306
10	left-middle-finger-fal-1-V20-(h)	0.759003161	0.911319492	1.373055189	1.083811135	0.63696731
11	left-middle-finger-fal-1-V21-(h)	0.679820783	0.586052486	0.618309645	0.428247412	0.719049912
12	left-middle-finger-fal-1-V25-(h)	0.638249742	0.692788225	1.113707102	0.732154954	0.384569804
13	left-middle-finger-fal-1-V2-(h)	0.731038104	0.492487007	0.625241734	0.517790261	0.765672818
14	left-middle-finger-fal-1-V3-(h)	0.928190851	0.808390026	0.639257382	0.785317949	1.001986477
15	left-middle-finger-fal-1-V4-(h)	0.686760359	0.565622923	0.558611643	0.490021643	0.789773547
16	left-middle-finger-fal-1-V5-(h)	0.563366457	0.550345272	0.982758741	0.583068567	0.52391906
17	left-middle-finger-fal-1-V6-(h)	0.814641116	0.765841143	0.623567659	0.708296248	0.880616863
18	left-middle-finger-fal-1-V7-(h)	0.731377797	0.61294673	0.528221054	0.548768267	0.810562526
19	left-middle-finger-fal-1-V9-(h)	0.695619535	0.494068978	0.517707162	0.407521626	0.88464759
20	left-middle-finger-fal-1-VE35-(h)	1.257093554	0.862417397	0.753912584	0.880846286	1.396928074
21	left-middle-finger-fal-1-VF561-2014-(h)	1.099801183	0.76988274	0.712637486	0.759037044	1.159565271
22	left-middle-finger-fal-1-VF772-2015-(h)	0.895070344	0.580339391	0.719620266	0.60842537	1.068722975

Before recording Macro, select the option ‘Use Relative References’ in the Macros button list*:

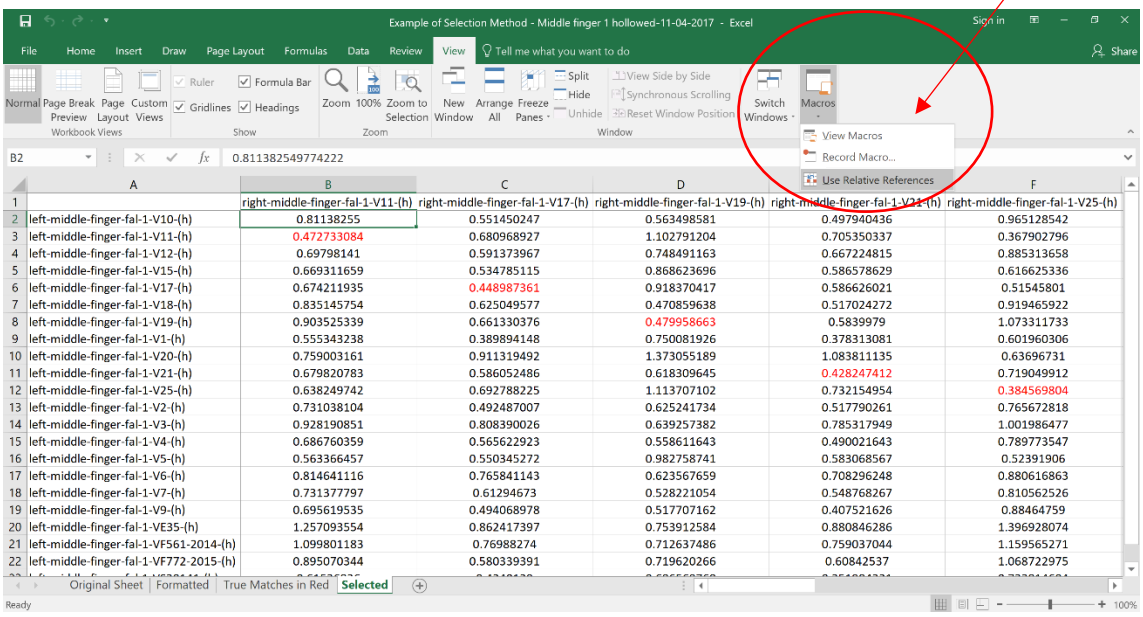

	A	B	C	D	E	F
1		right-middle-finger-fal-1-V11-(h)	right-middle-finger-fal-1-V17-(h)	right-middle-finger-fal-1-V19-(h)	right-middle-finger-fal-1-V21-(h)	right-middle-finger-fal-1-V25-(h)
2	left-middle-finger-fal-1-V10-(h)	0.81138255	0.551450247	0.563498581	0.497940436	0.965128542
3	left-middle-finger-fal-1-V11-(h)	0.472733084	0.680968927	1.102791204	0.705350337	0.367902796
4	left-middle-finger-fal-1-V12-(h)	0.69798141	0.591373967	0.748491163	0.667224815	0.885313658
5	left-middle-finger-fal-1-V15-(h)	0.669311659	0.534785115	0.868623696	0.586578629	0.616625336
6	left-middle-finger-fal-1-V17-(h)	0.674211935	0.448987361	0.918370417	0.586626021	0.51545801
7	left-middle-finger-fal-1-V18-(h)	0.835145754	0.625049577	0.470859638	0.517024272	0.919465922
8	left-middle-finger-fal-1-V19-(h)	0.903525339	0.661330376	0.479958663	0.5839979	1.073311733
9	left-middle-finger-fal-1-V1-(h)	0.555343238	0.389894148	0.750081926	0.378313081	0.601960306
10	left-middle-finger-fal-1-V20-(h)	0.759003161	0.911319492	1.373055189	1.083811135	0.63696731
11	left-middle-finger-fal-1-V21-(h)	0.679820783	0.586052486	0.618309645	0.428247412	0.719049912
12	left-middle-finger-fal-1-V25-(h)	0.638249742	0.692788225	1.113707102	0.732154954	0.384569804
13	left-middle-finger-fal-1-V2-(h)	0.731038104	0.492487007	0.625241734	0.517790261	0.765672818
14	left-middle-finger-fal-1-V3-(h)	0.928190851	0.808390026	0.639257382	0.785317949	1.001986477
15	left-middle-finger-fal-1-V4-(h)	0.686760359	0.565622923	0.558611643	0.490021643	0.789773547
16	left-middle-finger-fal-1-V5-(h)	0.563366457	0.550345272	0.982758741	0.583068567	0.52391906
17	left-middle-finger-fal-1-V6-(h)	0.814641116	0.765841143	0.623567659	0.708296248	0.880616863
18	left-middle-finger-fal-1-V7-(h)	0.731377797	0.61294673	0.528221054	0.548768267	0.810562526
19	left-middle-finger-fal-1-V9-(h)	0.695619535	0.494068978	0.517707162	0.407521626	0.88464759
20	left-middle-finger-fal-1-VE35-(h)	1.257093554	0.862417397	0.753912584	0.880846286	1.396928074
21	left-middle-finger-fal-1-VF561-2014-(h)	1.099801183	0.76988274	0.712637486	0.759037044	1.159565271
22	left-middle-finger-fal-1-VF772-2015-(h)	0.895070344	0.580339391	0.719620266	0.60842537	1.068722975

*Note – You can double-check this has worked as when you click on the ‘Macro’ button again, as the colour behind the box on the relative references should now be grey:

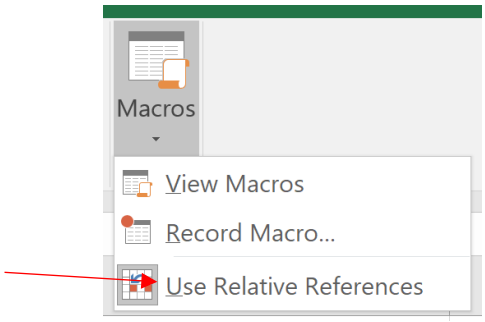

To record a Macro, click on the ‘Macro’ button and select ‘Record Macro’:

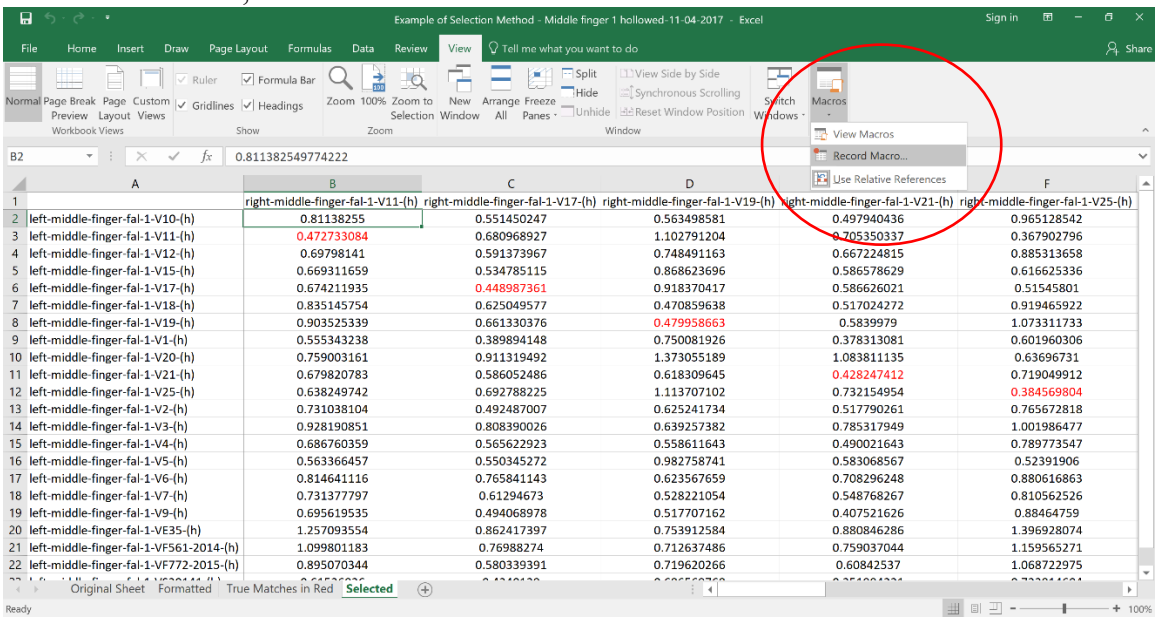

	A	B	C	D	E	F
1		right-middle-finger-fal-1-V11-(h)	right-middle-finger-fal-1-V17-(h)	right-middle-finger-fal-1-V19-(h)	right-middle-finger-fal-1-V21-(h)	right-middle-finger-fal-1-V25-(h)
2	left-middle-finger-fal-1-V10-(h)	0.81138255	0.551450247	0.563498581	0.497940436	0.965128542
3	left-middle-finger-fal-1-V11-(h)	0.472733084	0.680968927	1.102791204	0.705350337	0.367902796
4	left-middle-finger-fal-1-V12-(h)	0.69798141	0.591373967	0.748491163	0.667224815	0.885313658
5	left-middle-finger-fal-1-V15-(h)	0.669311659	0.534785115	0.868623696	0.586578629	0.616625336
6	left-middle-finger-fal-1-V17-(h)	0.674211935	0.448987361	0.918370417	0.586626021	0.51545801
7	left-middle-finger-fal-1-V18-(h)	0.835145754	0.625049577	0.470859638	0.517024272	0.919465922
8	left-middle-finger-fal-1-V19-(h)	0.903525339	0.661330376	0.479958663	0.5839979	1.073311733
9	left-middle-finger-fal-1-V1-(h)	0.555343238	0.389894148	0.750081926	0.378313081	0.601960306
10	left-middle-finger-fal-1-V20-(h)	0.759003161	0.911319492	1.373055189	1.083811135	0.63696731
11	left-middle-finger-fal-1-V21-(h)	0.679820783	0.586052486	0.618309645	0.428247412	0.719049912
12	left-middle-finger-fal-1-V25-(h)	0.638249742	0.692788225	1.113707102	0.732154954	0.384569804
13	left-middle-finger-fal-1-V2-(h)	0.731038104	0.492487007	0.625241734	0.517790261	0.765672818
14	left-middle-finger-fal-1-V3-(h)	0.928190851	0.808390026	0.639257382	0.785317949	1.001986477
15	left-middle-finger-fal-1-V4-(h)	0.686760359	0.565622923	0.558611643	0.490021643	0.789773547
16	left-middle-finger-fal-1-V5-(h)	0.563366457	0.550345272	0.982758741	0.583068567	0.52391906
17	left-middle-finger-fal-1-V6-(h)	0.814641116	0.765841143	0.623567659	0.708296248	0.880616863
18	left-middle-finger-fal-1-V7-(h)	0.731377797	0.61294673	0.528221054	0.548768267	0.810562526
19	left-middle-finger-fal-1-V9-(h)	0.695619535	0.494068978	0.517707162	0.407521626	0.88464759
20	left-middle-finger-fal-1-VE35-(h)	1.257093554	0.862417397	0.753912584	0.880846286	1.396928074
21	left-middle-finger-fal-1-VF561-2014-(h)	1.099801183	0.76988274	0.712637486	0.759037044	1.159565271
22	left-middle-finger-fal-1-VF772-2015-(h)	0.895070344	0.580339391	0.719620266	0.60842537	1.068722975

This will bring up this window:

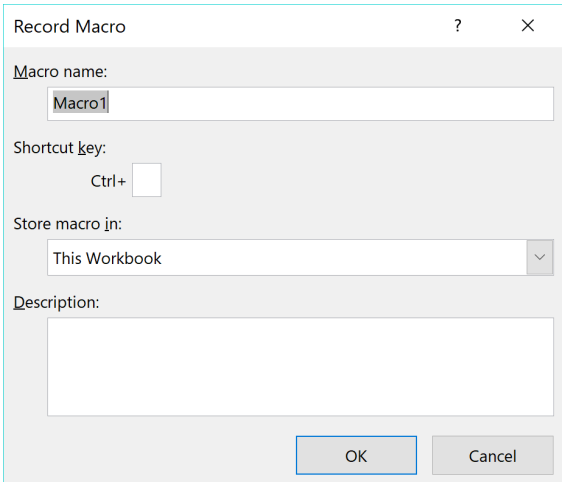

In that window, type in the following and select ‘Okay’:

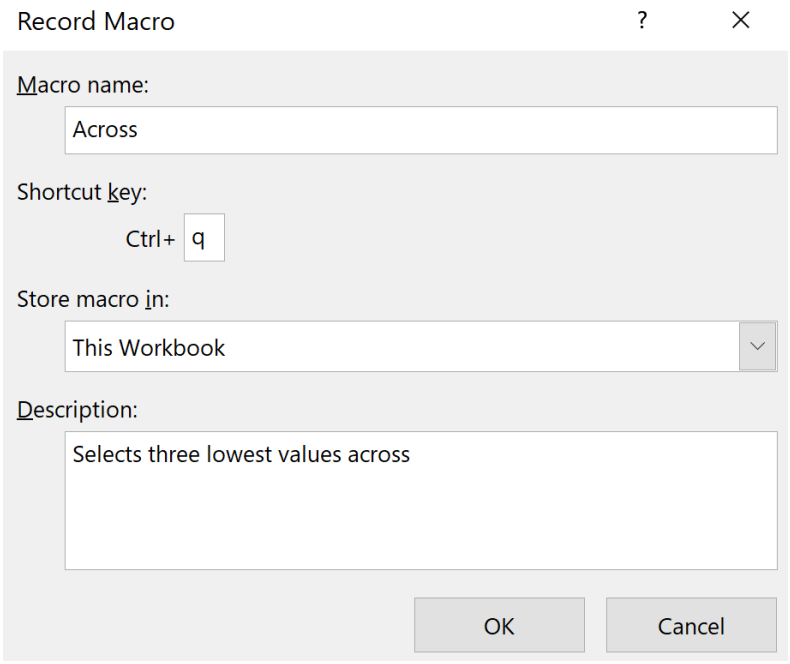

Then, select all the values in the top row (first left bone):

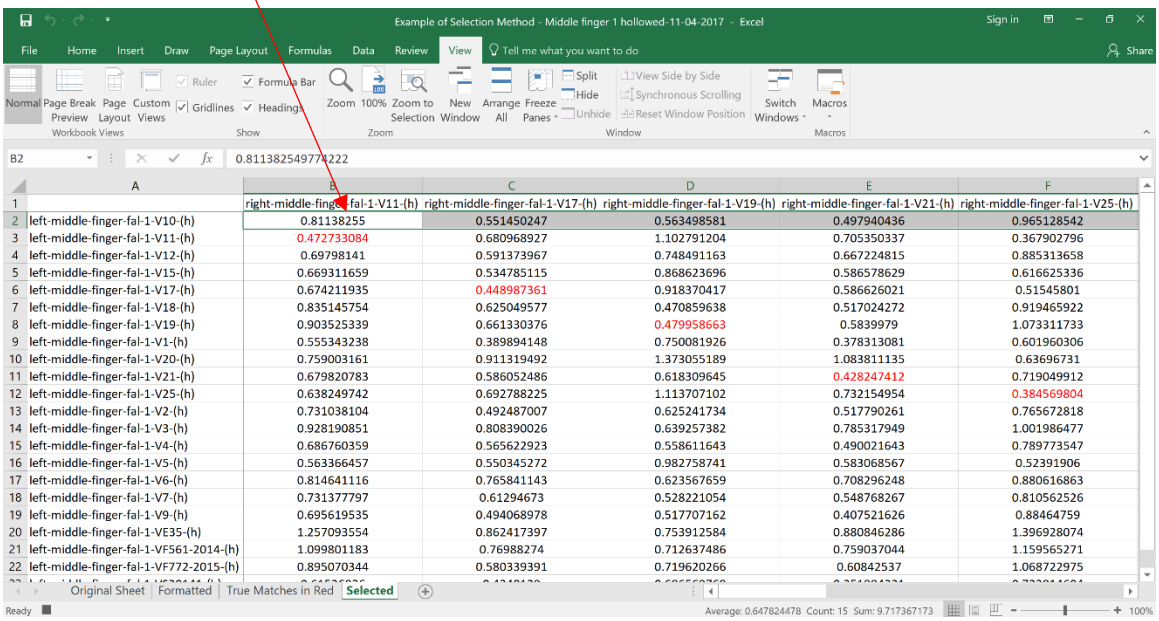

	A	B	C	D	E	F
1		right-middle-finger-fal-1-V11-(h)	right-middle-finger-fal-1-V17-(h)	right-middle-finger-fal-1-V19-(h)	right-middle-finger-fal-1-V21-(h)	right-middle-finger-fal-1-V25-(h)
2	left-middle-finger-fal-1-V10-(h)	0.81138255	0.551450247	0.563498581	0.497940436	0.965128542
3	left-middle-finger-fal-1-V11-(h)	0.472733084	0.680968927	1.102791204	0.705350337	0.367902796
4	left-middle-finger-fal-1-V12-(h)	0.69798141	0.591373967	0.748491163	0.667224815	0.885313658
5	left-middle-finger-fal-1-V15-(h)	0.669311659	0.534785115	0.868623696	0.586578629	0.616625336
6	left-middle-finger-fal-1-V17-(h)	0.674211935	0.448987361	0.918370417	0.586626021	0.51545801
7	left-middle-finger-fal-1-V18-(h)	0.835145754	0.625049577	0.470859638	0.517024272	0.919465922
8	left-middle-finger-fal-1-V19-(h)	0.903525339	0.661330376	0.479958663	0.5839979	1.073311733
9	left-middle-finger-fal-1-V1-(h)	0.555343238	0.389894148	0.750081926	0.378313081	0.601960306
10	left-middle-finger-fal-1-V20-(h)	0.759003161	0.911319492	1.373055189	1.083811135	0.63696731
11	left-middle-finger-fal-1-V21-(h)	0.679820783	0.586052486	0.618309645	0.428247412	0.719049912
12	left-middle-finger-fal-1-V25-(h)	0.638249742	0.692788225	1.113707102	0.732154954	0.384569804
13	left-middle-finger-fal-1-V2-(h)	0.731038104	0.492487007	0.625241734	0.517790261	0.765672818
14	left-middle-finger-fal-1-V3-(h)	0.928190851	0.808390026	0.639257382	0.785317949	1.001986477
15	left-middle-finger-fal-1-V4-(h)	0.686760359	0.565622923	0.558611643	0.490021643	0.789773547
16	left-middle-finger-fal-1-V5-(h)	0.563366457	0.550345272	0.982758741	0.583068567	0.52391906
17	left-middle-finger-fal-1-V6-(h)	0.814641116	0.765841143	0.623567659	0.708296248	0.880616863
18	left-middle-finger-fal-1-V7-(h)	0.731377797	0.61294673	0.528221054	0.548768267	0.810562526
19	left-middle-finger-fal-1-V9-(h)	0.695619535	0.494068978	0.517707162	0.407521626	0.88464759
20	left-middle-finger-fal-1-VE35-(h)	1.257093554	0.862417397	0.753912584	0.880846286	1.396928074
21	left-middle-finger-fal-1-VF561-2014-(h)	1.099801183	0.76988274	0.712637486	0.759037044	1.159565271
22	left-middle-finger-fal-1-VF772-2015-(h)	0.895070344	0.580339391	0.719620266	0.60842537	1.068722975

Next, go to the ‘Conditional Formatting’ button on the ‘Home’ tab, hover the mouse over ‘Top/Bottom Rules’ and select ‘Bottom 10 items’:

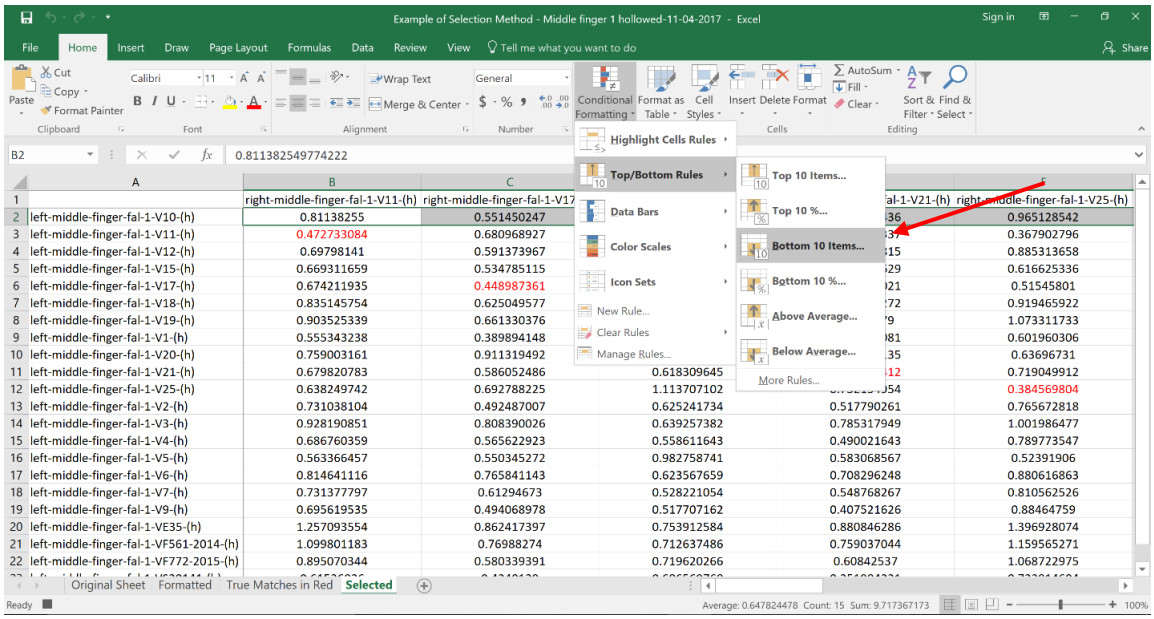

The window will look like this:

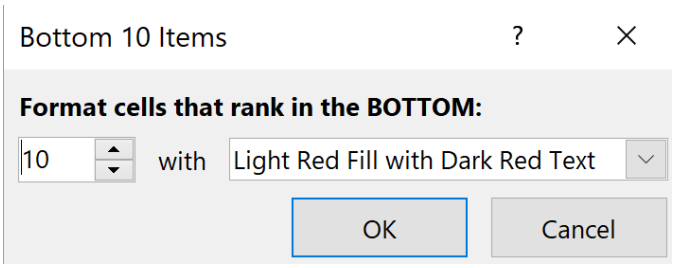

In that window, type in the following and click ‘Okay’:

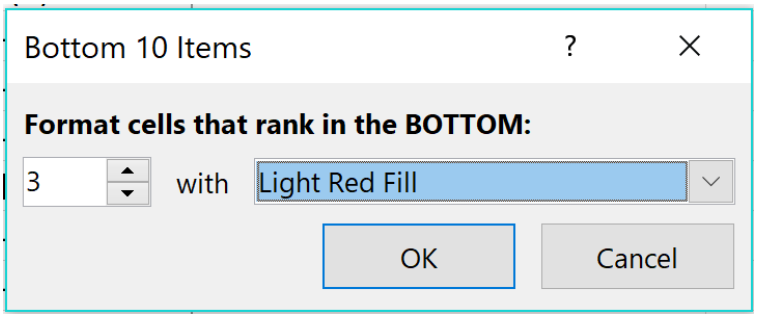

This should highlight the three lowest values in the top row:

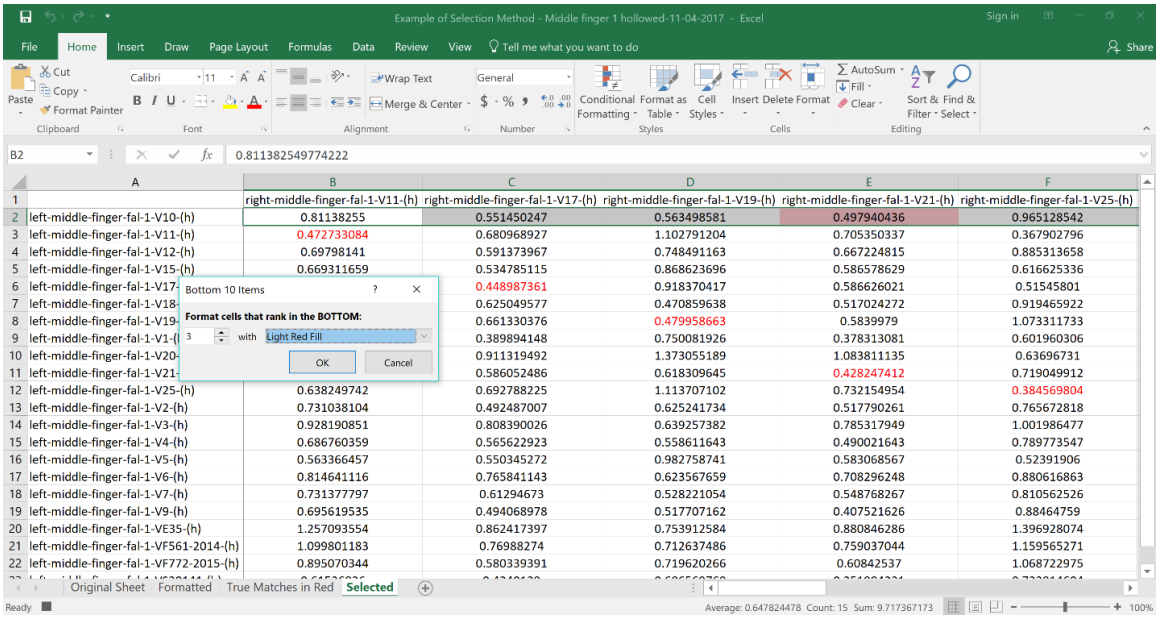

	A	B	C	D	E	F
1		right-middle-finger-fal-1-V11-(h)	right-middle-finger-fal-1-V17-(h)	right-middle-finger-fal-1-V19-(h)	right-middle-finger-fal-1-V21-(h)	right-middle-finger-fal-1-V25-(h)
2	left-middle-finger-fal-1-V10-(h)	0.81138255	0.551450247	0.563498581	0.497940436	0.965128542
3	left-middle-finger-fal-1-V11-(h)	0.472733084	0.680968927	1.102791204	0.705350337	0.367902796
4	left-middle-finger-fal-1-V12-(h)	0.69798141	0.591373967	0.748491163	0.667224815	0.885313658
5	left-middle-finger-fal-1-V15-(h)	0.669311659	0.534785115	0.868623696	0.586578629	0.616625336
6	left-middle-finger-fal-1-V17-	0.674211935	0.448987361	0.918370417	0.586626021	0.51545801
7	left-middle-finger-fal-1-V18-	0.835145754	0.625049577	0.470859638	0.517024272	0.919465922
8	left-middle-finger-fal-1-V19-	0.903525339	0.661330376	0.479958663	0.5839979	1.073311733
9	left-middle-finger-fal-1-V1-(	0.555343238	0.389894148	0.750081926	0.378313081	0.601960306
10	left-middle-finger-fal-1-V20-	0.759003161	0.911319492	1.373055189	1.083811135	0.63696731
11	left-middle-finger-fal-1-V21-	0.679820783	0.586052486	0.618309645	0.428247412	0.719049912
12	left-middle-finger-fal-1-V25-(h)	0.638249742	0.692788225	1.113707102	0.732154954	0.384569804
13	left-middle-finger-fal-1-V2-(h)	0.731038104	0.492487007	0.625241734	0.517790261	0.765672818
14	left-middle-finger-fal-1-V3-(h)	0.928190851	0.808390026	0.639257382	0.785317949	1.001986477
15	left-middle-finger-fal-1-V4-(h)	0.686760359	0.565622923	0.558611643	0.490021643	0.789773547
16	left-middle-finger-fal-1-V5-(h)	0.563366457	0.550345272	0.982758741	0.583068567	0.52391906
17	left-middle-finger-fal-1-V6-(h)	0.814641116	0.765841143	0.623567659	0.708296248	0.880616863
18	left-middle-finger-fal-1-V7-(h)	0.731377797	0.61294673	0.528221054	0.548768267	0.810562526
19	left-middle-finger-fal-1-V9-(h)	0.695619535	0.494068978	0.517707162	0.407521626	0.88464759
20	left-middle-finger-fal-1-VE35-(h)	1.257093554	0.862417397	0.753912584	0.880846286	1.396928074
21	left-middle-finger-fal-1-VF561-2014-(h)	1.099801183	0.76988274	0.712637486	0.759037044	1.159565271
22	left-middle-finger-fal-1-VF772-2015-(h)	0.895070344	0.580339391	0.719620266	0.60842537	1.068722975

After clicking ‘Okay’, select the first value in the second row:

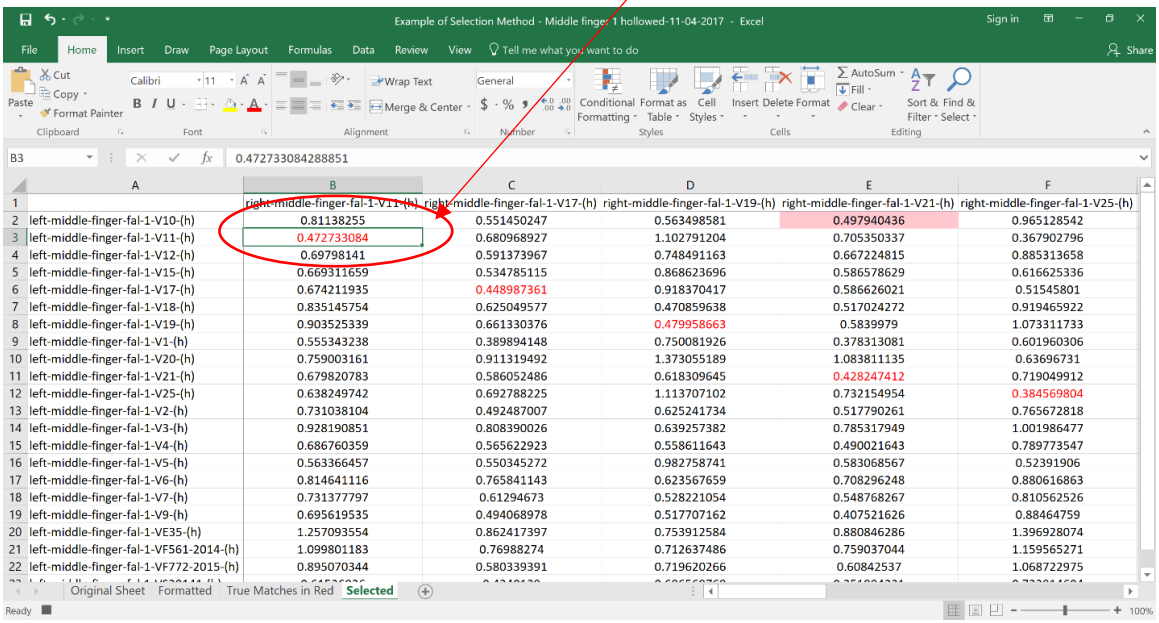

	A	B	C	D	E	F
1		right-middle-finger-fal-1-V11-(h)	right-middle-finger-fal-1-V17-(h)	right-middle-finger-fal-1-V19-(h)	right-middle-finger-fal-1-V21-(h)	right-middle-finger-fal-1-V25-(h)
2	left-middle-finger-fal-1-V10-(h)	0.81138255	0.551450247	0.563498581	0.497940436	0.965128542
3	left-middle-finger-fal-1-V11-(h)	0.472733084	0.680968927	1.102791204	0.705350337	0.367902796
4	left-middle-finger-fal-1-V12-(h)	0.69798141	0.591373967	0.748491163	0.667224815	0.885313658
5	left-middle-finger-fal-1-V15-(h)	0.669311659	0.534785115	0.868623696	0.586578629	0.616625336
6	left-middle-finger-fal-1-V17-(h)	0.674211935	0.448987361	0.918370417	0.586626021	0.51545801
7	left-middle-finger-fal-1-V18-(h)	0.835145754	0.625049577	0.470859638	0.517024272	0.919465922
8	left-middle-finger-fal-1-V19-(h)	0.903525339	0.661330376	0.479958663	0.5839979	1.073311733
9	left-middle-finger-fal-1-V1-(h)	0.555343238	0.389894148	0.750081926	0.378313081	0.601960306
10	left-middle-finger-fal-1-V20-(h)	0.759003161	0.911319492	1.373055189	1.083811135	0.63696731
11	left-middle-finger-fal-1-V21-(h)	0.679820783	0.586052486	0.618309645	0.428247412	0.719049912
12	left-middle-finger-fal-1-V25-(h)	0.638249742	0.692788225	1.113707102	0.732154954	0.384569804
13	left-middle-finger-fal-1-V2-(h)	0.731038104	0.492487007	0.625241734	0.517790261	0.765672818
14	left-middle-finger-fal-1-V3-(h)	0.928190851	0.808390026	0.639257382	0.785317949	1.001986477
15	left-middle-finger-fal-1-V4-(h)	0.686760359	0.565622923	0.558611643	0.490021643	0.789773547
16	left-middle-finger-fal-1-V5-(h)	0.563366457	0.550345272	0.982758741	0.583068567	0.52391906
17	left-middle-finger-fal-1-V6-(h)	0.814641116	0.765841143	0.623567659	0.708296248	0.880616863
18	left-middle-finger-fal-1-V7-(h)	0.731377797	0.61294673	0.528221054	0.548768267	0.810562526
19	left-middle-finger-fal-1-V9-(h)	0.695619535	0.494068978	0.517707162	0.407521626	0.88464759
20	left-middle-finger-fal-1-VE35-(h)	1.257093554	0.862417397	0.753912584	0.880846286	1.396928074
21	left-middle-finger-fal-1-VF561-2014-(h)	1.099801183	0.76988274	0.712637486	0.759037044	1.159565271
22	left-middle-finger-fal-1-VF772-2015-(h)	0.895070344	0.580339391	0.719620266	0.60842537	1.068722975

Then return to the ‘View’ tab, click the ‘Macro’ button and select ‘Stop Recording’:

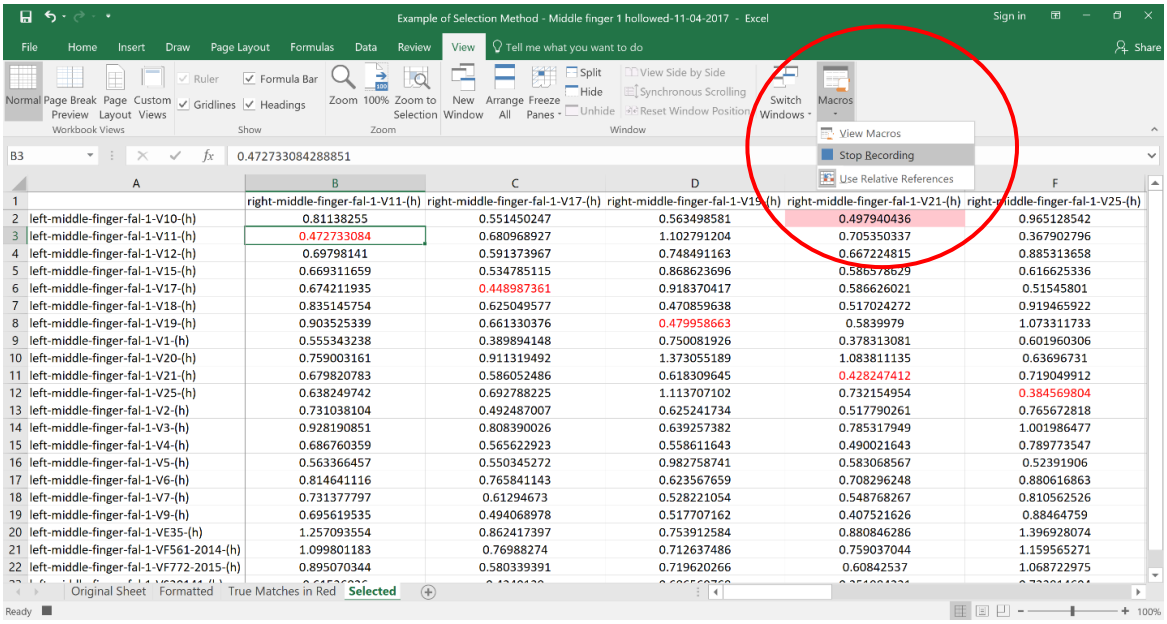

	A	B	C	D	E	F
1		right-middle-finger-fal-1-V11-(h)	right-middle-finger-fal-1-V17-(h)	right-middle-finger-fal-1-V19-(h)	right-middle-finger-fal-1-V21-(h)	right-middle-finger-fal-1-V25-(h)
2	left-middle-finger-fal-1-V10-(h)	0.81138255	0.551450247	0.563498581	0.497940436	0.965128542
3	left-middle-finger-fal-1-V11-(h)	0.472733084	0.680968927	1.102791204	0.705350337	0.367902796
4	left-middle-finger-fal-1-V12-(h)	0.69798141	0.591373967	0.748491163	0.667224815	0.885313658
5	left-middle-finger-fal-1-V15-(h)	0.669311659	0.534785115	0.868623696	0.586578629	0.616625336
6	left-middle-finger-fal-1-V17-(h)	0.674211935	0.448987361	0.918370417	0.586626021	0.51545801
7	left-middle-finger-fal-1-V18-(h)	0.835145754	0.625049577	0.470859638	0.517024272	0.919465922
8	left-middle-finger-fal-1-V19-(h)	0.903525339	0.661330376	0.479958663	0.5839979	1.073311733
9	left-middle-finger-fal-1-V1-(h)	0.555343238	0.389894148	0.750081926	0.378313081	0.601960306
10	left-middle-finger-fal-1-V20-(h)	0.759003161	0.911319492	1.373055189	1.083811135	0.63696731
11	left-middle-finger-fal-1-V21-(h)	0.679820783	0.586052486	0.618309645	0.428247412	0.719049912
12	left-middle-finger-fal-1-V25-(h)	0.638249742	0.692788225	1.113707102	0.732154954	0.384569804
13	left-middle-finger-fal-1-V2-(h)	0.731038104	0.492487007	0.625241734	0.517790261	0.765672818
14	left-middle-finger-fal-1-V3-(h)	0.928190851	0.808390026	0.639257382	0.785317949	1.001986477
15	left-middle-finger-fal-1-V4-(h)	0.686760359	0.565622923	0.558611643	0.490021643	0.789773547
16	left-middle-finger-fal-1-V5-(h)	0.563366457	0.550345272	0.982758741	0.583068567	0.52391906
17	left-middle-finger-fal-1-V6-(h)	0.814641116	0.765841143	0.623567659	0.708296248	0.880616863
18	left-middle-finger-fal-1-V7-(h)	0.731377797	0.61294673	0.528221054	0.548768267	0.810562526
19	left-middle-finger-fal-1-V9-(h)	0.695619535	0.494068978	0.517707162	0.407521626	0.88464759
20	left-middle-finger-fal-1-VE35-(h)	1.257093554	0.862417397	0.753912584	0.880846286	1.396928074
21	left-middle-finger-fal-1-VF561-2014-(h)	1.099801183	0.76988274	0.712637486	0.759037044	1.159565271
22	left-middle-finger-fal-1-VF772-2015-(h)	0.895070344	0.580339391	0.719620266	0.60842537	1.068722975

Now, to use this macro, press the CTRL key and the ‘q’ key at the same time. This should select the three lowest values for the next row:

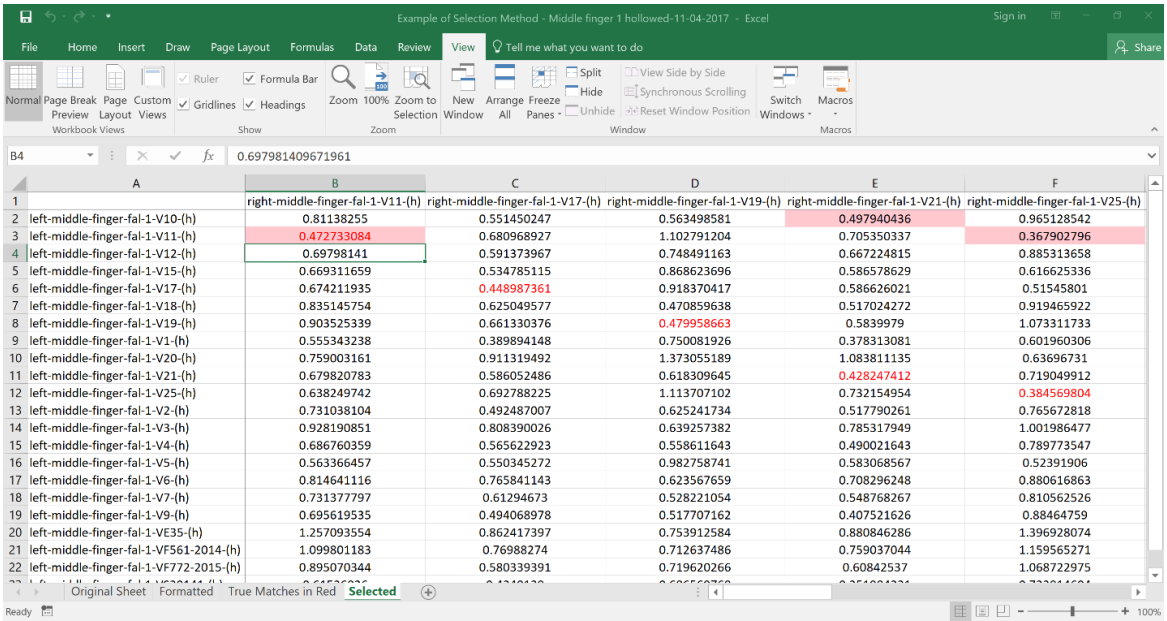

	A	B	C	D	E	F
1		right-middle-finger-fal-1-V11-(h)	right-middle-finger-fal-1-V17-(h)	right-middle-finger-fal-1-V19-(h)	right-middle-finger-fal-1-V21-(h)	right-middle-finger-fal-1-V25-(h)
2	left-middle-finger-fal-1-V10-(h)	0.81138255	0.551450247	0.563498581	0.497940436	0.965128542
3	left-middle-finger-fal-1-V11-(h)	0.472733084	0.680968927	1.102791204	0.705350337	0.367902796
4	left-middle-finger-fal-1-V12-(h)	0.69798141	0.591373967	0.748491163	0.667224815	0.885313658
5	left-middle-finger-fal-1-V15-(h)	0.669311659	0.534785115	0.868623696	0.586578629	0.616625336
6	left-middle-finger-fal-1-V17-(h)	0.674211935	0.448987361	0.918370417	0.586626021	0.51545801
7	left-middle-finger-fal-1-V18-(h)	0.835145754	0.625049577	0.470859638	0.517024272	0.919465922
8	left-middle-finger-fal-1-V19-(h)	0.903525339	0.661330376	0.479958663	0.5839979	1.073311733
9	left-middle-finger-fal-1-V1-(h)	0.555343238	0.389894148	0.750081926	0.378313081	0.601960306
10	left-middle-finger-fal-1-V20-(h)	0.759003161	0.911319492	1.373055189	1.083811135	0.63696731
11	left-middle-finger-fal-1-V21-(h)	0.679820783	0.586052486	0.618309645	0.428247412	0.719049912
12	left-middle-finger-fal-1-V25-(h)	0.638249742	0.692788225	1.113707102	0.732154954	0.384569804
13	left-middle-finger-fal-1-V2-(h)	0.731038104	0.492487007	0.625241734	0.517790261	0.765672818
14	left-middle-finger-fal-1-V3-(h)	0.928190851	0.808390026	0.639257382	0.785317949	1.001986477
15	left-middle-finger-fal-1-V4-(h)	0.686760359	0.565622923	0.558611643	0.490021643	0.789773547
16	left-middle-finger-fal-1-V5-(h)	0.563366457	0.550345272	0.982758741	0.583068567	0.52391906
17	left-middle-finger-fal-1-V6-(h)	0.814641116	0.765841143	0.623567659	0.708296248	0.880616863
18	left-middle-finger-fal-1-V7-(h)	0.731377797	0.61294673	0.528221054	0.548768267	0.810562526
19	left-middle-finger-fal-1-V9-(h)	0.695619535	0.494068978	0.517707162	0.407521626	0.88464759
20	left-middle-finger-fal-1-VE35-(h)	1.257093554	0.862417397	0.753912584	0.880846286	1.396928074
21	left-middle-finger-fal-1-VF561-2014-(h)	1.099801183	0.76988274	0.712637486	0.759037044	1.159565271
22	left-middle-finger-fal-1-VF772-2015-(h)	0.895070344	0.580339391	0.719620266	0.60842537	1.068722975

Keep pressing this combination (CTRL + q) until all the rows (lefts, across) have had their lowest values selected:

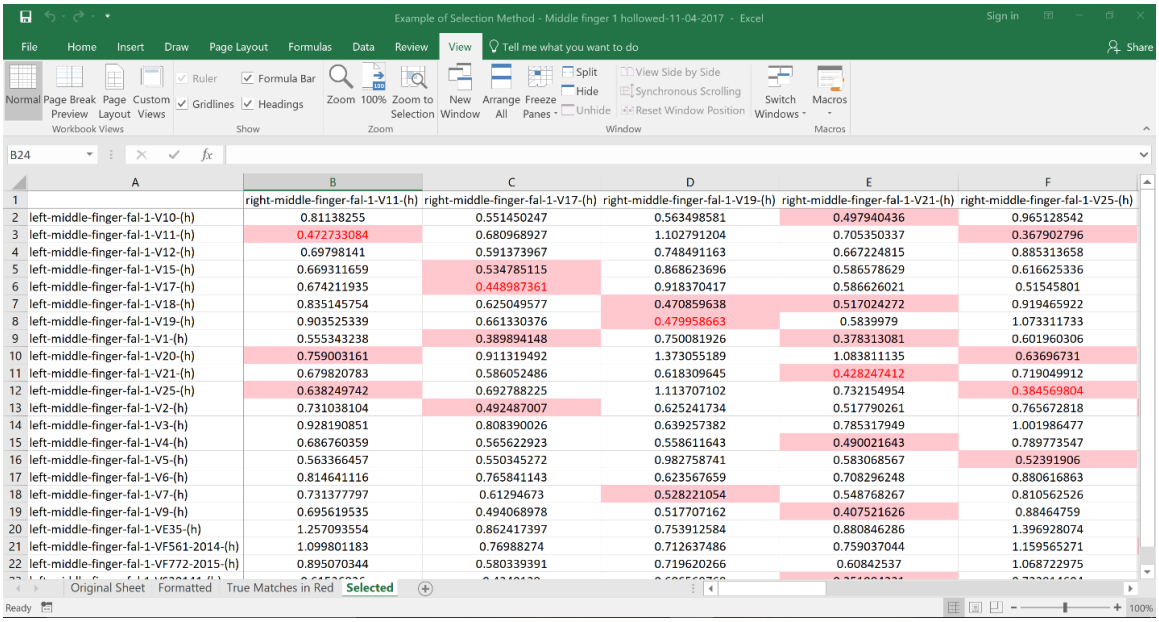

	right-middle-finger-fal-1-V11-(h)	right-middle-finger-fal-1-V17-(h)	right-middle-finger-fal-1-V19-(h)	right-middle-finger-fal-1-V21-(h)	right-middle-finger-fal-1-V25-(h)
left-middle-finger-fal-1-V10-(h)	0.81138255	0.551450247	0.563498581	0.497940436	0.965128542
left-middle-finger-fal-1-V11-(h)	0.472733084	0.680968927	1.102791204	0.705350337	0.367902796
left-middle-finger-fal-1-V12-(h)	0.69798141	0.591373967	0.748491163	0.667224815	0.885313658
left-middle-finger-fal-1-V15-(h)	0.669311659	0.534785115	0.868623696	0.586578629	0.616625336
left-middle-finger-fal-1-V17-(h)	0.674211935	0.448987361	0.918370417	0.586626021	0.51545801
left-middle-finger-fal-1-V18-(h)	0.835145754	0.625049577	0.470859638	0.517024272	0.919465922
left-middle-finger-fal-1-V19-(h)	0.903525339	0.661330376	0.479958663	0.5839979	1.073311733
left-middle-finger-fal-1-V1-(h)	0.555343238	0.389894148	0.750081926	0.378313081	0.601960306
left-middle-finger-fal-1-V20-(h)	0.759003161	0.911319492	1.373055189	1.083811135	0.63696731
left-middle-finger-fal-1-V21-(h)	0.679820783	0.586052486	0.618309645	0.428247412	0.719049912
left-middle-finger-fal-1-V25-(h)	0.638249742	0.692788225	1.113707102	0.732154954	0.384569804
left-middle-finger-fal-1-V2-(h)	0.731038104	0.492487007	0.625241734	0.517790261	0.765672818
left-middle-finger-fal-1-V3-(h)	0.928190851	0.808390026	0.639257382	0.785317949	1.001986477
left-middle-finger-fal-1-V4-(h)	0.686760359	0.565622923	0.558611643	0.490021643	0.789773547
left-middle-finger-fal-1-V5-(h)	0.563366457	0.550345272	0.982758741	0.583068567	0.52391906
left-middle-finger-fal-1-V6-(h)	0.814641116	0.765841143	0.623567659	0.708296248	0.880616863
left-middle-finger-fal-1-V7-(h)	0.731377797	0.61294673	0.528221054	0.548768267	0.810562526
left-middle-finger-fal-1-V9-(h)	0.695619535	0.494068978	0.517707162	0.407521626	0.88464759
left-middle-finger-fal-1-VE35-(h)	1.257093554	0.862417397	0.753912584	0.880846286	1.396928074
left-middle-finger-fal-1-VF561-2014-(h)	1.099801183	0.76988274	0.712637486	0.759037044	1.159565271
left-middle-finger-fal-1-VF772-2015-(h)	0.895070344	0.580339391	0.719620266	0.60842537	1.068722975

Now, to select the three lowest values for the rights (down, columns). Click on the first cell in the first column and then start to record another macro by clicking the arrow under the ‘Macro’ button and select ‘Record Macro’:

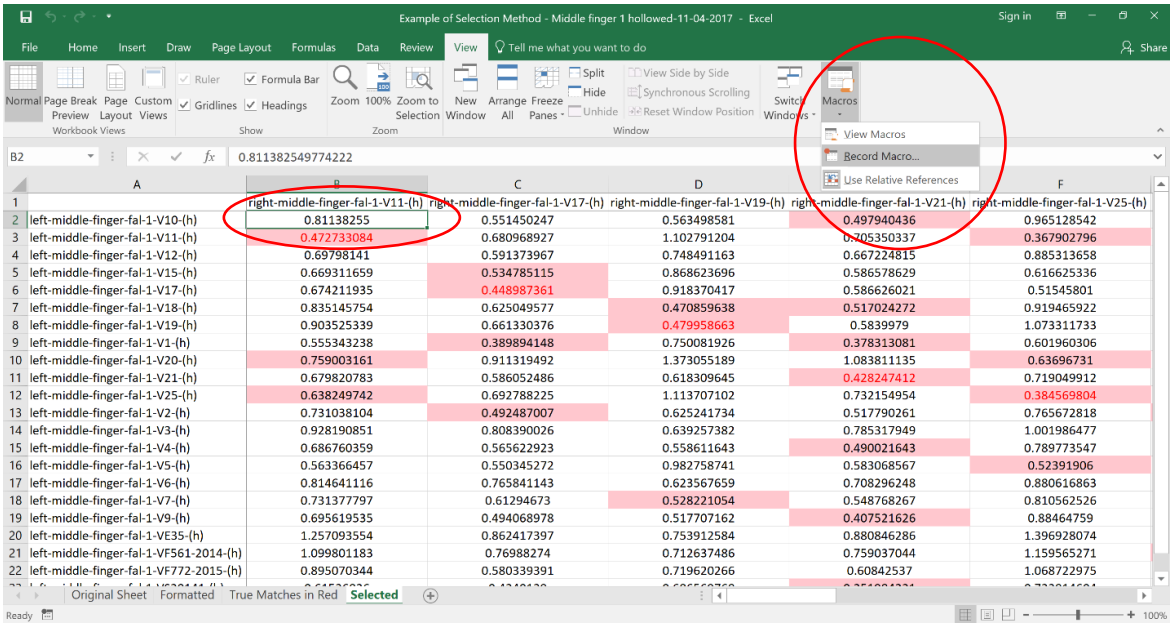

	right-middle-finger-fal-1-V11-(h)	right-middle-finger-fal-1-V17-(h)	right-middle-finger-fal-1-V19-(h)	right-middle-finger-fal-1-V21-(h)	right-middle-finger-fal-1-V25-(h)
left-middle-finger-fal-1-V10-(h)	0.81138255	0.551450247	0.563498581	0.497940436	0.965128542
left-middle-finger-fal-1-V11-(h)	0.472733084	0.680968927	1.102791204	0.705350337	0.367902796
left-middle-finger-fal-1-V12-(h)	0.69798141	0.591373967	0.748491163	0.667224815	0.885313658
left-middle-finger-fal-1-V15-(h)	0.669311659	0.534785115	0.868623696	0.586578629	0.616625336
left-middle-finger-fal-1-V17-(h)	0.674211935	0.448987361	0.918370417	0.586626021	0.51545801
left-middle-finger-fal-1-V18-(h)	0.835145754	0.625049577	0.470859638	0.517024272	0.919465922
left-middle-finger-fal-1-V19-(h)	0.903525339	0.661330376	0.479958663	0.5839979	1.073311733
left-middle-finger-fal-1-V1-(h)	0.555343238	0.389894148	0.750081926	0.378313081	0.601960306
left-middle-finger-fal-1-V20-(h)	0.759003161	0.911319492	1.373055189	1.083811135	0.63696731
left-middle-finger-fal-1-V21-(h)	0.679820783	0.586052486	0.618309645	0.428247412	0.719049912
left-middle-finger-fal-1-V25-(h)	0.638249742	0.692788225	1.113707102	0.732154954	0.384569804
left-middle-finger-fal-1-V2-(h)	0.731038104	0.492487007	0.625241734	0.517790261	0.765672818
left-middle-finger-fal-1-V3-(h)	0.928190851	0.808390026	0.639257382	0.785317949	1.001986477
left-middle-finger-fal-1-V4-(h)	0.686760359	0.565622923	0.558611643	0.490021643	0.789773547
left-middle-finger-fal-1-V5-(h)	0.563366457	0.550345272	0.982758741	0.583068567	0.52391906
left-middle-finger-fal-1-V6-(h)	0.814641116	0.765841143	0.623567659	0.708296248	0.880616863
left-middle-finger-fal-1-V7-(h)	0.731377797	0.61294673	0.528221054	0.548768267	0.810562526
left-middle-finger-fal-1-V9-(h)	0.695619535	0.494068978	0.517707162	0.407521626	0.88464759
left-middle-finger-fal-1-VE35-(h)	1.257093554	0.862417397	0.753912584	0.880846286	1.396928074
left-middle-finger-fal-1-VF561-2014-(h)	1.099801183	0.76988274	0.712637486	0.759037044	1.159565271
left-middle-finger-fal-1-VF772-2015-(h)	0.895070344	0.580339391	0.719620266	0.60842537	1.068722975

This will bring up this window again:

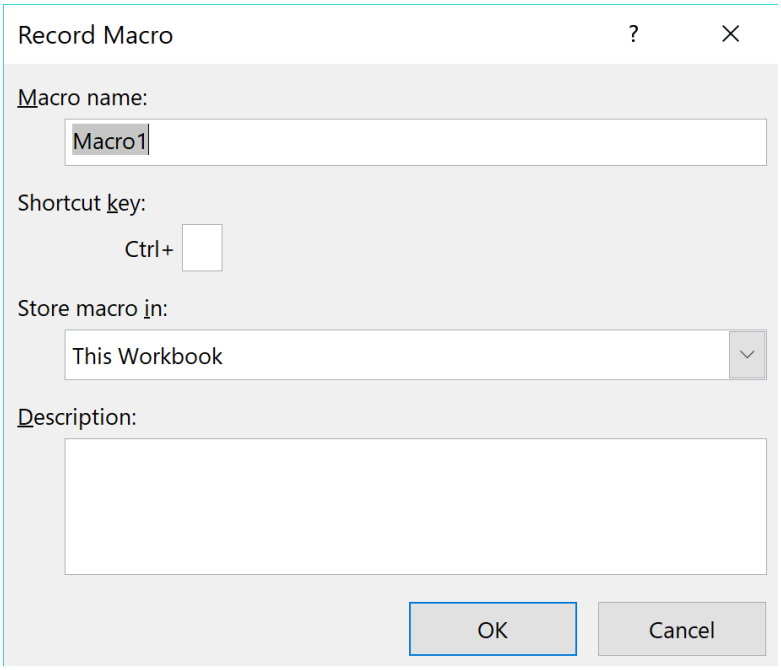

In that window, type in the following and select ‘Okay’:

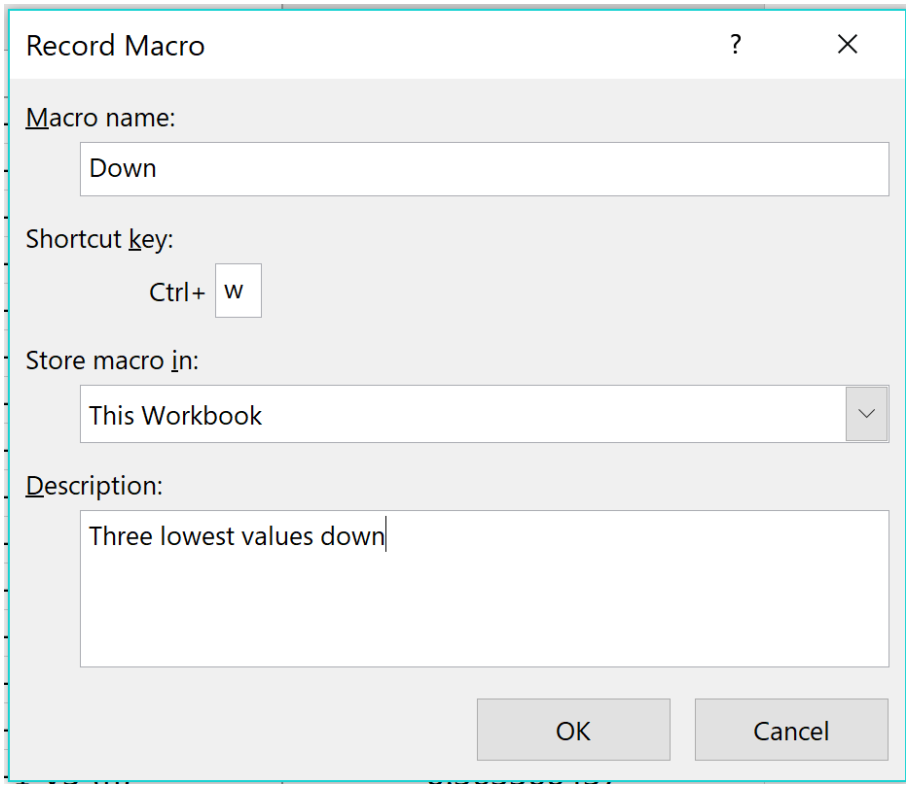

Then, select all the values in the first column (first right bone):

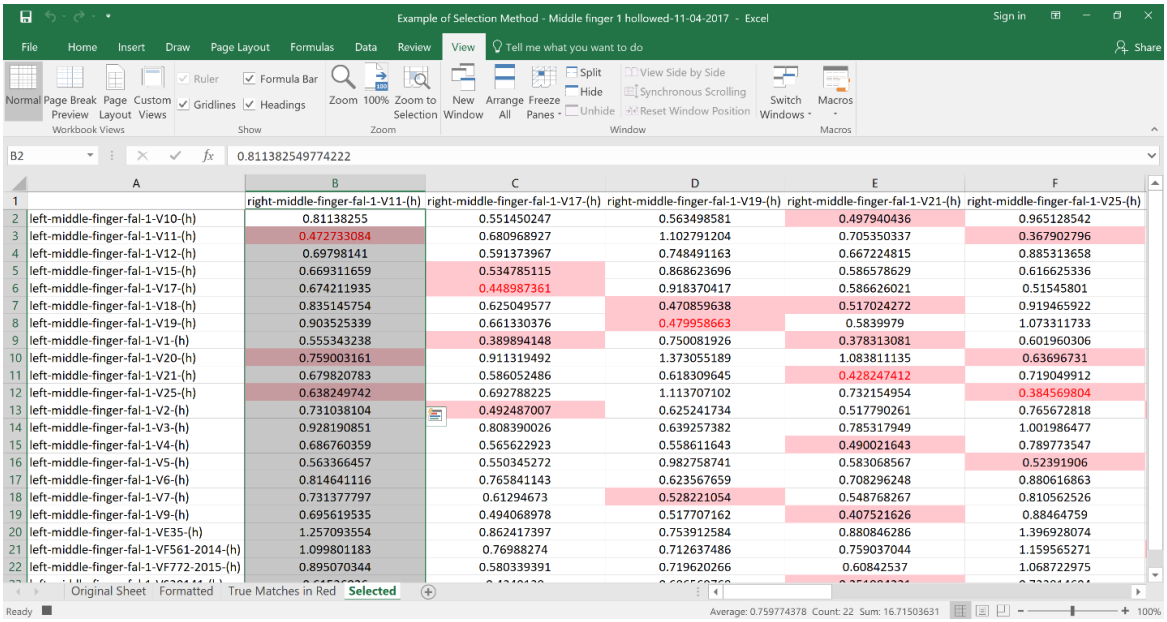

	A	B	C	D	E	F
1		right-middle-finger-fal-1-V11-(h)	right-middle-finger-fal-1-V17-(h)	right-middle-finger-fal-1-V19-(h)	right-middle-finger-fal-1-V21-(h)	right-middle-finger-fal-1-V25-(h)
2	left-middle-finger-fal-1-V10-(h)	0.81138255	0.551450247	0.563498581	0.497940436	0.965128542
3	left-middle-finger-fal-1-V11-(h)	0.472733084	0.680968927	1.102791204	0.705350337	0.367902796
4	left-middle-finger-fal-1-V12-(h)	0.69798141	0.591373967	0.748491163	0.667224815	0.885313658
5	left-middle-finger-fal-1-V15-(h)	0.669311659	0.534785115	0.868623696	0.586578629	0.616625336
6	left-middle-finger-fal-1-V17-(h)	0.674211935	0.448987361	0.918370417	0.586626021	0.51545801
7	left-middle-finger-fal-1-V18-(h)	0.835145754	0.625049577	0.470859638	0.517024272	0.919465922
8	left-middle-finger-fal-1-V19-(h)	0.903525339	0.661330376	0.479958663	0.5839979	1.073311733
9	left-middle-finger-fal-1-V1-(h)	0.555343238	0.389894148	0.750081926	0.378313081	0.601960306
10	left-middle-finger-fal-1-V20-(h)	0.759003161	0.911319492	1.373055189	1.083811135	0.63696731
11	left-middle-finger-fal-1-V21-(h)	0.679820783	0.586052486	0.618309645	0.428247412	0.719049912
12	left-middle-finger-fal-1-V25-(h)	0.638249742	0.692788225	1.113707102	0.732154954	0.384569804
13	left-middle-finger-fal-1-V2-(h)	0.731038104	0.492487007	0.625241734	0.517790261	0.765672818
14	left-middle-finger-fal-1-V3-(h)	0.928190851	0.808390026	0.639257382	0.785317949	1.001986477
15	left-middle-finger-fal-1-V4-(h)	0.686760359	0.565622923	0.558611643	0.490021643	0.789773547
16	left-middle-finger-fal-1-V5-(h)	0.563366457	0.550345272	0.982758741	0.583068567	0.52391906
17	left-middle-finger-fal-1-V6-(h)	0.814641116	0.765841143	0.623567659	0.708296248	0.880616863
18	left-middle-finger-fal-1-V7-(h)	0.731377797	0.61294673	0.528221054	0.548768267	0.810562526
19	left-middle-finger-fal-1-V9-(h)	0.695619535	0.494068978	0.517707162	0.407521626	0.88464759
20	left-middle-finger-fal-1-VE35-(h)	1.257093554	0.862417397	0.753912584	0.880846286	1.396928074
21	left-middle-finger-fal-1-VF561-2014-(h)	1.099801183	0.76988274	0.712637486	0.759037044	1.159565271
22	left-middle-finger-fal-1-VF772-2015-(h)	0.895070344	0.580339391	0.719620266	0.60842537	1.068722975

Next, go to the ‘Conditional Formatting’ button on the ‘Home’ tab, hover the mouse over ‘Top/Bottom Rules’ and select ‘Bottom 10 items’:

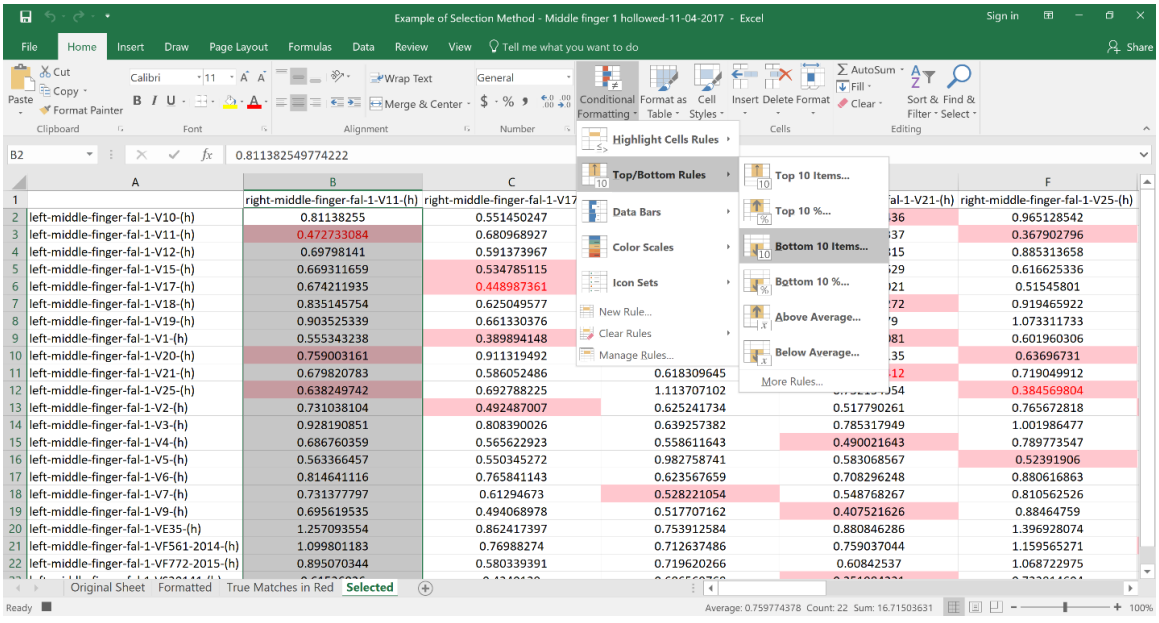

	A	B	C	F
1		right-middle-finger-fal-1-V11-(h)	right-middle-finger-fal-1-V17	right-middle-finger-fal-1-V25-(h)
2	left-middle-finger-fal-1-V10-(h)	0.81138255	0.551450247	0.965128542
3	left-middle-finger-fal-1-V11-(h)	0.472733084	0.680968927	0.367902796
4	left-middle-finger-fal-1-V12-(h)	0.69798141	0.591373967	0.885313658
5	left-middle-finger-fal-1-V15-(h)	0.669311659	0.534785115	0.616625336
6	left-middle-finger-fal-1-V17-(h)	0.674211935	0.448987361	0.51545801
7	left-middle-finger-fal-1-V18-(h)	0.835145754	0.625049577	0.919465922
8	left-middle-finger-fal-1-V19-(h)	0.903525339	0.661330376	1.073311733
9	left-middle-finger-fal-1-V1-(h)	0.555343238	0.389894148	0.601960306
10	left-middle-finger-fal-1-V20-(h)	0.759003161	0.911319492	0.63696731
11	left-middle-finger-fal-1-V21-(h)	0.679820783	0.586052486	0.719049912
12	left-middle-finger-fal-1-V25-(h)	0.638249742	0.692788225	0.384569804
13	left-middle-finger-fal-1-V2-(h)	0.731038104	0.492487007	0.765672818
14	left-middle-finger-fal-1-V3-(h)	0.928190851	0.808390026	1.001986477
15	left-middle-finger-fal-1-V4-(h)	0.686760359	0.565622923	0.789773547
16	left-middle-finger-fal-1-V5-(h)	0.563366457	0.550345272	0.52391906
17	left-middle-finger-fal-1-V6-(h)	0.814641116	0.765841143	0.880616863
18	left-middle-finger-fal-1-V7-(h)	0.731377797	0.61294673	0.810562526
19	left-middle-finger-fal-1-V9-(h)	0.695619535	0.494068978	0.88464759
20	left-middle-finger-fal-1-VE35-(h)	1.257093554	0.862417397	1.396928074
21	left-middle-finger-fal-1-VF561-2014-(h)	1.099801183	0.76988274	1.159565271
22	left-middle-finger-fal-1-VF772-2015-(h)	0.895070344	0.580339391	1.068722975

The window will look like this:

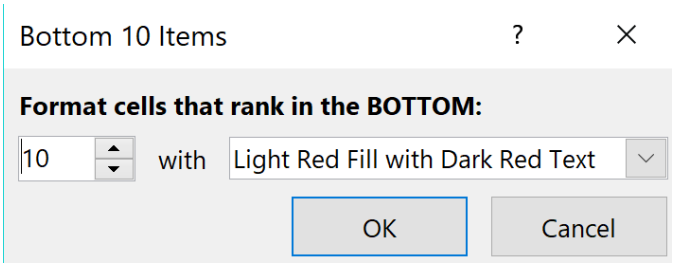

Fill in the window like this, selecting '3' instead of '10' and 'Custom Format':

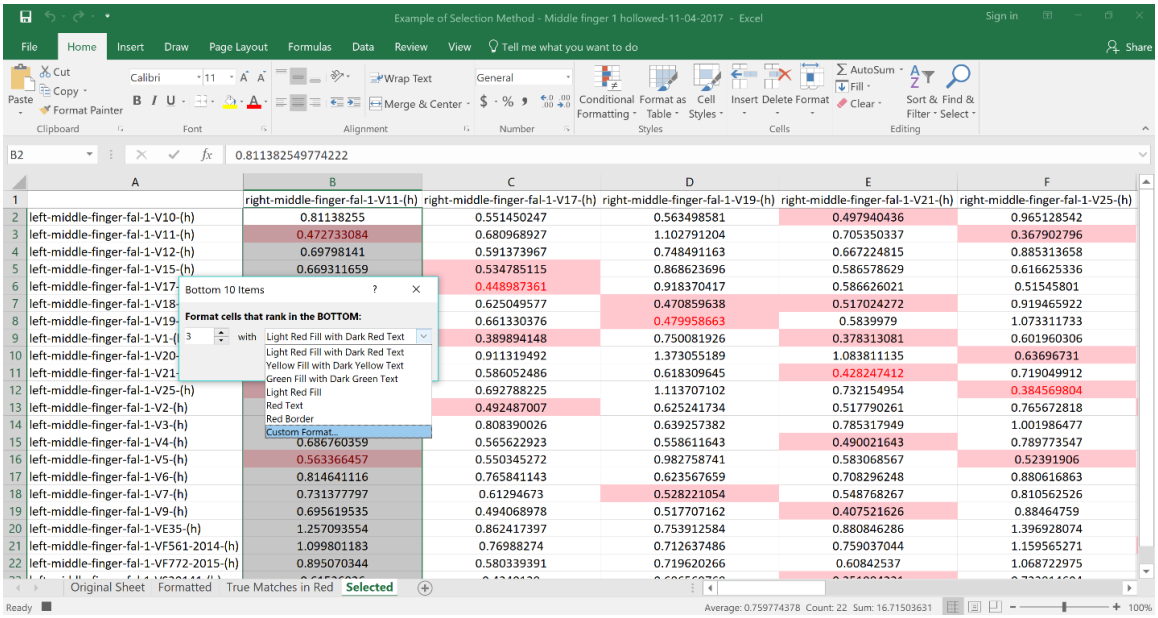

The custom formatting box will look like this:

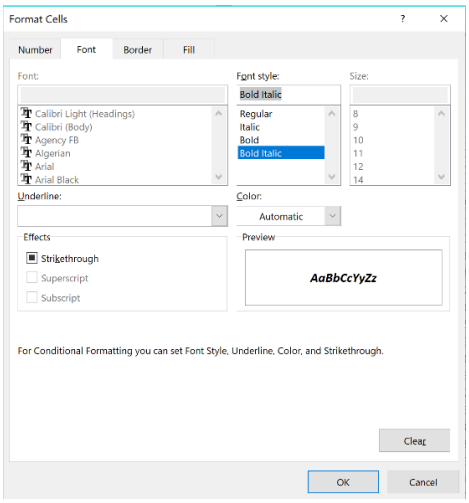

In the ‘Font’ tab, select ‘Bold Italic’:

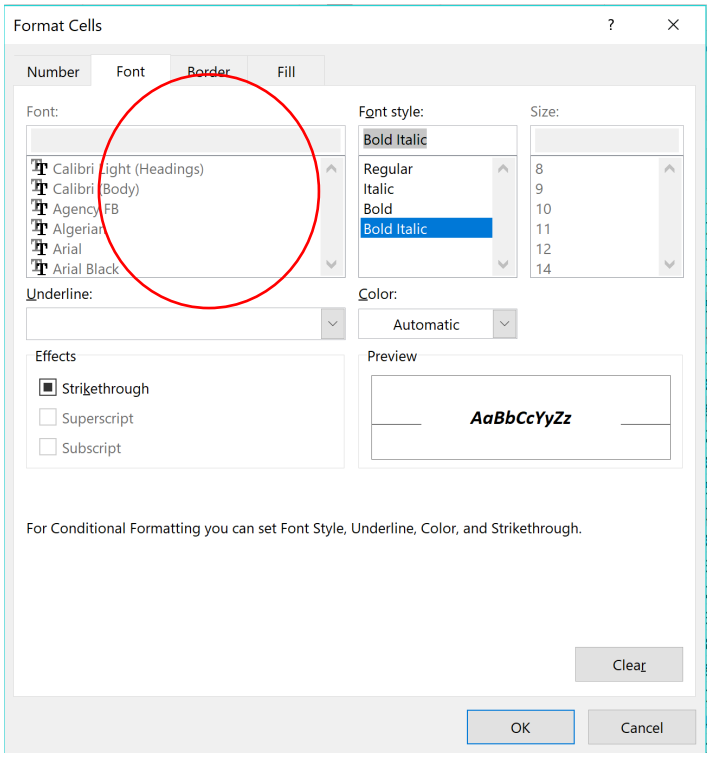

In the ‘Border’ tab, select the ‘Outline’ box (it will turn blue), then click ‘Okay’:

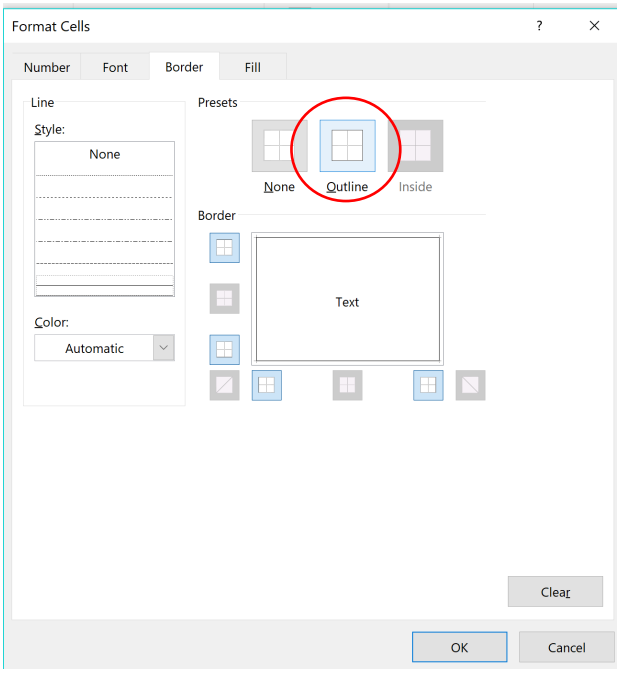

This should result in the conditional window looking like this, then click ‘Okay’:

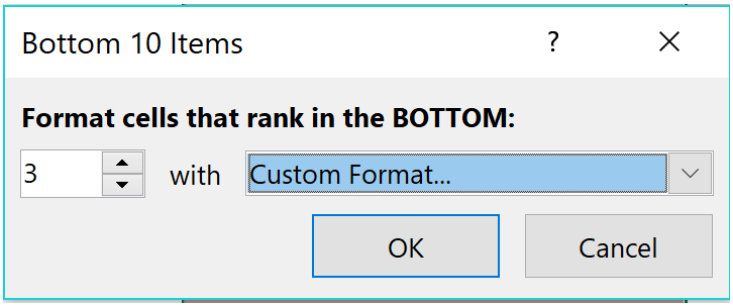

After clicking ‘Okay’, select the first value in the second column:

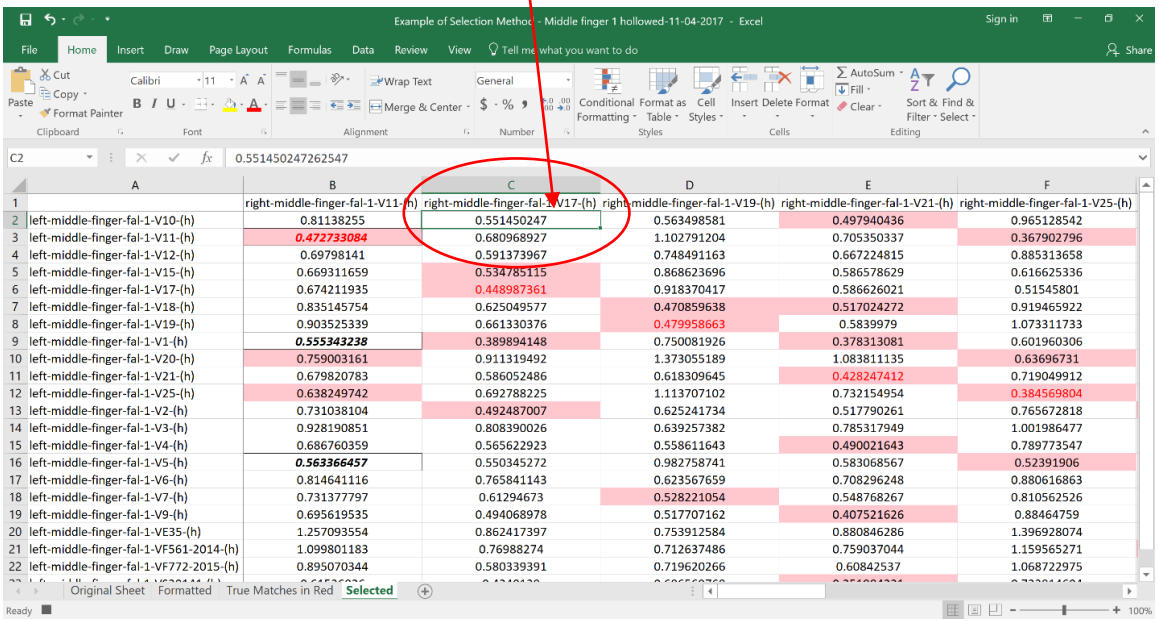

	A	B	C	D	E	F
1		right-middle-finger-fal-1-V11-(h)	right-middle-finger-fal-1-V17-(h)	right-middle-finger-fal-1-V19-(h)	right-middle-finger-fal-1-V21-(h)	right-middle-finger-fal-1-V25-(h)
2	left-middle-finger-fal-1-V10-(h)	0.81138255	0.551450247	0.563498581	0.497940436	0.965128542
3	left-middle-finger-fal-1-V11-(h)	***0.472733084***	0.680968927	1.102791204	0.705350337	0.367902796
4	left-middle-finger-fal-1-V12-(h)	0.69798141	0.591373967	0.748491163	0.667224815	0.885313658
5	left-middle-finger-fal-1-V15-(h)	0.669311659	0.534785115	0.868623696	0.586578629	0.616625336
6	left-middle-finger-fal-1-V17-(h)	0.674211935	0.448987361	0.918370417	0.586626021	0.51545801
7	left-middle-finger-fal-1-V18-(h)	0.835145754	0.625049577	0.470859638	0.517024272	0.919465922
8	left-middle-finger-fal-1-V19-(h)	0.903525339	0.661330376	0.479958663	0.5839979	1.073311733
9	left-middle-finger-fal-1-V1-(h)	***0.555343238***	0.389894148	0.750081926	0.378313081	0.601960306
10	left-middle-finger-fal-1-V20-(h)	0.759003161	0.911319492	1.373055189	1.083811135	0.63696731
11	left-middle-finger-fal-1-V21-(h)	0.679820783	0.586052486	0.618309645	0.428247412	0.719049912
12	left-middle-finger-fal-1-V25-(h)	0.638249742	0.692788225	1.113707102	0.732154954	0.384569804
13	left-middle-finger-fal-1-V2-(h)	0.731038104	0.492487007	0.625241734	0.517790261	0.765672818
14	left-middle-finger-fal-1-V3-(h)	0.928190851	0.808390026	0.639257382	0.785317949	1.001986477
15	left-middle-finger-fal-1-V4-(h)	0.686760359	0.565622923	0.558611643	0.490021643	0.789773547
16	left-middle-finger-fal-1-V5-(h)	***0.563366457***	0.550345272	0.982758741	0.583068567	0.52391906
17	left-middle-finger-fal-1-V6-(h)	0.814641116	0.765841143	0.623567659	0.708296248	0.880616863
18	left-middle-finger-fal-1-V7-(h)	0.731377797	0.61294673	0.528221054	0.548768267	0.810562526
19	left-middle-finger-fal-1-V9-(h)	0.695619535	0.494068978	0.517707162	0.407521626	0.88464759
20	left-middle-finger-fal-1-VE35-(h)	1.257093554	0.862417397	0.753912584	0.880846286	1.396928074
21	left-middle-finger-fal-1-VF561-2014-(h)	1.099801183	0.76988274	0.712637486	0.759037044	1.159565271
22	left-middle-finger-fal-1-VF772-2015-(h)	0.895070344	0.580339391	0.719620266	0.60842537	1.068722975

Then return to the ‘View’ tab, click the ‘Macro’ button and select ‘Stop Recording’:

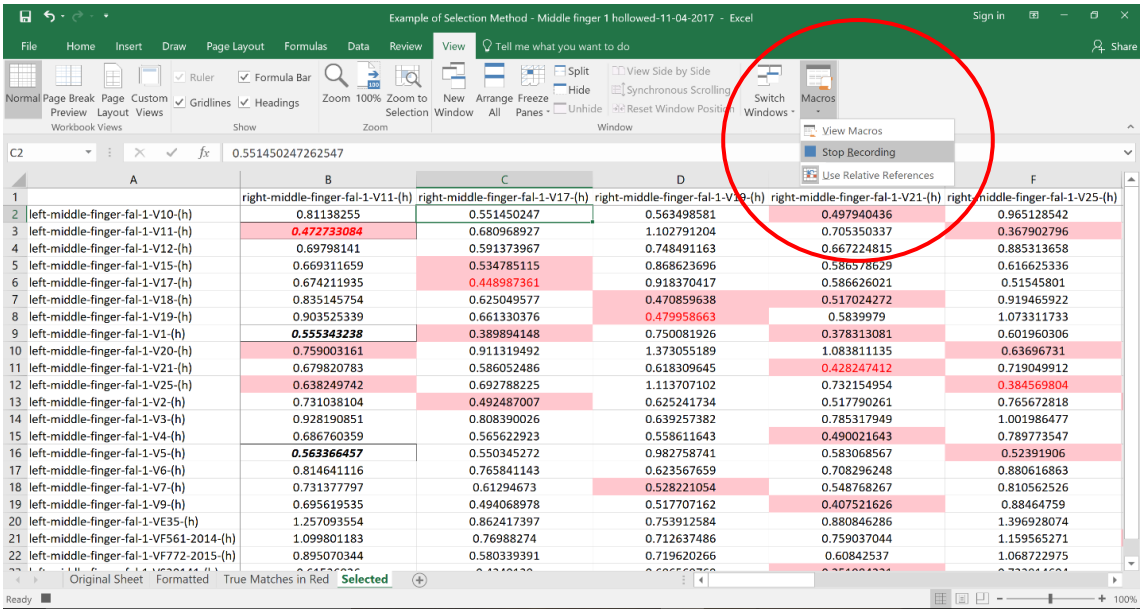

	A	B	C	D	E	F
1		right-middle-finger-fal-1-V11-(h)	right-middle-finger-fal-1-V17-(h)	right-middle-finger-fal-1-V19-(h)	right-middle-finger-fal-1-V21-(h)	right-middle-finger-fal-1-V25-(h)
2	left-middle-finger-fal-1-V10-(h)	0.81138255	0.551450247	0.563498581	0.497940436	0.965128542
3	left-middle-finger-fal-1-V11-(h)	***0.472733084***	0.680968927	1.102791204	0.705350337	0.367902796
4	left-middle-finger-fal-1-V12-(h)	0.69798141	0.591373967	0.748491163	0.667224815	0.885313658
5	left-middle-finger-fal-1-V15-(h)	0.669311659	0.534785115	0.868623696	0.586578629	0.616625336
6	left-middle-finger-fal-1-V17-(h)	0.674211935	0.448987361	0.918370417	0.586626021	0.51545801
7	left-middle-finger-fal-1-V18-(h)	0.835145754	0.625049577	0.470859638	0.517024272	0.919465922
8	left-middle-finger-fal-1-V19-(h)	0.903525339	0.661330376	0.479958663	0.5839979	1.073311733
9	left-middle-finger-fal-1-V1-(h)	***0.555343238***	0.389894148	0.750081926	0.378313081	0.601960306
10	left-middle-finger-fal-1-V20-(h)	0.759003161	0.911319492	1.373055189	1.083811135	0.63696731
11	left-middle-finger-fal-1-V21-(h)	0.679820783	0.586052486	0.618309645	0.428247412	0.719049912
12	left-middle-finger-fal-1-V25-(h)	0.638249742	0.692788225	1.113707102	0.732154954	0.384569804
13	left-middle-finger-fal-1-V2-(h)	0.731038104	0.492487007	0.625241734	0.517790261	0.765672818
14	left-middle-finger-fal-1-V3-(h)	0.928190851	0.808390026	0.639257382	0.785317949	1.001986477
15	left-middle-finger-fal-1-V4-(h)	0.686760359	0.565622923	0.558611643	0.490021643	0.789773547
16	left-middle-finger-fal-1-V5-(h)	***0.563366457***	0.550345272	0.982758741	0.583068567	0.52391906
17	left-middle-finger-fal-1-V6-(h)	0.814641116	0.765841143	0.623567659	0.708296248	0.880616863
18	left-middle-finger-fal-1-V7-(h)	0.731377797	0.61294673	0.528221054	0.548768267	0.810562526
19	left-middle-finger-fal-1-V9-(h)	0.695619535	0.494068978	0.517707162	0.407521626	0.88464759
20	left-middle-finger-fal-1-VE35-(h)	1.257093554	0.862417397	0.753912584	0.880846286	1.396928074
21	left-middle-finger-fal-1-VF561-2014-(h)	1.099801183	0.76988274	0.712637486	0.759037044	1.159565271
22	left-middle-finger-fal-1-VF772-2015-(h)	0.895070344	0.580339391	0.719620266	0.60842537	1.068722975

Original Sheet | Formatted | True Matches in Red | Selected

Now, to use this macro, press the CTRL key and the ‘w’ key at the same time. This should select the three lowest values for the next column:

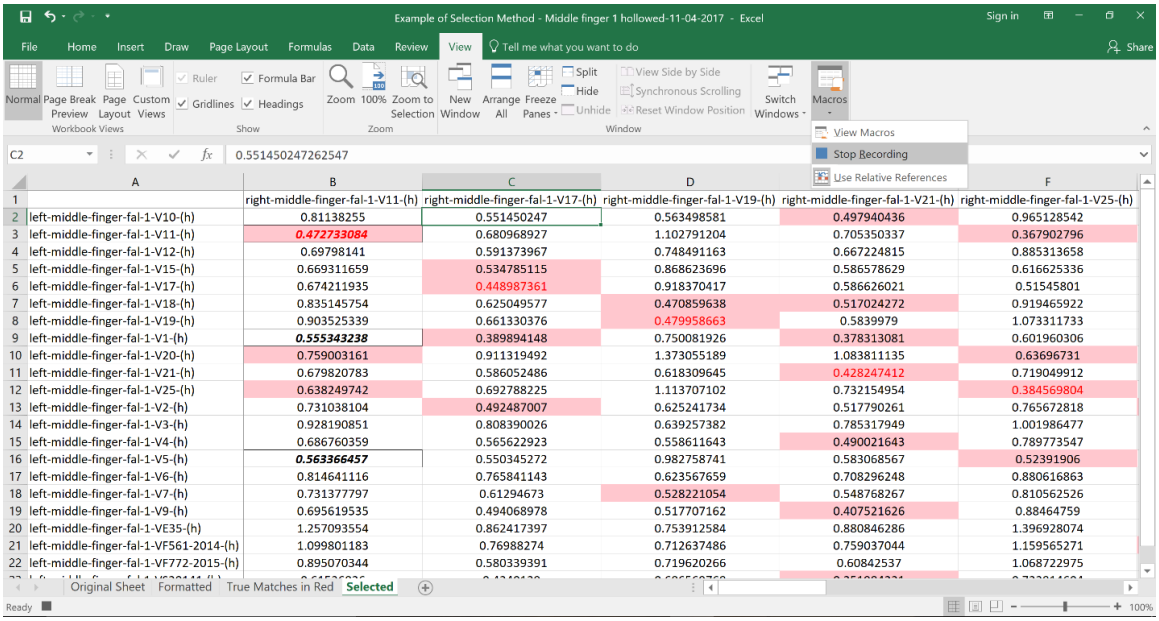

	A	B	C	D	E	F
1		right-middle-finger-fal-1-V11-(h)	right-middle-finger-fal-1-V17-(h)	right-middle-finger-fal-1-V19-(h)	right-middle-finger-fal-1-V21-(h)	right-middle-finger-fal-1-V25-(h)
2	left-middle-finger-fal-1-V10-(h)	0.81138255	0.551450247	0.563498581	0.497940436	0.965128542
3	left-middle-finger-fal-1-V11-(h)	***0.472733084***	0.680968927	1.102791204	0.705350337	0.367902796
4	left-middle-finger-fal-1-V12-(h)	0.69798141	0.591373967	0.748491163	0.667224815	0.885313658
5	left-middle-finger-fal-1-V15-(h)	0.669311659	0.534785115	0.868623696	0.586578629	0.616625336
6	left-middle-finger-fal-1-V17-(h)	0.674211935	0.448987361	0.918370417	0.586626021	0.51545801
7	left-middle-finger-fal-1-V18-(h)	0.835145754	0.625049577	0.470859638	0.517024272	0.919465922
8	left-middle-finger-fal-1-V19-(h)	0.903525339	0.661330376	0.479958663	0.5839979	1.073311733
9	left-middle-finger-fal-1-V1-(h)	***0.555343238***	0.389894148	0.750081926	0.378313081	0.601960306
10	left-middle-finger-fal-1-V20-(h)	0.759003161	0.911319492	1.373055189	1.083811135	0.63696731
11	left-middle-finger-fal-1-V21-(h)	0.679820783	0.586052486	0.618309645	0.428247412	0.719049912
12	left-middle-finger-fal-1-V25-(h)	0.638249742	0.692788225	1.113707102	0.732154954	0.384569804
13	left-middle-finger-fal-1-V2-(h)	0.731038104	0.492487007	0.625241734	0.517790261	0.765672818
14	left-middle-finger-fal-1-V3-(h)	0.928190851	0.808390026	0.639257382	0.785317949	1.001986477
15	left-middle-finger-fal-1-V4-(h)	0.686760359	0.565622923	0.558611643	0.490021643	0.789773547
16	left-middle-finger-fal-1-V5-(h)	***0.563366457***	0.550345272	0.982758741	0.583068567	0.52391906
17	left-middle-finger-fal-1-V6-(h)	0.814641116	0.765841143	0.623567659	0.708296248	0.880616863
18	left-middle-finger-fal-1-V7-(h)	0.731377797	0.61294673	0.528221054	0.548768267	0.810562526
19	left-middle-finger-fal-1-V9-(h)	0.695619535	0.494068978	0.517707162	0.407521626	0.88464759
20	left-middle-finger-fal-1-VE35-(h)	1.257093554	0.862417397	0.753912584	0.880846286	1.396928074
21	left-middle-finger-fal-1-VF561-2014-(h)	1.099801183	0.76988274	0.712637486	0.759037044	1.159565271
22	left-middle-finger-fal-1-VF772-2015-(h)	0.895070344	0.580339391	0.719620266	0.60842537	1.068722975

Original Sheet | Formatted | True Matches in Red | Selected

Keep pressing this combination (CTRL + w) until all the columns (rights, down) have had their lowest values selected:

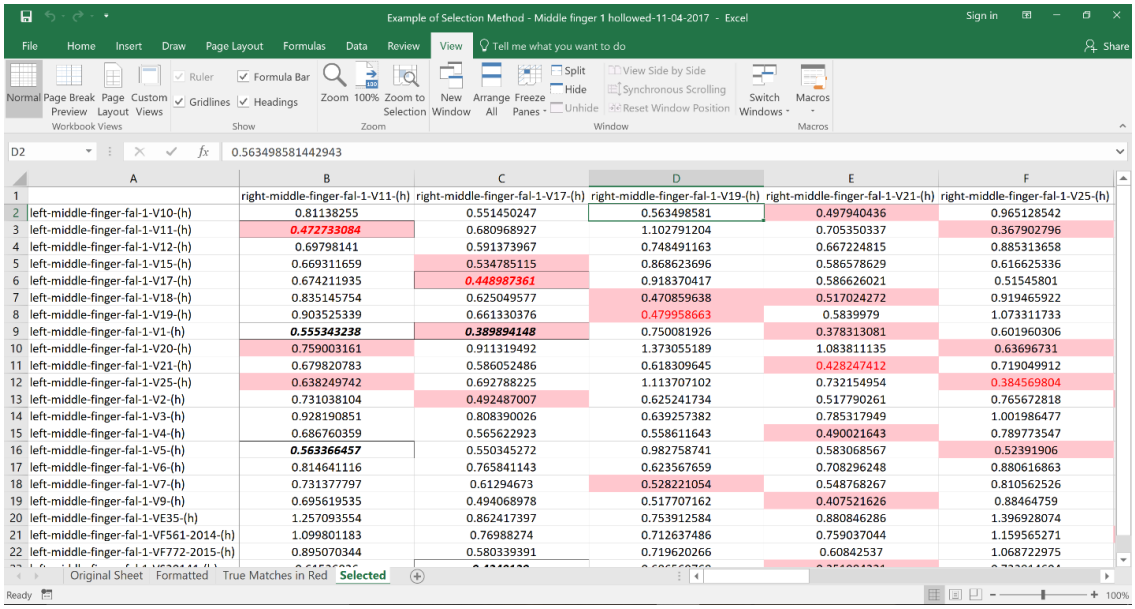

	A	B	C	D	E	F
1		right-middle-finger-fal-1-V11-(h)	right-middle-finger-fal-1-V17-(h)	right-middle-finger-fal-1-V19-(h)	right-middle-finger-fal-1-V21-(h)	right-middle-finger-fal-1-V25-(h)
2	left-middle-finger-fal-1-V10-(h)	0.81138255	0.551450247	0.563498581	0.497940436	0.965128542
3	left-middle-finger-fal-1-V11-(h)	***0.472733084***	0.680968927	1.102791204	0.705350337	0.367902796
4	left-middle-finger-fal-1-V12-(h)	0.69798141	0.591373967	0.748491163	0.667224815	0.885313658
5	left-middle-finger-fal-1-V15-(h)	0.669311659	0.534785115	0.868623696	0.586578629	0.616625336
6	left-middle-finger-fal-1-V17-(h)	0.674211935	***0.448987361***	0.918370417	0.586626021	0.51545801
7	left-middle-finger-fal-1-V18-(h)	0.835145754	0.625049577	0.470859638	0.517024272	0.919465922
8	left-middle-finger-fal-1-V19-(h)	0.903525339	0.661330376	0.479958663	0.5839979	1.073311733
9	left-middle-finger-fal-1-V1-(h)	***0.555343238***	***0.389894148***	0.750081926	0.378313081	0.601960306
10	left-middle-finger-fal-1-V20-(h)	0.759003161	0.911319492	1.373055189	1.083811135	0.63696731
11	left-middle-finger-fal-1-V21-(h)	0.679820783	0.586052486	0.618309645	0.428247412	0.719049912
12	left-middle-finger-fal-1-V25-(h)	0.638249742	0.692788225	1.113707102	0.732154954	0.384569804
13	left-middle-finger-fal-1-V2-(h)	0.731038104	0.492487007	0.625241734	0.517790261	0.765672818
14	left-middle-finger-fal-1-V3-(h)	0.928190851	0.808390026	0.639257382	0.785317949	1.001986477
15	left-middle-finger-fal-1-V4-(h)	0.686760359	0.565622923	0.558611643	0.490021643	0.789773547
16	left-middle-finger-fal-1-V5-(h)	***0.563366457***	0.550345272	0.982758741	0.583068567	0.52391906
17	left-middle-finger-fal-1-V6-(h)	0.814641116	0.765841143	0.623567659	0.708296248	0.880616863
18	left-middle-finger-fal-1-V7-(h)	0.731377797	0.61294673	0.528221054	0.548768267	0.810562526
19	left-middle-finger-fal-1-V9-(h)	0.695619535	0.494068978	0.517707162	0.407521626	0.88464759
20	left-middle-finger-fal-1-VE35-(h)	1.257093554	0.862417397	0.753912584	0.880846286	1.396928074
21	left-middle-finger-fal-1-VF561-2014-(h)	1.099801183	0.76988274	0.712637486	0.759037044	1.159565271
22	left-middle-finger-fal-1-VF772-2015-(h)	0.895070344	0.580339391	0.719620266	0.60842537	1.068722975

Now, duplicate this sheet in the same manner as before:
To do this, ‘Right Click’ on the tab to duplicate and select the ‘Move or Copy’ option:

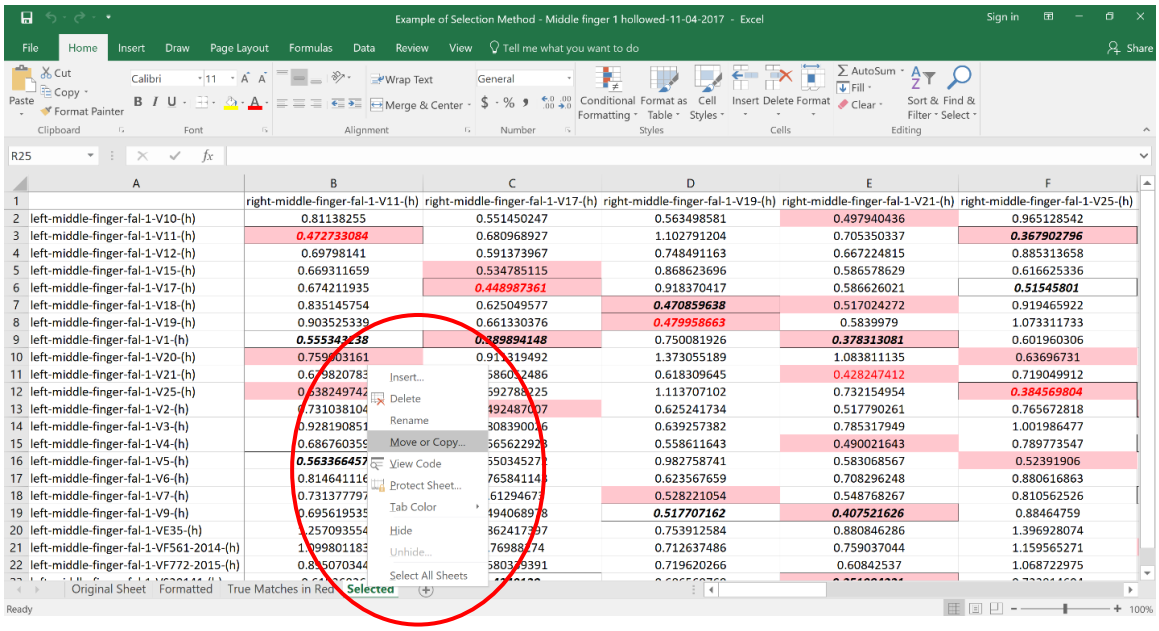

	A	B	C	D	E	F
1		right-middle-finger-fal-1-V11-(h)	right-middle-finger-fal-1-V17-(h)	right-middle-finger-fal-1-V19-(h)	right-middle-finger-fal-1-V21-(h)	right-middle-finger-fal-1-V25-(h)
2	left-middle-finger-fal-1-V10-(h)	0.81138255	0.551450247	0.563498581	0.497940436	0.965128542
3	left-middle-finger-fal-1-V11-(h)	***0.472733084***	0.680968927	1.102791204	0.705350337	***0.367902796***
4	left-middle-finger-fal-1-V12-(h)	0.69798141	0.591373967	0.748491163	0.667224815	0.885313658
5	left-middle-finger-fal-1-V15-(h)	0.669311659	0.534785115	0.868623696	0.586578629	0.616625336
6	left-middle-finger-fal-1-V17-(h)	0.674211935	***0.448987361***	0.918370417	0.586626021	***0.51545801***
7	left-middle-finger-fal-1-V18-(h)	0.835145754	0.625049577	***0.470859638***	0.517024272	0.919465922
8	left-middle-finger-fal-1-V19-(h)	0.903525339	0.661330376	***0.479958663***	0.5839979	1.073311733
9	left-middle-finger-fal-1-V1-(h)	***0.555343238***	***0.389894148***	0.750081926	***0.378313081***	0.601960306
10	left-middle-finger-fal-1-V20-(h)	0.759003161	0.911319492	1.373055189	1.083811135	0.63696731
11	left-middle-finger-fal-1-V21-(h)	0.679820783	0.586052486	0.618309645	0.428247412	0.719049912
12	left-middle-finger-fal-1-V25-(h)	0.638249742	0.692788225	1.113707102	0.732154954	***0.384569804***
13	left-middle-finger-fal-1-V2-(h)	0.731038104	0.492487007	0.625241734	0.517790261	0.765672818
14	left-middle-finger-fal-1-V3-(h)	0.928190851	0.808390026	0.639257382	0.785317949	1.001986477
15	left-middle-finger-fal-1-V4-(h)	0.686760359	0.565622923	0.558611643	0.490021643	0.789773547
16	left-middle-finger-fal-1-V5-(h)	***0.563366457***	0.550345272	0.982758741	0.583068567	0.52391906
17	left-middle-finger-fal-1-V6-(h)	0.814641116	0.765841143	0.623567659	0.708296248	0.880616863
18	left-middle-finger-fal-1-V7-(h)	0.731377797	0.61294673	0.528221054	0.548768267	0.810562526
19	left-middle-finger-fal-1-V9-(h)	0.695619535	0.494068978	***0.517707162***	***0.407521626***	0.88464759
20	left-middle-finger-fal-1-VE35-(h)	1.257093554	0.862417397	0.753912584	0.880846286	1.396928074
21	left-middle-finger-fal-1-VF561-2014-(h)	1.099801183	0.76988274	0.712637486	0.759037044	1.159565271
22	left-middle-finger-fal-1-VF772-2015-(h)	0.895070344	0.580339391	0.719620266	0.60842537	1.068722975

In the Move or Copy box, tick the ‘Create a copy’ box and highlight the ‘(move to end)’ and then click ‘Okay’

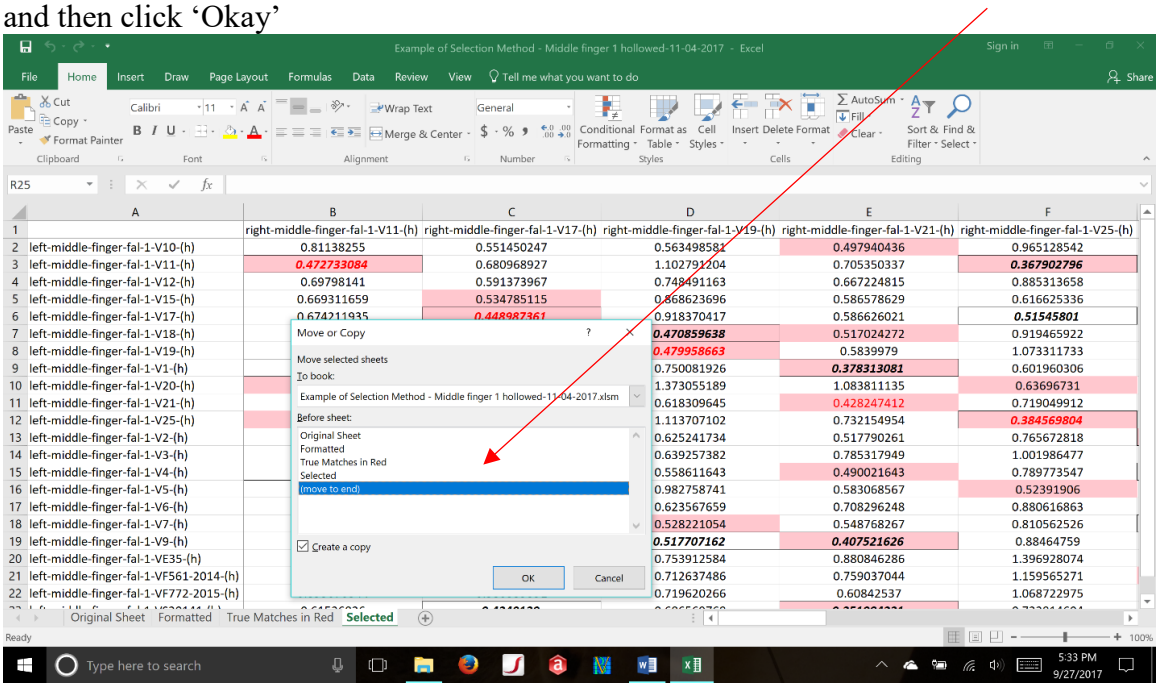

6) Now the lowest <u>agreed-upon</u> values need to be identified and highlighted.
This will ultimately result in one value for each ‘pair’ or no value at all for a non-match, instead of multiple possibilities at the end of the process.

So, take the previously duplicated sheet and rename it ‘Highlighted’ by Right-Clicking on the tab name:

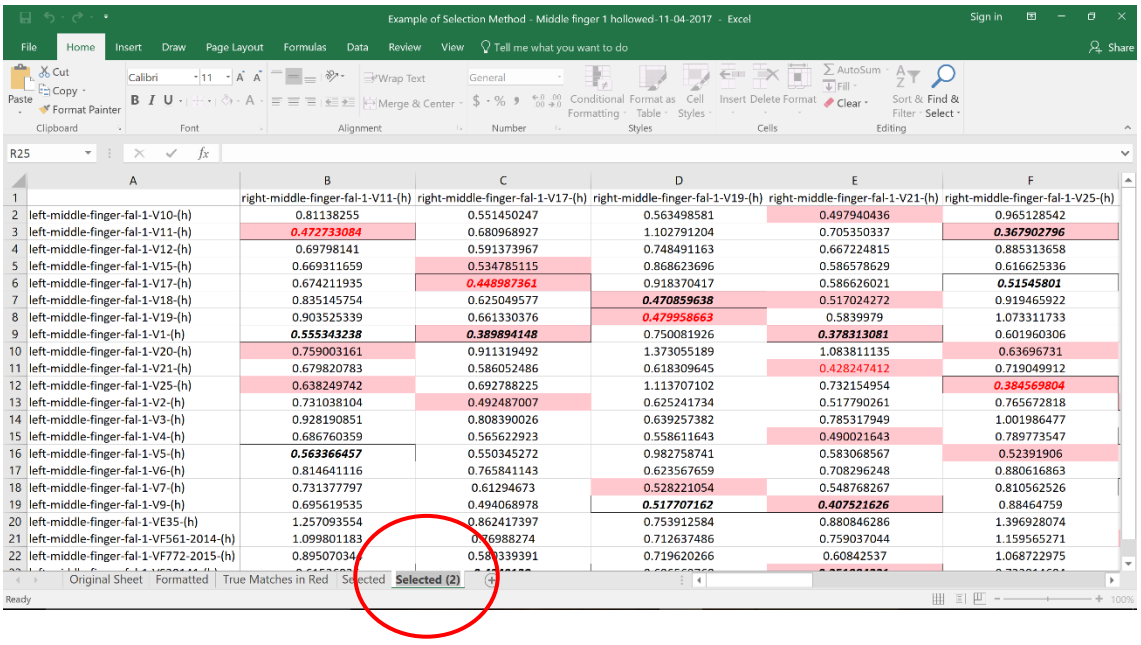

	right-middle-finger-fal-1-V11-(h)	right-middle-finger-fal-1-V17-(h)	right-middle-finger-fal-1-V19-(h)	right-middle-finger-fal-1-V21-(h)	right-middle-finger-fal-1-V25-(h)
left-middle-finger-fal-1-V10-(h)	0.81138255	0.551450247	0.563498581	0.497940436	0.965128542
left-middle-finger-fal-1-V11-(h)	***0.472733084***	0.680968927	1.102791204	0.705350337	***0.367902796***
left-middle-finger-fal-1-V12-(h)	0.69798141	0.591373967	0.748491163	0.667224815	0.885313658
left-middle-finger-fal-1-V15-(h)	0.669311659	0.534785115	0.868623696	0.586578629	0.616625336
left-middle-finger-fal-1-V17-(h)	0.674211935	***0.448987361***	0.918370417	0.586626021	***0.51545801***
left-middle-finger-fal-1-V18-(h)	0.835145754	0.625049577	***0.470859638***	0.517024272	0.919465922
left-middle-finger-fal-1-V19-(h)	0.903525339	0.661330376	***0.479958663***	0.5839979	1.073311733
left-middle-finger-fal-1-V1-(h)	***0.555343238***	***0.389894148***	0.750081926	***0.378313081***	0.601960306
left-middle-finger-fal-1-V20-(h)	0.759003161	0.911319492	1.373055189	1.083811135	0.63696731
left-middle-finger-fal-1-V21-(h)	0.679820783	0.586052486	0.618309645	0.428247412	0.719049912
left-middle-finger-fal-1-V25-(h)	0.638249742	0.692788225	1.113707102	0.732154954	***0.384569804***
left-middle-finger-fal-1-V2-(h)	0.731038104	0.492487007	0.625241734	0.517790261	0.765672818
left-middle-finger-fal-1-V3-(h)	0.928190851	0.808390026	0.639257382	0.785317949	1.001986477
left-middle-finger-fal-1-V4-(h)	0.686760359	0.565622923	0.558611643	0.490021643	0.789773547
left-middle-finger-fal-1-V5-(h)	***0.563366457***	0.550345272	0.982758741	0.583068567	0.52391906
left-middle-finger-fal-1-V6-(h)	0.814641116	0.765841143	0.623567659	0.708296248	0.880616863
left-middle-finger-fal-1-V7-(h)	0.731377797	0.61294673	0.528221054	0.548768267	0.810562526
left-middle-finger-fal-1-V9-(h)	0.695619535	0.494068978	***0.517707162***	***0.407521626***	0.88464759
left-middle-finger-fal-1-VE35-(h)	1.257093554	0.862417397	0.753912584	0.880846286	1.396928074
left-middle-finger-fal-1-VF561-2014-(h)	1.099801183	0.76988274	0.712637486	0.759037044	1.159565271
left-middle-finger-fal-1-VF772-2015-(h)	0.895070341	0.580339391	0.719620266	0.60842537	1.068722975

And writing ‘Highlighted’ in its space:

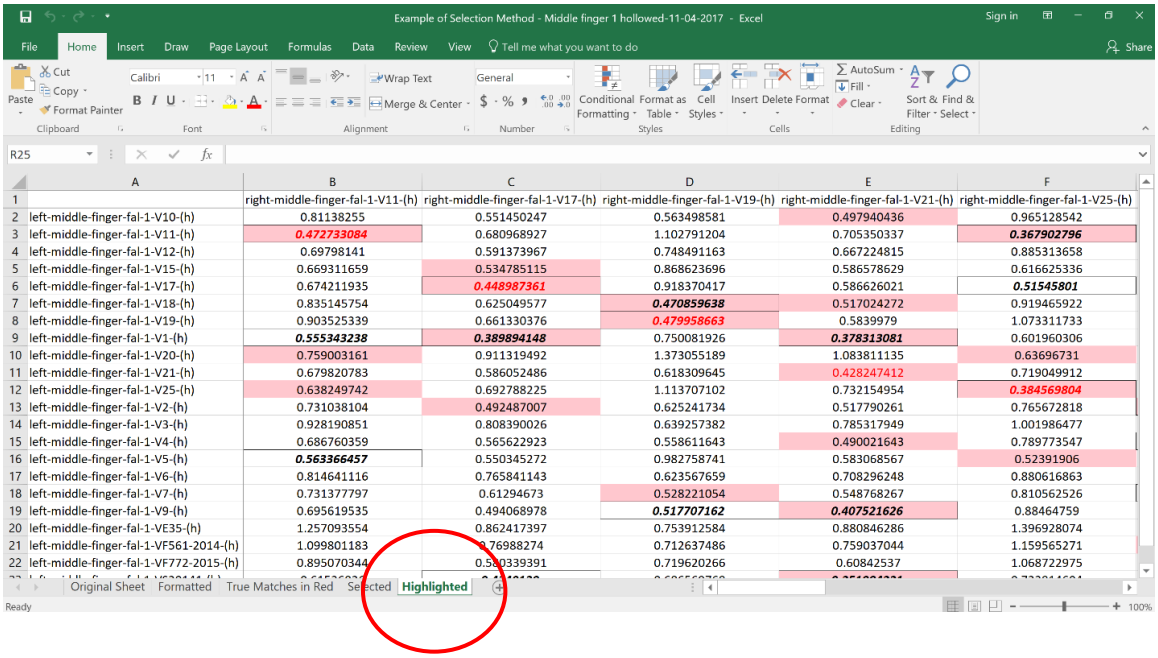

	A	B	C	D	E	F
1		right-middle-finger-fal-1-V11-(h)	right-middle-finger-fal-1-V17-(h)	right-middle-finger-fal-1-V19-(h)	right-middle-finger-fal-1-V21-(h)	right-middle-finger-fal-1-V25-(h)
2	left-middle-finger-fal-1-V10-(h)	0.81138255	0.551450247	0.563498581	0.497940436	0.965128542
3	left-middle-finger-fal-1-V11-(h)	***0.472733084***	0.680968927	1.102791204	0.705350337	***0.367902796***
4	left-middle-finger-fal-1-V12-(h)	0.69798141	0.591373967	0.748491163	0.667224815	0.885313658
5	left-middle-finger-fal-1-V15-(h)	0.669311659	0.534785115	0.868623696	0.586578629	0.616625336
6	left-middle-finger-fal-1-V17-(h)	0.674211935	***0.448987361***	0.918370417	0.586626021	***0.51545801***
7	left-middle-finger-fal-1-V18-(h)	0.835145754	0.625049577	***0.470859638***	0.517024272	0.919465922
8	left-middle-finger-fal-1-V19-(h)	0.903525339	0.661330376	***0.479958663***	0.5839979	1.073311733
9	left-middle-finger-fal-1-V1-(h)	***0.555343238***	***0.389894148***	0.750081926	***0.378313081***	0.601960306
10	left-middle-finger-fal-1-V20-(h)	0.759003161	0.911319492	1.373055189	1.083811135	0.63696731
11	left-middle-finger-fal-1-V21-(h)	0.679820783	0.586052486	0.618309645	0.428247412	0.719049912
12	left-middle-finger-fal-1-V25-(h)	0.638249742	0.692788225	1.113707102	0.732154954	***0.384569804***
13	left-middle-finger-fal-1-V2-(h)	0.731038104	0.492487007	0.625241734	0.517790261	0.765672818
14	left-middle-finger-fal-1-V3-(h)	0.928190851	0.808390026	0.639257382	0.785317949	1.001986477
15	left-middle-finger-fal-1-V4-(h)	0.686760359	0.565622923	0.558611643	0.490021643	0.789773547
16	left-middle-finger-fal-1-V5-(h)	***0.563366457***	0.550345272	0.982758741	0.583068567	0.52391906
17	left-middle-finger-fal-1-V6-(h)	0.814641116	0.765841143	0.623567659	0.708296248	0.880616863
18	left-middle-finger-fal-1-V7-(h)	0.731377797	0.61294673	0.528221054	0.548768267	0.810562526
19	left-middle-finger-fal-1-V9-(h)	0.695619535	0.494068978	***0.517707162***	***0.407521626***	0.88464759
20	left-middle-finger-fal-1-VE35-(h)	1.257093554	0.862417397	0.753912584	0.880846286	1.396928074
21	left-middle-finger-fal-1-VF561-2014-(h)	1.099801183	0.76988274	0.712637486	0.759037044	1.159565271
22	left-middle-finger-fal-1-VF772-2015-(h)	0.895070344	0.580339391	0.719620266	0.60842537	1.068722975

So, now all the ‘agreed-upon’ values should be formatted in the combination of the left (across/row) and the right (down/column) formatting. In other words, the agreed-upon values should have a light red background, black outline of the cell, and bold + italic text (either in black or red) like so:

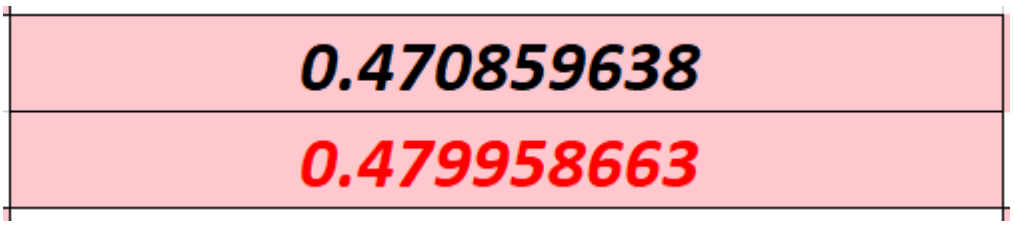

To only have these values present, go through the entire sheet, select *only* the cells with the formatting above and Highlight them in Yellow*:

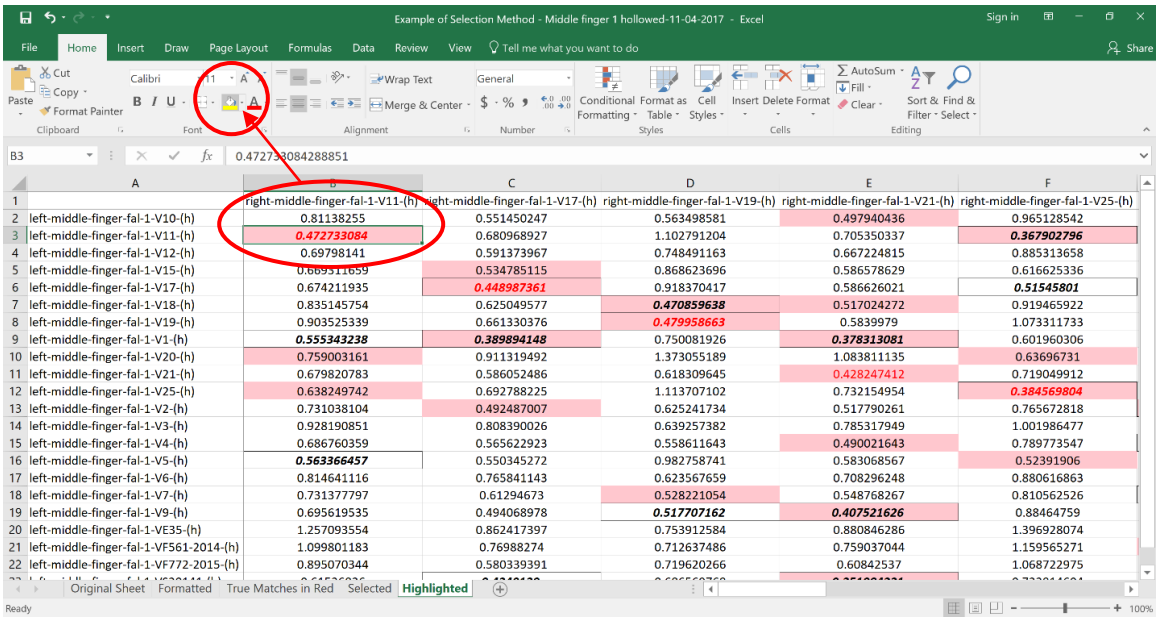

	A	B	C	D	E	F
1		right-middle-finger-fal-1-V11-(h)	right-middle-finger-fal-1-V17-(h)	right-middle-finger-fal-1-V19-(h)	right-middle-finger-fal-1-V21-(h)	right-middle-finger-fal-1-V25-(h)
2	left-middle-finger-fal-1-V10-(h)	0.81138255	0.551450247	0.563498581	0.497940436	0.965128542
3	left-middle-finger-fal-1-V11-(h)	***0.472733084***	0.680968927	1.102791204	0.705350337	***0.367902796***
4	left-middle-finger-fal-1-V12-(h)	0.69798141	0.591373967	0.748491163	0.667224815	0.885313658
5	left-middle-finger-fal-1-V15-(h)	0.689311659	0.534785115	0.868623696	0.586578629	0.616625336
6	left-middle-finger-fal-1-V17-(h)	0.674211935	***0.448987361***	0.918370417	0.586626021	***0.51545801***
7	left-middle-finger-fal-1-V18-(h)	0.835145754	0.625049577	***0.470859638***	0.517024272	0.919465922
8	left-middle-finger-fal-1-V19-(h)	0.903525339	0.661330376	***0.479958663***	0.5839979	1.073311733
9	left-middle-finger-fal-1-V1-(h)	***0.555343238***	***0.389894148***	0.750081926	***0.378313081***	0.601960306
10	left-middle-finger-fal-1-V20-(h)	0.759003161	0.911319492	1.373055189	1.083811135	0.63696731
11	left-middle-finger-fal-1-V21-(h)	0.679820783	0.586052486	0.618309645	0.428247412	0.719049912
12	left-middle-finger-fal-1-V25-(h)	0.638249742	0.692788225	1.113707102	0.732154954	***0.384569804***
13	left-middle-finger-fal-1-V2-(h)	0.731038104	0.492487007	0.625241734	0.517790261	0.765672818
14	left-middle-finger-fal-1-V3-(h)	0.928190851	0.808390026	0.639257382	0.785317949	1.001986477
15	left-middle-finger-fal-1-V4-(h)	0.686760359	0.565622923	0.558611643	0.490021643	0.789773547
16	left-middle-finger-fal-1-V5-(h)	***0.563366457***	0.550345272	0.982758741	0.583068567	0.52391906
17	left-middle-finger-fal-1-V6-(h)	0.814641116	0.765841143	0.623567659	0.708296248	0.880616863
18	left-middle-finger-fal-1-V7-(h)	0.731377797	0.61294673	0.528221054	0.548768267	0.810562526
19	left-middle-finger-fal-1-V9-(h)	0.695619535	0.494068978	***0.517707162***	***0.407521626***	0.88464759
20	left-middle-finger-fal-1-VE35-(h)	1.257093554	0.862417397	0.753912584	0.880846286	1.396928074
21	left-middle-finger-fal-1-VF561-2014-(h)	1.099801183	0.76988274	0.712637486	0.759037044	1.159565271
22	left-middle-finger-fal-1-VF772-2015-(h)	0.895070344	0.580339391	0.719620266	0.60842537	1.068722975

*Nothing will appear to happen when you press the highlight button, but that is okay
** I suggest going methodically through the Excel sheet column by column to make sure you select every cell correctly

Now, duplicate this sheet in the same manner as before:
To do this, 'Right Click' on the tab to duplicate and select the 'Move or Copy' option:

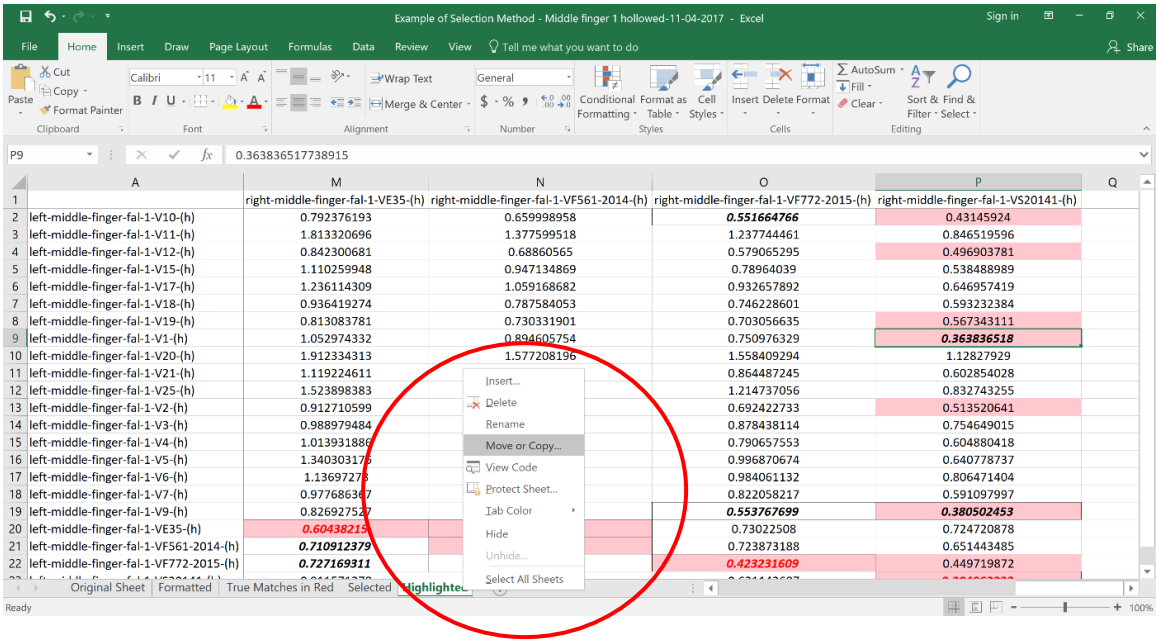

	A	M	N	O	P	Q
1		right-middle-finger-fal-1-VE35-(h)	right-middle-finger-fal-1-VF561-2014-(h)	right-middle-finger-fal-1-VF772-2015-(h)	right-middle-finger-fal-1-VS20141-(h)	
2	left-middle-finger-fal-1-V10-(h)	0.792376193	0.659998958	***0.551664766***	0.43145924	
3	left-middle-finger-fal-1-V11-(h)	1.813320696	1.377599518	1.237744461	0.846519596	
4	left-middle-finger-fal-1-V12-(h)	0.842300681	0.68860565	0.579065295	0.496903781	
5	left-middle-finger-fal-1-V15-(h)	1.110259948	0.947134869	0.78964039	0.538488989	
6	left-middle-finger-fal-1-V17-(h)	1.236114309	1.059168682	0.932657892	0.646957419	
7	left-middle-finger-fal-1-V18-(h)	0.936419274	0.787584053	0.746228601	0.593232384	
8	left-middle-finger-fal-1-V19-(h)	0.813083781	0.730331901	0.703056635	0.567343111	
9	left-middle-finger-fal-1-V1-(h)	1.052974332	0.894605754	0.750976329	***0.363836518***	
10	left-middle-finger-fal-1-V20-(h)	1.912334313	1.577208196	1.558409294	1.12827929	
11	left-middle-finger-fal-1-V21-(h)	1.119224611		0.864487245	0.602854028	
12	left-middle-finger-fal-1-V25-(h)	1.523898383		1.214737056	0.832743255	
13	left-middle-finger-fal-1-V2-(h)	0.912710599		0.692422733	0.513520641	
14	left-middle-finger-fal-1-V3-(h)	0.988979484		0.878438114	0.754649015	
15	left-middle-finger-fal-1-V4-(h)	1.013931886		0.790657553	0.604880418	
16	left-middle-finger-fal-1-V5-(h)	1.340303175		0.996870674	0.640778737	
17	left-middle-finger-fal-1-V6-(h)	1.13697278		0.984061132	0.806471404	
18	left-middle-finger-fal-1-V7-(h)	0.977686367		0.822058217	0.591097997	
19	left-middle-finger-fal-1-V9-(h)	0.826927527		***0.553767699***	***0.380502453***	
20	left-middle-finger-fal-1-VE35-(h)	***0.604382215***		0.73022508	0.724720878	
21	left-middle-finger-fal-1-VF561-2014-(h)	***0.710912379***		0.723873188	0.651443485	
22	left-middle-finger-fal-1-VF772-2015-(h)	***0.727169311***		***0.423231609***	0.449719872	

In the Move or Copy box, tick the ‘Create a copy’ box and highlight the ‘(move to end)’ and then click ‘Okay’

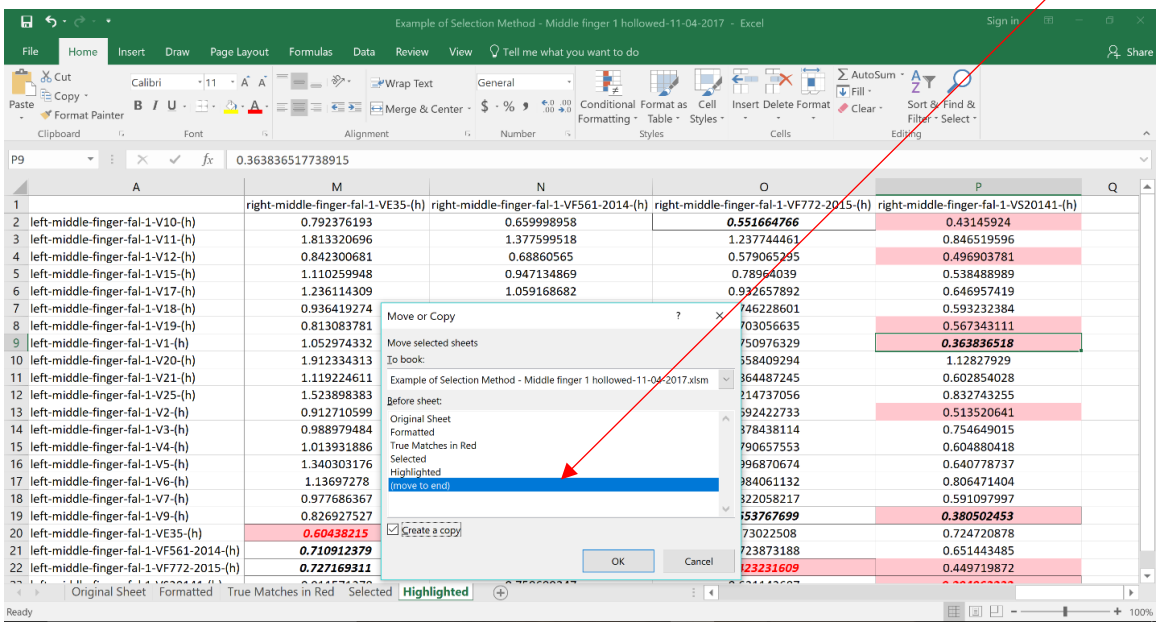

So, take the previously duplicated sheet and rename it ‘Deleted’ by Right-Clicking on the tab name:

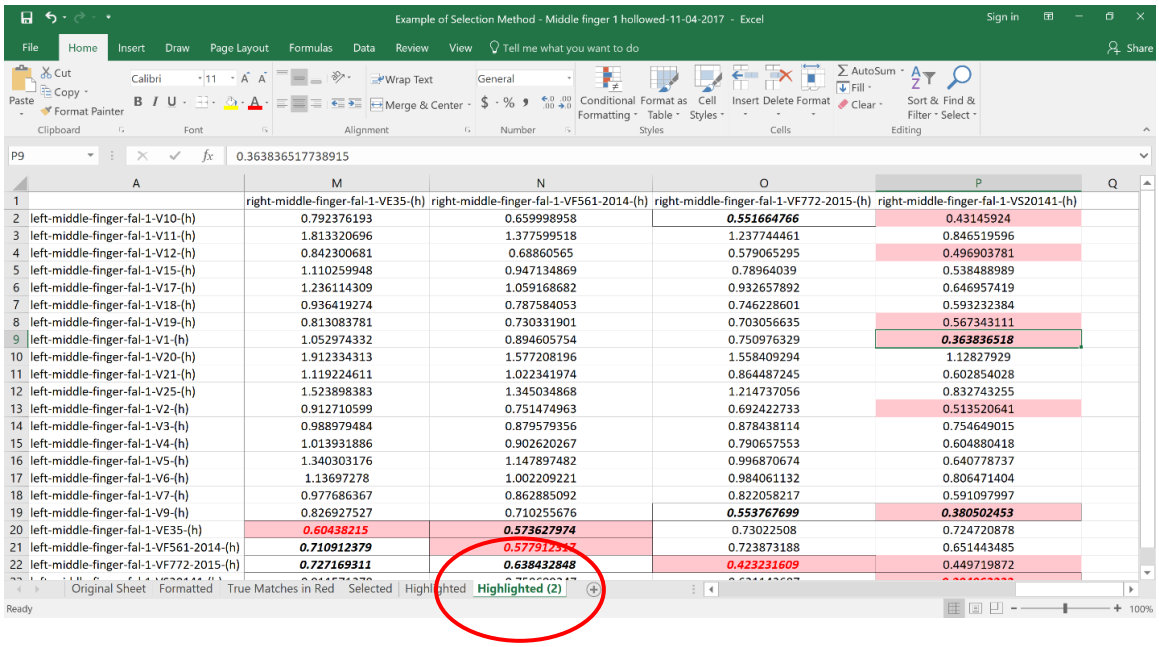

And writing ‘Deleted’ in its space:

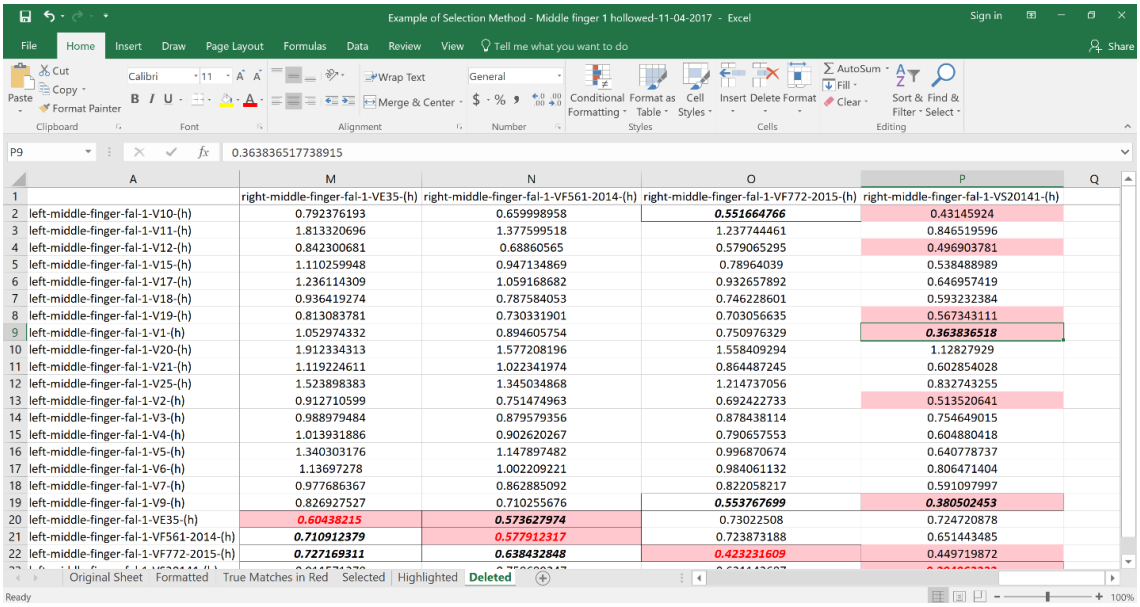

	A	M	N	O	P	Q
1		right-middle-finger-fal-1-VE35-(h)	right-middle-finger-fal-1-VF561-2014-(h)	right-middle-finger-fal-1-VF772-2015-(h)	right-middle-finger-fal-1-VS20141-(h)	
2	left-middle-finger-fal-1-V10-(h)	0.792376193	0.659998958	***0.551664766***	0.43145924	
3	left-middle-finger-fal-1-V11-(h)	1.813320696	1.377599518	1.237744461	0.846519596	
4	left-middle-finger-fal-1-V12-(h)	0.842300681	0.68860565	0.579065295	0.496903781	
5	left-middle-finger-fal-1-V15-(h)	1.110259948	0.947134869	0.78964039	0.538488989	
6	left-middle-finger-fal-1-V17-(h)	1.236114309	1.059168682	0.932657892	0.646957419	
7	left-middle-finger-fal-1-V18-(h)	0.936419274	0.787584053	0.746228601	0.593232384	
8	left-middle-finger-fal-1-V19-(h)	0.813083781	0.730331901	0.703056635	0.567343111	
9	left-middle-finger-fal-1-V1-(h)	1.052974332	0.894605754	0.750976329	***0.363836518***	
10	left-middle-finger-fal-1-V20-(h)	1.912334313	1.577208196	1.558409294	1.12827929	
11	left-middle-finger-fal-1-V21-(h)	1.119224611	1.022341974	0.864487245	0.602854028	
12	left-middle-finger-fal-1-V25-(h)	1.523898383	1.345034868	1.214737056	0.832743255	
13	left-middle-finger-fal-1-V2-(h)	0.912710599	0.751474963	0.692422733	0.513520641	
14	left-middle-finger-fal-1-V3-(h)	0.988979484	0.879579356	0.878438114	0.754649015	
15	left-middle-finger-fal-1-V4-(h)	1.013931886	0.902620267	0.790657553	0.604880418	
16	left-middle-finger-fal-1-V5-(h)	1.340303176	1.147897482	0.996870674	0.640778737	
17	left-middle-finger-fal-1-V6-(h)	1.13697278	1.002209221	0.984061132	0.806471404	
18	left-middle-finger-fal-1-V7-(h)	0.977686367	0.862885092	0.822058217	0.591097997	
19	left-middle-finger-fal-1-V9-(h)	0.826927527	0.710255676	***0.553767699***	***0.380502453***	
20	left-middle-finger-fal-1-VE35-(h)	***0.60438215***	***0.573627974***	0.73022508	0.724720878	
21	left-middle-finger-fal-1-VF561-2014-(h)	***0.710912379***	***0.577912317***	0.723873188	0.651443485	
22	left-middle-finger-fal-1-VF772-2015-(h)	***0.727169311***	***0.638432848***	***0.423231609***	0.449719872	

Now to reveal all the highlighted cells, first select all the cells in the sheet:

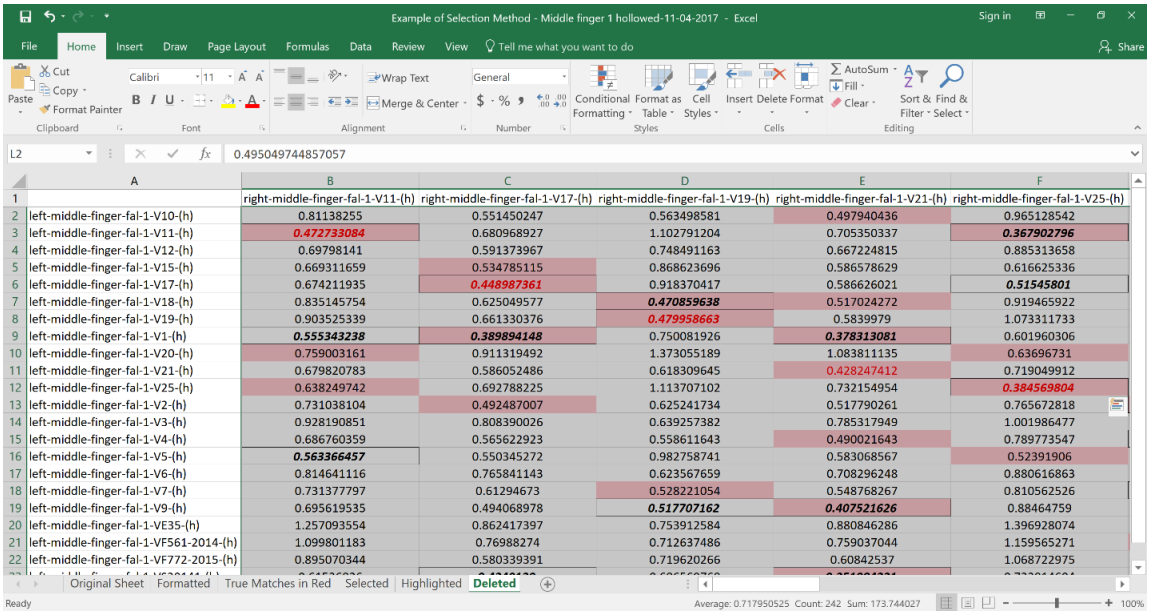

	A	B	C	D	E	F
1		right-middle-finger-fal-1-V11-(h)	right-middle-finger-fal-1-V17-(h)	right-middle-finger-fal-1-V19-(h)	right-middle-finger-fal-1-V21-(h)	right-middle-finger-fal-1-V25-(h)
2	left-middle-finger-fal-1-V10-(h)	0.81138255	0.551450247	0.563498581	0.497940436	0.965128542
3	left-middle-finger-fal-1-V11-(h)	***0.472733084***	0.680968927	1.102791204	0.705350337	***0.367902796***
4	left-middle-finger-fal-1-V12-(h)	0.69798141	0.591373967	0.748491163	0.667224815	0.885313658
5	left-middle-finger-fal-1-V15-(h)	0.669311659	0.534785115	0.868623696	0.586578629	0.616625336
6	left-middle-finger-fal-1-V17-(h)	0.674211935	***0.448987361***	0.918370417	0.586626021	***0.51545801***
7	left-middle-finger-fal-1-V18-(h)	0.835145754	0.625049577	***0.470859638***	0.517024272	0.919465922
8	left-middle-finger-fal-1-V19-(h)	0.903525339	0.661330376	***0.479958663***	0.5839979	1.073311733
9	left-middle-finger-fal-1-V1-(h)	***0.555343238***	***0.389894148***	0.750081926	***0.378313081***	0.601960306
10	left-middle-finger-fal-1-V20-(h)	0.759003161	0.911319492	1.373055189	1.083811135	0.63696731
11	left-middle-finger-fal-1-V21-(h)	0.679820783	0.586052486	0.618309645	0.428247412	0.719049912
12	left-middle-finger-fal-1-V25-(h)	0.638249742	0.692788225	1.113707102	0.732154954	***0.384569804***
13	left-middle-finger-fal-1-V2-(h)	0.731038104	0.492487007	0.625241734	0.517790261	0.765672818
14	left-middle-finger-fal-1-V3-(h)	0.928190851	0.808390026	0.639257382	0.785317949	1.001986477
15	left-middle-finger-fal-1-V4-(h)	0.686760359	0.565622923	0.558611643	0.490021643	0.789773547
16	left-middle-finger-fal-1-V5-(h)	***0.563366457***	0.550345272	0.982758741	0.583068567	0.52391906
17	left-middle-finger-fal-1-V6-(h)	0.814641116	0.765841143	0.623567659	0.708296248	0.880616863
18	left-middle-finger-fal-1-V7-(h)	0.731377797	0.61294673	0.528221054	0.548768267	0.810562526
19	left-middle-finger-fal-1-V9-(h)	0.695619535	0.494068978	***0.517707162***	***0.407521626***	0.88464759
20	left-middle-finger-fal-1-VE35-(h)	1.257093554	0.862417397	0.753912584	0.880846286	1.396928074
21	left-middle-finger-fal-1-VF561-2014-(h)	1.099801183	0.76988274	0.712637486	0.759037044	1.159565271
22	left-middle-finger-fal-1-VF772-2015-(h)	0.895070344	0.580339391	0.719620266	0.60842537	1.068722975

Go to ‘Conditional Formatting > Clear Rules’ and click on ‘Clear Rules from Selected Cells:

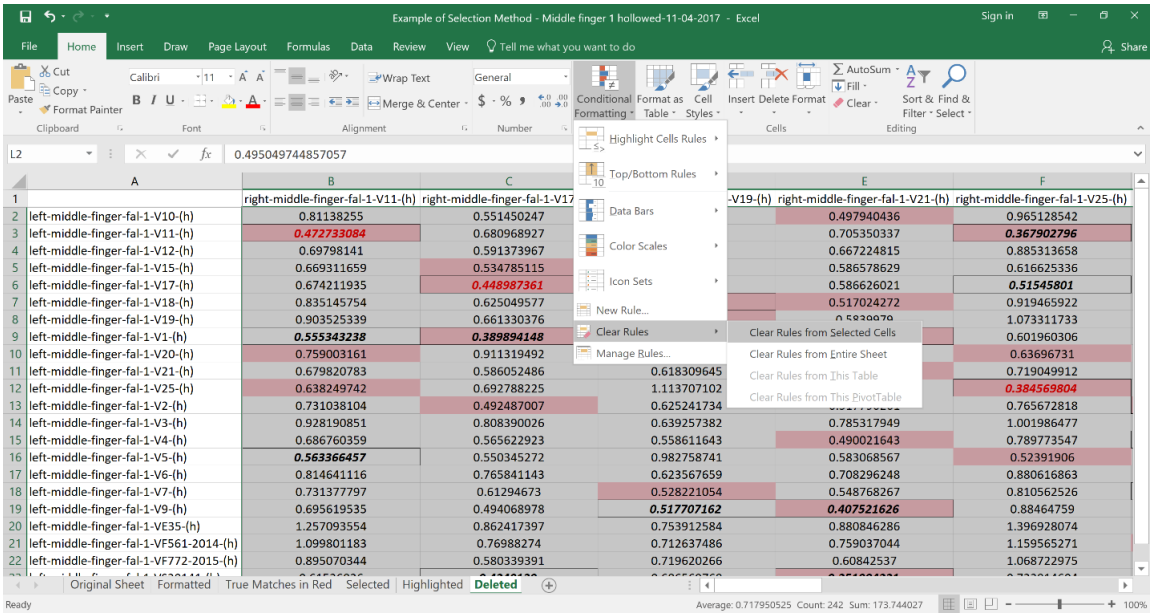

This should reveal the yellow highlighted cells like so:

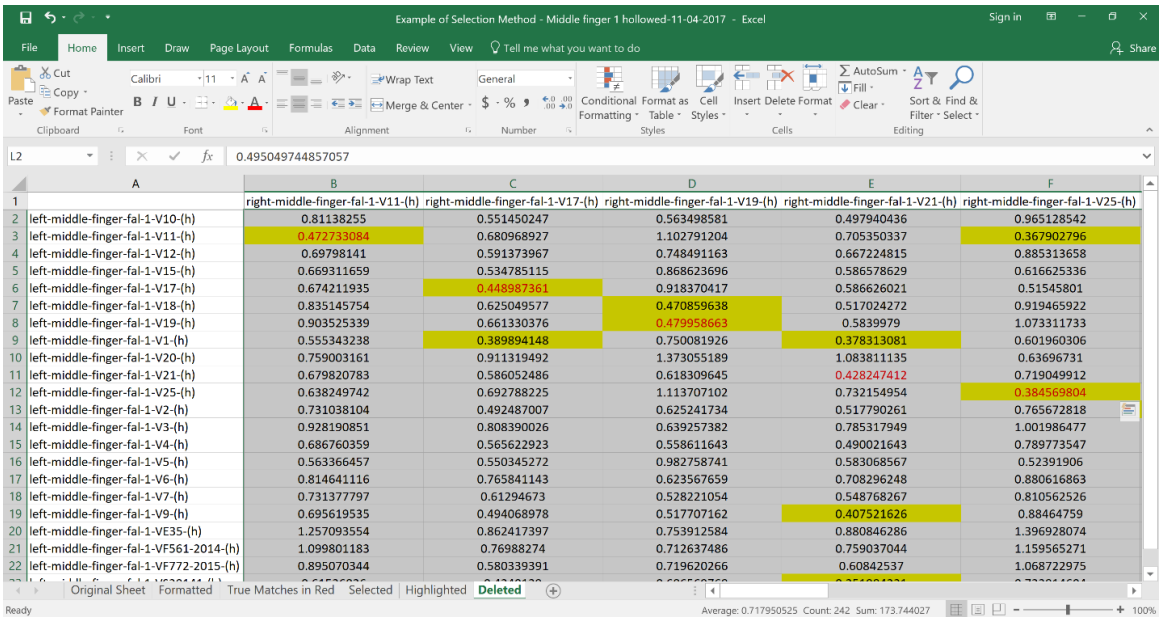

*Note that there should be significantly fewer values highlighted in yellow than there were selected by the across/down macros. This is good.

7) Now to select the *single* agreed-upon lowest value for each pair.

This is very important, and must be done in exactly this way each time, or else the results won't be the same/comparable.

Thus, the first step is going **across** each row (left by left) and deleting all but the lowest value. So start at the first cell, and go to the left, looking for duplicates:

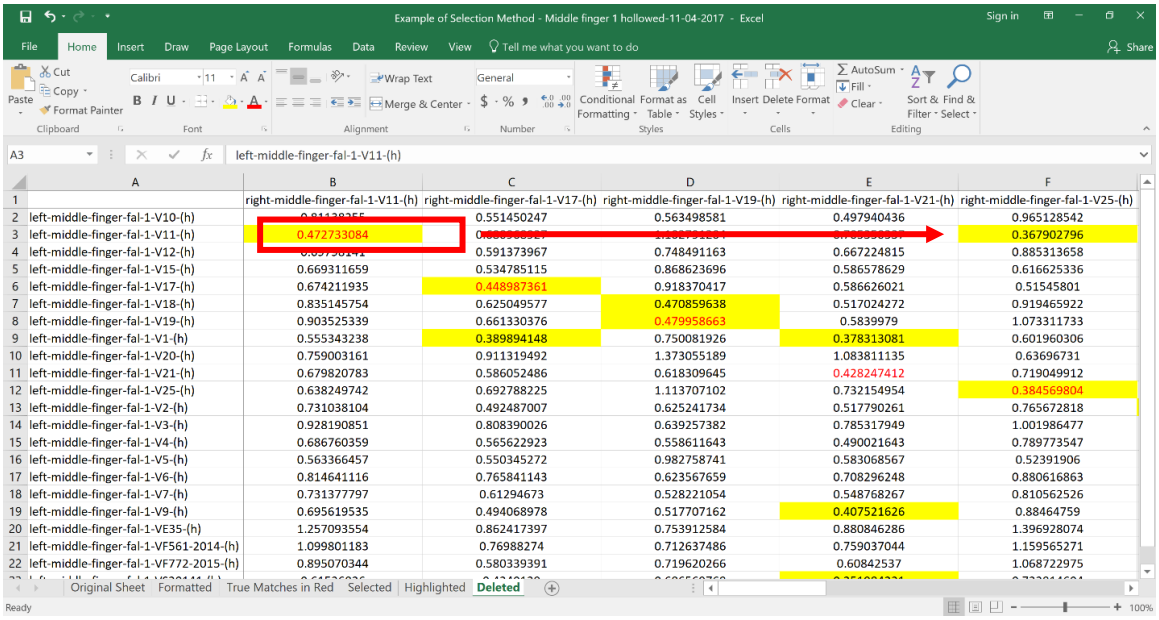

In this case, there are none for the first row, but there are for the second row:

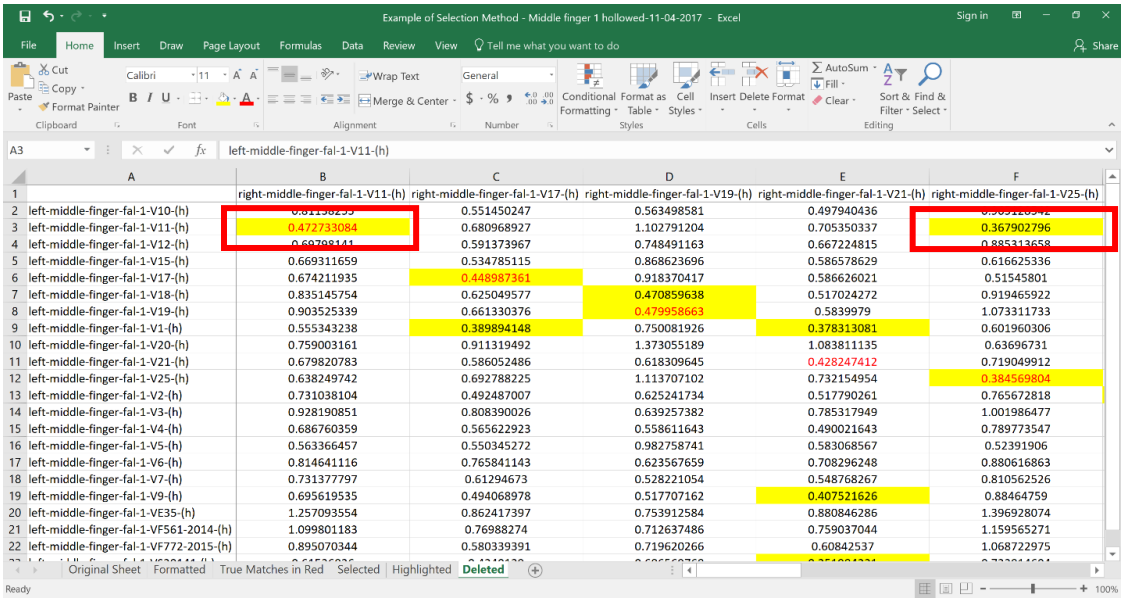

There can only be one final value, so the lowest is kept by un-highlighting the higher value using the ‘No Fill’ feature in the selected cell:

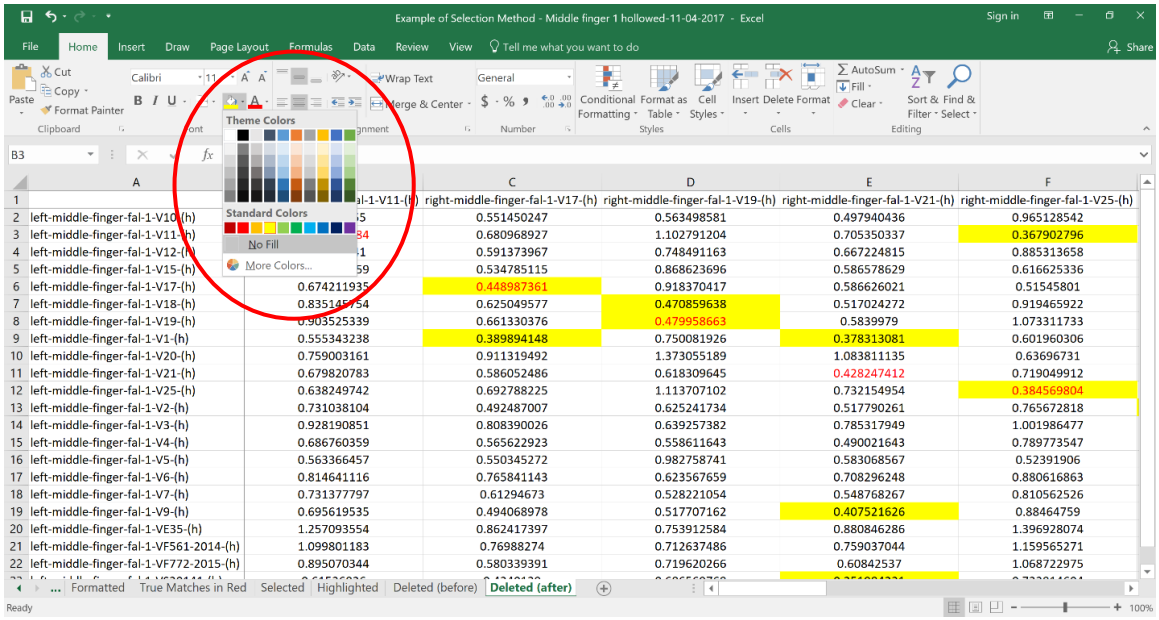

Resulting in:

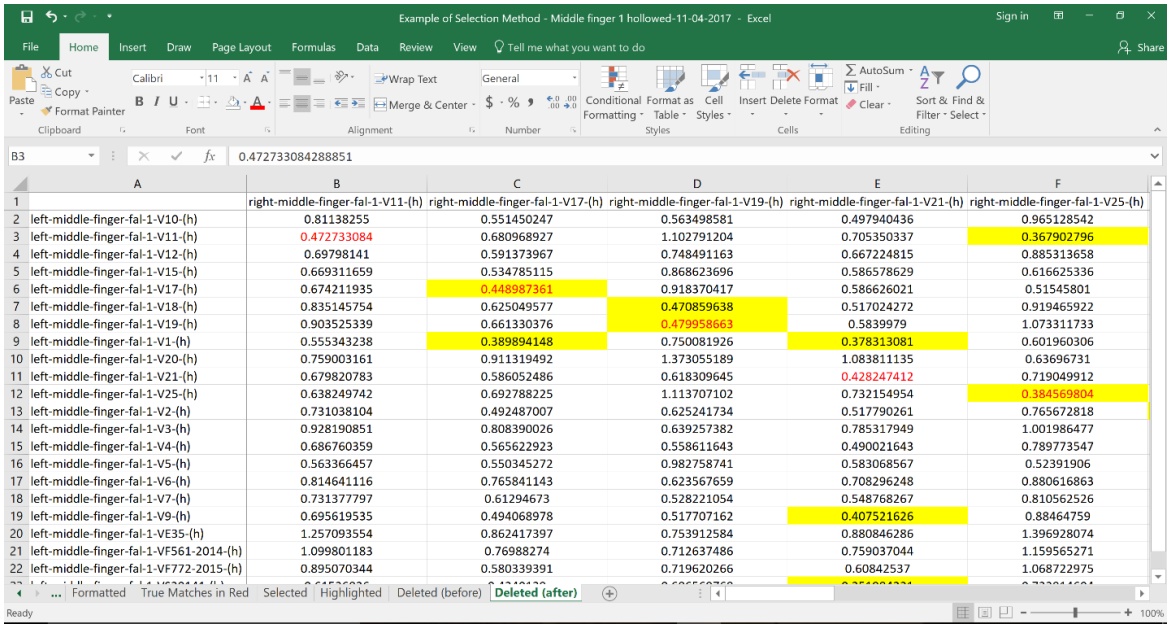

This is done for all the rows:

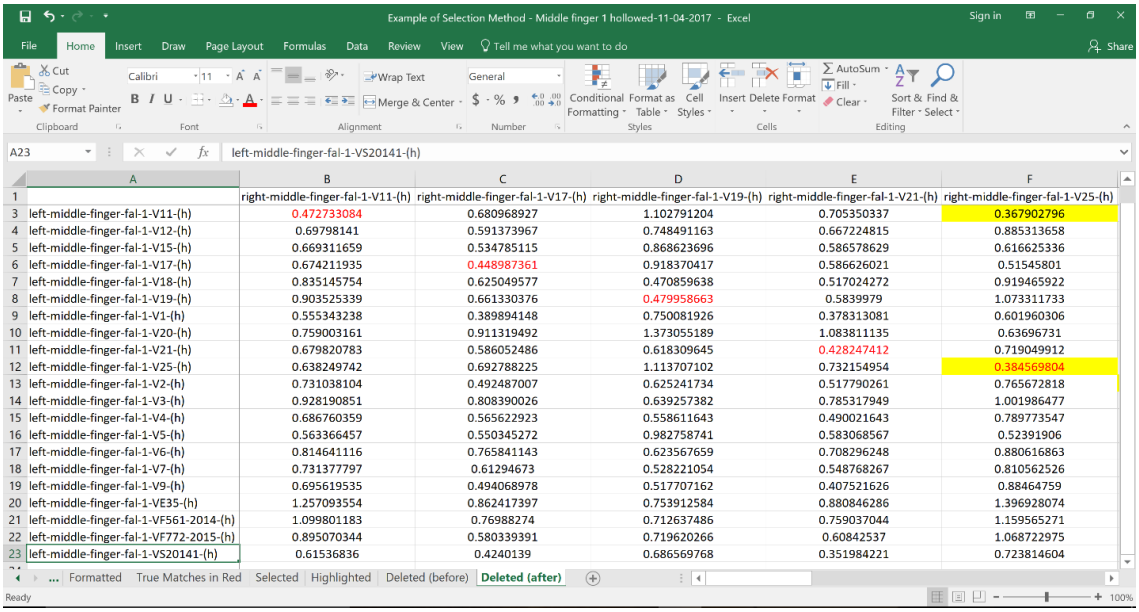

	right-middle-finger-fal-1-V11-(h)	right-middle-finger-fal-1-V17-(h)	right-middle-finger-fal-1-V19-(h)	right-middle-finger-fal-1-V21-(h)	right-middle-finger-fal-1-V25-(h)
left-middle-finger-fal-1-V11-(h)	0.472733084	0.680968927	1.102791204	0.705350337	0.367902796
left-middle-finger-fal-1-V12-(h)	0.69798141	0.591373967	0.748491163	0.667224815	0.885313658
left-middle-finger-fal-1-V15-(h)	0.669311659	0.534785115	0.868623696	0.586578629	0.616625336
left-middle-finger-fal-1-V17-(h)	0.674211935	0.448987361	0.918370417	0.586626021	0.51545801
left-middle-finger-fal-1-V18-(h)	0.835145754	0.625049577	0.470859638	0.517024272	0.919465922
left-middle-finger-fal-1-V19-(h)	0.903525339	0.661330376	0.479958663	0.5839979	1.073311733
left-middle-finger-fal-1-V1-(h)	0.555343238	0.389894148	0.750081926	0.378313081	0.601960306
left-middle-finger-fal-1-V20-(h)	0.759003161	0.911319492	1.373055189	1.083811135	0.63696731
left-middle-finger-fal-1-V21-(h)	0.679820783	0.586052486	0.618309645	0.428247412	0.719049912
left-middle-finger-fal-1-V25-(h)	0.638249742	0.692788225	1.113707102	0.732154954	0.384569804
left-middle-finger-fal-1-V2-(h)	0.731038104	0.492487007	0.625241734	0.517790261	0.765672818
left-middle-finger-fal-1-V3-(h)	0.928190851	0.808390026	0.639257382	0.785317949	1.001986477
left-middle-finger-fal-1-V4-(h)	0.686760359	0.565622923	0.558611643	0.490021643	0.789773547
left-middle-finger-fal-1-V5-(h)	0.563366457	0.550345272	0.982758741	0.583068567	0.52391906
left-middle-finger-fal-1-V6-(h)	0.814641116	0.765841143	0.623567659	0.708296248	0.880616863
left-middle-finger-fal-1-V7-(h)	0.731377797	0.61294673	0.528221054	0.548768267	0.810562526
left-middle-finger-fal-1-V9-(h)	0.695619535	0.494068978	0.517707162	0.407521626	0.88464759
left-middle-finger-fal-1-VE35-(h)	1.257093554	0.862417397	0.753912584	0.880846286	1.396928074
left-middle-finger-fal-1-VF561-2014-(h)	1.099801183	0.76988274	0.712637486	0.759037044	1.159565271
left-middle-finger-fal-1-VF772-2015-(h)	0.895070344	0.580339391	0.719620266	0.60842537	1.068722975
left-middle-finger-fal-1-VS20141-(h)	0.61536836	0.4240139	0.686569768	0.351984221	0.723814604

The second step is going **down** each column (right by right) and deleting all but the lowest value. So start at the first cell, and go down, looking for duplicates:

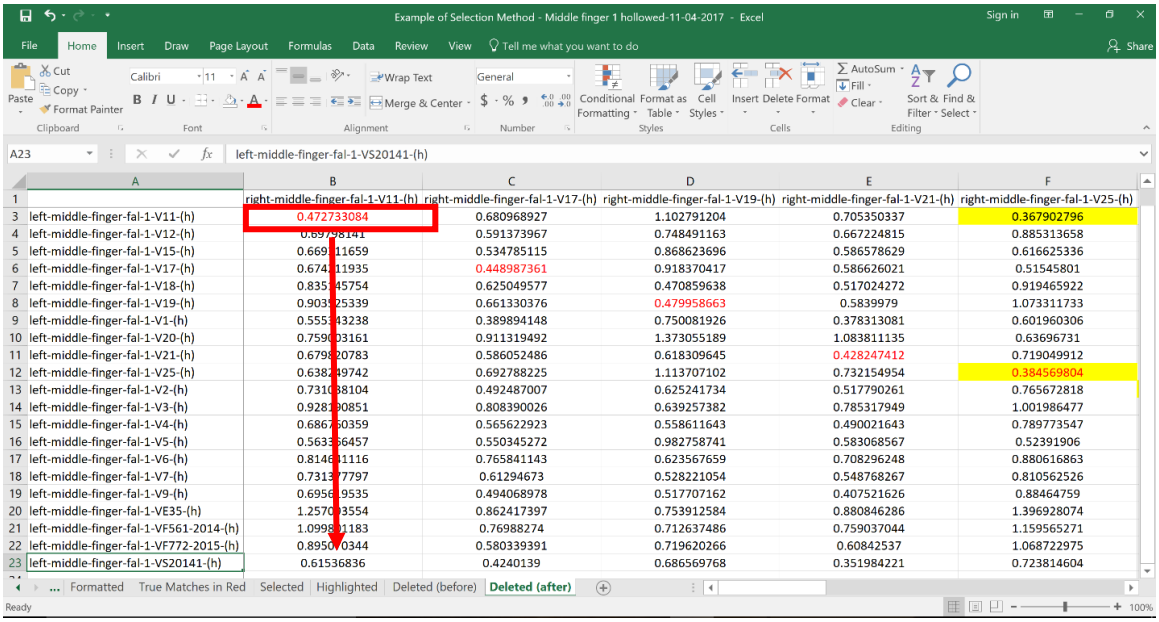

	right-middle-finger-fal-1-V11-(h)	right-middle-finger-fal-1-V17-(h)	right-middle-finger-fal-1-V19-(h)	right-middle-finger-fal-1-V21-(h)	right-middle-finger-fal-1-V25-(h)
left-middle-finger-fal-1-V11-(h)	0.472733084	0.680968927	1.102791204	0.705350337	0.367902796
left-middle-finger-fal-1-V12-(h)	0.69798141	0.591373967	0.748491163	0.667224815	0.885313658
left-middle-finger-fal-1-V15-(h)	0.669311659	0.534785115	0.868623696	0.586578629	0.616625336
left-middle-finger-fal-1-V17-(h)	0.674211935	0.448987361	0.918370417	0.586626021	0.51545801
left-middle-finger-fal-1-V18-(h)	0.835145754	0.625049577	0.470859638	0.517024272	0.919465922
left-middle-finger-fal-1-V19-(h)	0.903525339	0.661330376	0.479958663	0.5839979	1.073311733
left-middle-finger-fal-1-V1-(h)	0.555343238	0.389894148	0.750081926	0.378313081	0.601960306
left-middle-finger-fal-1-V20-(h)	0.759003161	0.911319492	1.373055189	1.083811135	0.63696731
left-middle-finger-fal-1-V21-(h)	0.679820783	0.586052486	0.618309645	0.428247412	0.719049912
left-middle-finger-fal-1-V25-(h)	0.638249742	0.692788225	1.113707102	0.732154954	0.384569804
left-middle-finger-fal-1-V2-(h)	0.731038104	0.492487007	0.625241734	0.517790261	0.765672818
left-middle-finger-fal-1-V3-(h)	0.928190851	0.808390026	0.639257382	0.785317949	1.001986477
left-middle-finger-fal-1-V4-(h)	0.686760359	0.565622923	0.558611643	0.490021643	0.789773547
left-middle-finger-fal-1-V5-(h)	0.563366457	0.550345272	0.982758741	0.583068567	0.52391906
left-middle-finger-fal-1-V6-(h)	0.814641116	0.765841143	0.623567659	0.708296248	0.880616863
left-middle-finger-fal-1-V7-(h)	0.731377797	0.61294673	0.528221054	0.548768267	0.810562526
left-middle-finger-fal-1-V9-(h)	0.695619535	0.494068978	0.517707162	0.407521626	0.88464759
left-middle-finger-fal-1-VE35-(h)	1.257093554	0.862417397	0.753912584	0.880846286	1.396928074
left-middle-finger-fal-1-VF561-2014-(h)	1.099801183	0.76988274	0.712637486	0.759037044	1.159565271
left-middle-finger-fal-1-VF772-2015-(h)	0.895070344	0.580339391	0.719620266	0.60842537	1.068722975
left-middle-finger-fal-1-VS20141-(h)	0.61536836	0.4240139	0.686569768	0.351984221	0.723814604

In this case, there are none for the first column, but there are for the fifth column:

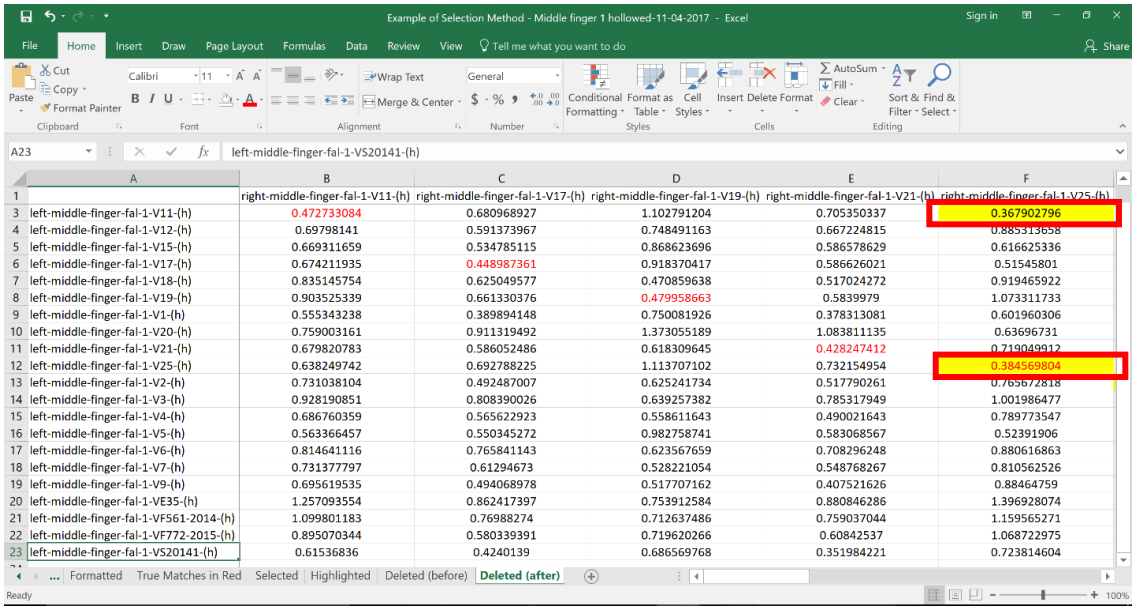

	A	B	C	D	E	F
1		right-middle-finger-fal-1-V11-(h)	right-middle-finger-fal-1-V17-(h)	right-middle-finger-fal-1-V19-(h)	right-middle-finger-fal-1-V21-(h)	right-middle-finger-fal-1-V25-(h)
3	left-middle-finger-fal-1-V11-(h)	0.472733084	0.680968927	1.102791204	0.705350337	0.367902796
4	left-middle-finger-fal-1-V12-(h)	0.69798141	0.591373967	0.748491163	0.667224815	0.885313658
5	left-middle-finger-fal-1-V15-(h)	0.669311659	0.534785115	0.868623696	0.586578629	0.616625336
6	left-middle-finger-fal-1-V17-(h)	0.674211935	0.448987361	0.918370417	0.586626021	0.51545801
7	left-middle-finger-fal-1-V18-(h)	0.835145754	0.625049577	0.470859638	0.517024272	0.919465922
8	left-middle-finger-fal-1-V19-(h)	0.903525339	0.661330376	0.479958663	0.5839979	1.073311733
9	left-middle-finger-fal-1-V1-(h)	0.555343238	0.389894148	0.750081926	0.378313081	0.601960306
10	left-middle-finger-fal-1-V20-(h)	0.759003161	0.911319492	1.373055189	1.083811135	0.63696731
11	left-middle-finger-fal-1-V21-(h)	0.679820783	0.586052486	0.618309645	0.428247412	0.719049912
12	left-middle-finger-fal-1-V25-(h)	0.638249742	0.692788225	1.113707102	0.732154954	0.384569804
13	left-middle-finger-fal-1-V2-(h)	0.731038104	0.492487007	0.625241734	0.517790261	0.765672818
14	left-middle-finger-fal-1-V3-(h)	0.928190851	0.808390026	0.639257382	0.785317949	1.001986477
15	left-middle-finger-fal-1-V4-(h)	0.686760359	0.565622923	0.558611643	0.490021643	0.789773547
16	left-middle-finger-fal-1-V5-(h)	0.563366457	0.550345272	0.982758741	0.583068567	0.52391906
17	left-middle-finger-fal-1-V6-(h)	0.814641116	0.765841143	0.623567659	0.708296248	0.880616863
18	left-middle-finger-fal-1-V7-(h)	0.731377797	0.61294673	0.528221054	0.548768267	0.810562526
19	left-middle-finger-fal-1-V9-(h)	0.695619535	0.494068978	0.517707162	0.407521626	0.88464759
20	left-middle-finger-fal-1-VE35-(h)	1.257093554	0.862417397	0.753912584	0.880846286	1.396928074
21	left-middle-finger-fal-1-VF561-2014-(h)	1.099801183	0.76988274	0.712637486	0.759037044	1.159565271
22	left-middle-finger-fal-1-VF772-2015-(h)	0.895070344	0.580339391	0.719620266	0.60842537	1.068722975
23	left-middle-finger-fal-1-VS20141-(h)	0.61536836	0.4240139	0.686569768	0.351984221	0.723814604

There can only be one final value, so the lowest is kept by un-highlighting the higher value using the ‘No Fill’ feature in the selected cell:

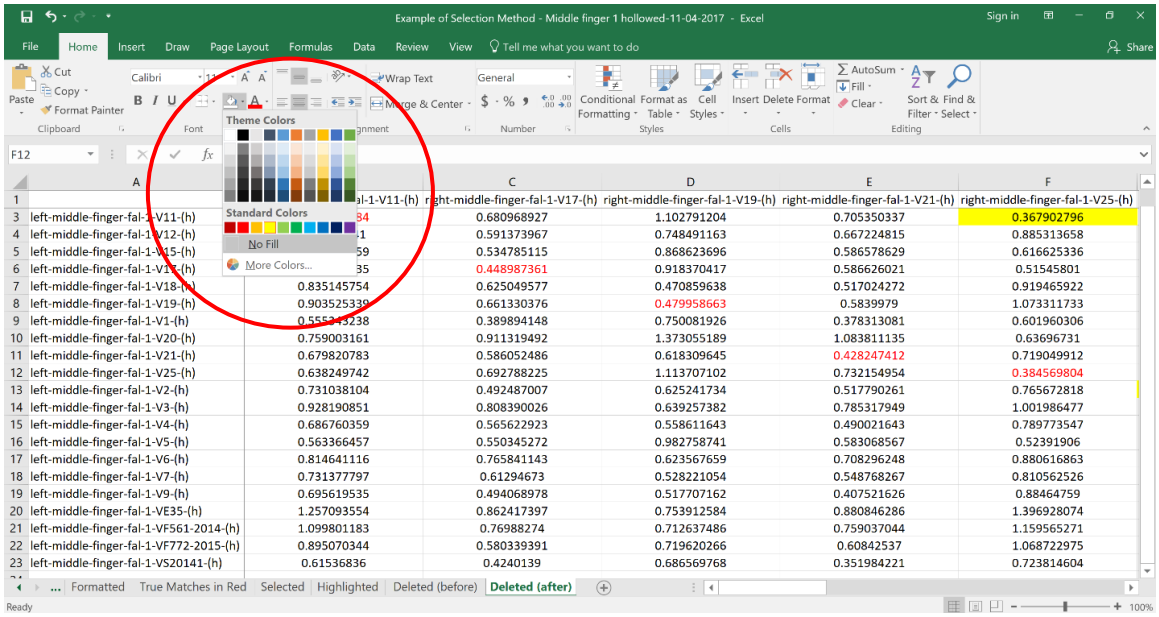

	A	C	D	E	F
1		right-middle-finger-fal-1-V17-(h)	right-middle-finger-fal-1-V19-(h)	right-middle-finger-fal-1-V21-(h)	right-middle-finger-fal-1-V25-(h)
3	left-middle-finger-fal-1-V11-(h)	0.680968927	1.102791204	0.705350337	0.367902796
4	left-middle-finger-fal-1-V12-(h)	0.591373967	0.748491163	0.667224815	0.885313658
5	left-middle-finger-fal-1-V15-(h)	0.534785115	0.868623696	0.586578629	0.616625336
6	left-middle-finger-fal-1-V17-(h)	0.448987361	0.918370417	0.586626021	0.51545801
7	left-middle-finger-fal-1-V18-(h)	0.625049577	0.470859638	0.517024272	0.919465922
8	left-middle-finger-fal-1-V19-(h)	0.661330376	0.479958663	0.5839979	1.073311733
9	left-middle-finger-fal-1-V1-(h)	0.389894148	0.750081926	0.378313081	0.601960306
10	left-middle-finger-fal-1-V20-(h)	0.911319492	1.373055189	1.083811135	0.63696731
11	left-middle-finger-fal-1-V21-(h)	0.586052486	0.618309645	0.428247412	0.719049912
12	left-middle-finger-fal-1-V25-(h)	0.692788225	1.113707102	0.732154954	0.384569804
13	left-middle-finger-fal-1-V2-(h)	0.492487007	0.625241734	0.517790261	0.765672818
14	left-middle-finger-fal-1-V3-(h)	0.808390026	0.639257382	0.785317949	1.001986477
15	left-middle-finger-fal-1-V4-(h)	0.565622923	0.558611643	0.490021643	0.789773547
16	left-middle-finger-fal-1-V5-(h)	0.550345272	0.982758741	0.583068567	0.52391906
17	left-middle-finger-fal-1-V6-(h)	0.765841143	0.623567659	0.708296248	0.880616863
18	left-middle-finger-fal-1-V7-(h)	0.61294673	0.528221054	0.548768267	0.810562526
19	left-middle-finger-fal-1-V9-(h)	0.494068978	0.517707162	0.407521626	0.88464759
20	left-middle-finger-fal-1-VE35-(h)	0.862417397	0.753912584	0.880846286	1.396928074
21	left-middle-finger-fal-1-VF561-2014-(h)	0.76988274	0.712637486	0.759037044	1.159565271
22	left-middle-finger-fal-1-VF772-2015-(h)	0.580339391	0.719620266	0.60842537	1.068722975
23	left-middle-finger-fal-1-VS20141-(h)	0.4240139	0.686569768	0.351984221	0.723814604

Resulting in:

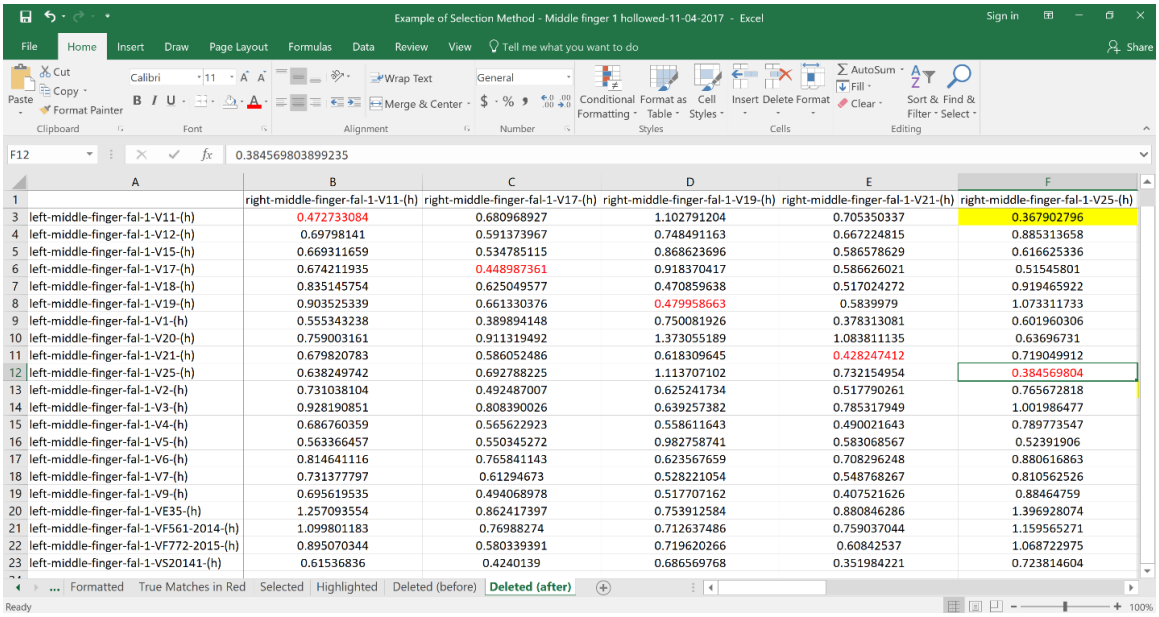

	A	B	C	D	E	F
1		right-middle-finger-fal-1-V11-(h)	right-middle-finger-fal-1-V17-(h)	right-middle-finger-fal-1-V19-(h)	right-middle-finger-fal-1-V21-(h)	right-middle-finger-fal-1-V25-(h)
3	left-middle-finger-fal-1-V11-(h)	0.472733084	0.680968927	1.102791204	0.705350337	0.367902796
4	left-middle-finger-fal-1-V12-(h)	0.69798141	0.591373967	0.748491163	0.667224815	0.885313658
5	left-middle-finger-fal-1-V15-(h)	0.669311659	0.534785115	0.868623696	0.586578629	0.616625336
6	left-middle-finger-fal-1-V17-(h)	0.674211935	0.448987361	0.918370417	0.586626021	0.51545801
7	left-middle-finger-fal-1-V18-(h)	0.835145754	0.625049577	0.470859638	0.517024272	0.919465922
8	left-middle-finger-fal-1-V19-(h)	0.903525339	0.661330376	0.479958663	0.5839979	1.073311733
9	left-middle-finger-fal-1-V1-(h)	0.555343238	0.389894148	0.750081926	0.378313081	0.601960306
10	left-middle-finger-fal-1-V20-(h)	0.759003161	0.911319492	1.373055189	1.083811135	0.63696731
11	left-middle-finger-fal-1-V21-(h)	0.679820783	0.586052486	0.618309645	0.428247412	0.719049912
12	left-middle-finger-fal-1-V25-(h)	0.638249742	0.692788225	1.113707102	0.732154954	0.384569804
13	left-middle-finger-fal-1-V2-(h)	0.731038104	0.492487007	0.625241734	0.517790261	0.765672818
14	left-middle-finger-fal-1-V3-(h)	0.928190851	0.808390026	0.639257382	0.785317949	1.001986477
15	left-middle-finger-fal-1-V4-(h)	0.686760359	0.565622923	0.558611643	0.490021643	0.789773547
16	left-middle-finger-fal-1-V5-(h)	0.563366457	0.550345272	0.982758741	0.583068567	0.52391906
17	left-middle-finger-fal-1-V6-(h)	0.814641116	0.765841143	0.623567659	0.708296248	0.880616863
18	left-middle-finger-fal-1-V7-(h)	0.731377797	0.61294673	0.528221054	0.548768267	0.810562526
19	left-middle-finger-fal-1-V9-(h)	0.695619535	0.494068978	0.517707162	0.407521626	0.88464759
20	left-middle-finger-fal-1-VE35-(h)	1.257093554	0.862417397	0.753912584	0.880846286	1.396928074
21	left-middle-finger-fal-1-VF561-2014-(h)	1.099801183	0.76988274	0.712637486	0.759037044	1.159565271
22	left-middle-finger-fal-1-VF772-2015-(h)	0.895070344	0.580339391	0.719620266	0.60842537	1.068722975
23	left-middle-finger-fal-1-VS20141-(h)	0.61536836	0.4240139	0.686569768	0.351984221	0.723814604

This is done for all the columns (view from further along in the sheet):

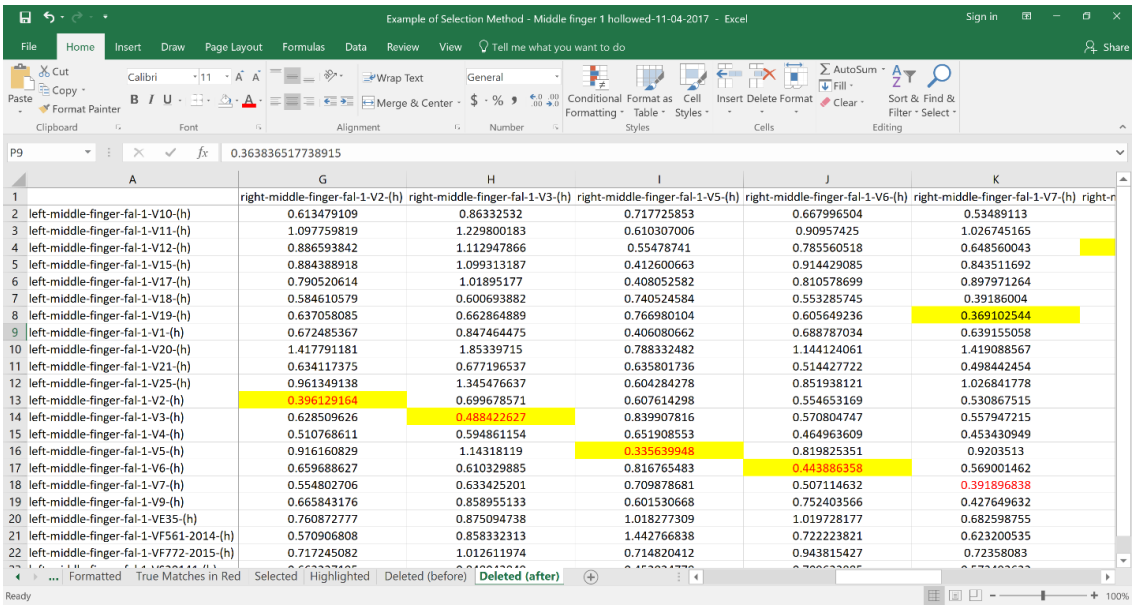

	A	G	H	I	J	K
1		right-middle-finger-fal-1-V2-(h)	right-middle-finger-fal-1-V3-(h)	right-middle-finger-fal-1-V5-(h)	right-middle-finger-fal-1-V6-(h)	right-middle-finger-fal-1-V7-(h)
2	left-middle-finger-fal-1-V10-(h)	0.613479109	0.86332532	0.717725853	0.667996504	0.53489113
3	left-middle-finger-fal-1-V11-(h)	1.097759819	1.229800183	0.610307006	0.90957425	1.026745165
4	left-middle-finger-fal-1-V12-(h)	0.886593842	1.112947866	0.55478741	0.785560518	0.648560043
5	left-middle-finger-fal-1-V15-(h)	0.884388918	1.099313187	0.412600663	0.914429085	0.843511692
6	left-middle-finger-fal-1-V17-(h)	0.790520614	1.01895177	0.408052582	0.810578699	0.897971264
7	left-middle-finger-fal-1-V18-(h)	0.584610579	0.600693882	0.740524584	0.553285745	0.39186004
8	left-middle-finger-fal-1-V19-(h)	0.637058085	0.662864889	0.766980104	0.605649236	0.369102544
9	left-middle-finger-fal-1-V1-(h)	0.672485367	0.847464475	0.406080662	0.688787034	0.639155058
10	left-middle-finger-fal-1-V20-(h)	1.417791181	1.85339715	0.788332482	1.144124061	1.419088567
11	left-middle-finger-fal-1-V21-(h)	0.634117375	0.677196537	0.635801736	0.514427722	0.498442454
12	left-middle-finger-fal-1-V25-(h)	0.961349138	1.345476637	0.604284278	0.851938121	1.026841778
13	left-middle-finger-fal-1-V2-(h)	0.396129164	0.699678571	0.607614298	0.554653169	0.530867515
14	left-middle-finger-fal-1-V3-(h)	0.628509626	0.488422627	0.839907816	0.570804747	0.557947215
15	left-middle-finger-fal-1-V4-(h)	0.510768611	0.594861154	0.651908553	0.464963609	0.453430949
16	left-middle-finger-fal-1-V5-(h)	0.916160829	1.14318119	0.335639948	0.819825351	0.9203513
17	left-middle-finger-fal-1-V6-(h)	0.659688627	0.610329885	0.816765483	0.443886358	0.569001462
18	left-middle-finger-fal-1-V7-(h)	0.554802706	0.633425201	0.709878681	0.507114632	0.391896838
19	left-middle-finger-fal-1-V9-(h)	0.665843176	0.858955133	0.601530668	0.752403566	0.427649632
20	left-middle-finger-fal-1-VE35-(h)	0.760872777	0.875094738	1.018277309	1.019728177	0.682598755
21	left-middle-finger-fal-1-VF561-2014-(h)	0.570906808	0.858332313	1.442766838	0.722223821	0.623200535
22	left-middle-finger-fal-1-VF772-2015-(h)	0.717245082	1.012611974	0.714820412	0.943815427	0.72358083

8) Now these values are then classed as true positive match, true negative, false positive, and false negative, again following the same pattern as before with across first, then down.

A *true positive* pair match is the left and rights both agree on the lowest value – formatting wise this means that the text of the cell should be **RED** and it should be highlighted in yellow like so:

A *true negative* should not have a match – formatting wise this means the entire row/column should have nothing in red text or highlighted in yellow.

1		left-middle-finger-fal-1-V10-(h)
2	right-middl	0.811383
3	right-middl	0.55145
4	right-middl	0.563499
5	right-middl	0.49794
6	right-middl	0.965129
7	right-middl	0.613479
8	right-middl	0.863325
9	right-middl	0.717726
10	right-middl	0.667997
11	right-middl	0.534891
12	right-middl	0.49505
13	right-middl	0.792376
14	right-middl	0.659999
15	right-middl	0.551665
16	right-middl	0.431459
17		true neg

(Example, but it's transposed – so you will never actually see lefts and rights in this exact position)

A *false positive* is when either the bone is mismatched to the wrong pair, or when a negative is mismatched with a pair at all – formatting wise this will appear as **black** text highlighted in yellow like so:

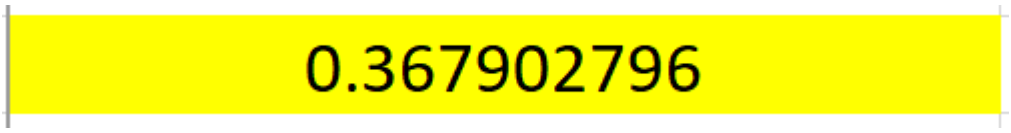

A false negative is when a bone has a match, but it was not selected– formatting wise this will appear as **RED** text but nothing will be highlighted in yellow like so:

		right-middle-finger-fal-1-V19-(h)
2	left-middle-finger-fal-1-V10-(h)	0.563498581
3	left-middle-finger-fal-1-V11-(h)	1.102791204
4	left-middle-finger-fal-1-V12-(h)	0.748491163
5	left-middle-finger-fal-1-V15-(h)	0.868623696
6	left-middle-finger-fal-1-V17-(h)	0.918370417
7	left-middle-finger-fal-1-V18-(h)	0.470859638
8	left-middle-finger-fal-1-V19-(h)	0.479958663
9	left-middle-finger-fal-1-V1-(h)	0.750081926
10	left-middle-finger-fal-1-V20-(h)	1.373055189
11	left-middle-finger-fal-1-V21-(h)	0.618309645
12	left-middle-finger-fal-1-V25-(h)	1.113707102
13	left-middle-finger-fal-1-V2-(h)	0.625241734
14	left-middle-finger-fal-1-V3-(h)	0.639257382
15	left-middle-finger-fal-1-V4-(h)	0.558611643
16	left-middle-finger-fal-1-V5-(h)	0.982758741
17	left-middle-finger-fal-1-V6-(h)	0.623567659
18	left-middle-finger-fal-1-V7-(h)	0.528221054
19	left-middle-finger-fal-1-V9-(h)	0.517707162
20	left-middle-finger-fal-1-VE35-(h)	0.753912584
21	left-middle-finger-fal-1-VF561-2014-(h)	0.712637486
22	left-middle-finger-fal-1-VF772-2015-(h)	0.719620266
23	left-middle-finger-fal-1-VS20141-(h)	0.686569768
24		false neg

So, to determine this, follow the same procedure for going **across** first, row by row and decide if each row is a true positive, true negative, false positive or false negative:

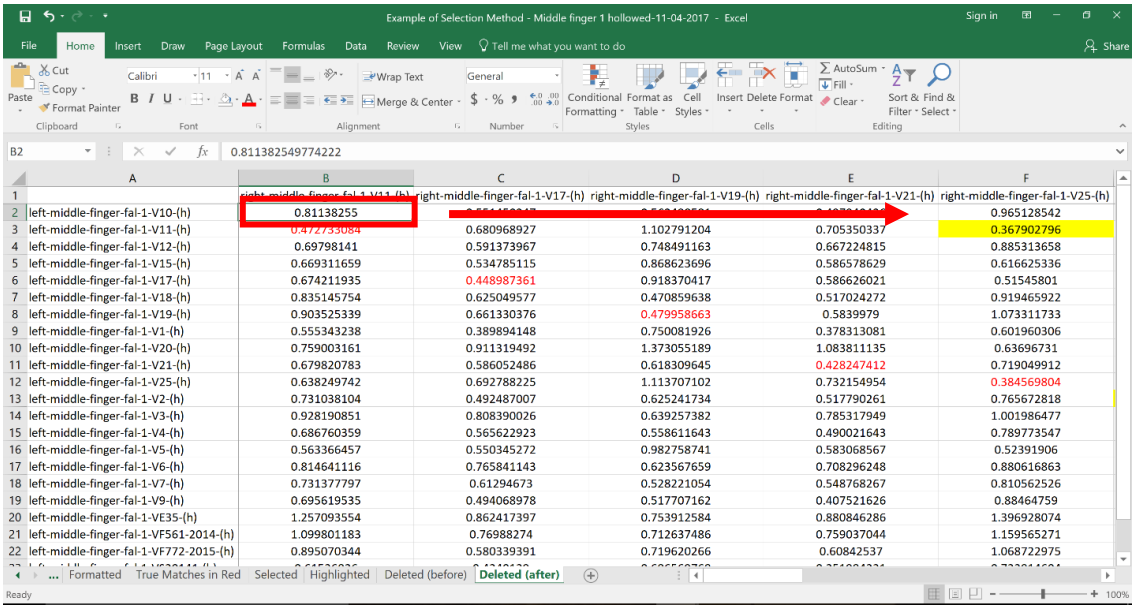

	A	B	C	D	E	F
1		right-middle-finger-fal-1-V11-(h)	right-middle-finger-fal-1-V17-(h)	right-middle-finger-fal-1-V19-(h)	right-middle-finger-fal-1-V21-(h)	right-middle-finger-fal-1-V25-(h)
2	left-middle-finger-fal-1-V10-(h)	0.81138255				0.965128542
3	left-middle-finger-fal-1-V11-(h)	0.472733084	0.680968927	1.102791204	0.705350337	0.367902796
4	left-middle-finger-fal-1-V12-(h)	0.69798141	0.591373967	0.748491163	0.667224815	0.885313658
5	left-middle-finger-fal-1-V15-(h)	0.669311659	0.534785115	0.868623696	0.586578629	0.616625336
6	left-middle-finger-fal-1-V17-(h)	0.674211935	0.448987361	0.918370417	0.586626021	0.51545801
7	left-middle-finger-fal-1-V18-(h)	0.835145754	0.625049577	0.470859638	0.517024272	0.919465922
8	left-middle-finger-fal-1-V19-(h)	0.903525339	0.661330376	0.479958663	0.5839979	1.073311733
9	left-middle-finger-fal-1-V1-(h)	0.555343238	0.389894148	0.750081926	0.378313081	0.601960306
10	left-middle-finger-fal-1-V20-(h)	0.759003161	0.911319492	1.373055189	1.083811135	0.63696731
11	left-middle-finger-fal-1-V21-(h)	0.679820783	0.586052486	0.618309645	0.428247412	0.719049912
12	left-middle-finger-fal-1-V25-(h)	0.638249742	0.692788225	1.113707102	0.732154954	0.384569804
13	left-middle-finger-fal-1-V2-(h)	0.731038104	0.492487007	0.625241734	0.517790261	0.765672818
14	left-middle-finger-fal-1-V3-(h)	0.928190851	0.808390026	0.639257382	0.785317949	1.001986477
15	left-middle-finger-fal-1-V4-(h)	0.686760359	0.565622923	0.558611643	0.490021643	0.789773547
16	left-middle-finger-fal-1-V5-(h)	0.563366457	0.550345272	0.982758741	0.583068567	0.52391906
17	left-middle-finger-fal-1-V6-(h)	0.814641116	0.765841143	0.623567659	0.708296248	0.880616863
18	left-middle-finger-fal-1-V7-(h)	0.731377797	0.61294673	0.528221054	0.548768267	0.810562526
19	left-middle-finger-fal-1-V9-(h)	0.695619535	0.494068978	0.517707162	0.407521626	0.88464759
20	left-middle-finger-fal-1-VE35-(h)	1.257093554	0.862417397	0.753912584	0.880846286	1.396928074
21	left-middle-finger-fal-1-VF561-2014-(h)	1.099801183	0.76988274	0.712637486	0.759037044	1.159565271
22	left-middle-finger-fal-1-VF772-2015-(h)	0.895070344	0.580339391	0.719620266	0.60842537	1.068722975

This will result in this:

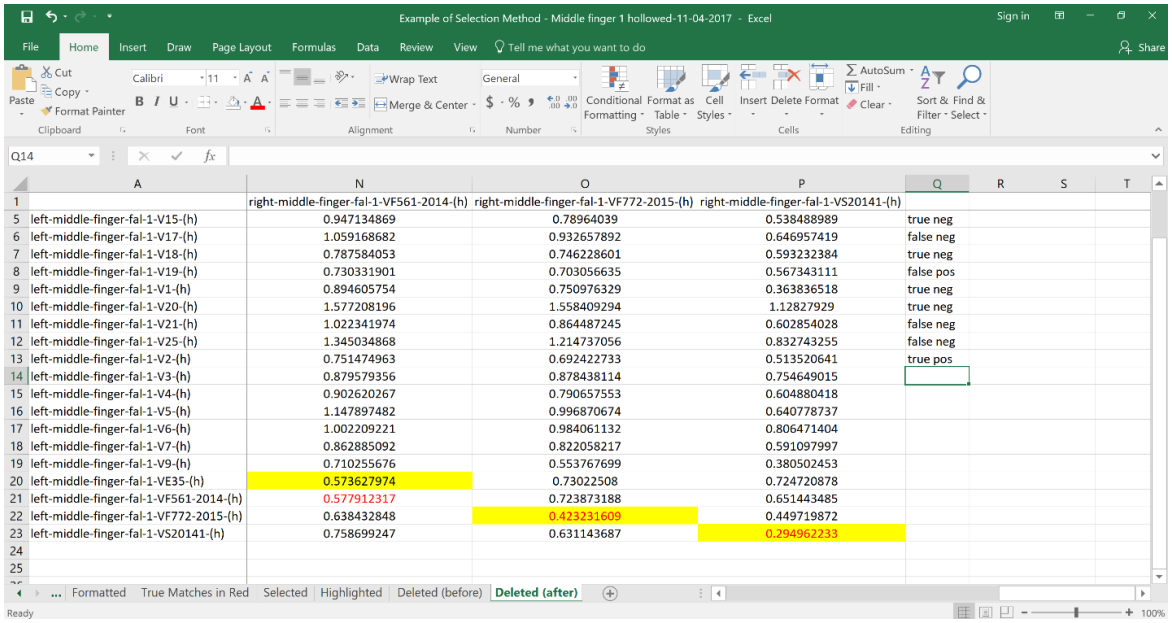

	A	N	O	P	Q
1		right-middle-finger-fal-1-VF561-2014-(h)	right-middle-finger-fal-1-VF772-2015-(h)	right-middle-finger-fal-1-VS20141-(h)	
5	left-middle-finger-fal-1-V15-(h)	0.947134869	0.78964039	0.538488989	true neg
6	left-middle-finger-fal-1-V17-(h)	1.059168682	0.932657892	0.646957419	false neg
7	left-middle-finger-fal-1-V18-(h)	0.787584053	0.746228601	0.593232384	true neg
8	left-middle-finger-fal-1-V19-(h)	0.730331901	0.703056635	0.567343111	false pos
9	left-middle-finger-fal-1-V1-(h)	0.894605754	0.750976329	0.363836518	true neg
10	left-middle-finger-fal-1-V20-(h)	1.577208196	1.558409294	1.12827929	true neg
11	left-middle-finger-fal-1-V21-(h)	1.022341974	0.864487245	0.602854028	false neg
12	left-middle-finger-fal-1-V25-(h)	1.345034868	1.214737056	0.832743255	false neg
13	left-middle-finger-fal-1-V2-(h)	0.751474963	0.692422733	0.513520641	true pos
14	left-middle-finger-fal-1-V3-(h)	0.879579356	0.878438114	0.754649015	
15	left-middle-finger-fal-1-V4-(h)	0.902620267	0.790657553	0.604880418	
16	left-middle-finger-fal-1-V5-(h)	1.147897482	0.996870674	0.640778737	
17	left-middle-finger-fal-1-V6-(h)	1.002209221	0.984061132	0.806471404	
18	left-middle-finger-fal-1-V7-(h)	0.862885092	0.822058217	0.591097997	
19	left-middle-finger-fal-1-V9-(h)	0.710255676	0.553767699	0.380502453	
20	left-middle-finger-fal-1-VE35-(h)	0.573627974	0.73022508	0.724720878	
21	left-middle-finger-fal-1-VF561-2014-(h)	0.577912317	0.723873188	0.651443485	
22	left-middle-finger-fal-1-VF772-2015-(h)	0.638432848	0.423231609	0.449719872	
23	left-middle-finger-fal-1-VS20141-(h)	0.758699247	0.631143687	0.294962233	

And finally this once all the rows are complete:

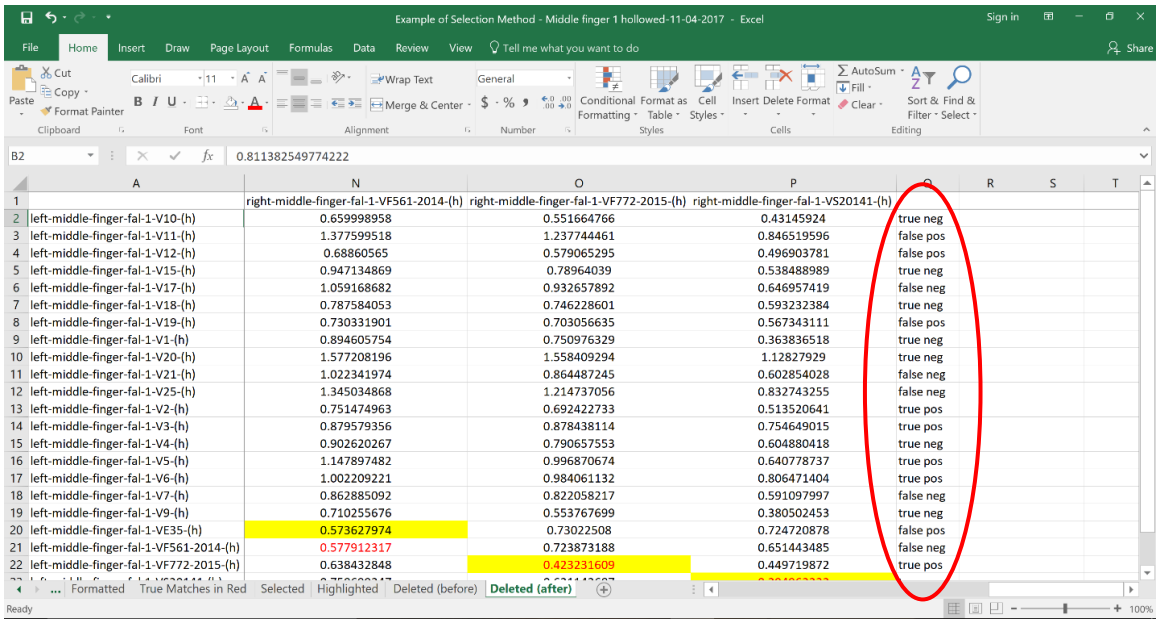

	A	N	O	P	Q
1		right-middle-finger-fal-1-VF561-2014-(h)	right-middle-finger-fal-1-VF772-2015-(h)	right-middle-finger-fal-1-VS20141-(h)	
2	left-middle-finger-fal-1-V10-(h)	0.659998958	0.551664766	0.43145924	true neg
3	left-middle-finger-fal-1-V11-(h)	1.377599518	1.237744461	0.846519596	false pos
4	left-middle-finger-fal-1-V12-(h)	0.68860565	0.579065295	0.496903781	false pos
5	left-middle-finger-fal-1-V15-(h)	0.947134869	0.78964039	0.538488989	true neg
6	left-middle-finger-fal-1-V17-(h)	1.059168682	0.932657892	0.646957419	false neg
7	left-middle-finger-fal-1-V18-(h)	0.787584053	0.746228601	0.593232384	true neg
8	left-middle-finger-fal-1-V19-(h)	0.730331901	0.703056635	0.567343111	false pos
9	left-middle-finger-fal-1-V1-(h)	0.894605754	0.750976329	0.363836518	true neg
10	left-middle-finger-fal-1-V20-(h)	1.577208196	1.558409294	1.12827929	true neg
11	left-middle-finger-fal-1-V21-(h)	1.022341974	0.864487245	0.602854028	false neg
12	left-middle-finger-fal-1-V25-(h)	1.345034868	1.214737056	0.832743255	false neg
13	left-middle-finger-fal-1-V2-(h)	0.751474963	0.692422733	0.513520641	true pos
14	left-middle-finger-fal-1-V3-(h)	0.879579356	0.878438114	0.754649015	true pos
15	left-middle-finger-fal-1-V4-(h)	0.902620267	0.790657553	0.604880418	true neg
16	left-middle-finger-fal-1-V5-(h)	1.147897482	0.996870674	0.640778737	true pos
17	left-middle-finger-fal-1-V6-(h)	1.002209221	0.984061132	0.806471404	true pos
18	left-middle-finger-fal-1-V7-(h)	0.862885092	0.822058217	0.591097997	false neg
19	left-middle-finger-fal-1-V9-(h)	0.710255676	0.553767699	0.380502453	true neg
20	left-middle-finger-fal-1-VE35-(h)	0.573627974	0.73022508	0.724720878	false pos
21	left-middle-finger-fal-1-VF561-2014-(h)	0.577912317	0.723873188	0.651443485	false neg
22	left-middle-finger-fal-1-VF772-2015-(h)	0.638432848	0.423231609	0.449719872	true pos

Next, follow the same procedure for going **down**, column by column and decide if each column is a true positive, true negative, false positive or false negative:

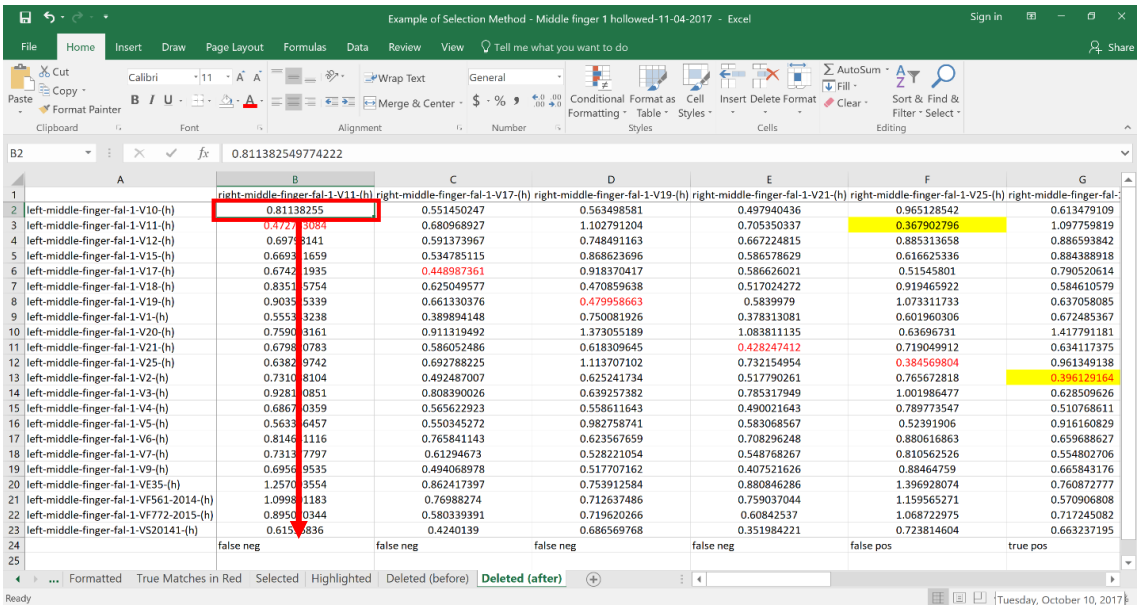

This will result in this:

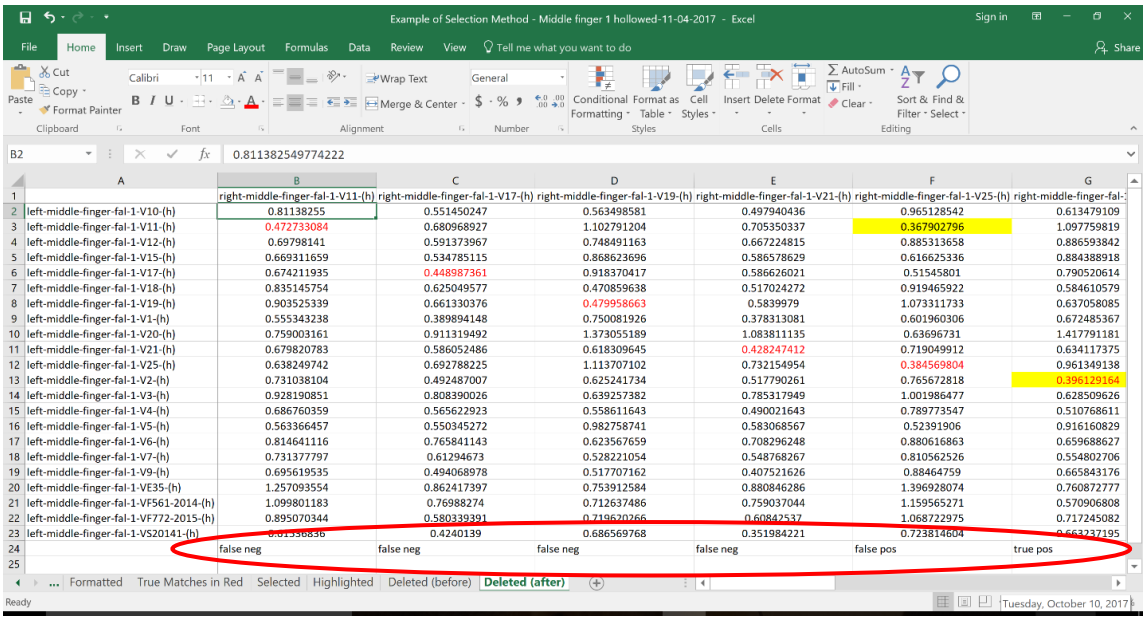

9) All of these results are combined in order to calculate sensitivity and specificity
First, create a new sheet by pressing the + button:

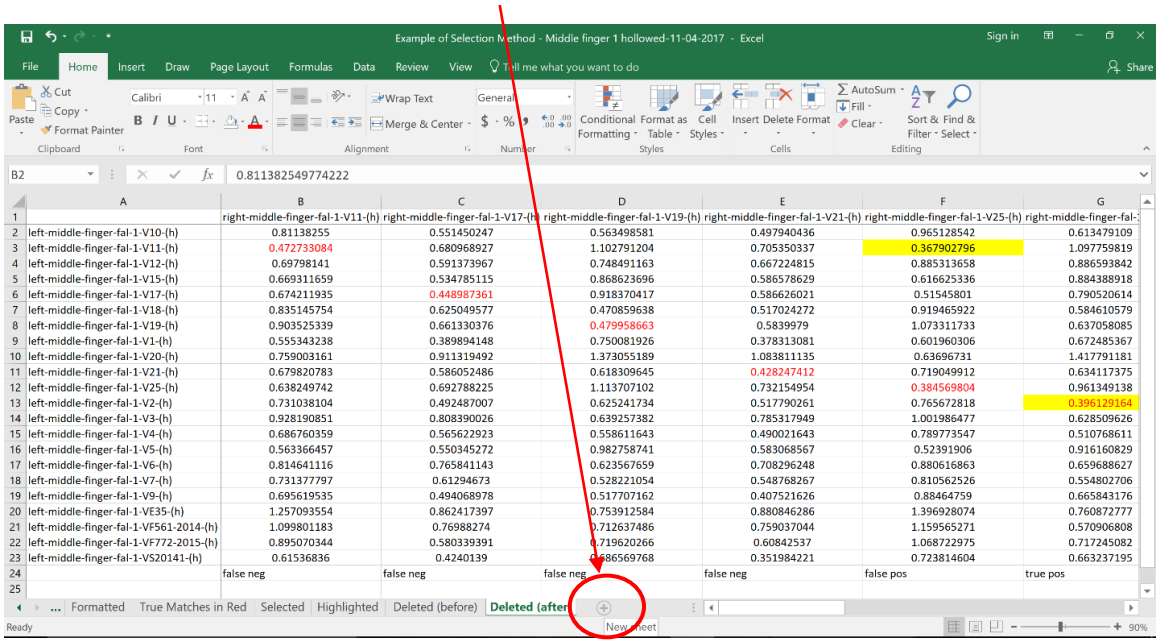

Rename this sheet ‘Sensitivity and Specificity’ by Right-Clicking on the tab name:

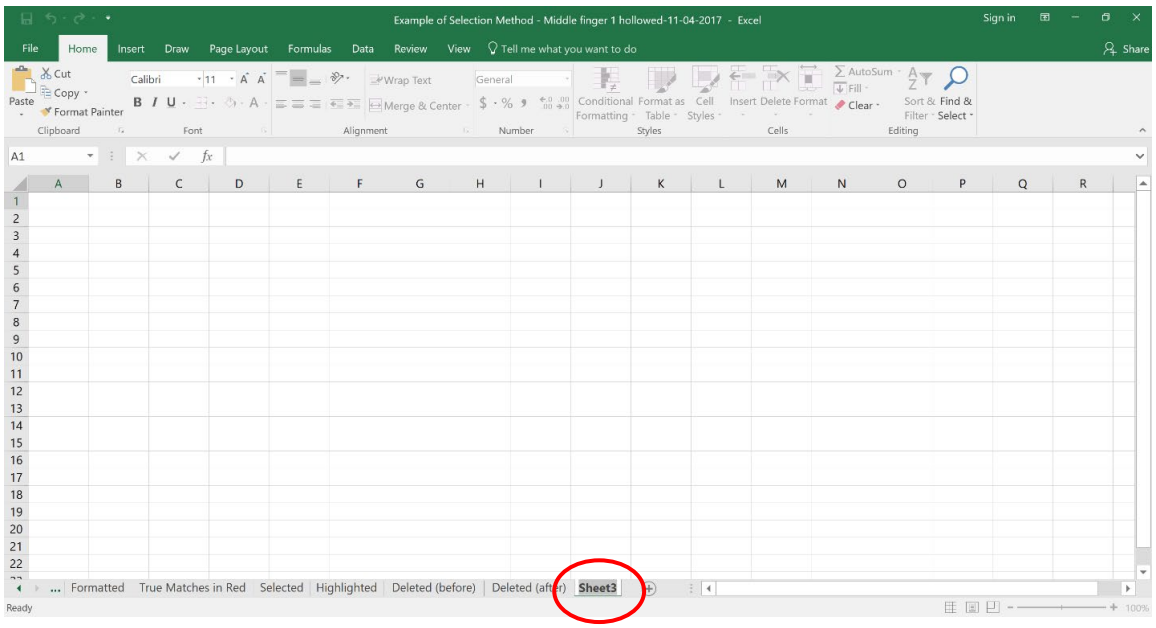

Resulting in this:

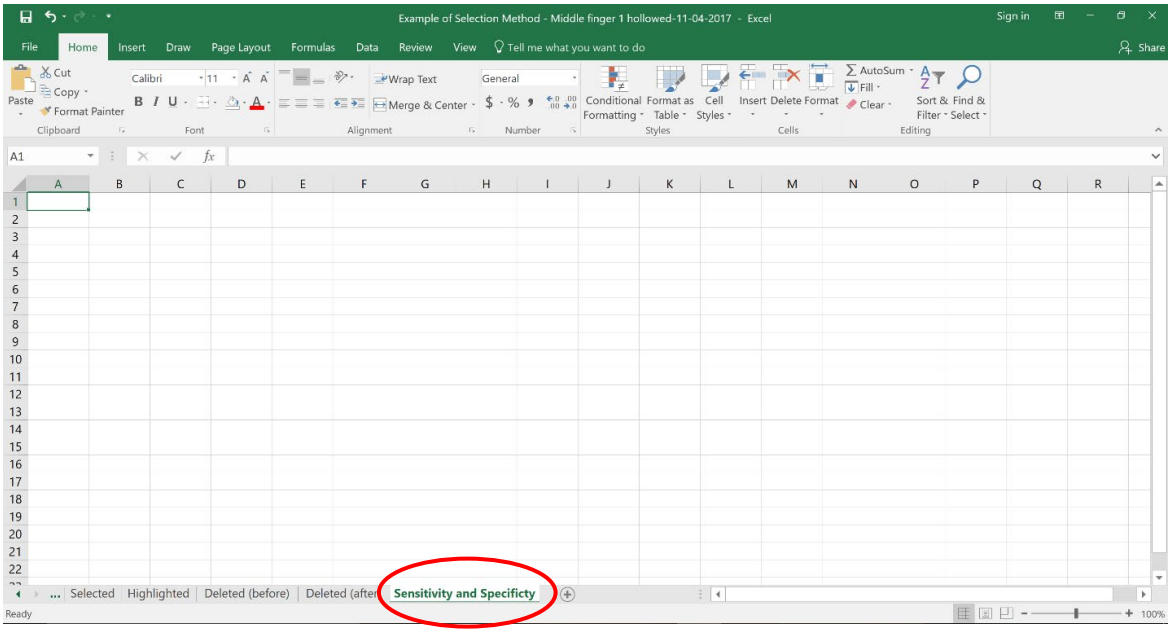

Next, select the **across** values:

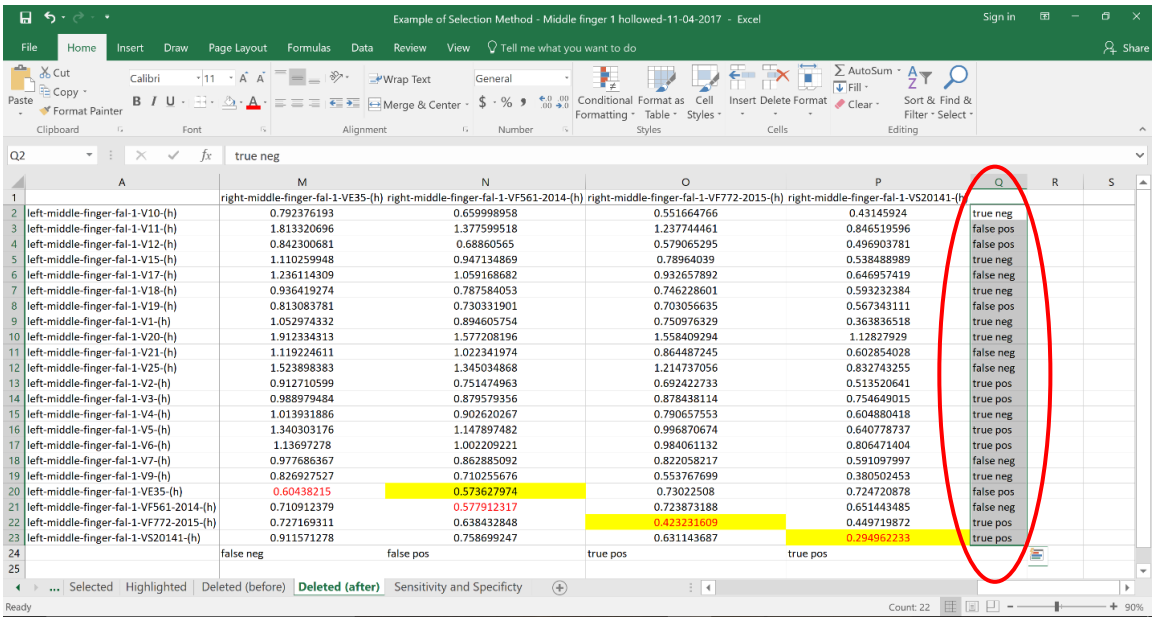

	right-middle-finger-fal-1-VE35-(h)	right-middle-finger-fal-1-VF561-2014-(h)	right-middle-finger-fal-1-VF772-2015-(h)	right-middle-finger-fal-1-VS20141-(h)	
left-middle-finger-fal-1-V10-(h)	0.792376193	0.659998958	0.551664766	0.43145924	true neg
left-middle-finger-fal-1-V11-(h)	1.813320696	1.377599518	1.237744461	0.846519596	false pos
left-middle-finger-fal-1-V12-(h)	0.842300681	0.68860565	0.579065295	0.496903781	false pos
left-middle-finger-fal-1-V15-(h)	1.110259948	0.947134869	0.78964039	0.538488989	true neg
left-middle-finger-fal-1-V17-(h)	1.236114309	1.059168682	0.932657892	0.646957419	false neg
left-middle-finger-fal-1-V18-(h)	0.936419274	0.787584053	0.746228601	0.593232384	true neg
left-middle-finger-fal-1-V19-(h)	0.813083781	0.730331901	0.703056635	0.567343111	false pos
left-middle-finger-fal-1-V1-(h)	1.052974332	0.894605754	0.750976329	0.363836518	true neg
left-middle-finger-fal-1-V20-(h)	1.912334313	1.577208196	1.558409294	1.12827929	true neg
left-middle-finger-fal-1-V21-(h)	1.119224611	1.022341974	0.864487245	0.602854028	false neg
left-middle-finger-fal-1-V25-(h)	1.523898383	1.345034868	1.214737056	0.832743255	false neg
left-middle-finger-fal-1-V2-(h)	0.912710599	0.751474963	0.692422733	0.513520641	true pos
left-middle-finger-fal-1-V3-(h)	0.988979484	0.879579356	0.878438114	0.754649015	true pos
left-middle-finger-fal-1-V4-(h)	1.013931886	0.902620267	0.790657553	0.604880418	true neg
left-middle-finger-fal-1-V5-(h)	1.340303176	1.147897482	0.996870674	0.640778737	true pos
left-middle-finger-fal-1-V6-(h)	1.13697278	1.002209221	0.984061132	0.806471404	true pos
left-middle-finger-fal-1-V7-(h)	0.977686367	0.862885092	0.822058217	0.591097997	false neg
left-middle-finger-fal-1-V9-(h)	0.826927527	0.710255676	0.553767699	0.380502453	true neg
left-middle-finger-fal-1-VE35-(h)	0.60438215	0.573627974	0.73022508	0.724720878	false pos
left-middle-finger-fal-1-VF561-2014-(h)	0.710912379	0.577912317	0.723873188	0.651443485	false neg
left-middle-finger-fal-1-VF772-2015-(h)	0.727169311	0.638432848	0.423231609	0.449719872	true pos
left-middle-finger-fal-1-VS20141-(h)	0.911571278	0.758699247	0.631143687	0.294962233	true pos
	false neg	false pos	true pos	true pos	

Right Click and select ‘Copy’:

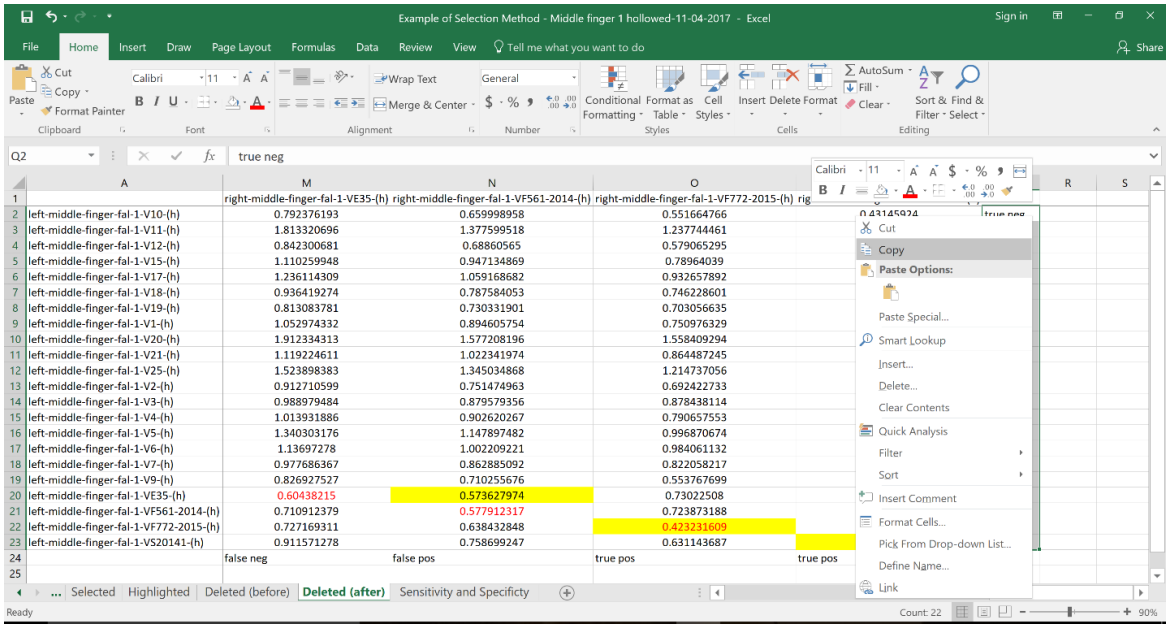

Go to the ‘Sensitivity and Specificity’ tab, select the first cell and Right Click to Paste:

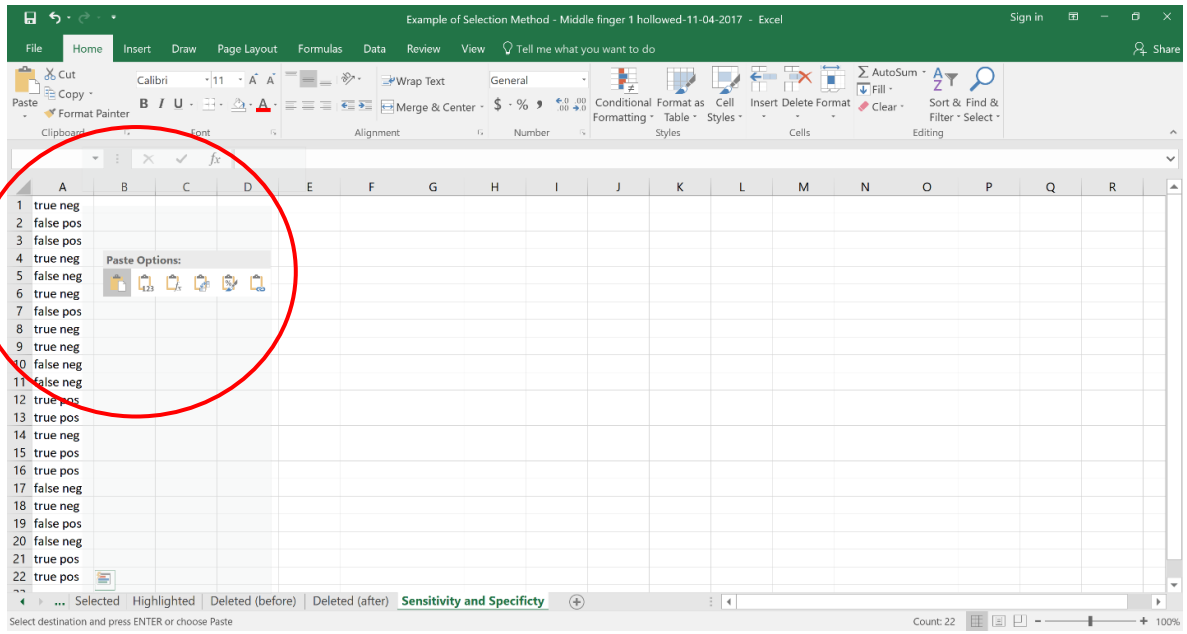

Next, select the **down** values:

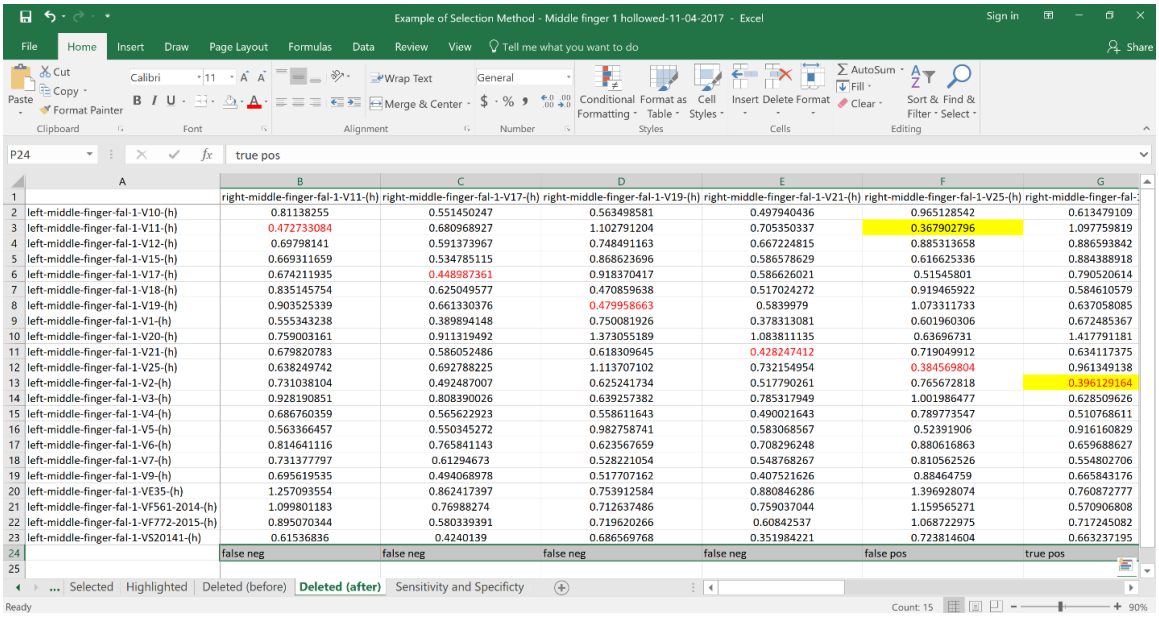

Right Click and select ‘Copy’:

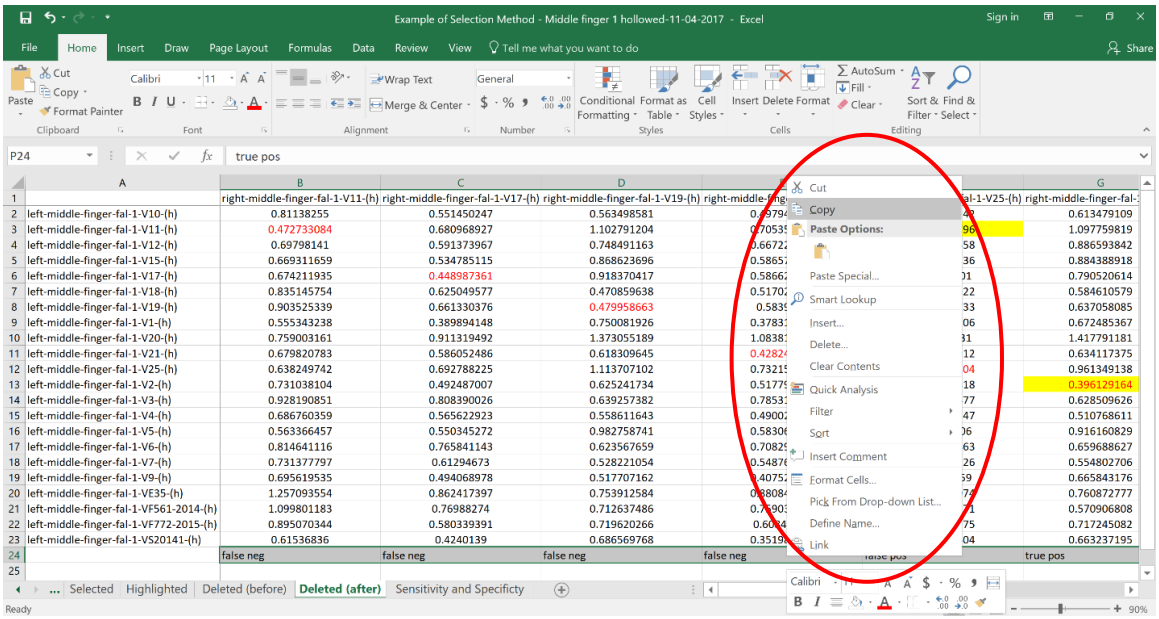

Go to the ‘Sensitivity and Specificity’ tab, select the cell at the end of the previous list and Right Click to Paste, selecting ‘TRANSPOSE’:

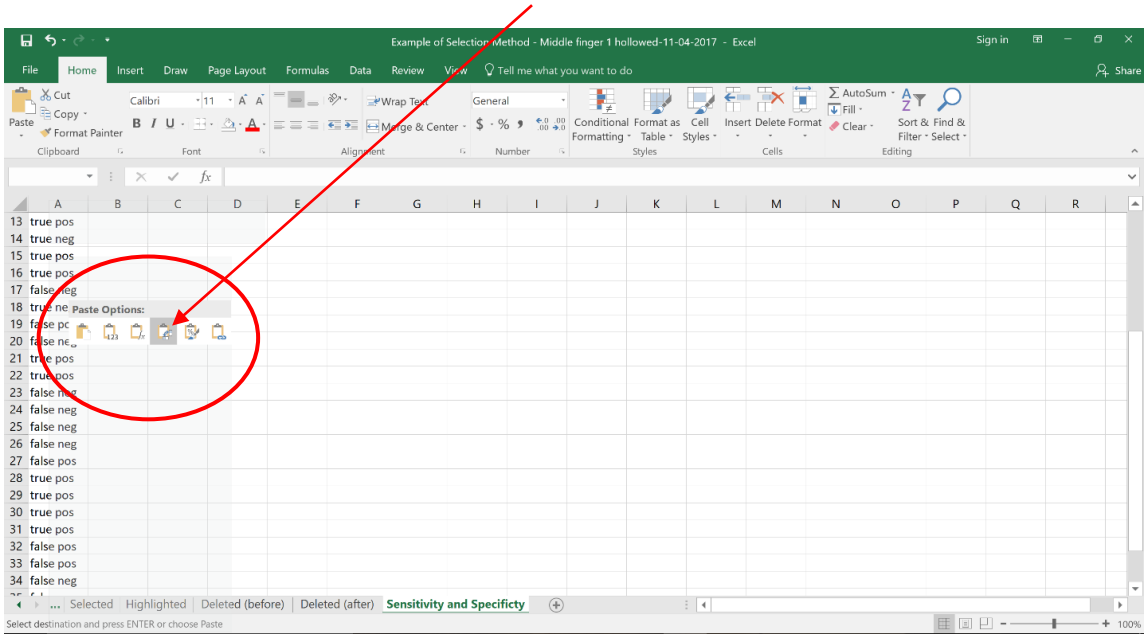

Now there should be one column with the combined results:

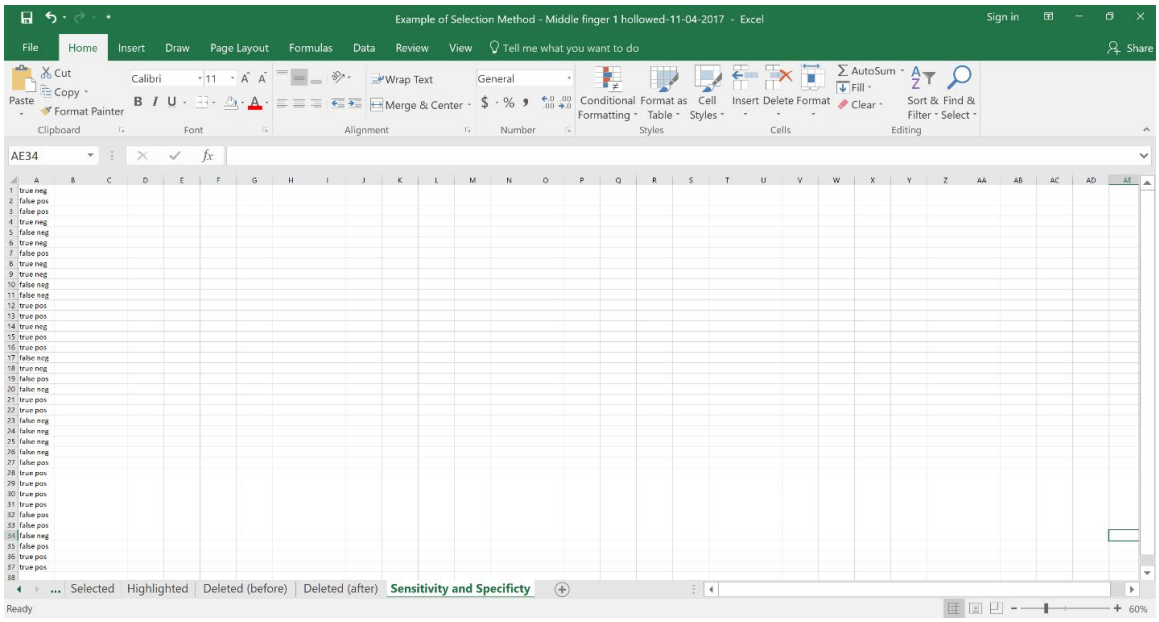

10) Calculate Sensitivity and Specificity

To calculate sensitivity and specificity, there needs to be a total number of true positives, true negatives, false positives and false negatives.
To do this, select the column:

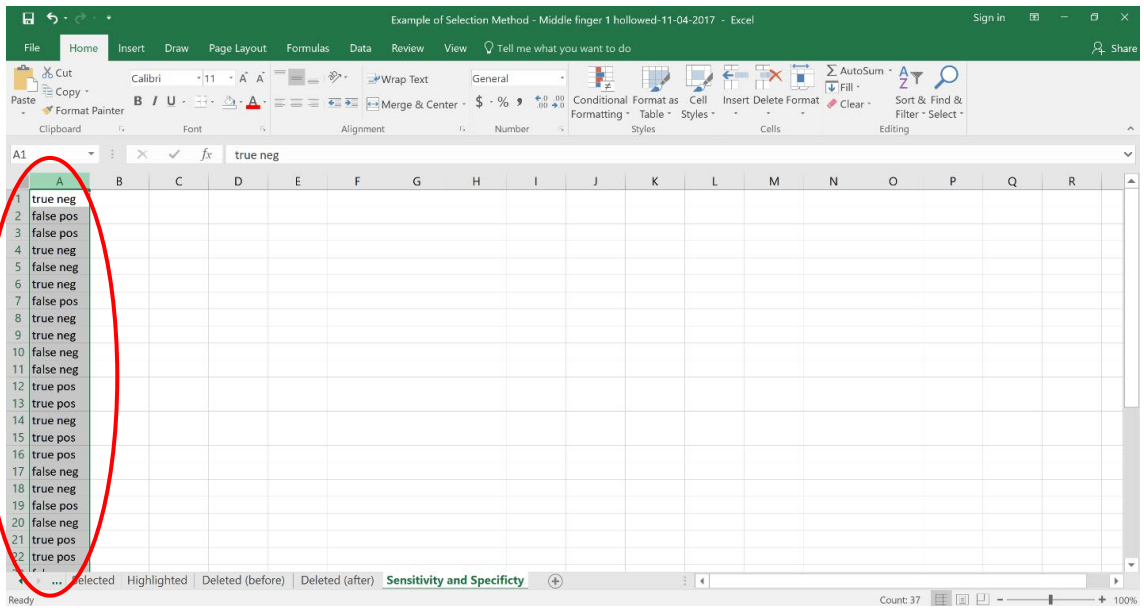

Then press the ‘Sort & Filter’ button, ‘Sort A to Z’:

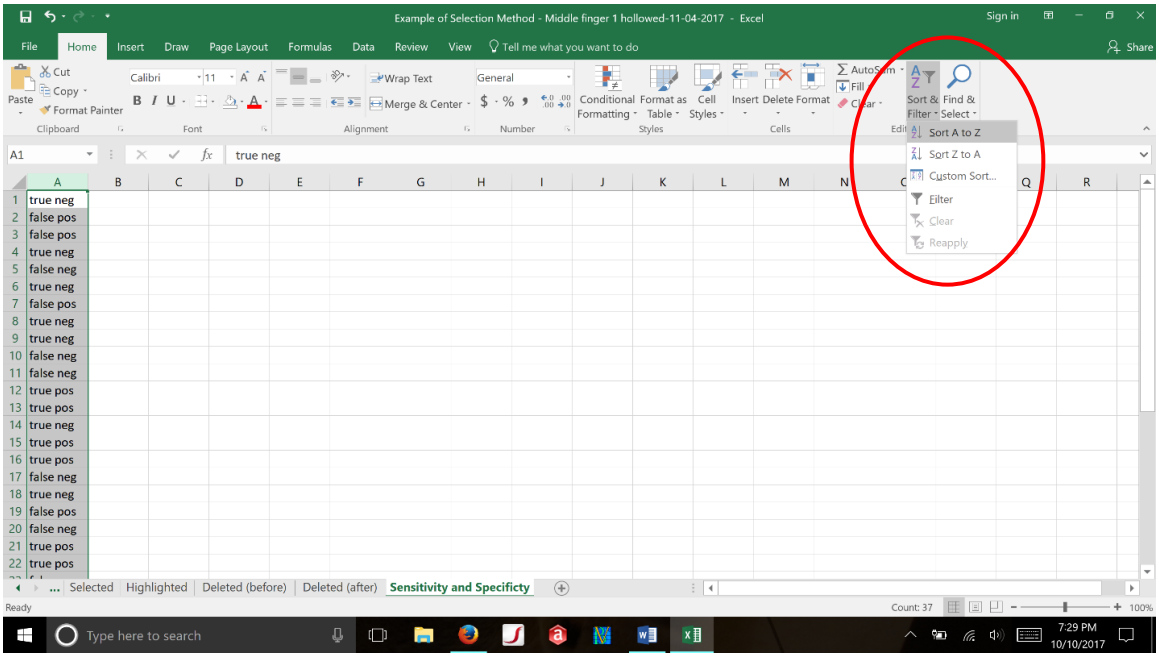

This should result in everything being sorted and grouped together:

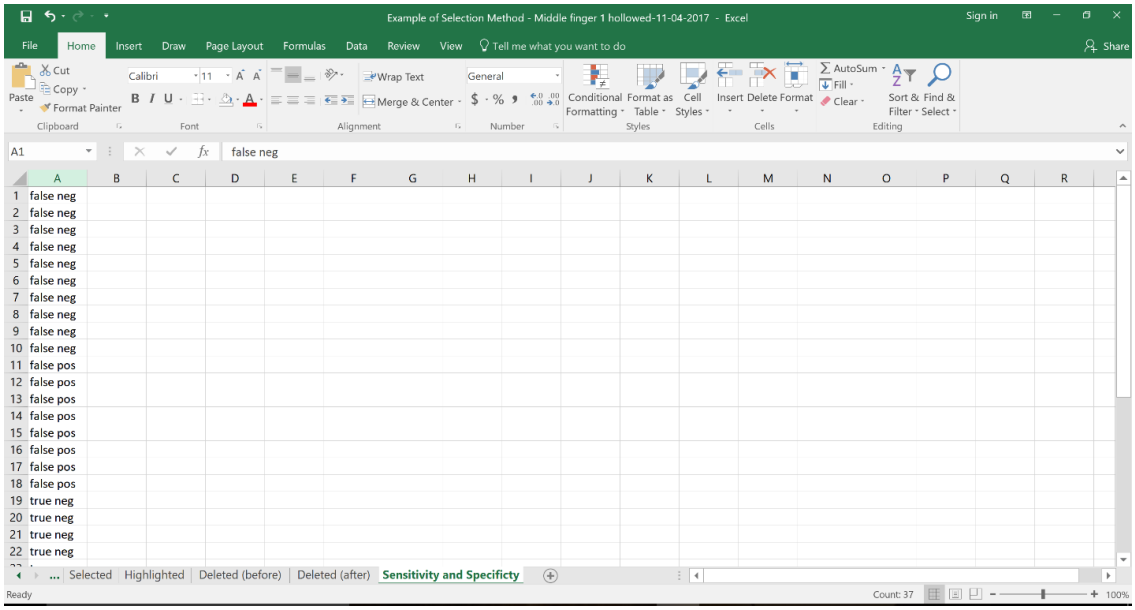

To accurate count each category, when highlighted, Excel will automatically count the selected cells:

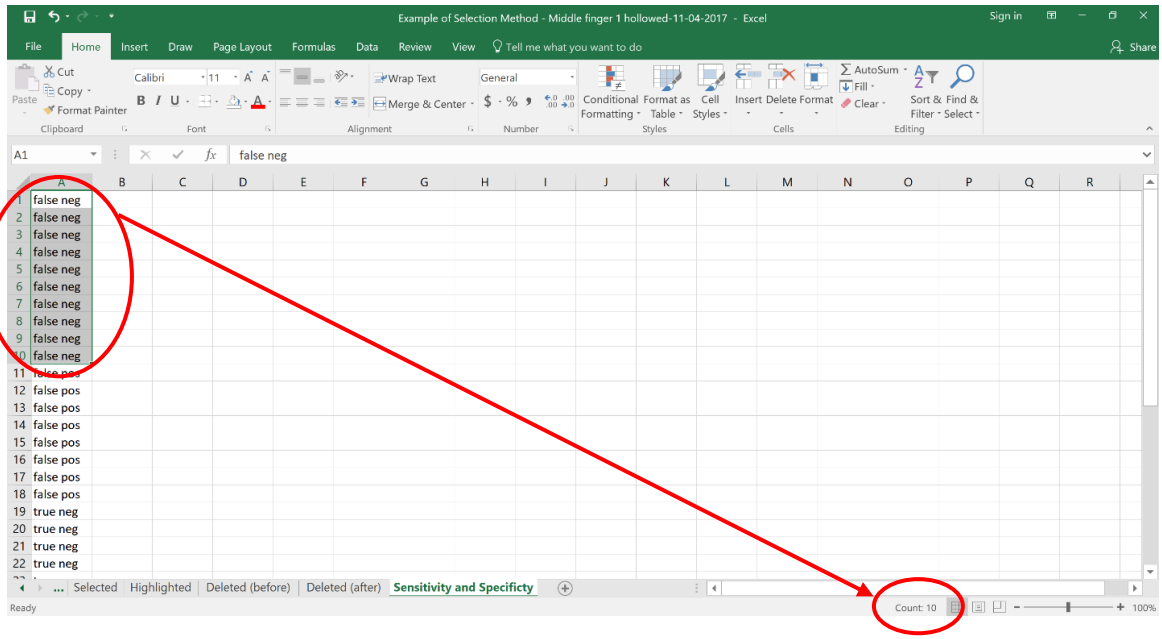

Repeat this for each category and then record these numbers like so:

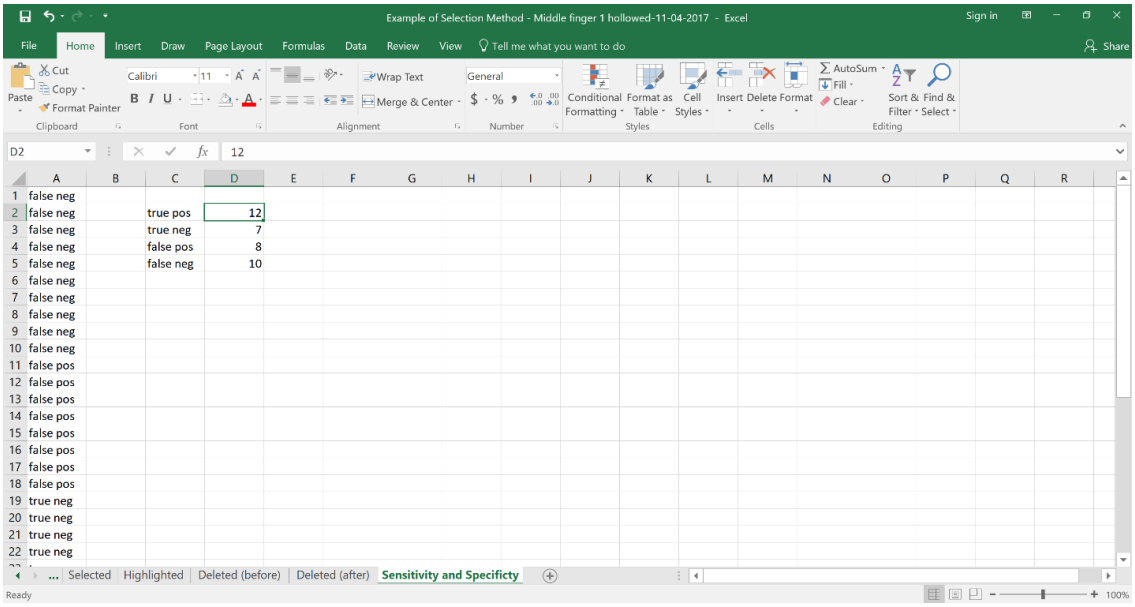

To calculate sensitivity, the formula is True Positive / (True Positives + False Negatives), so to do this in Excel, enter the formula below, selecting the appropriate values by clicking on the respective cells to add them into the formula:

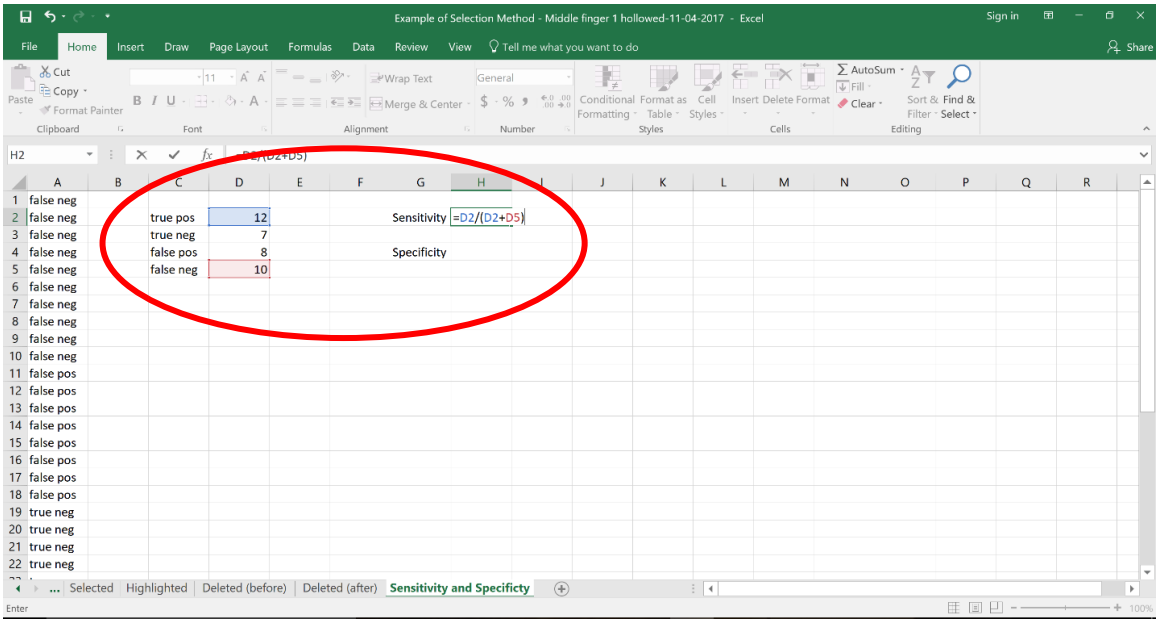

Once the formula is typed in, hit ENTER, and this will calculate the formula:

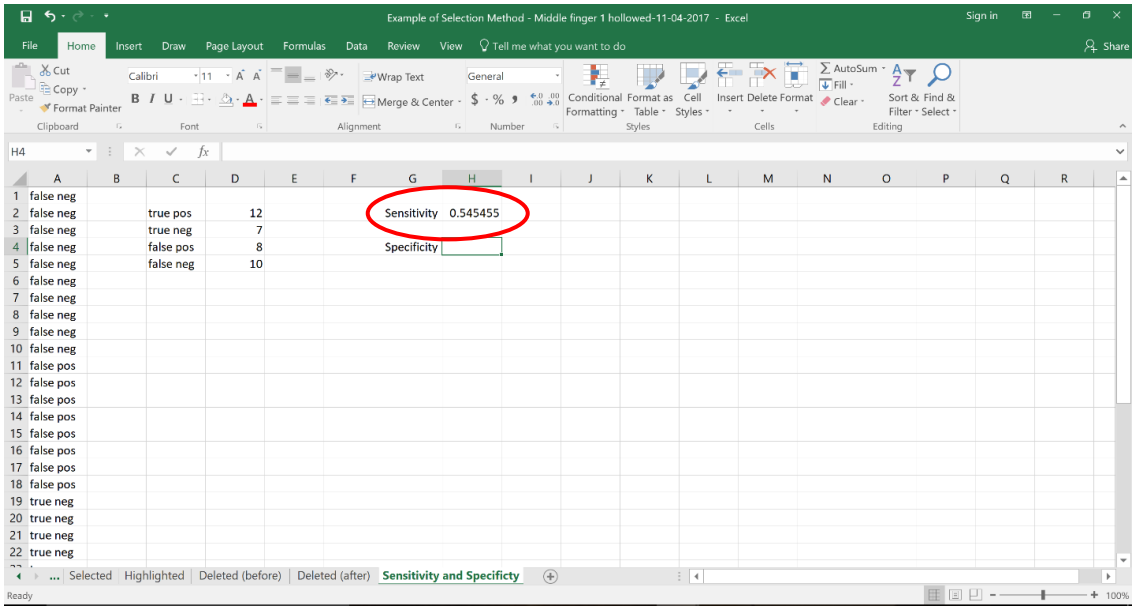

To calculate specificity, the formula is True Negative / (True Negative + False Positives), so to do this in Excel, enter the formula below, selecting the appropriate values by clicking on the respective cells to add them into the formula:

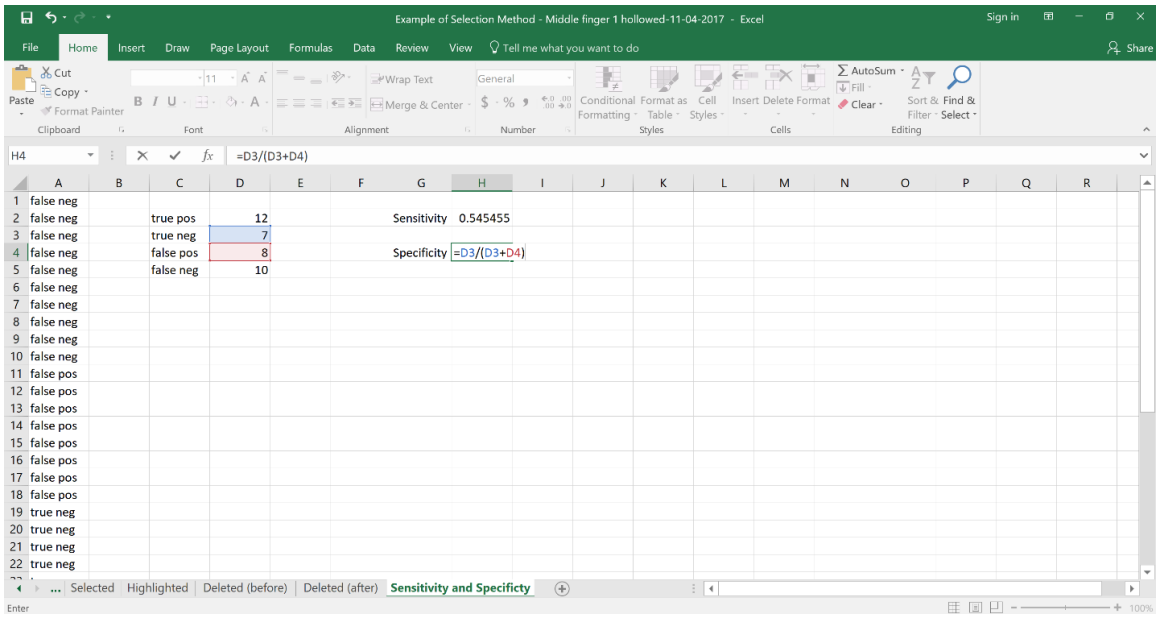

Once the formula is typed in, hit ENTER, and this will calculate the formula:

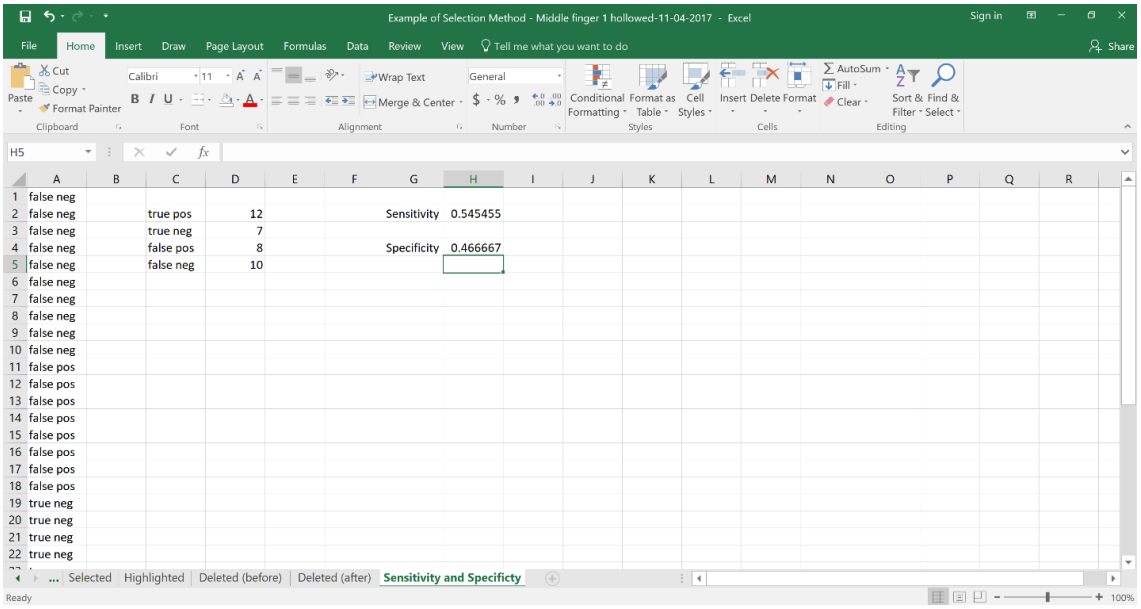

11) Feel accomplished! You're finished!

Appendix D

Batch	Time (Hours)	Computer	Location	Link Speed	Iterations	Iterations/Time
First 20 Decimated	183:30:00	Elena's	D Drive		1560	0:07:03
Second 20 - Decimated	183:33:00	Elena's	D Drive		1560	0:07:04
5 First Right 1	0:33:00	Romulus	Desktop Off		5	0:06:36
5 First Right 2	0:57:00	Remus	Desktop Off		5	0:11:24
15 First Right 1	1:34:00	Romulus	Desktop Off		15	0:06:16
15 First Right 2	22:01:00	Remus	Desktop Off		15	1:28:04
100 First Right 1	10:30:00	Romulus	Desktop Off		100	0:06:18
100 First Right 2	63:12:00	Remus	Desktop Off		100	0:37:55
100 First Right 3	4:49:00	Romulus	Desktop Off		100	0:02:53
40 First Rights - 1	18:21:00	Romulus	Desktop		40	0:27:32
40 Second Rights - 1	13:31:00	Elena's	D Drive	1 GB	40	0:20:17
20 First Rights - 1	0:56:00	Romulus	Desktop Off		20	0:02:48
80 First Rights - 1	19:45:00	Romulus	Desktop Off		80	0:14:49
80 First Rights - 2	112:09:00	Remus	Desktop Off		80	1:24:07
80 First Rights - 3	4:46:00	Romulus	Desktop Off		80	0:03:34
80 First Rights - 4	3:44:00	Romulus	Desktop Off		80	0:02:48
80 First Rights - 5	8:12:00	Romulus	Desktop Off		80	0:06:09
80 First Rights - 6	21:07:00	Romulus	Desktop Off	1 GB	80	0:15:50
80 First Rights - 7	23:15:00	Romulus	Desktop Off	1 GB	80	0:17:26
80 First Rights - 8	4:04:00	Romulus	Desktop	1 GB	80	0:03:03

80 First Rights - 9	3:31:00	Romulus	Off Desktop	1 GB	80	0:02:38
80 First Rights - 10	30:03:00	Romulus	Off Desktop	1 GB	80	0:22:32
80 First Rights - 11	28:52:00	Romulus	Off Desktop	1 GB	80	0:21:39
80 First Rights - 12	4:18:00	Amarna	D Drive	1 GB	80	0:03:14
80 First Rights - 13	9:09:00	Amarna	D Drive	1 GB	80	0:06:52
80 First Rights - 14	40:28:00	Amarna	D Drive	1 GB	80	0:30:21
80 First Rights - 15	3:28:00	Amarna	D Drive	1 GB	80	0:02:36
80 First Rights - 16	16:01:00	Amarna	D Drive	1 GB	80	0:12:01
80 First Rights - 17	17:19:00	Amarna	D Drive	1 GB	80	0:12:59
80 First Rights - 18	4:45:00	Elena's	D Drive	1 GB	80	0:03:34
80 First Rights - 19	22:35:00	Amarna	D Drive	1 GB	80	0:16:56
80 First Rights - 20	1:55:00	Elena's	D Drive	1 GB	80	0:01:26
40 Final Rights - 1	2:58:00	Romulus	Off Desktop		40	0:04:27
Total	885:51:00				5200	0:10:13